SELECTED ION FLOW DRIFT TUBE (SIFDT) STUDIES OF REACTIVE ION-NEUTRAL ENCOUNTERS

A Thesis
Presented for the Degree
of Doctor of Philosophy in Chemistry
In the
University of Canterbury

by
David Andrew Fairley

University of Canterbury
1998

TABLE OF CONTENTS

ACKNOWLEDGEMENTS

I wish to extend my gratitude, first and foremost, to my academic supervisor, Professor Murray McEwan for his guidance and wisdom during the course of this research. Many thanks also to Dr Colin Freeman for his role as joint supervisor of the research presented herein.

I have enjoyed numerous collaborations with Dr Robert Maclagan on the theoretical calculations performed during the course of this research and his patience and advice have been greatly appreciated.

Thanks go to my co-workers in the ion-molecule laboratory who assisted in gathering much of the data presented in this thesis, namely Dr Paul Wilson, Dr Graham Scott, Mr Daniel Milligan and Ms Louise Wheadon.

I have enjoyed immensely meeting and working alongside numerous visitors to the ion-molecule laboratory, including Professors Nigel Adams and Lucia Babcock, Dr Vincent Anicich and Dr Michael Mautner. Special mention goes to Professor David Smith and Dr Patrik Spanel, who visited the laboratory twice during the course of my research. Professor Smith's advice and encouragement, not only during his visits but via regular e-mail contact, was greatly appreciated. It is also fair to say that Dr Spanel's efforts in installing, upgrading and customising his "SIFT for Windows" software for use in the laboratory here at Canterbury represented a revolution in data acquisition and analysis.

I wish to extend warm thanks to the technical staff of the mechanical, electronics and glassblowing workshops in the Chemistry Department for their unstinting efforts in maintaining and upgrading the SIFDT apparatus, especially for their considerable labours during the relocation of the apparatus within the department. Thanks also go to the departmental secretarial staff for their assistance with the preparation of manuscripts for publication.

I thank the many fellow students and academic staff members I have been fortunate to work with in teaching laboratories during the past few years. Special mention goes to the "Honours class of '93" and in particular Dr Vaughan Langford and Dr Dave Bull for their encouragement of my research.

I thank the Chemistry Department for the provision of a Teaching Assistantship during the first three years of my Ph.D. and the Marsden Fund for funding during the latter part of my research.

Special thanks go to my old high school friends (and fellow morning fillers): Aaron Mikaere, Grant Samuels and Ross Edwards for their friendship during the past 12 or so years.

Last, but by no means least, I wish to thank my family, both immediate (Mum, Dad, Steven and Jacquie) and extended, for their support and encouragement during the course of my university studies.

LIST OF TABLES

LIST OF FIGURES

PUBLICATIONS

The following publications are related to the research presented in this thesis:

Fairley, D.A., Scott, G.B.I., Freeman, C.G., Maclagan, R.G.A.R., and McEwan, M.J., *J. Chem. Soc., Faraday Trans.*, **92**, 1305 (1996).
Ion-molecule association of H_3O^+ and C_2H_2: Interstellar CH_3CHO.

Fairley, D.A., Scott, G.B.I., Freeman, C.G., Maclagan, R.G.A.R., and McEwan, M.J., *J. Phys. Chem. A*, **101**, 2848 (1997).
$C_2H_7O^+$ potential surface and ion-molecule association between H_3O^+ and C_2H_4.

Fairley, D.A., Scott, G.B.I., Milligan, D.B., Maclagan, R.G.A.R., and McEwan, M.J., *Int. J. Mass Spectrom. Ion Proc.*, **172**, 79 (1998).
SIFDT study of the SO_2^+/H_2 H-atom abstraction reaction.

Fairley, D.A., Milligan, D.B., Wheadon, L.M., Freeman, C.G., Maclagan, R.G.A.R., and McEwan, M.J., *Int. J. Mass Spectrom.*, In Press (1998).
A flow tube and theoretical study of proton transfer reactions of $C_3H_5^+$ ions.

Fairley, D.A., Milligan, D.B., Freeman, C.G., McEwan, M.J., Spanel, P., and Smith, D., In Preparation.
Association and charge transfer: NO^+ + ketones – A SIFDT study.

ABSTRACT

Data is presented for a series of experiments performed using a selected ion flow drift tube (SIFDT) apparatus operated at room temperature (300 ± 5 K) and at helium pressures typically between 0.3 – 0.5 Torr. Several of the experiments described utilised the apparatus as a conventional selected ion flow tube (SIFT), i.e. the drift capability was only employed in some of the experiments.

Three termolecular ion-molecule association reactions proposed to play a potential role in the chemistry of the interstellar medium were investigated in an effort to elucidate the isomeric structures formed and thereby infer the structures likely to be formed in the analogous radiative association reactions at interstellar pressures. The termolecular association of H_3O^+ with C_2H_2 is shown to produce a mixture of $C_2H_5O^+$ isomers and efforts to identify the individual isomers are described. The termolecular association of H_3O^+ with C_2H_4 produces a $C_2H_7O^+$ isomer that exhibits reactivity with the neutrals 2-fluorotoluene and acrylonitrile identical to that observed from protonated ethanol, $C_2H_5OH_2^+$. The termolecular association of $CH_2NH_2^+$ with HCOOH is shown to produce an electrostatic adduct which undergoes facile ligand switching reactions with NH_3 and the amines, CH_3NH_2 and $C_2H_5NH_2$. The radiative association of $CH_2NH_2^+$ with HCOOH is therefore not considered to be a plausible synthetic route to protonated glycine in the interstellar medium.

Dissociative charge transfer from Kr^+, CO^+ or CO_2^+ to chlorobenzene is shown to produce the cyclic phenylium cation exclusively. Electron impact on halobenzenes and consecutive ion-molecule reactions of acetylene are known to produce a mixture of $C_6H_5^+$ isomers. It is shown that the more reactive of these isomers has the phenylium structure. Low energy dissociative charge transfer to cycloheptatriene or benzyl bromide is used to selectively form the tropylium and benzyl cations respectively. The experiments lead to an estimate of the barrier height for the isomerisation benzyl $\rightleftharpoons$ tropylium of 2.7 ± 0.9 eV. Reaction with benzene is used as a diagnostic for distinguishing the isomeric $C_7H_7^+$ product(s) formed in a series of ion-molecule reactions.

The allyl, $CH_2CHCH_2^+$, and 2-propenyl, $CH_3CCH_2^+$, cations are observed as distinct isomeric species in the SIFT. Reaction with methanol is used to distinguish

between the two isomers. The isomeric ratio of allyl:2-propenyl formed via protonation of allene or propyne by a protonated base, BH^+, is shown to be dependent on the proton affinity of the base, B. The experiments yield an estimate of the barrier height for the rearrangement allyl $\longrightarrow$ 2-propenyl of 110 ± 30 kJ mol^{-1}, which is in excellent accord with ab initio calculations performed at the G2(MP2) level of theory.

The exothermic H-atom abstraction reaction of SO_2^+ with H_2 has been studied in a SIFDT apparatus over a range of centre-of-mass energies from thermal (300 K) to ~ 0.12 eV. The observed increase in rate coefficient with ion kinetic energy gives a linear pseudo-Arrhenius plot with a slope that indicates a barrier of ~ 5 kJ mol^{-1} exists on the potential energy surface. The $H_2SO_2^+$ potential surface was also explored in an ab initio investigation using the G2(MP2) procedure. An $(SO_2^+ \cdot H_2)^*$ transition state between reactants and products is identified, corresponding to the barrier found from experiment.

The competition between charge transfer and association was investigated in a SIFDT study of the reactions of NO^+ with the ketones: acetone, butanone and 3-pentanone. Association is the sole process observed in all three reactions at 300 K (the 3-pentanone reaction possesses a minor channel to the slightly endothermic charge transfer product). As the ion-neutral centre-of-mass energy is increased the rate coefficient for termolecular association decreases markedly, as a result of the decreasing lifetime of the intermediate ($NO^+ \cdot$ketone) complex with increasing temperature. Bimolecular charge transfer can compete with association once sufficient energy is available to overcome the endothermicity and at higher energies dissociative charge transfer channels open up.

The association reactions of CH_3^+ with CH_3CN and C_2N_2 were also investigated in the SIFDT. The CH_3^+/CH_3CN reaction exhibits competitive binary and ternary channels. The bimolecular channels to $C_2H_5^+ + HCN$ and $HCNH^+ + C_2H_4$ both involve extensive intramolecular rearrangement of the intermediate $(CH_3^+ \cdot CH_3CN)^*$ collision complex and the rate coefficients for both channels exhibit a marked (negative) dependence on the ion-neutral centre-of-mass energy.

CHAPTER 1.

BRIDGING THE ENERGY GAP IN ION-MOLECULE REACTION STUDIES: THE FLOW DRIFT TUBE AND ITS VARIANTS

1.1 The Flowing Afterglow and SIFT Techniques.

Among the techniques available for the study of ion-molecule reaction kinetics, few have proved to be as reliable and productive as the fast flow tube techniques, the flowing afterglow (FA) and the selected ion flow tube (SIFT). The flowing afterglow (Figure 1.1) was developed in the early 1960s by Ferguson, Fehsenfeld and Schmeltekopf [1-4] in Boulder, Colorado and was first applied to the study of ion-neutral reactions that control the loss of helium ions in the earth's ionosphere. [1] The ability to operate the FA over a wide temperature range [5] (as low as 80 K and up to 900 K) permitted the study of weakly bound cluster ions, which dissociate readily at room temperature, and the determination of the temperature dependence of reactive ion-neutral encounters. The upper temperature limit for FA experiments has recently been extended to ~1600 K by workers in the Massachusetts laboratory of Viggiano and Paulson, where a new high temperature flowing afterglow (HTFA) [6-10] has been developed. The apparatus utilises a ceramic flow tube heated by a commercial furnace, and the basic principles of operation are the same as any flowing afterglow. [6] The principal disadvantage of the flowing afterglow is the method by which reactant ions are created. Ionization is created in the upstream region of a fast flowing carrier gas (usually helium) by electrical discharge through the carrier gas, forming He^+ and $He(2\,^3S)$ metastables. Ions other than He^+ are then formed by direct addition of a source gas to the He^+ plasma. This process may generate more than one reactant ion by virtue of the thermochemistry of charge

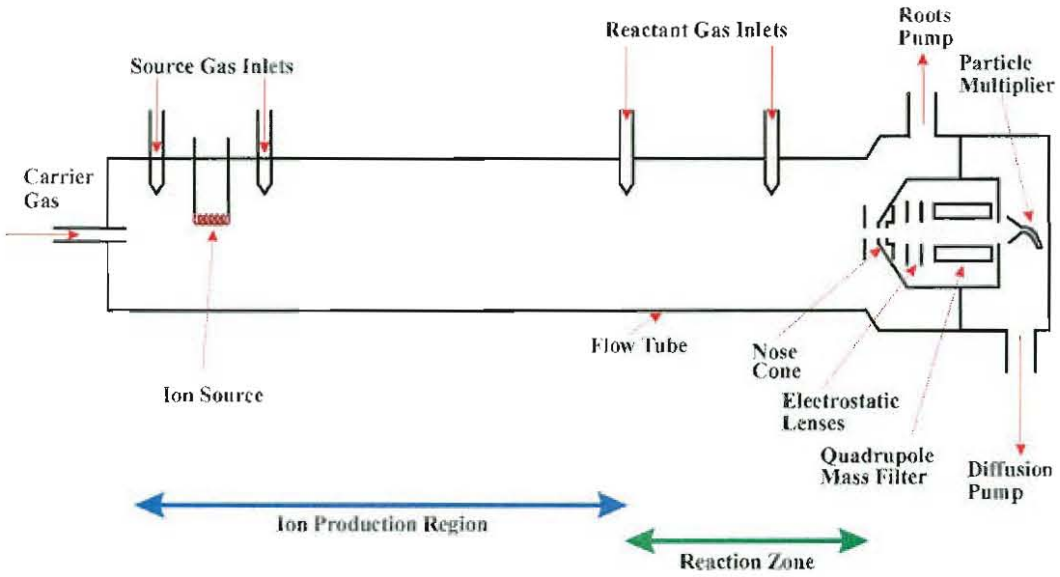

Figure 1.1. Schematic diagram of a flowing afterglow (FA) apparatus.

transfer and Penning ionisation processes and via reactions of primary ions with the parent reactant gas. This may prevent the unequivocal identification of the product ions of a given ion-molecule reaction. The difficulties inherent in interpreting flowing afterglow data prompted the development of the selected ion flow tube (SIFT) technique by Smith and Adams in the late 1970s. [11,12] In the SIFT technique ions are created in an ion source remote from the flow reactor tube, from which ions of a single m/z ratio are selected in a differentially pumped quadrupole mass filter, and injected (free of all other ions), at low energies, through a small orifice into the flow tube. The ions are then convected downstream in a fast flowing carrier gas, sampled through another small orifice, mass selected in a second quadrupole mass filter and detected using ion counting techniques. Reactions of these thermalised primary ions can be observed by adding a reactant neutral to the carrier gas flow in the reaction region and measuring the reduction in the primary ion signal as a function of neutral flow. A schematic diagram of a SIFT apparatus is given in Figure 1.2. The parallel development of the ion cyclotron resonance (ICR) technique [13-18] has also contributed greatly to an understanding of reactive ion-neutral encounters. The flowing afterglow [2,3,19] SIFT [19-23] and ICR [13-17] techniques have all been extensively reviewed.

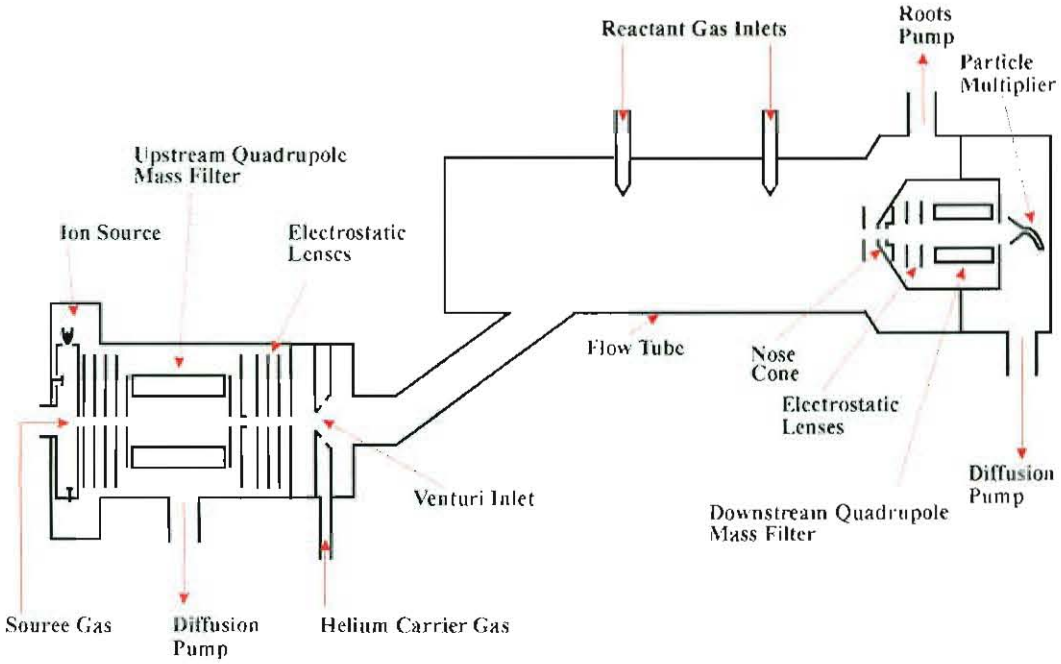

Figure 1.2. Schematic diagram of a selected ion flow tube (SIFT) apparatus.

1.2 The Flow Drift Tube Technique.

Flowing afterglow and SIFT experiments provide kinetic data for ion-neutral reactions in the thermal range of interaction energies, i.e. up to about 0.1 eV (3/2 kT at 900 K).[‡] Ion beam experiments [24-29] provide cross sections for such reactions at energies in excess of a few tenths of an electron volt in most cases (although some sophisticated beam experiments [28] operate at lower energies). A desire to develop an instrument to "bridge the gap" between thermal energies and the smallest beam experiment energies led to the development of the flow-drift tube (FDT) in the NOAA laboratories in Boulder, Colorado. [30-32]

1.2.1 A brief history of drift tubes.

Shortly after the discovery of X-rays in 1895, drift tubes were developed to study the behaviour of slow ions drifting in gases. A drift tube apparatus consists of an ion

[‡] This range has been extended to ~ 0.2 eV with the development of the HTFA instrument, [6] which operates at temperatures up to ~ 1800 K.

source, an enclosure containing gas at a "high" pressure, a set of electrodes that establish a uniform electric field along which the ions drift and a detector at the end of the drift region. Most early drift tubes contained internal ion sources and were used almost exclusively (prior to about 1960) to measure ionic drift velocities to the exclusion of quantitative studies of diffusion and ion-molecule reactions. Interested readers are referred to the excellent historical reviews by Mason and McDaniel [33] and McDaniel et al [34] and references cited therein for a discussion of the development of drift tube technology.

1.2.2 The Flow Drift Tube (FDT).

McFarland constructed the original NOAA flow drift tube (Figure 1.3) for his Ph.D. thesis. [30] In the FDT, the downstream half of the flow tube is made up of a series of narrow ring sections (7.5 mm in width) clamped together via O-rings to form a vacuum tight cylindrical tube, with the individual ring sections electrically insulated from each other. By applying suitable potentials to the rings, a uniform electric field can be established along the axis of the flow tube. Thus ions can be constrained to drift through the carrier gas under the influence of the applied field, thereby increasing their laboratory energy and hence their interaction energy with the carrier gas and any added reactant gas. By varying the electric field strength, E, or more correctly the ratio E/N (where N is the carrier gas number density), reactions can be studied over a range of energies. In the original NOAA FDT, the ionization was created in the field free region upstream of the drift region. This method has all the inherent disadvantages of the flowing afterglow as described above, and thus it was a natural development to incorporate a SIFT-type injector in the FDT, creating a selected ion flow drift tube (SIFDT) [35], greatly enhancing the versatility of the instrument. Another natural extension of the SIFDT technique was to incorporate a variable temperature facility, as in the variable temperature flowing afterglow and variable temperature SIFT (VT-SIFT) apparatuses. This was successfully achieved by Smith and Adams, who developed a variable temperature selected ion flow drift tube (VT-SIFDT). [21] Variable temperature operation necessitated a change in design of the drift tube region. Rather than constructing the drift region from ring sections

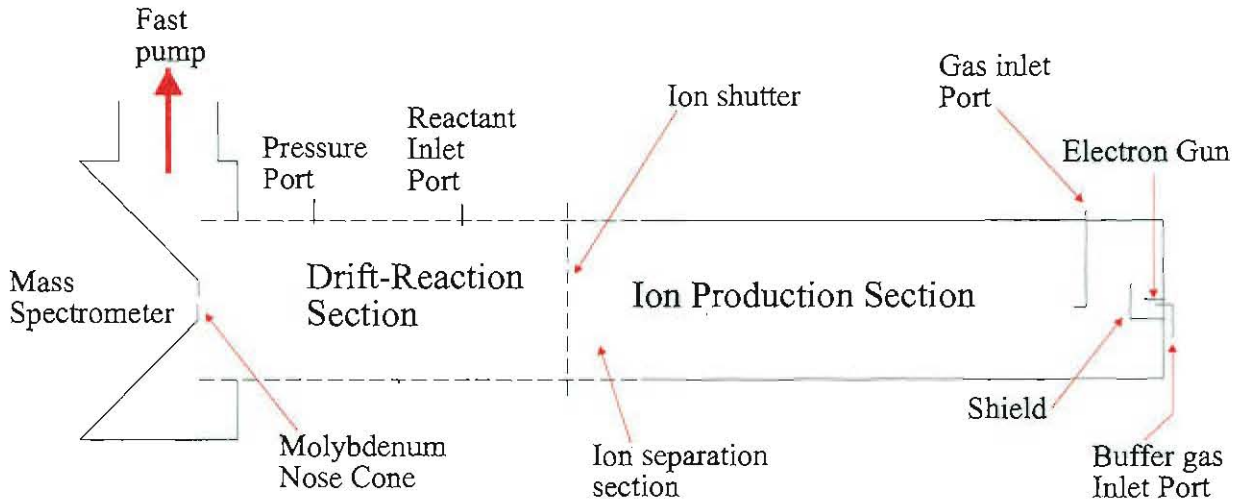

Figure 1.3. Schematic diagram of a flow-drift tube (FDT) apparatus.

clamped together with O-rings, the Birmingham design utilized a drift tube section consisting of 50 metal rings (diameter 60 mm, width 9 mm) held 1 mm apart by ceramic insulators, which could be inserted into a standard VT-SIFT.

1.3 Theory of Drift Tube Operation

The basic principles of drift tube operation are simple. [21,33,36] Ions are produced in, or introduced into, a buffer gas at pressures typically between 0.1 and a few Torr. Metal rings held at appropriate potentials provide a homogeneous electric field of strength E along the axis of the drift tube (see Figure 1.4). The ions are accelerated by the action of the drift field and at the same time undergo many collisions with the carrier gas atoms or molecules. Therefore, rather than being constantly accelerated by E, the ions reach a steady mean drift velocity, v_d, in the direction of E. The average ion kinetic energy acquired from the electric field, which is proportional to v_d, is only a function of E/N, where N is the number density of the carrier gas. [33] This statement can be rationalised as follows. The electric force on an ion of charge e is eE and the resulting acceleration is eE/M_{ion}, where M_{ion} is the mass of the ion. The crude assumption can be made that when an ion undergoes a collision, it loses, on average, all the energy imparted to it by the field during the previous free path. Then, if the mean time between collisions is denoted τ, the ion velocity, v, immediately before a collision, will be $eE\tau/M_{ion}$. Since τ

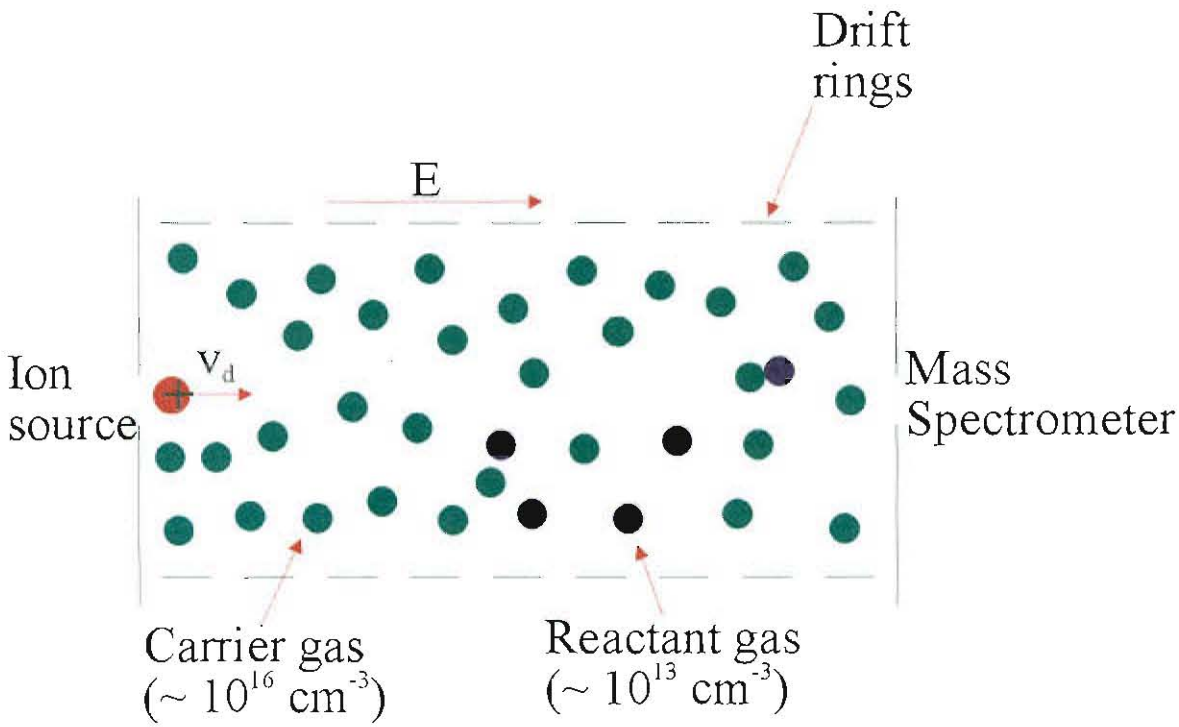

Figure 1.4. Schematic diagram of a drift tube used for the investigation of ion-neutral reactions.

is proportional to 1/N, the energy obtained between collisions is thus seen to be proportional to $(E/N)^2$, since kinetic energy = $\frac{1}{2}M_{ion}v^2$. Rigorous calculations also demonstrate that E/N is the parameter that determines the field energy of the ions. [33] v_d is a small fraction of the mean random velocity of the ions as long as E/N is small and increases as E/N increases.

Drift velocities have been determined experimentally for a wide variety of ions, both in their parent gases and other bath gases and are essential parameters in the determination of rate coefficients for ion-molecule reactions in drift tubes. [37-40] The proportionality constant between the drift velocity and the applied field is called the ionic mobility, K, and is defined by the equation:

$$K = \frac{v_d}{E} \qquad \textbf{(1.1)}$$

Since K is inversely proportional to N at fixed temperature, T, and E/N, it is usual to report a reduced mobility K_o corresponding to a standard density (Loschmidt's constant, the density of an ideal gas at 0°C and 760 Torr).

$$K_o = K\left(\frac{P}{760}\right)\left(\frac{273.15}{T}\right) \quad \textbf{(1.2)}$$

K_o is usually tabulated as a function of E/N, where E/N is expressed in Townsends (1 Td = 10^{-17} V cm^2).

1.4 The Wannier Equations.

Swarms of drifting ions possess a random velocity distribution as well as a superimposed drift velocity in the direction of the applied field, E. Taking into account the ion-induced dipole interaction between the drifting ions and the carrier gas particles, Wannier [41] calculated the kinetic energy of the drifting ions, KE_{ion},

$$KE_{ion} = \tfrac{3}{2}k_bT + \frac{m_c v_d^2}{2} + \frac{M_{ion} v_d^2}{2} \quad \textbf{(1.3)}$$

where m_c is the mass of the carrier gas particles, M_{ion} is the mass of the ions and k_b is the Boltzmann constant. When considering a reaction of the ion swarm with a reactant neutral, the important parameter is E_r, the mean relative centre-of-mass energy between the ion-neutral pair, which is given by [31,33,36,41]:

$$E_r = \tfrac{1}{2} M M_{ion} \frac{(v_i^2 + v_n^2)}{(M + M_{ion})} \quad \textbf{(1.4)}$$

where M is the mass of the reactant neutral, v_n^2 is the mean square velocity of the reactant neutral (given by $\tfrac{3}{2}k_bT = \tfrac{1}{2}Mv_n^2$) and v_i^2 is the ion mean square velocity (obtained from $\tfrac{1}{2}M_{ion}v_i^2 = KE_{ion}$). Substitution for v_i^2 and v_n^2 in equation (1.4) gives:

$$E_r = \left[\frac{M}{M_{ion} + M}\right]\left(KE_{ion} - \tfrac{3}{2}k_bT\right) + \tfrac{3}{2}k_bT \quad \textbf{(1.5)}$$

The rate coefficients, k, for ion-neutral reactions studied using drift tubes are usually presented as a function of E_r. For atomic ions drifting in an atomic carrier gas, only elastic collisions can occur between the ions and the carrier gas atoms. Moreover, it has been shown [42-47] that atomic ions drifting in helium possess a near-Maxwellian energy distribution, described to a very good first approximation, by the centre-of-mass energy E_c, appropriate to the ion-carrier gas atom collisions:

$$E_c = \left[\frac{m_c}{(M_{ion}+m_c)}\right](KE_{ion} - \tfrac{3}{2}k_bT) + \tfrac{3}{2}k_bT \qquad \textbf{(1.6a)}$$

Substitution of equation (1.3) into (1.6a) yields:

$$E_c = \tfrac{1}{2}m_c v_d^2 + \tfrac{3}{2}k_bT = \tfrac{3}{2}k_bT_{eff}^c \qquad \textbf{(1.6b)}$$

where m_c is the mass of the carrier gas atoms. Indeed, it is now recognised that the accuracy of equation (1.6b) is a reflection of the closeness with which both the ions and carrier gas atoms possess, in the centre-of-mass reference frame, Maxwell-Boltzmann distribution functions characterised by T_{eff}^c. A similar argument extends to the accuracy of equation (1.5).

For atomic ions drifting in an atomic buffer gas, Wannier's formulas are believed to be generally accurate to ± 10%. [48] It follows that for an ***atomic*** ion drifting in helium the energy of the interaction between the ion and the carrier gas, E_c, and the energy of the interaction of the ion with the reactant neutral, E_r, can be correctly characterized to within the uncertainty of most experimental rate determinations. When the drifting ions are ***molecular***, however, internal excitation of the ions can occur in collisions with the carrier gas atoms. [49-54] Rotational excitation (and de-excitation) is generally facile in such collisions as verified by laser fluorescence measurements of the rotational temperature of N_2^+ ions in helium [55], equilibration being achieved in about ten collisions in the case of N_2^+, and a rotational temperature can generally be ascribed to the ions in terms of E_c, such that:

$$\tfrac{3}{2}k_bT_{rot} = E_c \qquad \textbf{(1.7)}$$

At high E/N and especially in heavier buffer gases (e.g. argon) ***vibrational*** excitation of the ions can occur. Theoretical calculations by Viehland et al [48,56-61] suggest that ***given sufficient collisions*** between the ions and (atomic) carrier gas particles, the internal energy state of the ions, T_{int}, will equilibrate to E_c, the ion-carrier gas centre-of-mass energy, viz.

$$\tfrac{3}{2}k_bT_{int} = E_c \qquad \textbf{(1.8)}$$

E_c is given to a first approximation by equation (1.6). A more accurate expression is: [56-61]

$$E_c = \frac{3}{2}k_bT_{int} = \left(1+\frac{m_c}{m_i}\xi\right)\left(\frac{3}{2}k_bT + \frac{1}{2}m_c v_d^2\right)(1+\beta) \qquad \textbf{(1.9)}$$

where m_i and m_c are the ion and carrier gas masses respectively, β is a small ($<< 1$) correction term and ξ is a dimensionless ratio of collision integrals which characterise the fractional energy loss due to inelastic collisions. Viehland and Robson [48] have recently introduced a new expression for the effective internal temperature involving only quantities that are measurable in traditional drift tube experiments (e.g. ionic mobility and diffusion coefficients).

$$\frac{3}{2}k_b T_{\text{int}} = E_c^{(1)} = E_c^{W} - \frac{m_c}{m_i + m_c}\left[\frac{3}{2}k_b T + \frac{1}{2}m_c v_d^{\,2} - \frac{qD_T}{K} - \frac{qD_L}{2K(1+K')}\right] \qquad \textbf{(1.10)}$$

Here, E_c^{W} is the centre-of-mass energy defined by the Wannier equation (1.6a), q is the ion charge, K (= v_d/E) is the ion mobility, and K' is the logarithmic derivative of K with respect to the logarithm of E/N, i.e.

$$K' = \frac{d\ln K}{d\ln(E/N)} \qquad \textbf{(1.11)}$$

A similar expression has been derived for E_r. The accuracy of equation (1.10) has yet to be tested for polyatomic ions, as a result of the dearth of transverse and longitudinal diffusion coefficients for polyatomic ions in atomic carrier gases. [48] It is anticipated, however, that the Wannier equations will prove to be accurate to the same ± 10% for polyatomic ions drifting in atomic buffer gases as has been shown for atomic ions. [48] Larger deviations are predicted for atomic and molecular ions drifting in molecular bath gases. However, while the internal energy of an ion is predicted to equilibrate to E_c at steady state, it is uncertain how many collisions with the carrier gas will be required for steady state to be reached. Indeed, achievement of a steady-state Boltzmann vibrational distribution may require a drift tube of infinite length! [62] Most of the available experimental data suggests that vibrational excitation in a helium carrier gas is inefficient at typical values of E/N. Although a value of E_c can be calculated, the internal energy of the drifting ions is often quite uncertain, i.e. a vibrational temperature cannot be readily ascribed to the ions. Federer et al [63] and Kriegel et al [64], using a SIFDT apparatus, have shown for example that N_2^+ and O_2^+ ions can be vibrationally excited in a helium carrier gas even at modest E/N values. However, this process is relatively slow and equilibrium among the v = 0 and v = 1 states of the N_2^+ and O_2^+ ions is barely achieved in the

available length of the drift field except at the highest values of E/N. Vibrational excitation, especially of polyatomic ions, must therefore be considered in SIFDT experiments even when a helium carrier gas is used, although, as already mentioned, caution must be exercised in ascribing a temperature to the internal excitation of ions drifting in monatomic buffer gases.

1.5 Determination of Rate Coefficients as a Function of Interaction Energy.

Reaction rate coefficients are determined in a SIFDT apparatus in a similar manner to that described for a conventional flowing afterglow or SIFT. [20-22,36] The decrease in the reactant ion signal and the appearance of the product ions are monitored as a function of the neutral reactant flow rate. The analysis of the data is greatly simplified compared to that for a SIFT or flowing afterglow, essentially due to the fact that the radial profile of the ion velocity for the drifting ions is uniform. "Plug" flow prevails rather than the parabolic radial velocity distribution present in a SIFT or FA. This is a consequence of the ion drift velocity being significantly greater than the gas flow velocity even for small values of E/N. For a generalised reaction:

$$A^+ + B \longrightarrow C^+ + D \qquad \textbf{(1.12)}$$

the rate of loss of A^+ in the drift region is given by:

$$v\frac{\partial A^+}{\partial z} = -k[A^+][B] \qquad \textbf{(1.13)}$$

where k is the reaction rate coefficient, and $[A^+]$ and [B] are the concentrations of A^+ and the reactant neutral B, and v is the ***sum*** of the flow velocity and drift velocity of the ions. Diffusive loss terms can be eliminated from the analysis. It follows that

$$[B] = Q/(\pi a^2 v_o) \qquad \textbf{(1.14)}$$

where Q is the reactant gas flow rate, a is the flow tube radius, and v_o is the bulk flow velocity of the carrier gas. Substitution of [B] into equation (1.13), followed by integration and rearrangement leads to a value for k.

$$k = \frac{\pi a^2 v v_o}{Q(L+z)} \ln \frac{[A^+]_o}{[A^+]} \qquad \textbf{(1.15)}$$

$[A^+]_o$ corresponds to $[A^+]$ at Q = 0, L is the distance between the reactant inlet and the sampling orifice and z is a (small) end correction to allow for non-instantaneous mixing of the reactant neutral. It should also be noted that excessive concentrations of a neutral reagent will reduce the drift velocity of an ion below that determined in the absence of the neutral, thus increasing the reaction time. This will have the effect of yielding erroneously high rate coefficients but will only be significant for very slow reactions ($k \leq 10^{-12}$ cm^3 s^{-1}). As discussed above it is usual to present rate coefficients measured in drift tubes as a function of E_r, determined from the ion drift velocity using the Wannier equations.

1.6 "Typical" drift tube reaction behaviour.

Reactions occurring in drift tubes can be loosely categorised into two classes, fast and slow reactions. [65,66] For fast reactions, e.g. exothermic proton transfer, the rate coefficients either remain constant [‡] or slowly decrease with increasing kinetic energy. For slow reactions the rate coefficients are found to decrease with increasing energy at low kinetic energies. At some intermediate energy the rate coefficient reaches a minimum and then begins to increase again at higher energies. This behaviour is rationalised in terms of ion-molecule reactions occurring on a double-minimum potential. The reactants form a long-lived encounter complex in the entrance channel and proceed to products over a tight barrier. The observed energy dependence in a drift tube can be understood in terms of a competition between returning to reactants over a loose barrier or proceeding on to products over a tight barrier. Dissociation back to reactants involves a looser transition state and hence a higher density of states ratio, which changes more rapidly with increasing energy than the density of states ratio for the tight transition state. Therefore the rate constant for the reverse process increases more rapidly with increasing energy than the rate constant for product formation. Consequently, a decreasing fraction of reactants will proceed through the tight transition state to products as the kinetic energy of the ion-molecule collision increases. The increase in rate coefficient at higher energies

[‡] In actuality the rate coefficient may increase slightly with increasing kinetic energy – see the section following equation (1.20).

usually indicates that a new mechanism has become important, such as a new vibrational or electronic state becoming energetically accessible or a completely new product.

Glosik et al [67,68] have measured the dependence of the rate coefficients, k, on the average centre-of-mass interaction energy, E_r, for the bimolecular reactions of several simple positive ions with HCl. Although most of the reactions are strongly exothermic and proceed at close to the collisional rates at thermal energies, some reactions show a pronounced decrease in their rate coefficients with increasing E_r. They interpreted the results in terms of a simple model based on the steady state approximation. The model allows information to be obtained on the unimolecular rate coefficients for the dissociation of the intermediate collision complex to products or back to reactants, k_2 and k_r respectively, and the rate coefficient k_f (often equal to the collision rate coefficient) for the formation of these complexes. The following reaction scheme is appropriate.

$$A^+ + B \underset{k_r}{\overset{k_f}{\rightleftharpoons}} (AB)^{+*} \xrightarrow{k_2} C^+ + D \qquad \textbf{(1.16)}$$

The ratio k_r/k_2 was extracted from the experimental data and it was found that the E_r dependence of this ratio could be expressed by a power law function, $(E_r / E_{r0})^m$, where E_{r0} and m are adjustable parameters.

$$\frac{k_r}{k_2} = \left(\frac{E_r}{E_{r0}}\right)^m \qquad \textbf{(1.17)}$$

For reactions in which a second, endothermic reaction channel becomes accessible at higher E_r, a second term was added to the expression describing the dependence of the observed rate coefficient on E_r, given by the familiar Arrhenius equation. The additional term equates the endothermicity of the "direct" channel to an Arrhenius activation energy. Combining the two terms yields the expression:

$$k(E_r) = k_I + k_{II}$$

$$= k_f \frac{1}{1+\left(\frac{E_r}{E_{r0}}\right)^m} + k_{IIo}\exp\left(\frac{-\Delta E_A}{\frac{2}{3}E_r}\right) \qquad \textbf{(1.18)}$$

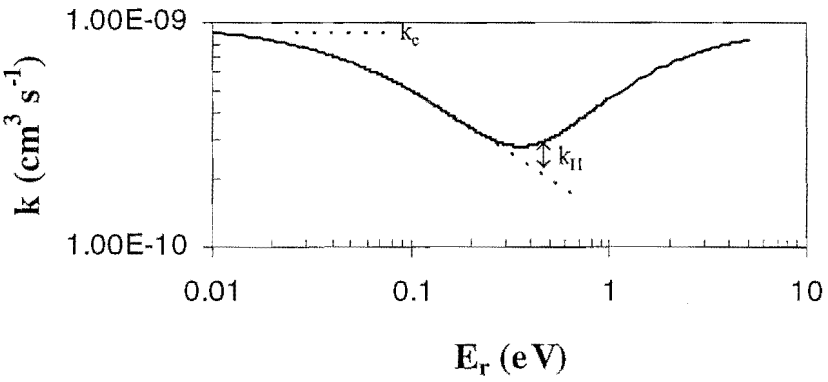

Figure 1.5. E_r dependence of the rate coefficient for an ion-molecule reaction proceeding via a mechanism described by equation (1.16) and formally expressed by equation (1.18). The parameters used are $k_f = k_{IIo} = 1 \times 10^{-9}$ cm^3 s^{-1}; $E_{r0} = 0.1$ eV; $\Delta E_A = 0.66$ eV; m = 2.

Here k_I and k_{II} are the rate coefficients for the "indirect" and "direct" processes respectively and k_{IIo} is a coefficient (Arrhenius pre-exponential factor) which is independent of E_r.

The steady state approximation when applied to the above reaction scheme yields:

$$k_I = \frac{k_f k_2}{k_r + k_2} = \frac{k_f}{1 + k_r/k_2} \qquad \textbf{(1.19)}$$

In order to visualize the dependence of the ratio k_r/k_2 on E_r, equation (1.17) can be rewritten in the form:

$$\frac{k_r}{k_2} = \frac{k_f}{k_f} - 1 \qquad \textbf{(1.20)}$$

In the original analysis the rate coefficient k_f was assumed to be independent of E_r. Subsequent experiments [69-72] showed that the measured rate coefficients for a number of fast ion-molecule reactions actually increased above the thermal rate coefficient at elevated E_r, leading to the incorporation of an empirical energy-dependent factor, β, derived from many experimental measurements, into equation (1.17).

$$\frac{\beta k_f}{k_f} - 1 = \frac{k_r}{k_2} = \left(\frac{E_r}{E_{r0}}\right)^m \qquad \textbf{(1.21)}$$

A theoretical discussion of the reasons for this energy dependence has been given by Smith et al [73], where the capture rate coefficient is predicted to increase as $T^{0.5}$ (i.e. as $(E_r)^{0.5}$ at suprathermal energies, such as those obtained in drift tube experiments.

Adams and Smith have investigated the variation of the ternary association reactions of CH_3^+ ions with N_2, H_2 and CO with E_c and E_r in a SIFDT apparatus. [74] The ternary association reactions are considered to proceed in two stages:

$$A^+ + BC \underset{k_r}{\overset{k_f}{\rightleftharpoons}} (ABC^+)^* \qquad \textbf{(1.22)}$$

$$(ABC^+)^* + M \xrightarrow{fk_c} ABC^+ + M \qquad \textbf{(1.23)}$$

In the first step A^+ and BC combine to form an excited intermediate complex, $(ABC^+)^*$, with rate coefficient k_f, which undergoes unimolecular dissociation back to reactants with rate coefficient k_r. In the second step the intermediate complex can be stabilised by collision with a third body, M, with a collisional rate coefficient, k_c, modified by an efficiency factor, f (which is ≤ 1). If it is assumed that the stabilisation step (1.23) does not significantly disturb the equilibrium in the first step, i.e. that $k_r >> fk_c[M]$, where [M] is the number density of the stabilising third body, then it can be shown that k_3 can be represented by:

$$k_3 = fk_c \frac{q'(ABC^+)^*}{q'(A^+ + BC)} = fk_c \frac{q'(ABC^+)^*}{q_{rel} q_{rot}(A^+) q_{rot}(BC)} \qquad \textbf{(1.24)}$$

where the q' are pseudo-partition functions. $q'(A^+ + BC)$ is approximated to the product of q_{rel}, the partition function for the relative translational motion of A^+ and BC, and $q_{rot}(A^+)$ and $q_{rot}(BC)$, the rotational partition functions for A^+ and BC respectively. After substitution of the appropriate partition functions, k_3 is predicted to vary with the various "temperatures" assignable to the reactants and the intermediate complex as:

$$k_3 \alpha \frac{T_c^{r_c/2}}{T_t^{3/2} T_i^{r_i/2} T_n^{r_n/2}} \qquad \textbf{(1.25)}$$

where r_c, r_i and r_n are, respectively, the number of rotational degrees of freedom in the complex (c), the reactant ion (i), and the reactant neutral (n), the T values are their

associated temperatures and T_t is the translational temperature appropriate to the A^+/BC interaction, i.e. $\frac{3}{2} k_b T_t = E_r$. Under thermal equilibrium conditions, as is appropriate to a normal SIFT experiment, all the T values are equal and k_3 is predicted to vary as $T^{-r/2}$, where r is the total number of rotational degrees of freedom in the separated reactants. In the drift field region of a SIFDT apparatus, the "temperatures" of the reactants and the intermediate complex are not all equal. The temperature of the reactant neutral, T_n, is equilibrated to that of the carrier gas and is not influenced by the drift field. For the reactions of CH_3^+ with diatomic molecules, k_3 is related to the various T values by:

$$k_3 \alpha \frac{T_c^{3/2}}{T_t^{3/2} T_i^{3/2} T_n} \qquad \textbf{(1.26)}$$

T_t is obtained directly from E_r and T_i is obtained from E_c. T_c would be expected to depend on T_t, T_i and T_n in some complicated way. However at any finite value of E/N, T_n will be small compared with T_t and T_i and thus T_c will be largely dependent on T_t and T_i. For the reactions of CH_3^+ with N_2 and CO in a He carrier, $T_t > T_i$ (since $E_r > E_c$) and it follows that T_c approximates to T_t. For the reaction of CH_3^+ with H_2, $T_i > T_t$ (since $E_c > E_r$), hence T_c approximates to T_i. This simple model therefore predicts the reactions of CH_3^+ with N_2 and CO to vary as $E_c^{-3/2}$ and the CH_3^+/H_2 reaction to vary as $E_r^{-3/2}$. These predictions were indeed substantiated by experiment. [74] Similar behaviour was observed in the reaction of CH_3^+ with HCl by Glosik et al. [69] It should be noted that for the reactions of l-C_3H^+ and c-$C_3H_2^+$ with CO a much steeper dependence of the termolecular rate coefficient on E_c was observed, k_3 varying as $E_c^{-2.9}$. k_3 is predicted by the model to vary as $E_c^{-1.0}$ for the linear ion and as $E_c^{-1.5}$ for the cyclic ion. The large difference observed between experiment and theoretical prediction was attributed to the population of low-frequency vibrational modes in the C_3H^+ and $C_3H_2^+$ ions, which would lead to a much steeper reduction in k_3 with increasing E_c. [74]

1.7 The utility of the SIFDT technique.

The utility of the SIFDT technique is not simply limited to the determination of the rate coefficients and ion product ratios of ion-molecule reactions as a function of ion energy. Judicious analysis of drift tube experimental data has provided information on

areas of ion chemistry as diverse as the production and quenching of vibrational excitation in different buffer gases [49-54, 75-79], the energy dependence of forward and reverse proton transfer reactions [80] and corresponding enthalpy and entropy changes derived from Arrhenius and van't Hoff plots [75,81-83], the energetics and reaction rates of collision induced dissociation [73,84-87], the mobilities of ions in gas mixtures from Blanc's law [88-92], correlating measured mobilities with ion structure [93], and the separate influences of internal and translational energy on ion-molecule reactions. [49,54,65,66,75,94] Some of these aspects will now be discussed. The following is not intended as a comprehensive review, but rather to give a feel for the versatility of the drift tube technique. Further, for the most part the discussion will focus on work performed after 1984. Extensive reviews of drift tube experiments, of the FDT and SIFDT type, performed prior to 1984, have been published elsewhere. [36,49,50,54,94]

1.7.1 The Determination of Proton Affinity Differences.

Tichy et al [82] measured the forward and reverse rate constants as a function of relative kinetic energy for several proton transfer reactions in a SIFDT apparatus. In all but two cases, van't Hoff plots of the equilibrium constant against reciprocal centre of mass collision energy were linear and it was possible to derive values for the enthalpy and entropy changes for each reaction from the slope and intercept respectively. The measured ΔH values were used to construct a proton affinity difference ladder that was anchored to the absolute proton affinity of Br. The ladder showed excellent agreement with the established PA scale, and the experimental entropy changes were in good accord with values calculated from the entropies of the individual ions and neutrals. The non-linearity of the pseudo-Arrhenius plots obtained for the two measured reactions of N_2OH^+ was attributed to the presence of two N_2OH^+ isomers (N- and O- protonated). [83] It was unclear, however, whether both ions had been injected from the ion source or whether the higher energy collisions of the SIFDT were inducing transitions between the two isomers, which are separated by only 25 ± 5 kJ mol^{-1}. Tichy et al speculated that the derivation of apparently accurate thermodynamic data from the non-thermal drift tube experiments via pseudo van't Hoff plots was due to the fact that such reactions depend only on the total

energy available, and not the individual rotational and vibrational states involved, except as they contribute to making an endoergic reaction exoergic.

1.7.2 Collision induced dissociation (CID) studies.

One of the earliest reported studies of collision induced dissociation in a flow drift tube was that of Dotan et al using the original NOAA FDT apparatus. [95] They measured the dissociation rates for the water cluster ions $H_3O^+.H_2O$ and $H_3O^+(H_2O)_2$ in a helium buffer using Ar, Ne and CO_2 respectively as the collision partner. For both clusters the rates were observed to increase rapidly with ion-collision partner centre-of-mass energy. The $H_3O^+(H_2O)_2$ cluster was observed to dissociate at much lower energies than the $H_3O^+.H_2O$ cluster in accord with its weaker bond. Dotan et al commented however that "while such data do provide some insight into the relative bonds of the dissociating clusters, using them to deduce bond energies or even relative bond energies, must await more knowledge about the speed distributions of the drifting cluster ions". [95] The lack of a detailed theory governing multi-collision CID in a drift tube does not, however, diminish the utility of the technique as a qualitative tool for identifying low energy ion fragmentation pathways and for distinguishing between isomeric ions via differences in fragmentation behaviour. There is also a limited, but growing amount of experimental evidence which suggests that in certain specific instances it may indeed be possible to extract reliable thermodynamic data from such experiments (see discussion below).

Smith et al [73] examined the pseudo-unimolecular decomposition of protonated ethanol, $C_2H_5OH_2^+$, in the Birmingham VT-SIFDT apparatus, measuring dissociation rate coefficients, k_{uni}, as a function of the mean ion-carrier gas centre-of-mass energy, E_c. The individual k_{uni} were determined as follows. For a fixed field strength E and a fixed carrier gas number density N, the length of the drift region (and hence the reaction time for collisional excitation and unimolecular dissociation) was varied by changing the number of rings to which the field was applied (to maintain a constant field strength, E, the drift length and voltage were changed in proportion). A plot of ln (I/I_0) vs reaction length (where I is the parent ion signal and I_0 is the sum of the parent ion and product ion signals) yielded the desired values of k_{uni}. Quantitative modelling of the decomposition was also carried out using RRKM theory, with the assumptions that: (1) the induction

period for attaining steady-state distributions is brief compared to the timescale of the experiment; (2) the translational energy distribution of the primary ions is Maxwellian with a mean energy E_c and that a thermal probability distribution function is appropriate for vibrational energy and angular momentum transfer in collisions between the primary ions and the helium carrier gas atoms. The experimental data indicated that assumption (1) was valid as the plots of ln (I/I_o) yielded linear single-exponential decays with zero intercepts indicating that the internal degrees of freedom of the $C_2H_5OH_2^+$ ions approach steady state rapidly on the timescale of the experiment. If the ions traversed a significant length of the drift region while steady state was attained one would observe apparently reduced rates of dissociation for shorter drift region lengths. The experimental results suggest that assumption (2) is not valid however, since the values of k_{uni} measured at different carrier gas temperatures but at the same value of E_c were not the same. Smith et al concluded, therefore, that the measured rate coefficients do not correspond to thermal rate coefficients at elevated temperatures, T, given by $E_c = \frac{3}{2} k_b T$. [73] They also suggested that in order to obtain an approximation to thermal data from drift tube data, some form of extrapolation of the results to zero field would be required. The best functional form of such an extrapolation is yet to be determined.

Using their SIFDT apparatus the Innsbruck group of Lindinger have had some success in deriving apparently accurate thermodynamic data from CID studies. [84-87] Utilising a similar methodology to that employed by Smith et al [73] described above, they measured the effective bimolecular dissociation rate for the ions Kr_2^+, N_2Ar^+, $(CO)_2^+$, CH_5^+ and $C_2H_5^+$ as a function of E_c in a helium carrier gas. [86] They also reported similar studies on N_4^+ [85] and $CH_3O_2^+$ [84]. Their derived values of Arrhenius activation energies towards dissociation showed excellent agreement with available literature values. Further, by calculating bimolecular dissociation rates from measured thermal termolecular association rates using the van't Hoff equation, and adding these points to their pseudo-Arrhenius plots they showed that the combined thermal and SIFDT data could be fitted, to a very good approximation, by a straight line over at least 15, and in some cases up to 50 orders of magnitude. They took this as an indication that the internal temperature of the drifting ions, T_i, ***was*** fully and quickly equilibrated with the ion-carrier

gas centre of mass energy, i.e. $E_c = \frac{3}{2} k_b T_i$. Departure from linearity in the plots for CH_5^+ at high field and short drift lengths indicated that CH_5^+ ions require a considerably longer time to reach internal equilibration, comparable with the time scale of the experiment (~ 1ms).

In another CID study, Glosik et al were able to distinguish between the isomeric ions H_2COOH^+ and $HC(OH)_2^+$. [84] The two structures produced different branching ratios to HCO^+ and H_3O^+ fragments, which were independent of E_c over the energy range covered. Also, the calculated Arrhenius activation energies for dissociation were different for each structure.

The efficient quenching of $CO^+(v=1)$ by N_2, prompted a SIFDT study of the formation and dissociation of $CO^+.N_2$ ions in a nitrogen carrier gas [87] in order to determine the bond energy of $CO^+.N_2$, since a strong correlation is known to exist between quenching efficiency and the attractive potential or complex bond strength between the respective collision partners. [76] To obtain rates of the processes taking place in the drift tube, the drift tube was divided into two sections, with different values of E/N.

$$CO^+ + N_2 + N_2 \underset{k_2}{\overset{k_3}{\rightleftharpoons}} CO^+.N_2 + N_2 \qquad (1.27)$$

Two specific sets of conditions were employed in order to extract rate values for termolecular association (k_3) and collision-induced dissociation (k_2). With the E/N high in the first section, association was suppressed and only CO^+ ions were present at the beginning of the second section, facilitating determination of k_3 as a function of E/N in the second section. With low E/N in the first section all injected CO^+ ions associate and only $CO^+.N_2$ ions are present at the beginning of the second section, enabling determination of k_2 as a function of E/N in the second section. Appropriate analysis of the data yielded a value for the $CO^+.N_2$ bond energy of 0.7 ± 0.2 eV, which was in fair agreement with an available ab initio value and sufficiently large to rationalise the fast vibrational quenching of $CO^+(v=1)$ by N_2.

Two other innovative uses of CID are also worthy of discussion. Baranov and Bohme have described a technique for utilising a conventional SIFT apparatus for studying collision induced dissociation. [96] By connecting a power supply to their

downstream sampling nose cone they are able to bias the nose cone up to –80 V (positive ion detection). This produces a region of elevated E/N directly in front of the sampling nose cone in which ions can undergo multi-collision CID. While the technique does not yield quantitative thermodynamic data it is an inexpensive method for establishing bond connectivities in reactant and product ions, for distinguishing between isomeric ion structures and for the elucidation of dissociation and reaction mechanisms. For example, the technique clearly distinguishes between the isomeric ions $CH_3NO_2^+$ and CH_3ONO^+, which exhibit quite different dissociation thresholds to NO^+. [97] This multi-collision CID technique is now routinely used in Bohme's laboratory for establishing bond connectivities and distinguishing isomeric ion structures. [98-102] Squires [103] has utilised a mini drift tube for performing "preparative CID", the formation of chemically interesting species not readily generated by conventional ionisation methods. He used the technique to generate a series of carbanions via collisional activation of the corresponding carboxylate ions, viz.

$$RCO_2^- \longrightarrow R^- + CO_2 \qquad \textbf{(1.28)}$$

The instrument described by Squires also utilises a triple quadrupole analyser, which can be used to verify the structure of the CID fragment either via ion-molecule chemistry or further CID with an inert target species. The triple quadrupole can also yield quantitative thermodynamic data as CID can be performed under single collision conditions.

1.7.3 Studies of ion mobility.

The mobility of a gas phase ion is a measure of how rapidly it moves through a buffer gas under the influence of an electric field. It is calculated as the ratio of the drift velocity to the electric field strength as given by equation (1.1). For atomic ions the mobility depends on the electronic state as demonstrated by Rowe et al [104] for O^+, Twiddy et al [105] for C^+ and by van Koppen et al [106] for transition metal ions. For a large polyatomic ion the mobility depends on the average collision cross-section. [93,107,108] An ion with a large average cross-section undergoes more collisions with the buffer gas and travels more slowly than an ion with a smaller average collision cross-section. Mobility measurements can therefore be used to separate ions with different geometries. Ion mobility measurements have been carried out on carbon cluster ions [109-115] and a

correlation has been observed between the structure of the clusters (linear chains, rings and three-dimensional spheres) and the measured mobilities. [116] Similar studies have been performed on silicon [117], germanium[118], aluminium [119] and metal-containing carbon clusters. [120-122] Tremendous interest has focussed recently on the use of ion mobility measurements to examine the conformations of peptides [123] and proteins [124-126] in the gas phase prompting Dugourd et al [127] to develop a new high-resolution ion mobility apparatus to improve resolution of isomeric structures. The drift tube temperature can be varied to study thermally activated isomerisation processes as a function of temperature as was demonstrated for the isomeric clusters of formula $(NaCl)_{35}Cl^-$. [127]

Krishnamurty et al [128] measured the mobilities of a series of ions derived from benzene, naphthalene and biphenyl in a SIFDT apparatus, to examine the possibility of differentiating small structural differences in ions based on their mobilities. The experimentally measured mobilities were compared with those computed (equation 1.29) by obtaining an angle-averaged hard sphere collision cross-section($\overline{\Omega'}$) from the geometric structure of the ions. To a good approximation the mobility of an ion is given by [33,129]:

$$K_o = \frac{3qe}{16N_o}\left[\frac{2\pi}{k_bT}\right]^{1/2}\left[\frac{1}{\mu^{1/2}\Omega^{(1,1)}}\right]$$

$$= \frac{1.85\times10^4}{\Omega^{(1,1)}\sqrt{T_{eff}}}\sqrt{\frac{m+M}{mM}}\ (\mathrm{cm^2\ V^{-1}\ s^{-1}}) \qquad \textbf{(1.29)}$$

where q is the total number of elementary charges, e is the elementary charge, N_o is the standard number density, k_b is the Boltzmann constant, μ is the reduced mass of the ion-buffer gas system, M and m are the buffer gas and ion masses respectively (in amu), T_{eff} is the effective temperature (taken as 273.15 K to obtain a reduced mobility), and $\Omega^{(1,1)}$ is the collision integral (in $Å^2$). The collision integral is approximated by the angle-averaged hard sphere collision cross-section, which is obtained by constructing a space-filled model of the ion using the van der Waals radii of the constituent atoms and averaging the cross-sectional area of the molecular ion over all orientations. The predicted zero-field mobilities were found to compare well with the experimentally determined values. This approach had previously been employed in the cluster ion

studies (see above), and the accuracy of the hard sphere projection approximation has been discussed. [130] More rigorous scattering models have been developed for calculating the gas-phase mobilities of polyatomic ions. [107,130]

1.7.4 Mobilities derived from Blanc's law.

Bierbaum and co-workers have examined the mobilities of cluster ions (e.g. $NO^+(CH_3CN)_n$, $H_3O^+(H_2O)_n$, $NH_4^+(NH_3)_n$, $NO^+(CH_3COCH_3)_n$) drifting in polar gases in a SIFDT apparatus. [89-92] Such cluster ions are among the most abundant species in the lower ionosphere of the Earth. Core ions (e.g. NO^+) are produced in an ion source, mass-selected and injected into the flow tube containing a He or N_2 buffer gas. The reagent gas (e.g. H_2O, CH_3CN) is added to the flow tube just downstream of the ion injector and cluster formation occurs in the remainder of the flow tube. The drift velocity and hence the ion mobility is determined using a pulsed ion-depletion technique, which is discussed in chapter 2 of this thesis. The ion mobility is observed to depend on the concentration of reagent molecules as the ions are drifting in a mixture of buffer gas and reagent molecules. Blanc's law [33,131] gives the measured mobility:

$$\frac{1}{K_{mix}} = \frac{x_b}{K_b} + \frac{x_R}{K_R} \qquad \textbf{(1.30)}$$

where K_b and K_R are the ionic mobilities in the buffer and reagent gases, and x_b and x_R are the mole fractions of the buffer and reagent gas respectively. Separate values of K_b and K_R can be determined from the slope and intercept of a plot of measured mobility versus mole fraction of reactant gas. The mobilities of the cluster ions are found to be much lower in the reagent gases compared to the mobilities in helium. This is a consequence of the much higher polarisabilities and dipole moments of the reagent gases compared to helium, which leads to a much larger momentum-transfer collision integral for the reagent gases and hence a lower mobility. Other factors that may be important include dipole-dipole interactions, ligand exchange reactions and the formation of long-lived quasi-bound complexes. In a helium carrier gas the measured mobilities of cluster ions are quantitatively explained using the hard-sphere collision model described above. The hard-sphere model does not accurately represent the mobility of cluster ions drifting in a nitrogen carrier. As a result of the stronger polarisability of N_2, the hard-sphere

collision model does not agree with the data, and better agreement was obtained using a simple model that included ion-induced dipole interactions.

1.7.5 Insights into reaction mechanisms.

The isomerisation of HCN^+ to HNC^+ in reactions with CO or CO_2 was originally investigated by Petrie et al [132], because of its relevance to the chemistry of the interstellar medium. A "forth and back" proton transfer mechanism was proposed to account for the isomerisation reaction.

$$NCH^+ + CO_2 \longrightarrow (NC\cdots H^+ - CO2) \quad \textbf{(1.31a)}$$

$$(CN\cdots H^+ - CO2) \longrightarrow CNH^+ + CO_2 \quad \textbf{(1.31b)}$$

Within the intermediate collision complex the proton is transferred towards the CO_2 moiety (the proton transfer is exothermic). The collision complex is sufficiently long-lived to enable the rotation of the CN dipole (dipole moment 1.45 D) which favours the $CN\cdots H^+ - CO_2$ orientation. The proton is then transferred back to form the more exothermic CNH^+ product.

As a critical test of this proposed mechanism Hansel et al [133] investigated the reaction of HCN^+ with CO_2 as a function of relative kinetic energy in a SIFDT. Their measured branching ratio as a function of E_r showed that at collision energies close to thermal, the isomerisation channel contributes more than 95% to the overall reaction. As E_r is increased, this contribution decreases to less than 5% at $E_r = 0.7$ eV. Concurrently the production of CO_2H^+ shows an increase from a few percent at room temperature to about 40% at $E_r = 0.7$ eV. The contribution of the endothermic charge transfer product CO_2^+ rises steeply, beginning at approximately 0.2 eV and becoming the dominant product (~55%) at $E_r = 0.7$ eV. These observations are entirely consistent with the mechanism proposed by Petrie et al. [132] At low collision energies the lifetime of the collision complex is sufficiently long to allow rotation of the CN dipole and back transfer of the proton to form CNH^+. At elevated E_r the translational energy converted to internal energy of the collision complex reduces the complex lifetime leading to enhanced production of CO_2H^+. A similar "forth and back" mechanism has been proposed to explain the isomerisation of $R\text{-}CO^+$ (R = H, CH_3) [134,135] and the isomerisation of $CH_3NO_2^+$ to CH_3ONO^+. [97] As an adjunct to their SIFDT study of HCN^+/HNC^+

isomerisation, Hansel et al determined enthalpies of formation for HNC and HNC^+. [136] The rate coefficient for the slightly endothermic reaction of HNC^+ with CO was measured as a function of relative kinetic energy, yielding a value for the endothermicity of equation (1.32) of 31 ± 1 kJ mol^{-1},

$$HNC^+_{(v=0)} + CO \longrightarrow HCO^+ + CN \qquad \textbf{(1.32)}$$

and a value for $\Delta_f H^\circ(HNC^+)$ of 1349 ± 4 kJ mol^{-1}. The heat of formation of HNC was determined similarly by measuring the kinetic energy dependence of the slightly endothermic charge transfer reaction:

$$HNC^+_{(v=0)} + Xe \longrightarrow Xe^+ + HNC \qquad \textbf{(1.33)}$$

The pseudo-Arrhenius plot of ln k versus E_r^{-1} yielded an endothermicity of 0.09 ± 0.01 eV (8.7 ± 1 kJ mol^{-1}) and $\Delta_f H^\circ(HNC)$ = 188.2 ± 4 kJ mol^{-1}.

Glosik et al [137] investigated the reaction of ground state silicon ions, $Si^+(^2P)$ with C_2H_4 over the pressure range from 0.14 to 0.52 Torr, for centre-of-mass energies, E_r, from near thermal to ~ 2 eV. The two observed product ions over the energy range covered were $SiC_2H_3^+$ and $SiC_2H_4^+$. The reaction rate coefficients for the binary (k_2) and ternary (k_3) channels were determined both from the measured branching ratio into products and from the pressure dependence of the effective bimolecular rate coefficient. At $E_r > 0.1$ eV, the termolecular rate coefficient determined from the branching ratio decreased more rapidly with E_r than the termolecular rate coefficient determined from the pressure dependence of the effective bimolecular rate coefficient. This was taken as an indication that in collisions of the helium bath gas atoms with the excited intermediate collision complex, the dissociation of $(SiC_2H_4^+)^*$ to $SiC_2H_3^+$ takes place. This is therefore an example of a ternary reaction having two product channels, collisional stabilisation (product $SiC_2H_4^+$) and collision induced dissociation (product $SiC_2H_3^+$) with probabilities α_1 and α_2, where $\alpha_2 = 1 - \alpha_1$.

1.7.6 Internal Energy Effects.

The effect of reactant ion vibrational excitation on rate coefficients measured in drift tubes has been the subject of many comprehensive discussions [36,49-54,65,66,94] and so only a few salient features will be mentioned here. As discussed previously, molecular ion reactions that are slow typically show a decreasing reactivity with increasing centre of

mass energy within the regime dominated by complex formation. Since vibrational excitation often dramatically enhances the reactivity, the rate coefficients of reactions involving molecular ions often show different E_r dependences in different buffer gases. This is because for a given E_r value the value of E_c and hence the extent of vibrational excitation is different in the different buffer gases (see Figure 1.6). If it is assumed that the observed enhancement in k is due to the vibrational excitation of the ions the total rate coefficient, k_t, can be separated into two components. The first component, k_K, describes the pure kinetic energy dependence and the second component, k_v, describes the influence of internal excitation, which is related to E_c. An Arrhenius treatment of data for the charge transfer reactions of CO_2^+ with O_2 and N_2O^+ with NO, in which ln k_v was plotted

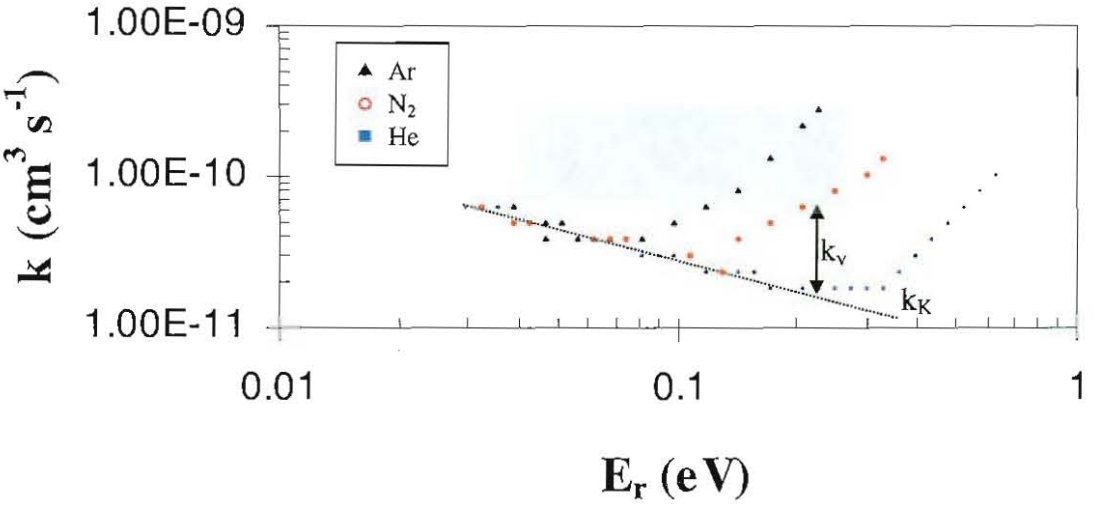

Figure 1.6. Typical energy dependences for a slow reaction of a molecular ion obtained in helium, nitrogen and argon buffer gases. [54] The internal temperature of the ions is changed with E_r to a degree that depends on the particular buffer gas, since the internal temperature is controlled by E_c.

against E_c^{-1} showed that the dependence of k_v on E_c was nearly identical for He and Ar buffer gases. [54]

Viggiano's group in Massachusetts has developed a VT-SIFDT technique for measuring the rate dependence on the neutral reactant internal energy. [65] By measuring rate constants (or branching ratios) as a function of drift field at several carrier gas temperatures, a separate E_r dependence curve is obtained for each temperature. If these curves do not fall on top of one another (Figure 1.7), then at a given E_r the difference between rate constants measured at different temperatures, results from the corresponding different internal temperatures of the reactants (since the kinetic energy of collision is fixed). This method has been the subject of a detailed review [65] and hence only a brief summary of the principal conclusions will be given.

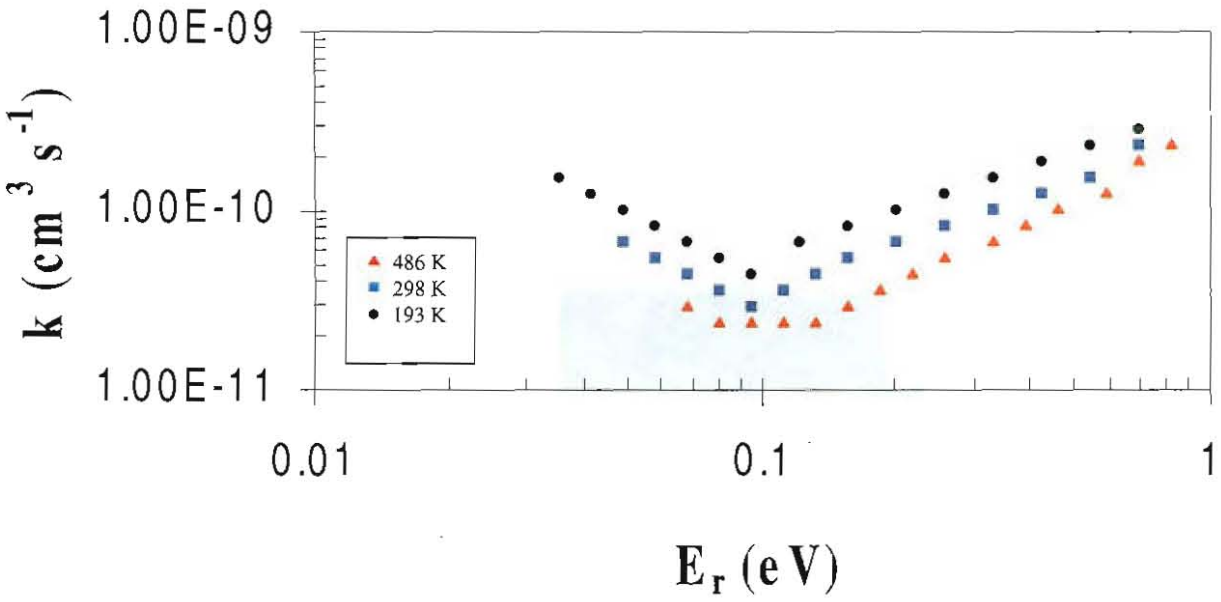

Figure 1.7. Rate constants for a reaction possessing a negative rotational temperature dependence. The three distinct curves describe the E_r dependence at three different buffer gas temperatures. Increased rotational temperature in the neutral reagent leads to a decrease in the reaction rate coefficient. The reaction of Kr^+ with HCl exhibits this kind of behaviour (see text for discussion).

By comparing the influence of neutral reactant rotational temperature on ion-reactivity for a variety of reaction systems, Viggiano and Morris [65] have divided the

results into three general catergories: (1) most reactions, in which rotational energy has little or no influence on reactivity, (2) endothermic reactions, where rotational energy contributes to the total energy used to overcome the reaction endothermicity, and (3) reactants with large rotational constants, where rotational excitation is observed to measurably affect the reaction kinetics (Figure 1.7). An example of a reaction in category (2) is the endothermic charge transfer reaction between Ar^+ and N_2 (this reaction is discussed further in chapter 2):

$$Ar^+(^2P_{3/2}) + N_2 \longrightarrow N_2^+ (v = 1) + Ar - 0.092 \text{ eV} \qquad \textbf{(1.34)}$$

The E_r dependences of the rate of reaction (1.34) were measured at 298, 428, and 552 K. The three E_r dependence curves do not coincide with one another at low E_r but begin to merge at higher energies. This lack of coincidence between the curves must indicate the rate dependence on N_2 rotational excitation, since Ar^+ cannot be internally excited and vibrational levels of N_2 are not accessible at the temperatures of the experiment. The pure temperature dependence of the rate yielded an activation energy of 0.07 eV in good agreement with the reaction endothermicity. Further, a plot of the rate data versus the average total energy illustrates that the three distinct E_r dependence curves collapse into a single curve, which is dependent on the average total energy only, independent of the type of energy (kinetic or rotational). This implies that rotational and translational energy are equally efficient at promoting reaction by supplying energy to overcome the reaction endothermicity. This conclusion is believed to be generally applicable to endothermic reactions.

An example of a reaction with a large rotational effect (category (3)) is the charge transfer reaction (1.35):

$$Kr^+(^2P_{3/2}) + HCl \longrightarrow HCl^+ + Kr + 1.25 \text{ eV} \qquad \textbf{(1.35)}$$

The E_r dependences measured at three different temperatures [138] do not coincide with one another, but define three distinct curves separated by more than the relative error bars. Increased rotational temperature leads to a decrease in the reaction rate coefficient. The effect found for DCl as the reactant neutral was similar to that observed for HCl. The observed rotational effect was attributed to: (1) the rotational dependence of the capture rate constant and (2) the fact that the charge transfer is facilitated by a collinear geometry,

as the rotational temperature of the HCl reactant temperature increases the dipole "locks" to the positive charge less efficiently.

As remarked above, the preceding review is by no means exhaustive or definitive, but is intended to give a flavour for the utility of the flow drift tube techniques and an introduction to some of the literature covering this area.

The ensuing chapters detail experimental and theoretical work performed during the period from January 1994 to June 1998. The experiments are a combination of SIFT and SIFDT studies. Some of the experimental work is of relevance to the chemistry of the interstellar medium, and where appropriate, the implications of the experimental results to interstellar chemistry will be discussed.

Chapter Two describes the experimental apparatus and modifications to the apparatus.

Chapter Three discusses three ion-molecule association reactions, $H_3O^+ + C_2H_2$, $H_3O^+ + C_2H_4$ and $CH_2NH_2^+ + HCOOH$ which have all been suggested to play roles in the chemistry of the interstellar medium. Efforts to identify the isomeric ions formed in each of the association reactions are described.

Chapter Four further explores methods for distinguishing isomeric ions based on differing ion-molecule reactivities. SIFT experiments are used to distinguish isomers in the well-studied $C_6H_5^+$, $C_7H_7^+$ and $C_3H_5^+$ systems.

Chapter Five examines the role of kinetic barriers in H-atom abstraction reactions. The exothermic reaction $SO_2^+ + H_2 \longrightarrow SO_2H^+ + H$ is explored both experimentally in the SIFDT apparatus and theoretically via ab initio calculations and it is demonstrated that the reaction possesses a kinetic barrier in the entrance channel.

Chapter Six describes SIFDT studies of termolecular association and the competition between bimolecular and termolecular reaction channels. The specific systems examined are CH_3^+ with C_2N_2 and CH_3CN and NO^+ with acetone, butanone and 3-pentanone.

Chapter Seven summarises the present work and offers suggestions for further work to expand the scope of the present studies.

CHAPTER 2.

EXPERIMENTAL

2.1 Equipment.

The experiments reported herein were obtained in part using the selected ion flow tube originally constructed in this department from 1982-1985, and in part using a newly constructed SIFT instrument possessing a flowing afterglow ion source. Previous workers in this laboratory have described most of the essential features of the original apparatus. [18,139-141]

Petrie [140] has described the modification of the original instrument, which included a co-linear ion source, to an off-axis ion source arrangement, and the development of a new high-pressure ion source. Wilson [18] discusses modifications to the particle multiplier assembly, the use of upstream facing ring inlets to replace the original finger inlets, and modifications to the electronics and software used for data analysis. He also describes structural modifications performed in preparation for the installation of a drift tube into the apparatus; I will return to a discussion of these modifications shortly. Scott [141] has given a detailed description of modifications to the apparatus, ancillary equipment and software performed during the course of the research described herein. Any further discussion will therefore focus only on modifications not discussed by Scott or those of particular pertinence to the present work.

In 1996 construction commenced on framework and chassis sections for a new SIFT apparatus and in the latter half of 1997 the ion-molecule laboratory was relocated within the Chemistry Department to share laboratory space with the ion cyclotron resonance spectrometer. The principal modifications to the apparatus were the incorporation of a flowing afterglow ion source, the addition of a new dual annulus Venturi orifice and greatly improved pumping of the upstream and downstream quadrupole chambers. Much of the experimental data presented herein was obtained using the new instrument. To differentiate between the two apparatuses I will utilise the

terms SIFT or SIFDT for the original apparatus and FA-SIFT or FA-SIFDT for the new apparatus, where appropriate, in the following chapters describing experimental results. A full description of the essential features of the new FA-SIFDT apparatus follows. I will first discuss however, the installation of the drift tube into the original SIFT apparatus.

2.2 Drift tube operation.

2.2.1 Preparations for drift tube operation.

The requirement to float the downstream end of the drift tube and the entire mass spectrometer detection region to high potential necessitated modifications to the construction of the downstream end of the SIFT apparatus. These modifications were performed prior to the commencement of the research described herein. [18] Since the nose cone is floated to high potential it was necessary to insulate the nose cone from the surrounding flanges using acetyl gaskets. A vacuum tight seal between the gaskets and stainless steel flanges was achieved using O-rings. Thin teflon sheets were also subsequently placed between the nose cone and the cradle supporting the T section at the downstream end of the SIFT to ensure good electrical insulation from chassis ground. A schematic diagram of the downstream region of the SIFT showing the acetyl insulators appears on page 31 of Wilson's thesis. [18] The anticipated installation of the drift tube also prompted the replacement of the existing finger inlets for introduction of neutral reagents into the flow tube by ring-type inlets. The upstream-facing ring inlet (Figure 2.1) incorporates a section of pyrex tubing which insulates the metal inlet from the flange which attaches to the flow tube chassis, and facilitates electrical connection of the inlet to the drift ring the inlet is inserted through. Another advantage of the ring-type inlet is the reduced end correction required for rate coefficient determinations relative to the end correction for the finger-type inlets. [142] Problems with the use of finger type inlets in a SIFDT apparatus have been discussed before. [138]

2.2.2 The drift tube.

The drift tube (Figure 2.2), resistor board and power supply were all constructed in the mechanical and electronics workshops of the University of Canterbury Chemistry Department prior to the commencement of the research described herein. The drift tube

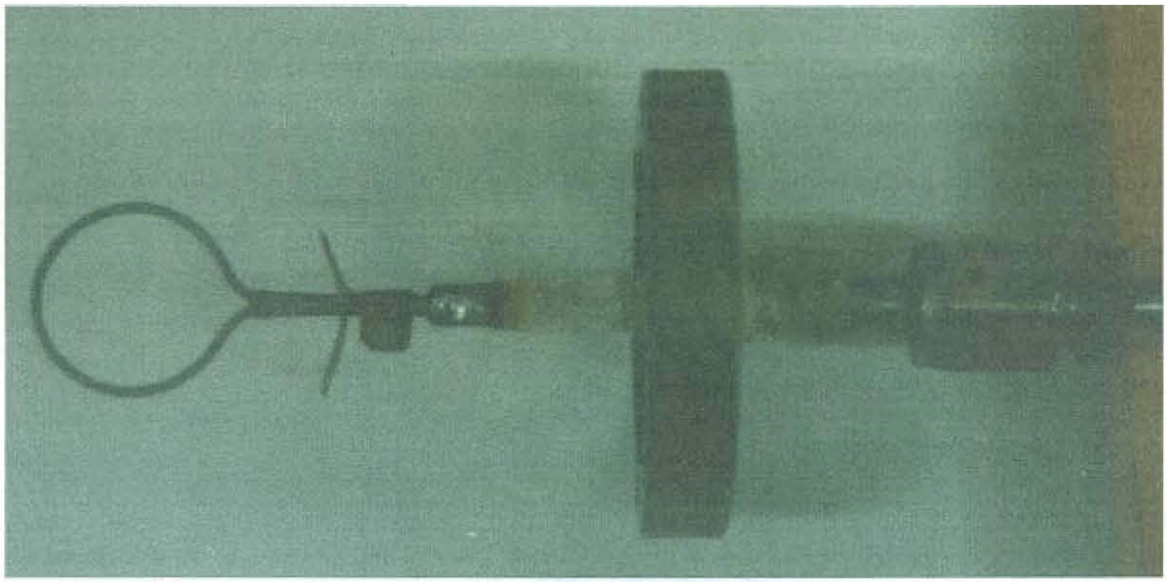

Figure 2.1. Photograph of the ring inlet used for neutral addition to the SIFDT.

is similar in design to that developed by Smith and Adams for use in their VT-SIFT instrument at Birmingham. [21] It consists of 50 stainless steel rings of 60.3 mm i.d. and 9 mm width held 1mm apart by ceramic insulators. The drift tube is inserted directly into the existing flow tube (i.d. = 73.2 mm). As a consequence of the resulting reduction in tube diameter, the drift tube assembly also incorporates a 17 cm field-free extension to the drift section to ensure that the carrier gas flow is settled to laminar prior to the drift field reaction region. The field free extension is electrically connected to the flow tube by a flexible stainless steel earthing clip. The end of the drift tube was positioned 0.5 cm from the molybdenum sampling disc on the downstream nose cone in the SIFDT apparatus and is 1.5 cm from the molybdenum disc in the new FA-SIFDT apparatus. The ring inlet is inserted through the eighth ring from the upstream end through a 2.5 mm wide slot in the ring and is electrically connected to the ring with a brass clip. Insertion of the atom inlets [141] into the SIFDT necessitated the cutting of a ~ 2 cm circular hole in

the seventh, eight and ninth drift rings. A separate tinned copper wire insulated in a fibreglass sheath connects each ring to the male half of a 50 pin D-type connector. The female half is connected in turn to a hermetically sealed multiple connector sealed in a plate that connects to a flange at the downstream end of the flow tube. The wires are arranged on the connectors in such a way that the voltage difference between adjacent pins is minimised. The drift tube resistor board connects to the multiple connector externally.

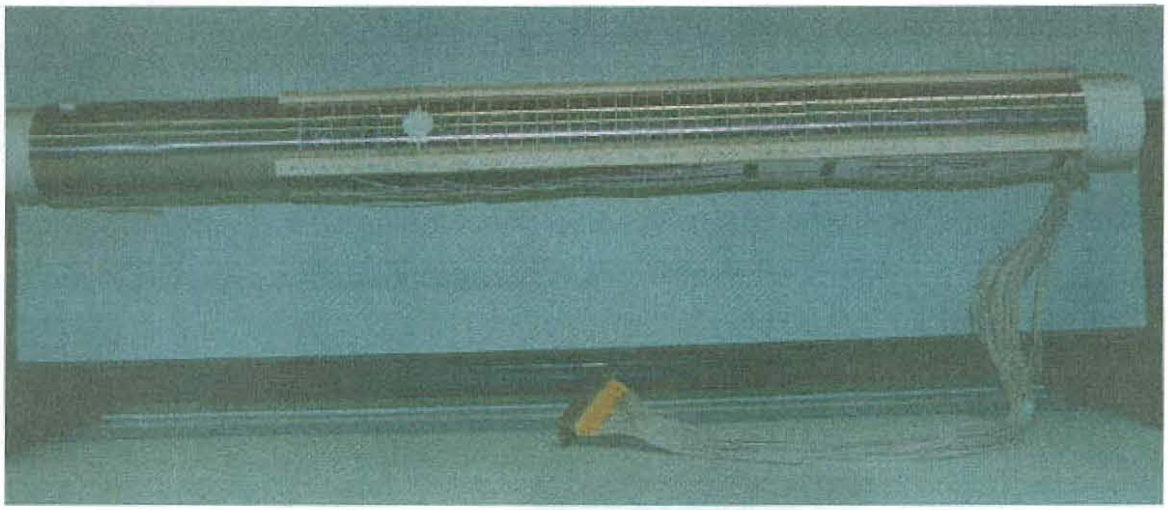

Figure 2.2. Photograph of the drift tube assembly.

2.2.3 Electronics.

A uniform electric field is established along the axis of the drift tube by applying a voltage to the end of a chain of fifty 100 kΩ resistors which terminates to ground. There is a 39 kΩ resistor between each 100 kΩ resistor and a drift ring (although it has subsequently been realised that the 39 kΩ resistors are redundant and serve no useful purpose in the circuit). Modulating voltage pulses are capacitively coupled to a selected ring through a .22 μF capacitor, and the two adjacent rings are capacitively coupled to ground via .01 μF capacitors (to prevent the effect of a voltage pulse being too large on those rings). This circuit is illustrated in Figure 2.3.

The (current-limited) drift tube power supply and pulsing circuitry are contained in a single unit. The drift tube voltage is adjustable from ± 0 – 600 V (negative for

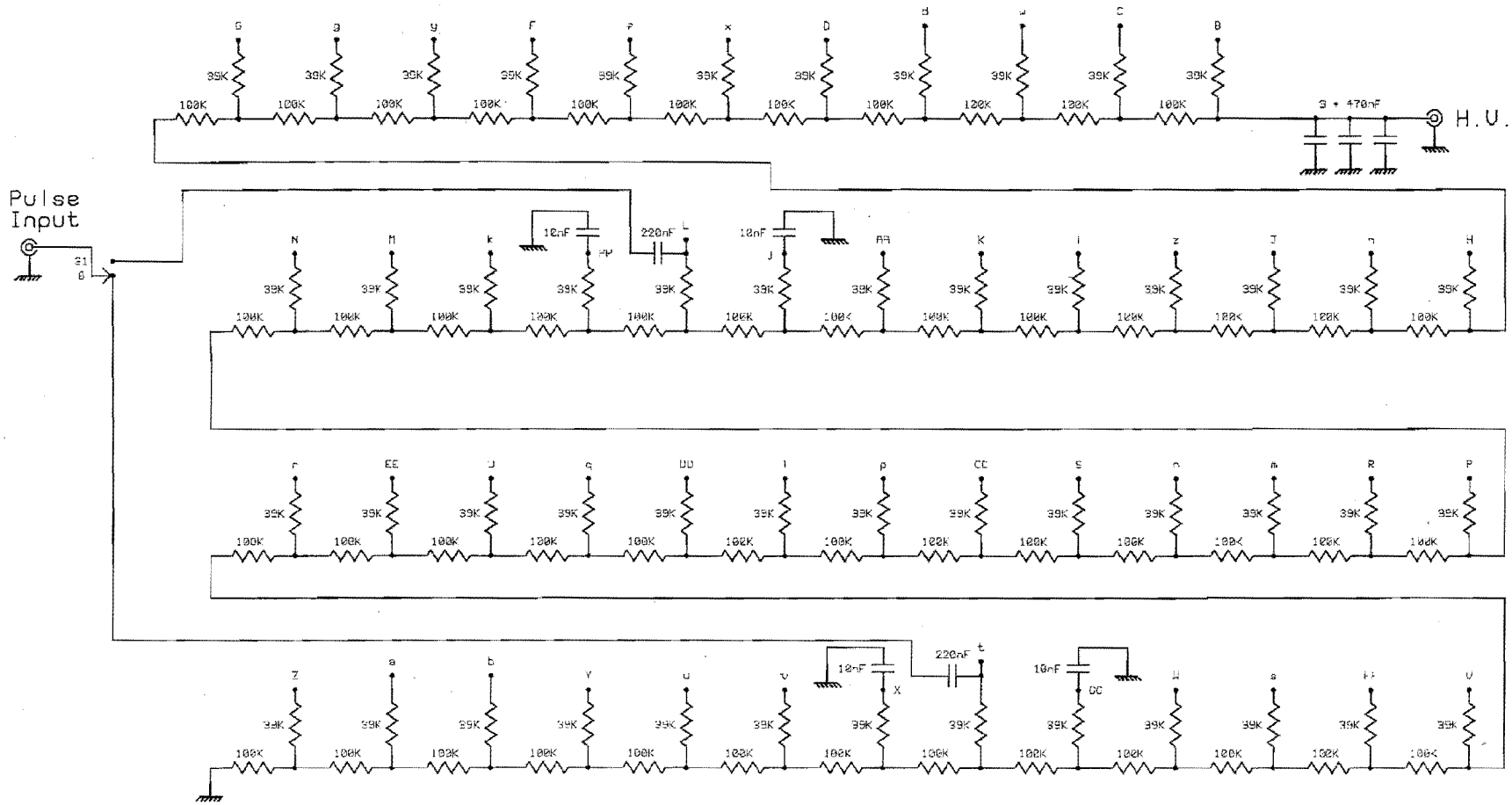

Figure 2.3. The drift tube resistor chain circuit.

positive ions and vice versa), although in practice the maximum voltage which can be applied before breakdown is ~ 400 V. Output pulses for modulating the ion signal during mobility measurements are adjustable from 0 –50 V, the pulse polarity is again adjustable from positive to negative. The pulse duration is adjustable from 1 – 20 μs and the pulse repetition rate can be set between 0.1 – 100 ms. A digital voltmeter attached to the unit is used to monitor the magnitude of the drift tube voltage or output pulse height. The power supply/pulse circuit unit also contains +200 V and –200 V power supplies which power the six adjustable supplies to the downstream ion optics. The drift tube voltage acts as the common reference for the downstream ion optics (i.e. the downstream lenses float relative to the voltage applied to the furthest downstream drift ring). The drift tube voltage is also connected to the CKT COMM (circuit common) terminal on the downstream quadrupole controller in order to float the quadrupole axis voltage relative to the drift tube. Adjustment of the zero potentiometer at the rear of the quadrupole controller adjusts the dc pole potentials symmetrically about the axis with respect to the CKT COMM terminal and has a range of about ± 8 Vdc. Both the upstream and downstream quadrupole controllers are normally operated with this setting adjusted full negative (for positive ion detection). With the shorting link between CKT COMM and GND removed, a potential of up to ± 400 Vdc can be applied to the circuit common. When operating the apparatus as a conventional SIFT a shorting link is placed between the CKT COMM and the GND (ground) terminal on the quadrupole controller.

In the original VT-SIFDT designed by Smith and Adams [21] the channeltron multiplier was electrically decoupled from the drift tube potential (i.e. the multiplier voltage was not floated relative to the drift tube). For reasons discussed more fully below it was decided to float the particle multiplier in the present system. This necessitated connecting the drift tube voltage to the + H.V. terminal on the triax flange for the particle multiplier and the floating ground of the Spellman Model RHR5PN30/FG/220 high voltage power supply which provides the high voltage for the particle multiplier. This arrangement greatly enhanced the level of noise appearing at the pulse counter. The problem was attributed to ripple from the drift tube power supply coupling to the signal input of the pulse preamplifier via the + H.V. terminal. A partial remedy was achieved by

connecting the drift tube voltage to the multiplier + H.V. terminal through a wire wound round a ferrite toroid in an alloy box with four large coupling capacitors (~ 0.5 μF) to ground. Even with this arrangement it was necessary to set the preamplifier discriminator to a higher level than would be necessary for conventional SIFT operation. Again, under conventional SIFT operation the floating ground of the Spellman high voltage supply should be tied to chassis ground. A block diagram of the drift tube electronics is illustrated in Figure 2.4.

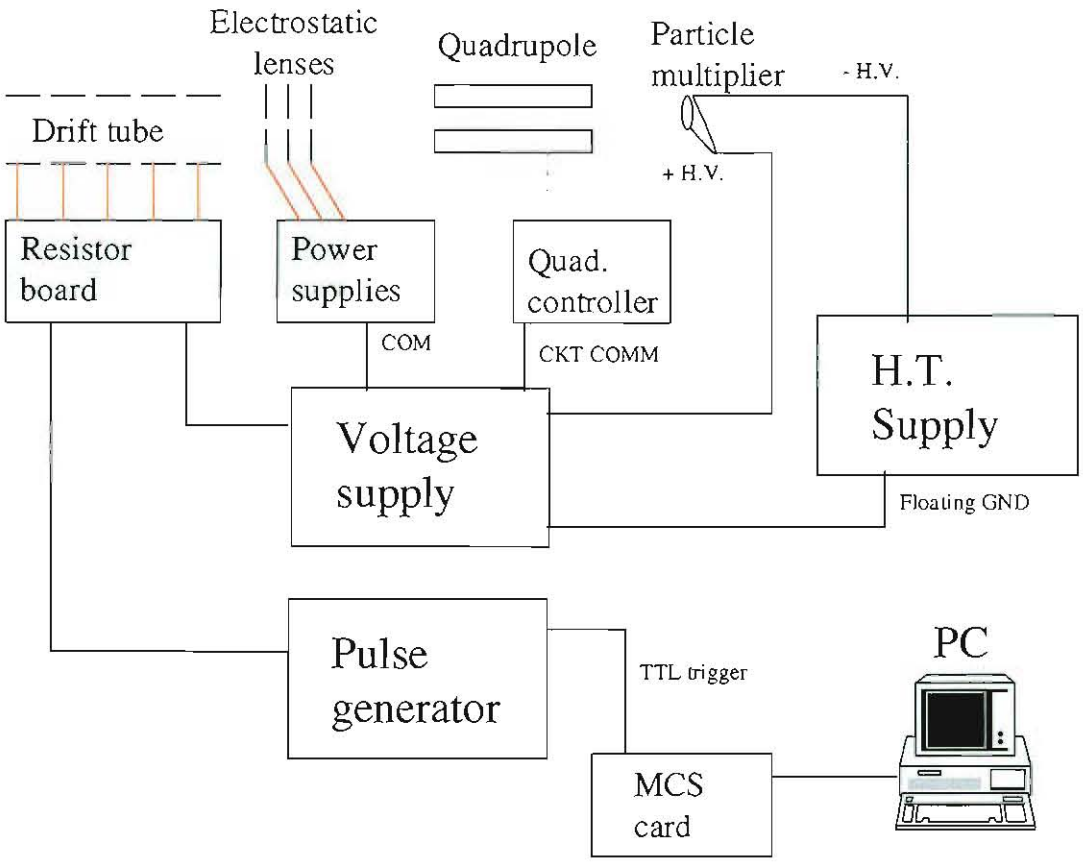

Figure 2.4. Block diagram of the drift tube and associated electronics.

2.2.4 Anomalous behaviour with drift tube voltage.

It became quickly apparent when an ion swarm was introduced into the drift tube and the voltage was increased, that the variation in ion signal with voltage did not behave as intuitively expected for normal drift tube operation. As the voltage is increased the

corresponding increase in ion velocity reduces the time spent by the ion in the flow tube. Thus the loss by diffusion diminishes and the ion signal increases. Ultimately the ion signal registered by the particle multiplier should plateau at a value limited by the total injected ion current and the size of the sampling orifice in the downstream nose cone. Instead, as the drift tube voltage was increased, the signal rose to a maximum and then began to decrease rapidly again. Typically the ion signal would increase up to ~ 150 V and then decrease, falling to a value equal to, or even less than, the zero field signal at ~ 300 V. Various theories were posited to explain this behaviour and were tested experimentally. The various explanations and the experimental test employed to confirm or contradict the explanation are given in Table 2.1. Two critical pieces of observational evidence narrowed down the search for the problem. Firstly, the fall off in ion signal was independent of the drift length and appeared to be a function of the drift tube voltage only. Secondly, it was possible, at least in part, to restore the ion signal by re-optimising the nose cone and molybdenum disc voltages, suggesting that the problem lay in the region immediately in front of the nose cone (in the vicinity of the last few drift rings). It was not until the drift tube was installed into the new FA-SIFT apparatus that this problem was satisfactorily addressed (see the discussion below). One major study (that of the SO_2^+/H_2 reaction described in chapter 5) was, however, carried out using the original SIFDT apparatus.

2.3 FA-SIFDT apparatus.

In 1996 construction began on the framework for a new FA-SIFT apparatus (Figure 2.5), in laboratory space adjoining that containing the Canterbury ion cyclotron resonance spectrometer. The principal motivation behind the upgrade was to significantly enhance injected ion signals and to improve the ion transmission and resolution of both the upstream and downstream quadrupoles with improved pumping. Many of the design features are similar to those developed by the Boulder group of Bierbaum and DePuy described by Van Doren et al. [143] Two other groups had constructed such an instrument previously, Smith and Adams [144] at Birmingham, and Bohme's group at York. [145] The

principal differences between the original Canterbury SIFT and the new FA-SIFT are outlined in Table 2.2. A general discussion of aspects of the new apparatus follows.

Theory	Experimental Test
Hole cut for atom inlet causing anomalous electric field in vicinity of neutral inlet.	Establish field over rings downstream of neutral inlet. The problem was still present.
Ion optics element or quad axis voltage not floating correctly.	Check that lens and quad axis voltages vary with drift tube voltage as expected.
Ion signal loss consequence of particle multiplier not floating.	Float particle multiplier.
End plate on particle multiplier housing not floating.	Remove end plate.
Anomalous field in region of the first lens (top hat/spring lens) behind the molybdenum disc, or charging of macor disc.	Wrap spring in gauze mesh to ensure uniform field; replace top hat lens with solid cylindrical lens and move closer to molybdenum disc.
Centre of drift tube not aligned with the orifice in the molybdenum disc.	Check alignment with laser and adjust position of flow tube relative to the nose cone.
Does behaviour depend on field length or drift tube voltage only?	Vary length of field free region and drift region.
Can refocusing the downstream ion optics (at least in part) restore the ion signal?	Re-optimise the focusing of the downstream ion optics.
Some other element charging up or not floating.	Carefully inspected quadrupole, nose cone and multiplier assemblies for evidence.

Table 2.1. Theories posited to explain the anomalous variation of ion signal with drift tube voltage and the experiment performed to test the theory.

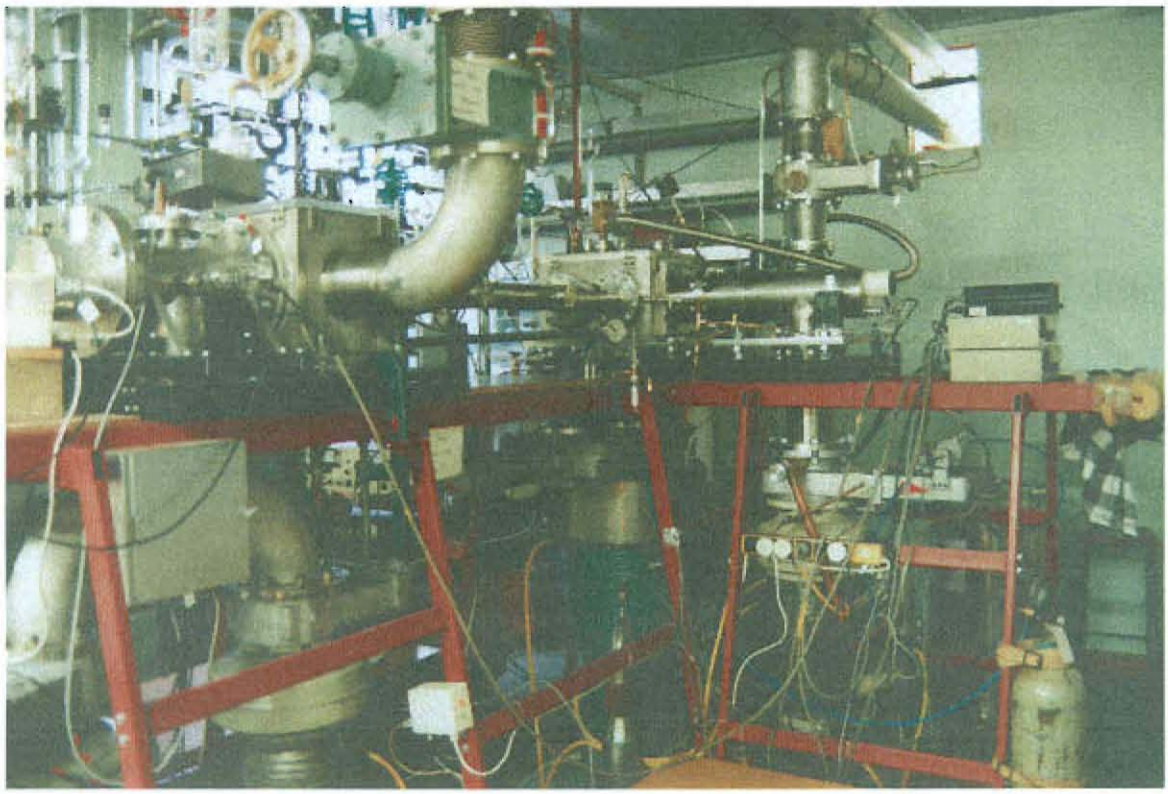

Figure 2.5. Photograph of the FA-SIFT apparatus at the University of Canterbury.

2.3.1 Flowing afterglow source.

The flowing afterglow source (Figure 2.7) consists of a 20.5 cm long stainless steel flow tube (4.76 cm i.d.) press-fitted inside a "T"-section which is stud-mounted on the upstream SIFT chamber. The flowing afterglow can be extended by up to 45 cm with flanged 15 cm lengths of 5.08 cm o.d., 4.76 cm i.d. stainless steel tubing. The tube at the downstream end extends to within ~ 46 mm of the plane of the nose cone orifice. The carrier gas flow is pumped through a 15 cm diameter pumping line by an Edwards EH 1200 mechanical booster pump backed by an Edwards E2M 80 double stage high vacuum backing pump. This combination has an effective pumping speed of 840 $m^3 h^{-1}$ at 0.3 mbar (air). The source is isolated from the pumping line by a 10 cm Temescal gate valve. The Roots blower and backing pump are isolated from the pumping line by a 15 cm pneumatic gate valve. A bellows by-pass connects the source to the upstream chamber and is opened during pump-down of the system. The flow tube is equipped with a pressure-measuring port connected to a MKS 122AA-00010AB 10 Torr capacitance

manometer. One of the removable sections has three trigonally arranged inlets for introduction of carrier gas into the FA. Two other stationary inlets (one in the same removable section and the other very close to the nose cone orifice) can be used for introducing neutral reagents into the carrier flow. The source also possesses a movable 40mm i.d. ring inlet, containing 10 evenly spaced holes in the upstream face for uniform reagent addition, which can traverse nearly the entire length of the flow tube (see Figure 2.8). The design details of the FA source and details of other aspects of the modified FA/SIFDT apparatus will be discussed by D.B. Milligan in his thesis.[‡]

SIFT apparatus	FA-SIFT apparatus
High-pressure electron impact ion source.	Flowing afterglow ion source with faciltity to form ions by electron impact or microwave discharge.
Upstream chamber and quadrupole pumped by single 4" diffusion pump.	Upstream chamber pumped by 10" diffusion pump; quadrupole differentially pumped by a separate 6" diffusion pump.
Venturi inlet with single annulus for introduction of carrier gas.	Venturi inlet with inner and outer annuli for introduction of carrier gas.
Downstream chamber and quadrupole pumped by single 4" diffusion pump.	Downstream chamber pumped by dual 4" diffusion pumps.
Downstream nose cone diameter = 4 ½".	Improved pumping of downstream nose cone – diameter = 6".
Ion optics as described in refs 140 and 141.	New upstream and downstream ion optics (see discussion below).

Table 2.2. A summary of differences between the Canterbury SIFT and FA-SIFT.

[‡] Milligan, D.B., Ph.D. Thesis, University of Canterbury, New Zealand, to be submitted.

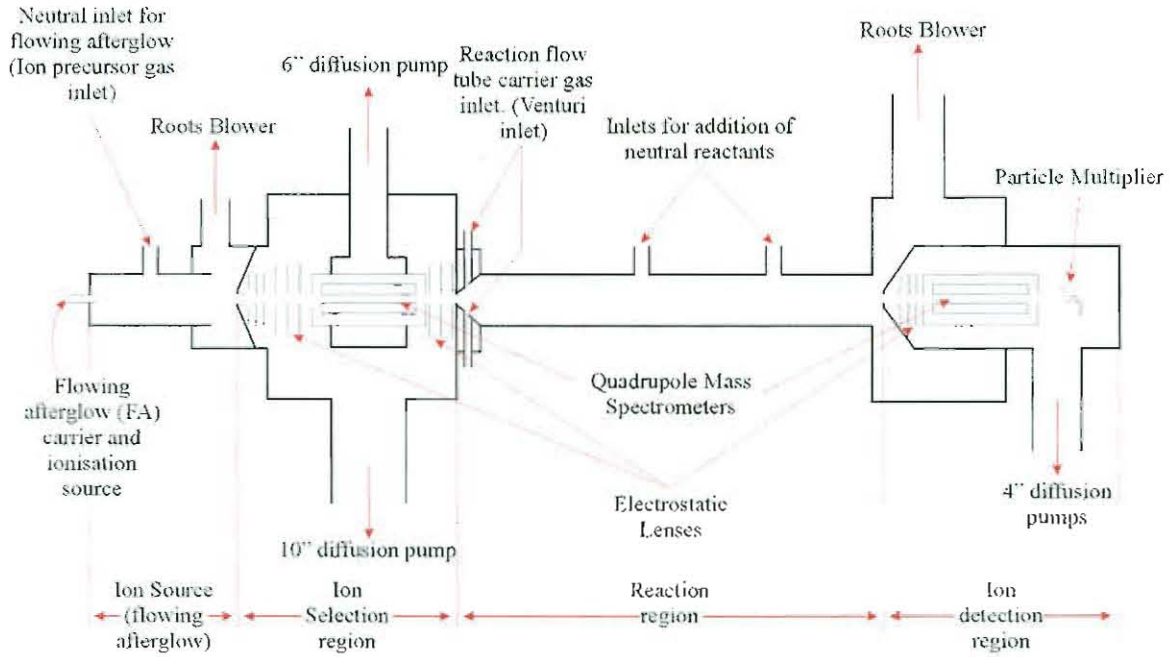

Figure 2.6. Schematic diagram of the flowing afterglow-selected ion flow tube (FA-SIFT) at the University of Canterbury.

2.3.2 Ionisation techniques.

At present, ions can be formed in the flowing afterglow either by microwave discharge (which generates He^+ ions and metastable excited helium atoms, $He(2\,^3S)$, when He is the carrier gas) or electron impact. There are also plans to construct a hollow cathode source to test its performance relative to the two other ionisation sources. The electron impact ioniser consists of a rhenium ribbon (~ 0.6 mm wide, ~ 180 μm thick) spot-welded between two tungsten electrodes approximately 15 mm apart and an extracting grid (maintained at ground potential) and is mounted on a movable tube which can traverse the entire length of the flow tube (Figure 2.8). The filament is typically operated at an emission current of ~ 1 mA. The filament is biased typically at –75 V with respect to ground. It should be noted that operation of the electron impact ioniser for extended periods, particularly when hydrocarbon precursor neutrals are used, rapidly contaminates the flowing afterglow sampling nose cone (i.e. within one to two weeks). This necessitates more regular cleaning of the nose cone compared to the use of the microwave discharge source.

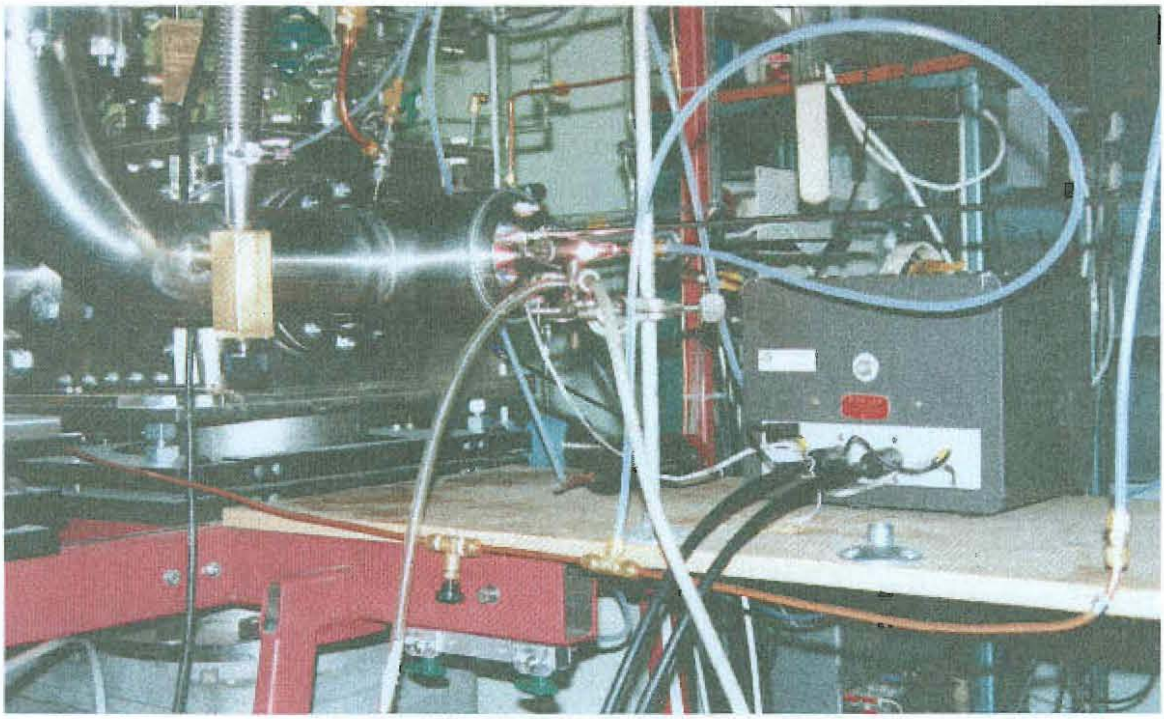

Figure 2.7. Photograph of the flowing afterglow source. A coaxial microwave discharge source is in use with the pink glow of a helium discharge clearly visible.

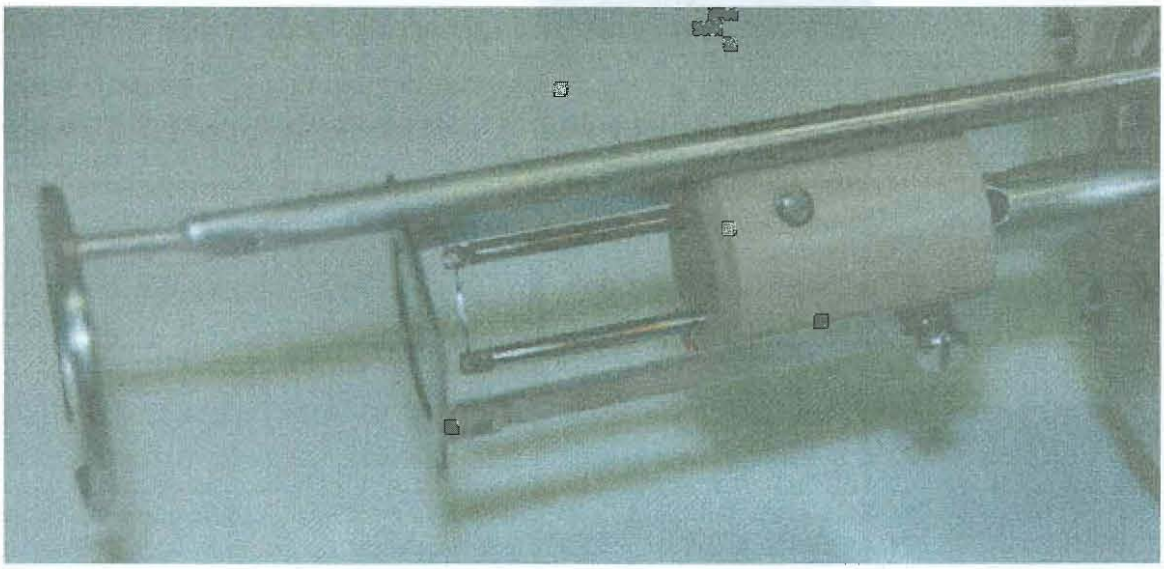

Figure 2.8. Photograph of the movable ioniser and ring inlet.

The microwave discharge cavity and power generator are the same as described by Scott [141] and used in his investigations of ion-atom reaction chemistry. The operating details are also identical to those described previously. Two discharge tubes have been

constructed: one a linear section of 12 mm o.d., 9 mm i.d. pyrex tubing and the second similar in design to the generic atom probe described by Scott [141] featuring a right angle bend and Wood's horn, again made of pyrex. The expense of incorporating quartz sections into the discharge tubes was deemed unnecessary as the microwave cavity can be operated around a pyrex tube without any problems provided a sufficient flow of cooling air is used to cool the cavity. When using the linear discharge tube it has been noted that photons from the discharge can traverse the upstream quadrupole and enter the flow tube through the Venturi orifice. This causes a small, but measurable amount of ionisation of of impurities in the carrier gas. One must therefore be careful to ensure that ion signals ascribed to reaction products do not in fact originate from this photo-ionisation. The presence of photo-ionisation in the reaction tube can be readily established by maintaining the source discharge while gating the injected ion signal, either by de-tuning the upstream quadrupole or switching the polarity on an upstream ion optics element to retard the ion signal. Any remaining signal detected at the downstream end must originate from photo-ionisation. Typically, the buffer gas pressure in the flowing afterglow is maintained between 0.2 – 1 Torr. At 0.5 Torr the flow velocity is ~ 8500 cm s^{-1}.

2.3.3 SIFT chamber, ion optics and quadrupole.

Ions are sampled into the upstream chamber through a 2 mm diameter orifice in a 24mm diameter molybdenum disc on a stainless steel nose cone (cone angle = 134°). The disc is electrically connected to the nose cone. A seal between the disc and nose cone is provided by a teflon gasket. The potential applied to the nose cone (and disc) determines the energy of the ions in the laboratory frame, since the ions exit the flowing afterglow at the potential of the nose cone and enter the flow reactor tube at ground potential. This voltage can be typically maintained at +20 – 25 V (for positive ion injection, provided the nose cone is clean) and is sufficiently low to inject most ions without significant collision-induced dissociation upon injection into a helium carrier. It is planned to float the Venturi orifice which should enable lower injection energies to be achieved, facilitating injection of, for example, weakly bound cluster ions such as $H_3O^+(H_2O)_n$, which cannot be injected without some dissociation at present. The nose cone voltage is

provided by a 10mA variable 100 V power supply; the current rating of the supply is necessary to prevent "loading" of the supply by the large ion currents (typically 1 mA) impinging on the flowing afterglow nose cone. Upon entering the SIFT chamber (Figure 2.9) the ions are focussed by a series of six electrostatic lenses (assembled on the back of the nose cone plate) into the upstream quadrupole (Extrel model 7-270-9). The quadrupole assembly also incorporates mounting plates at either end, which are used as additional focussing lenses. These two lenses are electrically connected to each other. The quadrupole case is also floated. Three further electrostatic lenses (an Einzel lens arrangement) focus ions exiting the quadrupole into a newly constructed dual annulus-type Venturi inlet.

Both the upstream and downstream ion optics were modeled using the SIMION 6.0 program [146] to ensure sensible focussing conditions could be achieved prior to settling on a final design for the ion optics. The first element of the upstream entrance lens system is a conically shaped extractor with a 4 mm diameter aperture (41 mm total diameter, 12.7 mm from apex to back plate) axially aligned with the nose cone orifice and located ~ 2 mm behind the orifice. The next two lenses are flat plate ring electrodes (25.4 mm i.d., 41 mm o.d.). The first three lenses are equi-spaced from one another and the next lens set by ~ 2 cm. The next three lens elements of the entrance lens system are also flat plate electrodes (16 mm i.d., 71 mm o.d., containing multiple 3 mm holes for optimal pumping) equi-spaced from one another and the upstream quadrupole by ~ 1.2 cm. The exit lenses from the upstream quadrupole are identical to the last three elements of the entrance lens system and are spaced ~ 22 mm apart, with the distance from the quadrupole end plate to the first of these lenses being 13.5 mm. The details of the quadrupole and its operation have been described previously by Scott. [141]

A 25.4 cm oil diffusion pump (Varian VHS-400, pumping speed 8000 L s^{-1} for air) backed by a Leybold-Heraeus Trivac® D65B backing pump (pumping speed 65 m^3 h^{-1} [‡]) pumps the upstream chamber. The pressure inside the SIFT chamber is measured by a HPS 421 cold cathode gauge and micro-controller. The quadrupole chamber is differentially pumped by a 15 cm oil diffusion pump (Varian VHS-6, pumping speed

[‡] Mean value of pumping speed between 1 bar and 133 mbar at an operating frequency of 50 Hz.

2400 L s^{-1} for air) backed by a Leybold-Heraeus Trivac® D30A backing pump (pumping speed 30 m^3 h^{-1}‡). The pressure in the quadrupole chamber is measured by a Varian Ratiomatic 843 vacuum ionisation gauge controller connected to a Duniway I-075-K ion gauge. Typically the pressure is a factor of ten lower in the quadrupole chamber than in the SIFT chamber and absolute pressures of ~ 9 x 10^{-8} Torr have been achieved in the quadrupole chamber with prolonged pumping.

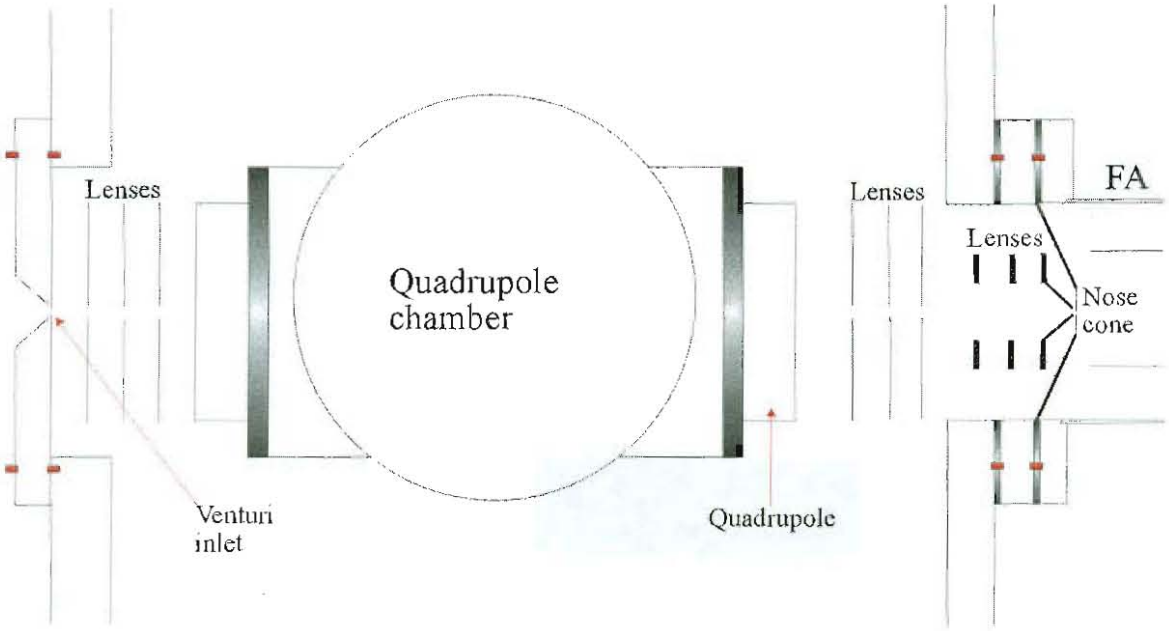

Figure 2.9. Schematic diagram of the SIFT chamber.

2.3.4 Venturi and flow tube.

The Venturi inlet possesses two annular slits for introduction of the carrier gas into the flow reactor tube. The essential features necessary for efficient performance of a Venturi have been discussed in detail elsewhere. [143,147] The stainless steel injector flange is 15.2 cm in diameter and 2.2 cm thick. The walls of the assembled injector slope away at 45° from the 2 mm diameter ion injection orifice. The carrier gas is directed to each annulus through separate radial channels. The inner annulus is 0.0025 cm wide and has an internal diameter of 0.87 cm. The outer annulus is 0.04 cm wide and has an internal diameter of 3.71 cm. The width of the inner annulus is such that positioning is critical

‡ Mean value of pumping speed between 1 bar and 133 mbar at an operating frequency of 50 Hz.

and difficult to optimise. Positioning is achieved by passing a small flow of argon through the annulus, squirting petroleum ether (acetone is unsuitable as it chemically attacks O-rings) at the orifice and adjusting the position of the annulus to achieve a symmetrical flow pattern (visualised by observing the flow of liquid). The proportion of gas admitted through each annulus can be varied by adjustment of a Nupro SS-VCR-4-VH needle valve, which controls the flow of carrier gas to the outer annulus. Experiments in which an ion signal was observed whilst adjusting the needle valve from fully closed to fully open indicate that the adjustment of the valve has little effect on the transmitted ion signal. The flow reactor tube present in the FA-SIFT apparatus is the same one used in the previous SIFT instrument. [141]

2.3.5 Carrier gas flow system.

The essential features of the carrier gas flow system are identical to those described by Scott. [141] The presence of the flowing afterglow source necessitates the requirement to introduce carrier gases individually into the flowing afterglow source region and the flow reactor tube. Helium (or hydrogen) to the flowing afterglow source is admitted via a MKS model 1179A14CS1BV-SPCAL mass flow controller, which is calibrated for helium and has a maximum flow rate of 10000 sccm. Helium to the flow reactor tube is measured by a Tylan FC 261 flowmeter connected to its own dedicated power supply and readout. [141] Other carrier gases (e.g. argon, nitrogen) are measured using a MKS 1179A14CS1BV mass flow controller, calibrated for nitrogen (10000 sccm max.). The two MKS flow controllers are connected to a MKS Type 247C 4-channel readout. The gas handling line is plumbed in such a way that different carrier gases can be admitted to the FA and flow reactor tube as required. A new molecular sieve trap was constructed to facilitate separate purification of FA and flow reactor tube carrier gases.

2.3.6 Neutral Reagent Addition.

The departmental glassblowers constructed a new glass gas handling line, which maintains all of the essential features of the handling line described previously. [18,140] Of the three available neutral inlets to the flow tube, the middle inlet is now dedicated to trace gas analysis measurements, however the first upstream inlet can be used for

performing ion-molecule chemistry in the flow tube. The inlet closest to the downstream end is the inlet routinely used for rate determinations. The uncorrected reaction distance for this inlet was 42.9 cm in the original SIFT apparatus and is now 43.9 cm in the new FA-SIFDT apparatus. An end correction of +1.8 cm is appropriate for the ring inlet used for rate coefficient measurements. The flow rate of a neutral species is monitored either by measuring the pressure drop from a calibrated volume or directly using one of two commercial flow controllers. The first is a MKS model 1259C calibrated for nitrogen with a maximum flow rate of 10sccm and the second is a model 1179A also calibrated for N_2 with a maximum throughput of 100sccm. Use of the model 1259C is recommended for measuring rate coefficients down to ~ 10^{-10} cm^3 $molecule^{-1}$ s^{-1}. When measuring smaller rate coefficients, use of the larger throughput controller is recommended. Both mass flow controllers are connected to a MKS Type 247C 4-channel readout and can be controlled manually (with the set point source switch set to "FLOW" on the 4-channel readout, or automatically via the PC (with the set point source switch set to "EXT"). Since there are only two D/A output channels available on the PC Labcard, one of which controls the downstream quadrupole, the set point inputs to channels 1 and 2 of the 4-channel readout are tied together. The 10 sccm flow controller is selected by picking flow gauge 1 in the ***"Measurement"*** window of the SIFT for Windows program and the 100 sccm flow controller is selected by picking flow gauge 3. Flow gauge 2 is selected when measuring neutral flows via a pressure drop from the calibrated volumes.

The channels of the Advantech PCL-812 PG Labcard and their associated inputs and outputs are listed in Table 2.3.

2.3.7 The ion detection region.

Following convection along the flow tube, the ions are sampled through a small orifice in a molybdenum disc at the apex of a 15 cm, 126° stainless steel nose cone. The ions are focussed by three electrostatic lens elements into the downstream quadrupole which has been described previously. [141]

The first lens element is a conical extractor (3 mm aperture, situated < 0.5 mm behind the molybdenum disc) similar to that used behind the flowing afterglow nose cone. The second and third elements are top-hat lenses. The nose cone and

quadrupole are differentially pumped by two 10 cm oil diffusion pumps (Varian model VHS-4, pumping speed 1200 L s^{-1} for air) each backed by a Welch Scientific Company

Channel	Input/Output
Connector 1 (CN1) – Analog Input	
A/D 0	-
A/D 1	-
A/D 2	Output of the 10 sccm reactant gas flow controller.
A/D 3	Output of the 10 Torr Baratron (flow reactor tube).
A/D 4	Output of the flow reactor tube carrier gas flowmeter (Tylan).
A/D 5	Output of the 100 sccm reactant gas flow controller.
A/D 6	Output of the downstream pressure transducer (Validyne DP15-20).
A/D 7	Output of the LM 335 temperature sensitive diode.[a]
A/D 8	Drift tube voltage.
A/D 9	Output of the 10 Torr Baratron (FA source).
Connector 2 (CN2) – Analog Output	
D/A 1	Set point input to the reactant gas flow controllers.
D/A 2	Mass input of the downstream quadrupole mass spectrometer.
Connector 5 (CN5) – Counter	
CLK[b]	TTL pulse output of the preamplifier/discriminator.

Table 2.3. Input and output channels used on the Advantech PCL 812-PG Labcard.

Duo-Seal vacuum pump. Ion currents reaching the molybdenum disc can be measured either with a Keithley 602 solid-state electrometer [141] or a newly constructed picoammeter, based on a design suggested by Dr Patrik Spanel. [148] The ions are detected by a particle multiplier (De-Tech Model 203 for most of the work described herein). Current pulses from the particle multiplier are capacitively coupled to a preamplifier/discriminator, which outputs TTL level pulses. The output TTL level signal is fed to a PC Lab Card [141] and a pulse counter/ratemeter circuit. [18] The preamplifier used

[a] Laboratory temperature is linearly proportional to output voltage, e.g. 2.98 V = 25°C. Output changes by 0.01 V/degree and is calibrated via a screwdriver adjustable potentiometer.

for most of the work contained herein was locally built based on a circuit from the Extranuclear 032-3 preamp counting head and generated TTL output pulses 0.2 μs wide. This has recently been replaced by an Advanced Research Instruments F-100T preamplifier/discriminator V6. The timing capacitor in the F-100T has been replaced by a 22 pF capacitor which sets the output pulse width at ~ 30 ns. The F-100T is used with 50 ohm termination to prevent ringing with consequent double counting. The chassis of the preamp requires good electrical grounding to the flow tube chassis to ensure noise-free operation. The preamp is powered by the same ± 15 V power supply used for the previous preamp.

2.4 Data Acquisition and Analysis.

For the most part, the details of data acquisition and analysis appropriate to the present work have been discussed previously by Scott. [141] A further update of the SIFT for Windows program (v 2.5) was supplied by Dr Patrik Spanel during a visit to the department in December 1997. A brief overview of the essential features of the program follows, with an emphasis on the features of the upgraded version of the program.

2.4.1 File menu.

This menu contains self-explanatory options for opening and saving data files as well as dumping data to a printer or copying the decay and branching ratio graphs to the Windows clipboard. Data files are saved with a *.sde extension.

2.4.2 Data menu.

The Data menu contains options for commencing data acquisition, editing experimental data, changing experimental parameters, and scrolling through data sets. It is worth noting that one of the editable experimental parameters is the reaction time. This option is useful for drift tube experiments where the ion velocity and hence the reaction time are measured in separate experiments (see section 2.5.1).

2.4.3 Calculations menu.

This menu contains two options, ***Add Model*** and ***Log Results***. The ***Add Model*** option can be used to fit a double exponential function to a curved decay. Although this

---

[b] Clock input for the 8253 counter.

is not an iterative, computer controlled procedure (and must be done by trial and error), it is quite useful for establishing approximate reaction rates and isomeric ratios. The ***Log Results*** option writes the experimental data table to a file (*.txt) that can be imported into a spreadsheet for further analysis if required.

2.4.4 Mass Spec Menu.

The Mass Spec menu contains two options, ***Mass Prog*** and ***Scan***. The ***Mass Prog*** option opens the mass programmer window, where ion masses to be recorded during an experimental measurement are entered. A mass program file can be saved for later use with a *.mpr extension. The mass scan window can be opened from the mass programmer by selecting the ***Scan*** option. Calibration of the mass range can be performed using the ***Calib*** option. One enters the observed masses of two peaks corresponding to two unequivocally known ions, preferably well separated in mass, e.g. Ar^+ at m/z = 40 and SF_5^+ at m/z = 127, plus the exact masses of the ions. The program scales the entire mass range (0-200 amu) in such a way that Ar^+ appears at exactly 40 amu and SF_5^+ at exactly 127 amu.

The ***Scan*** option opens the mass spectrum window, which is used to obtain a mass spectrum over any desired mass range at a pre-selected scan rate. Mass spectrum files are saved with a *.mse extension. The mass spectrum window has a separate menu for manipulating mass spectrum files. The File menu contains options for opening, saving and printing *.mse files, as well as copying the files to the Windows clipboard for use in other applications. The Graph menu is used to adjust the vertical and horizontal scales as required and to switch the vertical scale between linear and logarithmic. The Mass Spec menu contains options to start and stop mass spectral scans, switch to the mass programmer window, add a comment to the mass spectrum and smooth the peaks if required. The ***Analyse*** option can be used to give an instantaneous readout of relative peak height ratios, the exact masses where peaks appear and, in the case of a trace gas analysis measurement, the concentration of a pre-selected trace component (in ppb or ppm). Options for peak analysis are selected in the Options menu. The ***Analysis*** sub-menu gives options for peak analysis, e.g. ***Splitting*** adjusts the minimum relative well between peaks and ***Sensitivity*** is used to select the minimum signal to be counted as a

peak in the analysis. The ***Select Molecules*** option is used to select the molecules that will be accounted for in a trace gas analysis spectrum. The molecules are tabulated in a database file H3OP.TXT, which lists the names of the molecules plus the precursor ions, reaction rates and product ions appropriate to a particular trace species. The ***Edit MS*** option performs a similar task to the Calib option in the mass programmer window, i.e. it scales the mass spectrum relative to two pre-selected calibration peaks.

Another useful tool in the Mass Spectrum window is the ability to zoom in on a section of a mass spectrum by clicking and dragging the cursor around the section of interest.

2.5 Installation of the drift tube into the FA-SIFT.

When the drift tube was first installed into the FA-SIFT and tested, electrical breakdown was observed to occur at ~ 160 V at a helium pressure of ~ 0.35 Torr. The breakdown was evidenced by the appearance of large signals (> 10^5 c.p.s. in some cases) of "air ions" (e.g. N^+, O^+, OH^+, H_2O^+, N_2^+ and O_2^+) as a result of ionisation of impurities in the helium carrier by the glow discharge. In addition, a sudden enhancement in the injected ion signal (Ar^+) was observed following the voltage breakdown. The drift tube and nose cone power supplies became visibly "loaded" by this sudden increase in ion current. The Ar^+ signal was also observed to track sensibly with drift tube voltage following the breakdown, although the signal declined to a much lower level at zero field than that observed prior to the breakdown. In an effort to observe directly what was occurring inside the apparatus, a perspex lid was machined and fitted to the downstream chamber. A glow discharge was readily observed in the region surrounding the nose cone at the onset of breakdown. Electrical breakdown was occurring in two places: between the pins of the internal D-connector and the chassis of the downstream chamber and between the nose cone itself and the vacuum chamber. The first of these problems was remedied simply by wrapping the D-connector in a plastic bag and the second problem was addressed by sleeving the nose cone with a split length of 15 cm i.d. PVC tubing. It should be noted that at ~ 0.38 Torr and 300V, electrical breakdown will still occur in the region of the last three or four drift rings. Higher values of E/N are still achievable,

however, by lowering the flow tube pressure. In order to establish whether the observed enhancement in the injected Ar^+ ion signal following breakdown was due to ionisation of an Ar impurity in the helium carrier or due to some other phenomenon, CF_3^+ (formed from CF_4 in the ion source) was injected into the flow reactor tube. A similar enhancement in the m/z = 69 signal was observed following the onset of electrical breakdown, although no source of m/z = 69, other than the injected ion signal, was present in the helium carrier. As discussed in section 2.2.4 the most persistent problem following installation of the drift tube was the failure of the ion signal to track with the increase in drift tube voltage. At voltages above ~ 150 V the signal decreased noticeably. The observed enhancement in injected CF_3^+ ion signal following electrical breakdown suggested that the observed decline in ion signal prior to breakdown was due to some form of surface charging phenomenon, which was retarding the ion signal. This signal decline could be compensated for in part by refocusing the nose cone and molybdenum disc (see section 2.2.4). Almost certainly the problem was due to the fibreglass sheathing around the wires to each ring impinging slightly into the region immediately in front of the nose cone. When the wires and their insulation were repositioned well away from the internal surface of the last drift ring, a significant improvement in the tracking of the ion signal with drift voltage was observed. Presumably the external surface of the fibreglass was charging and therefore perturbing the ion signal in the region in front of the nose cone. This would explain the observed ability to, in part, refocus the ion signal via adjustment of the nose cone and molybdenum disc voltages, and the observed influence of the plasma generated by electrical breakdown on an injected ion signal.

2.5.1 Ion mobility measurements.

Ion arrival times are measured using the so-called dual-pulse depletion technique. Two drift rings of known separation (one near the beginning of the drift region and one near the end) are pulsed with a short duration ($\leq$ 20 μs, rise time ~ 100 ns) +50 V pulse. The voltage pulses cause a transient depletion of the ion density. The rings can be pulsed individually in separate measurements or simultaneously in the same experiment. The upstream ring pulsed was invariably the ring through which the neutral ring inlet was inserted. The effect of the voltage pulse being spread over the ring inlet is to cause a

larger perturbation to the ion density thereby reducing the time to measure an arrival time distribution. For this reason the second pulse was often applied to the molybdenum disc on the sampling nose cone. An EG & G Ortec ACE™ MCS multi-channel scaler card and associated software [149] was used to measure the ion signal as a function of time and record the arrival times of the "dips" in the ion density. The difference in the arrival times of the two depletion signals gives a measure of the time for the ions to traverse the distance between the two rings that are pulsed. The advantage of the dual-pulse depletion technique is that the residence time of ions in the detection region does not influence the arrival time measurements. The differences in arrival times are determined as a value Δt between the minima of the two depletion signals. The mobility at a given field, E, is obtained using equation (1.1), where the drift velocity, v_d, is the difference between the ion velocity measured at E and the measured ion velocity at zero field, viz:

$$v_d = \left(\frac{\Delta l}{\Delta t_E} - \frac{\Delta l}{\Delta t_0} \right) \qquad \textbf{(2.1)}$$

Δl is the distance between the two pulsed rings and Δt_E and Δt_0 are the arrival times at an applied field E and at zero field, respectively. For most ions in a helium carrier, the contribution to the total ion velocity from the bulk flow of the carrier gas, i.e. $\frac{\Delta l}{\Delta t_0}$, will be equal to 1.5 v_g (within ~ 10%), where v_g is the carrier gas velocity. A typical arrival time distribution is illustrated in Figure 2.10.

For measurement of an arrival time distribution, the pulse output of the preamplifier/discriminator is connected to the *Data In* cable of the multichannel scaler (MCS) card. A TTL pulse from the pulse generator unit is connected to the *Start In* cable of the MCS and triggers the MCS to start counting when a drift ring is pulsed. Data collection is initiated by opening the MCS program and adjusting the preset values of dwell time, number of channels and number of passes. The minimum dwell time per channel is 2 μs and is used for most measurements. The number of channels selected should be sufficient to ensure both ion depletion signals are observed, whilst keeping the total time in all channels less than the pulse repetition rate (1-2 ms was found to be sufficient "recovery time" between data acquisition into all channels and the next pulse).

Once a suitable arrival time distribution has been collected, data collection can be stopped and the data is copied into the PC buffer, where it can be smoothed if necessary and the data can be saved to file. Note that the arrival time distribution is displayed "live" on screen only for dwell times >10μs, but the screen can be updated with a keystroke for

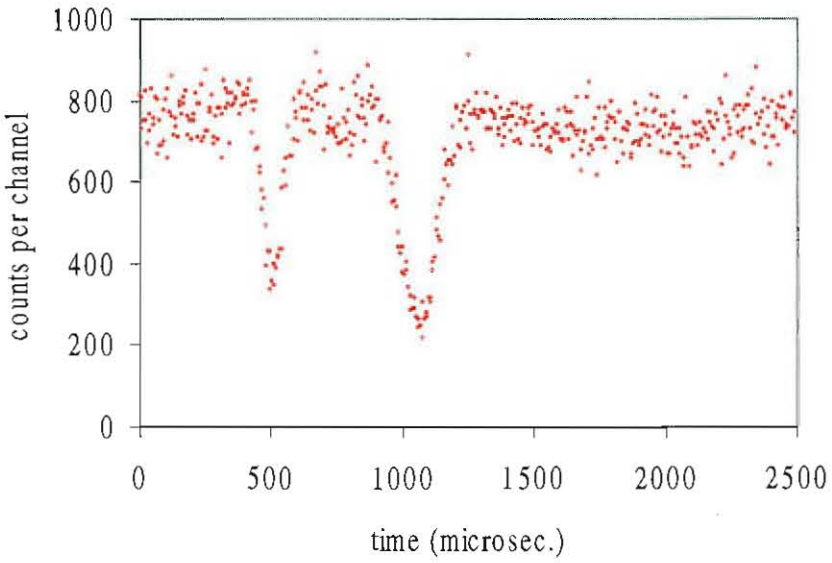

Figure 2.10. Arrival time distribution for CO_2^+ measured at 300 K, a helium carrier gas pressure of 0.35 Torr and an electric field of 0.5 V/cm. The distance between the two pulsed rings is 24 cm and the difference in arrival times for the two depletion signals is 580 μs.

times <10 μs. A program MCSREAD (see Appendix I) was written in QuickBASIC to enable the data to be written to a text file that can be imported, for example, into Microsoft Excel for further manipulation. The program DAFPROG (written in Borland Pascal, see Appendix I) takes the measured arrival times as input and outputs values of reduced mobility, E_r and E_c to a file SIFDT.TXT.

2.5.2 Early results.

The performance of the drift tube was assessed by selecting a simple, well-studied reaction for a test comparison. The reaction selected was the charge transfer reaction between Ar^+ and N_2, which has been examined by several workers using drift tubes,[149-154] and also at various temperatures using a VT-SIFT. [155] Interested readers are referred to

the compilation of Anicich [156] and reference 154 for a bibliography of experimental measurements of this well-studied reaction. The mobility of Ar^+ in He has been measured as a function of E/N at room temperature by Lindinger and Albritton [157] and more recently by Viehland et al. [47]

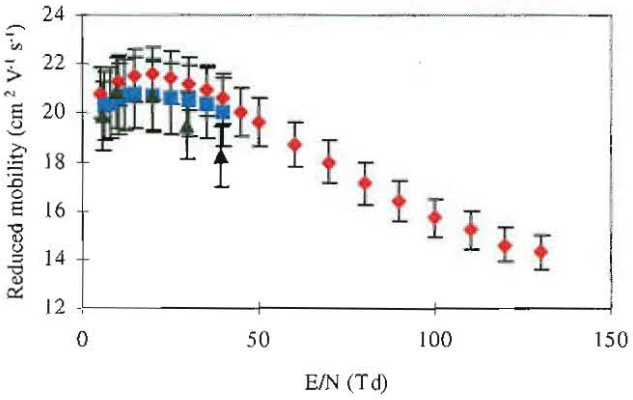

Figure 2.11. Reduced mobility of Ar^+ in He as a function of E/N. Data points are from ref. 157 (◆), ref. 47 (■) and the present work (▲).

$$Ar^+ + N_2 \longrightarrow N_2^+ + Ar \qquad \textbf{(2.2)}$$

The rate coefficient has been shown to increase continuously from ~1 x 10^{-11} cm^3 s^{-1} at room temperature to ~ 6 x 10^{-10} cm^3 s^{-1} at E_r = 2 eV, typical of an endoergic reaction. Hence the reaction does not proceed via the exoergic channel:

$$Ar^+ + N_2 \longrightarrow N_2^+ (X, v = 0) + Ar + 0.18\ eV \qquad \textbf{(2.3)}$$

but rather via the slightly endoergic channel:

$$Ar^+ + N_2 \longrightarrow N_2^+ (X, v = 1) + Ar - 0.09\ eV \qquad \textbf{(2.4)}$$

Calculation of the expected room temperature rate coefficient for reaction (2.4), assuming Arrhenius behaviour, i.e.

$$k = k_c \exp\left(\frac{-\Delta E}{kT}\right) \qquad \textbf{(2.5)}$$

where ΔE is the reaction endoergicity and k_c the Langevin capture rate, yields a room

temperature rate coefficient of 1.7 x 10^{-11} cm^3 s^{-1} in fair agreement with the value measured in the present work (1.2 x 10^{-11} cm^3 s^{-1}), which is in excellent agreement with previous measurements performed at room temperature [150,153-155]. Proof that reaction (2.4) dominates over reaction (2.3) was provided by Smith and Adams [155] when it was

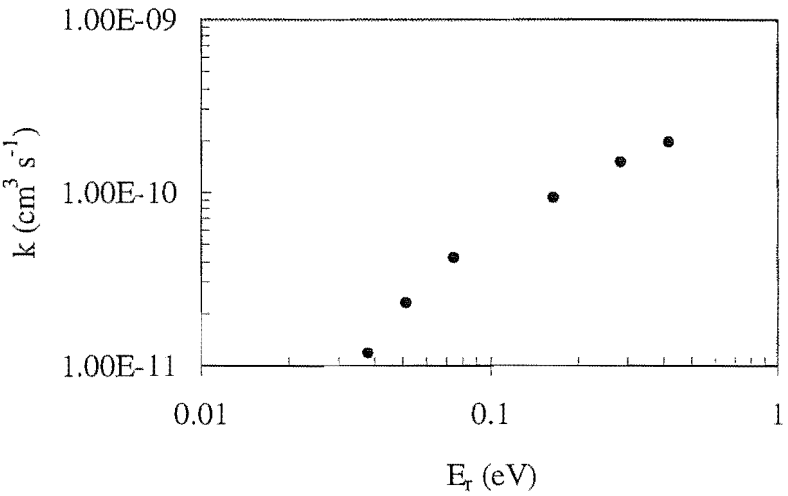

Figure 2.12. Variation in the rate coefficient, k, for the reaction $Ar^+ + N_2$ with E_r.

shown that the product N_2^+ reacted rapidly with the Ar, which meant that the N_2^+ was vibrationally excited. Measurements at lower temperatures performed using a VT-SIFT indicated that the rate coefficient did not continuously decrease with decreasing temperature, but that a minimum occurred in k. The product ion was solely $N_2^+(X, v = 0)$ at 80 K and thus the reaction path changes from reaction (2.4) at room temperature and above to reaction (2.3) at considerably lower temperatures. The reduced mobility of Ar^+ (calculated using equations (2.1), (1.1) and (1.2)) in helium as a function of E/N is given in figure 2.11, with the values of Lindinger and Albritton [157] and Viehland et al [47] shown for comparison. The measured rate coefficient for reaction (2.2) as a function of ion-neutral centre of mass energy, E_r, is depicted in figure 2.12. The measured values show good agreement with the values of Lindinger et al [151], Viggiano et al [154] and Hamdan et al [153] within the experimental uncertainty.

2.5.3 Qualitative CID Studies.

Some qualitative measurements of multi-collision induced dissociation (CID) were performed to illustrate the usefulness of the drift tube in this regard. The hydrated hydronium ions, $H_3O^+(H_2O)_n$ (n = 1,2), were formed by injecting H_3O^+ from a high pressure ion source containing H_2O into the flow reactor tube and adding water vapour to the carrier flow at the upstream neutral inlet. The ion signals were recorded as a function of drift tube voltage with the drift field applied over the last 10 cm of the drift tube (rings

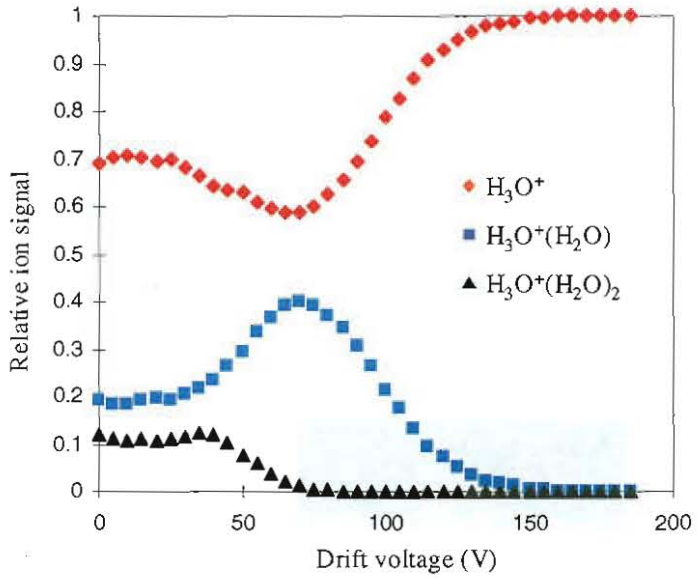

Figure 2.13. Multi-collision CID results for $H_3O^+(H_2O)_n$ (n = 1,2), generated by injecting H_3O^+ and adding H_2O vapour at the first neutral inlet. The graph plots the ratio of each ion signal to the total observed signal versus drift voltage for a drift length of 10 cm and a He pressure of 0.35 Torr.

1 - 40 were shorted to ground) at a helium pressure of 0.35 Torr. Figure 2.13 shows the relative ion signals as a function of drift voltage. The doubly hydrated adduct $H_3O^+(H_2O)_2$, clearly has a lower dissociation threshold than the monohydrated adduct, in accord with the established bond dissociation energies of H_3O^+-(H_2O) and $(H_2O)H_3O^+$-(H_2O) and in good qualitative agreement with the results of Baranov and Bohme [96] who examined the same system using their SIFT-CID technique. Quantitative

bond dissociation energies cannot be extracted directly from data in this form.[‡] The use of this technique as a qualitative tool for structure elucidation and for the elucidation of dissociation and reaction mechanisms is, however, self-evident. Similar measurements were performed on the solvated cluster ions $C_2H_5OH_2^+(C_2H_5OH)_n$, with n = 0 – 2 (see Figure 2.14). Again dissociation occurs via consecutive losses of a single solvent molecule and the observed thresholds are consistent with the known order of bond energies. Note that both H_3O^+ and $C_2H_5^+$ fragments were observed from $C_2H_5OH_2^+$ in accord with the earlier study by Smith et al. [73] The $C_2H_5^+$ fragment ion appears as a relatively minor channel and is not recorded in Figure 2.14.

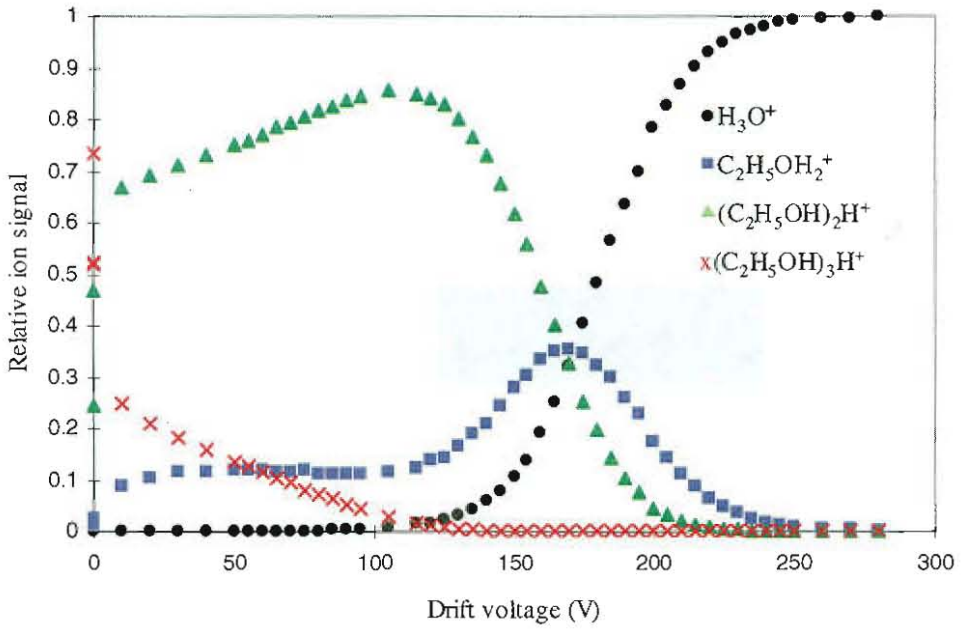

Figure 2.14. Multi-collision CID results for $(C_2H_5OH)_nH^+$ (n = 1,2,3), formed by injecting $HCNH^+$ and adding ethanol at the first neutral inlet. The graph plots each ion signal as a fraction of the total observed ion signal versus drift tube voltage for a drift length of 20 cm and a He pressure of 0.35 Torr.

[‡] Methods for determining thermodynamic quantities from CID experiments are discussed in chapter 1.7.

2.6 Ab initio calculations.

As an adjunct to experimental work described herein, theoretical calculations were performed on many of the systems studied to assist in the interpretation of the data. The theoretical procedure employed is the Gaussian-2 procedure (G2 theory) [158], an extension of the earlier Gaussian-1 (G1) theory [159], which is based on ab initio molecular orbital theory. Both procedures have been extensively described in the original papers and so will not discussed here. Some of the calculations presented herein were performed at the G2 (MP2) level of theory [160] which is a less computationally expensive method than G2 theory. The average absolute deviation of the G2 (MP2) theory from experiment is 6.61 kJ mol^{-1} (compared to 5.06 kJ mol^{-1} for G2 theory), based on the test set of 125 atomic and molecular systems used for validation of the G2 theory. [160]

2.7 Reagents and Physical Conditions.

Reagents used are as described previously [141] with the following exceptions. Acetaldehyde, CH_3CHO (99.5%), was obtained from BDH, and was additionally purified by vacuum distillation. Oxirane (ethylene oxide) was obtained from BDH. Dimethoxymethane, $(CH_3O)_2CH_2$ (99%) was obtained from Aldrich. n-butanol (AR grade) was obtained from BDH. 1,3-propanediol, was obtained from BDH. p-fluorotoluene (4-fluorotoluene) was obtained from BDH. d_4-methanol, CD_3OD (99.8 atom % D), was obtained from Aldrich. Ethyl bromide, C_2H_5Br (99+%) was obtained from May and Baker Limited. Methanol, CH_3OH, was HPLC grade. o-fluorotoluene (2-fluorotoluene) was obtained from L. Light and Co. Limited. Acrylonitrile, CH_2CHCN, reagent grade (stabilised with 0.005% p-methoxy phenol) was obtained from BDH. Formic acid, HCOOH (reagent grade) was obtained from BDH Limited. Acetic acid, CH_3COOH (AR grade) was obtained from Ajax Chemicals. Bromobenzene, C_6H_5Br, was obtained from May and Baker Limited. Chlorobenzene, C_6H_5Cl (AR grade) was obtained from BDH. Fluorobenzene, C_6H_5F, was obtained from BDH. m-bromotoluene (3-bromotoluene), was obtained from Koch-Light Laboratories. Benzyl bromide (98+%) was obtained from BDH. Cycloheptatriene, c-C_7H_8, was obtained from Koch-Light Laboratories, and was additionally purified by vacuum distillation. Propylene, C_3H_6, was

obtained from Alphagaz. Cyanogen bromide, BrCN, was prepared by reacting bromine with excess mercuric cyanide under vacuum. Methyl bromide, CH_3Br (99.5+%) was obtained from Aldrich. Acetonitrile, CH_3CN (98+%) was obtained from May and Baker Limited. Acetone, $(CH_3)_2CO$ (spectro grade), was obtained from Eastman Organic Chemicals. Nitric oxide (CP grade) was obtained from Matheson and was further purified by slow passage through a dry/ice acetone cooled molecular sieve trap. Diethylketone (3-pentanone), $(C_2H_5)_2CO$ (97%) was obtained from Aldrich. Butanone, $C_2H_5COCH_3$ (Ar grade), was obtained from BDH. Cyclopropane (99+%) was obtained from Aldrich. Dimethyl ether (99+%) was obtained from Aldrich. Liquified SO_2 was obtained from BDH. Ethanol (spectro grade) was obtained from Riedel-De Haën A.G.

All liquid reagents were further purified using multiple freeze-pump-thaw cycles. Unless stated otherwise, measurements were made using instrument grade (stated purity 99.99%) or in some cases zero grade (stated purity 99.995%) helium as the carrier gas at pressures between 0.300 and 0.500 Torr at a room temperature of 298 ± 5 K. Collision rate coefficients were calculated using the parameterised method of Su and Chesnavich. [161] Dipole moments and polarisabilities were obtained from the C.R.C. Handbook of Chemistry and Physics. [162] Thermodynamic quantities at 298 K were obtained from the compilations of Lias and co-workers. [163,164] Rate coefficients determined in this work are considered to have an experimental uncertainty of ± 20% for permanent gases and ± 30% for vapours, unless specifically stated otherwise. Product distributions have an estimated uncertainty of ± 20%.

CHAPTER 3.

DETERMINATION OF THE ISOMERIC PRODUCT STRUCTURE IN ION-MOLECULE ASSOCIATION REACTIONS

3.1 Introduction.

Reactivity studies have been used to identify the isomeric structures formed in three ion-molecule association reactions that have been proposed to play a role in the chemistry of the interstellar medium.

The termolecular association of H_3O^+ with C_2H_2 is shown to produce a mixture of $C_2H_5O^+$ isomers. Further, it is shown that the predominant ion has a structure which is different from the well-characterised ions: protonated acetaldehyde, protonated oxirane and the methoxymethyl cation. A combined theoretical and experimental study of the $C_2H_5O^+$ potential energy surface is used to identify the likely products of the termolecular (and by inference the radiative) association of H_3O^+ with C_2H_2. Several reactions of the ions: protonated acetaldehyde, protonated oxirane and the methoxymethyl cation are also reported. Radiative association of H_3O^+ with C_2H_4 followed by dissociative electron-ion recombination has been proposed as a synthetic route to the ethanol observed by radioastronomy in interstellar clouds. The reactivity of the $C_2H_7O^+$ ion product formed in the *termolecular* association of H_3O^+ with C_2H_4 is examined using the neutral reagents 2-fluorotoluene and acrylonitrile. Further, it is shown that the ion formed in the termolecular association of H_3O^+ with C_2H_4 exhibits identical reactivity to that of protonated ethanol with the same neutrals. It is concluded that formation of protonated ethanol ***is*** therefore a likely outcome of the analogous radiative association reaction of H_3O^+ with C_2H_4.

The proposal that radiative association of protonated imines with formic acid may lead to protonated amino acids in the interstellar medium is tested by examining the analogous termolecular association of protonated methanimine, $CH_2NH_2^+$ with formic

acid. The observation of ligand exchange reactions between the termolecular association product and the neutrals NH_3, CH_3NH_2 and $C_2H_5NH_2$ leads to the conclusion that the termolecular association of $CH_2NH_2^+$ with HCOOH yields an electrostatic, rather than covalently bonded, adduct. This observation is in accord with a previous collision-induced dissociation (CID) study of protonated glycine which indicated that loss of HCOOH occurs over a substantial barrier and that, as a consequence, there is a sizeable barrier to the reverse association of $CH_2NH_2^+$ with HCOOH.

3.2 Ion-molecule association of H_3O^+ and C_2H_2: Interstellar CH_3CHO.

Acetaldehyde is one of the molecules known to exist in interstellar gas clouds, having been first identified in 1971 via its characteristic emission spectrum at 1065.075 MHz. [165] Among the synthetic routes proposed to account for the formation of acetaldehyde in the ISM, is the radiative association of H_3O^+ with C_2H_2 [166,167]:

$$H_3O^+ + C_2H_2 \longrightarrow C_2H_5O^+ + h\nu \qquad (3.1)$$

followed by dissociative electron-ion recombination.

$$CH_3CHOH^+ + e \longrightarrow CH_3CHO + H \qquad (3.2)$$

Several isomeric forms of $C_2H_5O^+$ are known to exist, however, and it is not immediately obvious whether protonated acetaldehyde, CH_3CHOH^+, is the structure formed by radiative association in reaction (3.1). Calculations by Herbst et al [168] suggested that the structure of the product ion formed in the termolecular association reaction (3.3) ***does not*** correspond to CH_3CHOH^+, which is the lowest energy isomer of $C_2H_5O^+$.

$$H_3O^+ + C_2H_2 + M \longrightarrow C_2H_5O^+ + M \qquad (3.3)$$

In their study Herbst et al compared the measured termolecular rate coefficient for reaction (3.3) with that calculated assuming the product ion has the CH_3CHOH^+ structure. Their calculated rate coefficient disagreed with their experimentally determined value by more than two orders of magnitude, although they believe the computational method employed to be accurate to within one order of magnitude. They therefore concluded that the $C_2H_5O^+$ isomer formed in the association reaction (3.3) has a structure higher in energy than CH_3CHOH^+. Jarrold et al [166] compared the collision induced dissociation spectrum of the ion formed in reaction (3.3) with that of protonated acetaldehyde,

protonated oxirane, and the methoxymethyl cation. They concluded that the product of reaction (3.3) has the structure of *either* protonated acetaldehyde or protonated oxirane because of the similarities of the CID spectra of these two ions to that of the H_3O^+/C_2H_2 association ion. Burgers et al [169] presented evidence for the stability of the vinyloxonium cation (protonated vinyl alcohol) in the gas phase, based on collisional activation and charge stripping experiments. In accord with the suggestion of Herbst et al [168] we compared the reactivity of the ion formed in reaction (3.3) with that of protonated acetaldehyde and protonated oxirane and investigated some reactions of the methoxymethyl cation also.

3.2.1 Experimental.

The experiments were performed at room temperature (298 ± 5) K and at helium bath gas pressures between 0.3 and 0.35 Torr. Most of the reactions were measured in the original SIFT apparatus, however several measurements were subsequently checked in the new FA-SIFT apparatus. The $H_3O^+.C_2H_2$ association ion was formed in the flow tube by injecting mass-selected H_3O^+ from the SIFT ion source (formed via electron impact on water vapour, or, alternatively, by introducing water vapour into the FA source in the FA-SIFT) and adding C_2H_2 at the first inlet port.

$$H_3O^+ + C_2H_2 + He \longrightarrow C_2H_5O^+ + He \qquad (3.4)$$

The reactivity of the resultant $C_2H_5O^+$ species was probed via subsequent reactions performed at the downstream neutral inlet. Our measured pseudo-second-order rate coefficient for reaction (3.4) was 1.1×10^{-11} cm^3 s^{-1} at a He bath gas pressure of 0.3 Torr in the SIFT, which corresponds to an effective termolecular rate coefficient of $k_2/[He] = 1.1 \times 10^{-27}$ cm^6 s^{-1}. This agrees with the value of 8×10^{-28} cm^6 s^{-1} obtained by Herbst et al [168] within the experimental uncertainty. In most measurements the flow of C_2H_2 at the first neutral inlet was sufficient to reduce the injected H_3O^+ signal to less than 1% of the background level, to achieve near complete reaction of H_3O^+ with C_2H_2 before reaching the downstream reaction region. This was crucial as a "distributed source" of $C_2H_5O^+$ could lead to curvature in the measured reaction decays, which could confuse identification of the isomeric structure(s) of the ion(s) formed in reaction (3.4) (see the

discussion below). At the large flow rates of acetylene required, secondary (and tertiary) reaction chemistry was observed to occur, generating ions at m/z = 67, 69, and 71.

$$H_3O^+.C_2H_2 + C_2H_2 \xrightarrow{M} C_4H_7O^+ \quad \textbf{(3.5a)}$$

$$\longrightarrow C_4H_5O^+ + H_2 \text{ (major products)} \quad \textbf{(3.5b)}$$

$$C_4H_5O^+ + C_2H_2 \longrightarrow C_4H_3O^+ + C_2H_4 \quad \textbf{(3.6)}$$

The ion at m/z = 67 may also be produced from $H_3O^+.C_2H_2 + C_2H_2$ in a single step, although this would require direct elimination of two molecules of H_2, which is unlikely. Thus reaction (3.6) is the more probable route to formation of this ion. A mass spectrum showing the ions formed when acetylene is added to an H_3O^+ ion swarm is illustrated in Figure 3.1. The presence of these secondary ions and excess acetylene hampered the unequivocal identification of products in some of the reactions of $H_3O^+.C_2H_2$ discussed below.

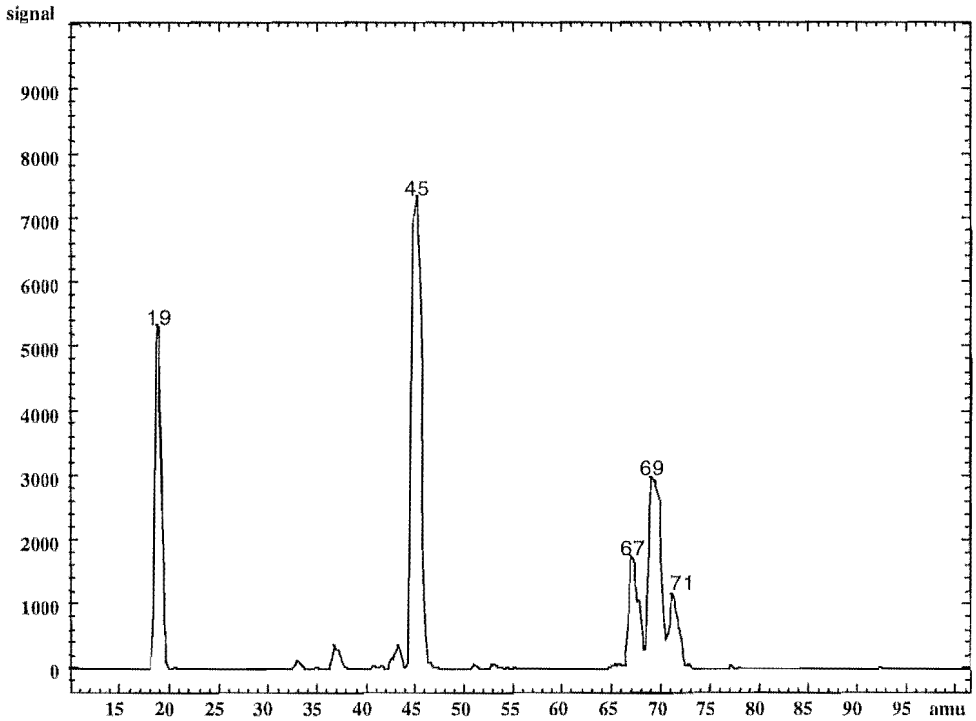

Figure 3.1. Mass spectrum obtained upon addition of acetylene to an H_3O^+ ion swarm.

The existence of multiple isomeric structures can be established via their differing reactivities with selected reagents. [170] The possibility that vibrational excitation of ions

formed via an association reaction might also give rise to curved semilogarithmic decays of ln(ion signal) versus neutral flow must also be considered. However, in the present case, eight atoms in the $C_2H_2.H_3O^+$ complex yield 18 (i.e. 3N – 6 for a non-linear species) normal modes for distribution of vibrational energy, which makes collisional stabilisation by the carrier gas a more efficient process than for smaller ions. The distance of 40 cm between the upstream and downstream inlet ports means that under typical experimental conditions (298 K, P = 0.3 – 0.35 Torr) the association ion would experience ~ 15,000 collisions with the carrier gas atoms before reaction with the diagnostic neutral species.

The ab initio calculations described below show that the proton affinities (PAs) of some C_2H_4O species are sufficiently different for proton transfer to be used as a probe of the structure of the protonated ions. Several neutral reactants were selected for reaction with the different isomers of $C_2H_5O^+$, on the basis of their known proton affinities.[‡] The neutral reagents chosen were C_2H_5Br (PA = 696.2 kJ mol^{-1}), 4-fluorotoluene (PA = 763.8 kJ mol^{-1}), benzene (PA = 750.4 kJ mol^{-1}), allene (PA = 775.3 kJ mol^{-1})[†], 2-fluorotoluene (PA = 773.3 kJ mol^{-1}) and CH_3OH (PA = 754.3 kJ mol^{-1}).

In the SIFT experiments protonated acetaldehyde, CH_3CHOH^+, was formed via electron impact on CH_3CHO in a high-pressure ion source. Protonated oxirane, c-$CH_2(OH)CH_2^+$, was formed similarly from pure oxirane in a high pressure ion source. The methoxymethyl cation, $CH_3OCH_2^+$, was formed via electron impact on dimethoxy methane, $(CH_3O)_2CH_2$. In the FA-SIFT experiments these three ions were formed by introducing acetaldehyde, oxirane or dimethoxy methane respectively into the flowing afterglow source. The desired $C_2H_5O^+$ isomer was then mass-selected (m/z = 45) and injected into the flow tube in the usual manner. These $C_2H_5O^+$ isomers have substantial barriers to isomerisation and retain their identity in the flow tube as the reaction chemistry described next bears out.

[‡] The PA values reported here have been amended from those reported in Appendix II following publication of the latest NIST database (ref.164).

[†] The protonation site in allene is dependent on the proton affinity of the base from which proton transfer is occurring (see chapter 4.4).

3.3 Results.

3.3.1 CH_3CHOH^+ Reactions.

The reactions of protonated acetaldehyde, CH_3CHOH^+ with the five neutral reagents 4-fluorotoluene, methanol, benzene, ethyl bromide and acetylene were examined. The only products observed in all five reactions were the termolecular association adducts. The measured pseudo-second-order rate coefficients for the reactions were k = 4.5 x 10^{-10} cm^3 s^{-1} (4-fluorotoluene, 0.300 Torr He), k = 4.4 x 10^{-10} cm^3 s^{-1} (CH_3OH, 0.300 Torr He), k = 1.3 x 10^{-10} cm^3 s^{-1} (C_6H_6, 0.345 Torr He), k = 5.8 x 10^{-11} cm^3 s^{-1} (C_2H_5Br, 0.345 Torr He) and k < 1 x 10^{-12} cm^3 s^{-1} (C_2H_2, 0.345 Torr He).

3.3.2 $CH_3OCH_2^+$ Reactions.

The five reagents: C_6H_6, 4-fluorotoluene, CH_3OH (CD_3OD), ethyl bromide and acetylene were also reacted with the methoxymethyl cation, $CH_3OCH_2^+$, with the following results.

$$CH_3OCH_2^+ + C_6H_6 \xrightarrow{1.0} C_7H_7^+ + CH_3OH \qquad \textbf{(3.7)}$$

$k_{3.7} = 5.0 \times 10^{-10}$ cm^3 s^{-1}

The observed reaction product corresponds to formal transfer of CH^+ from the methoxymethyl cation to benzene. This CH^+ transfer channel was observed by Wilson et al [18,171] in several reactions of the methoxymethyl cation in an investigation of the reactions of $CH_3OCH_2^+$ with a number of nitrogen bases.

$$CH_3OCH_2^+ + C_7H_7F \xrightarrow{>0.90} C_8H_8F^+ + CH_3OH \qquad \textbf{(3.8a)}$$

$$\xrightarrow{<0.10} \text{adduct} \qquad \textbf{(3.8b)}$$

$k_{3.8} = 2.6 \times 10^{-10}$ cm^3 s^{-1}

Again, the first channel in reaction (3.8) corresponds to CH^+ transfer.

$$CH_3OCH_2^+ + CD_3OD \xrightarrow{>0.9} \text{adduct} \qquad \textbf{(3.9a)}$$

$$\xrightarrow{<0.1} CD_3OCH_2^+ + CH_3OD \qquad \textbf{(3.9b)}$$

$k_{3.9} = 2 \times 10^{-11}$ cm^3 s^{-1}

The reaction of $CH_3OCH_2^+$ with CH_3OH was measured previously by Wilson [18,171], who obtained a rate coefficient of 1.3 x 10^{-11} cm^3 s^{-1}, which agrees with the present measurement within the combined uncertainties of the two measurements. The only

product ion observed was the collision stabilised adduct, although Wilson [18] commented that a CH^+ transfer channel could not be ruled out, without the use of isotopically labelled methanol, since it would produce a product ion identical to the reactant ion. d_4-methanol, CD_3OD, was therefore utilised in the present study. The results indicate that CH^+ transfer is only a minor channel in reaction (3.9).

$CH_3OCH_2^+ + C_2H_5Br \xrightarrow{1.0}$ adduct **(3.10)**

$k_{3.10} = 4 \times 10^{-12}$ cm^3 s^{-1} (0.345 Torr He)

This pseudo-bimolecular rate coefficient corresponds to an effective termolecular rate coefficient of $k_2/[He] \sim 3.6 \times 10^{-28}$ cm^3 s^{-1}.

$CH_3OCH_2^+ + C_2H_2 \longrightarrow$ no reaction **(3.11)**

$k_{3.11} < 5 \times 10^{-13}$ cm^3 s^{-1}

3.3.3 c-$CH_2(OH)CH_2^+$ Reactions.

The reactions of protonated oxirane with C_6H_6, 4-fluorotoluene, methanol, ethyl bromide and acetylene were examined.

$c\text{-}C_2H_5O^+ + C_7H_7F \xrightarrow{0.9} C_9H_{10}F^+ + H_2O$ **(3.12a)**

$\xrightarrow{0.1}$ adduct **(3.12b)**

$k_{3.12} = 6.3 \times 10^{-10}$ cm^3 s^{-1}

$c\text{-}C_2H_5O^+ + CH_3OH \xrightarrow{0.6} C_3H_7O^+ + H_2O$ **(3.13a)**

$\xrightarrow{0.4}$ adduct **(3.13b)**

$k_{3.13} = 5.0 \times 10^{-10}$ cm^3 s^{-1}

$c\text{-}C_2H_5O^+ + C_6H_6 \xrightarrow{0.8} C_8H_9^+ + H_2O$ **(3.14a)**

$\xrightarrow{0.2}$ adduct **(3.14b)**

$k_{3.14} = 1.7 \times 10^{-10}$ cm^3 s^{-1}

$c\text{-}C_2H_5O^+ + C_2H_5Br \xrightarrow{1.0}$ adduct **(3.15)**

$k_{3.15} = 6.5 \times 10^{-11}$ cm^3 s^{-1}

$c\text{-}C_2H_5O^+ + C_2H_2 \longrightarrow$ adduct **(3.16a)**

$\longrightarrow C_4H_5O^+ + H_2$ **(3.16b)**

$k_{3.16} \sim 3.6 \times 10^{-12}$ cm^3 s^{-1}

The $C_4H_5O^+$ product formed in reaction (3.16b) reacts rapidly with acetylene (probably at close to the collision rate, although this was not determined quantitatively) to yield a product ion at m/z = 67.

$$C_4H_5O^+ + C_2H_2 \longrightarrow C_4H_3O^+ + C_2H_4 \qquad \textbf{(3.17)}$$

This pattern of reactivity mirrors the secondary chemistry observed when C_2H_2 reacts with H_3O^+, discussed in a previous section, and may suggest that protonated oxirane is formed in the termolecular association of H_3O^+ and C_2H_2, although the measurements discussed below fail to support this contention.

The series of reactions listed above suggest that elimination of water as a neutral product may be a common channel in the reactions of protonated oxirane, which could potentially be used to identify the presence of protonated oxirane in a mixture of $C_2H_5O^+$ ions, since water elimination was not observed in the reactions of CH_3CHOH^+ and $CH_3OCH_2^+$ with the same neutral reagents.

3.3.4 $H_3O^+.C_2H_2$ reactions.

Six reagents were used to examine the reactivity of the H_3O^+/C_2H_2 association ion: C_2H_5Br, 4-fluorotoluene, C_6H_6, CH_3OH, 2-fluorotoluene and allene (propadiene). For the first three of these reagents the reaction behaviour was very different from the behaviour exhibited by the $C_2H_5O^+$ isomers discussed previously. For each reagent, *curved* semilogarithmic decays were observed, which indicates that more than one isomeric form of $C_2H_5O^+$ is formed in the association reaction (3.4). Further, the consistent linearity of the semilogarithmic decays obtained for the other three reagents (Figure 3.2) under typical experimental conditions indicates that the curvature is not due to an extended source of $C_2H_5O^+$ in the flow tube. Also, it seems very unlikely that the observed curvature is the result of formation of a product at m/z = 45, although the possibility of an isomerisation reaction cannot be ruled out. An example of a curved decay obtained for the reaction of $C_2H_2.H_3O^+$ and benzene is shown in Figure (3.3). The data points are fitted in the usual way using equation (3.18) which assumes that two isomeric forms of $C_2H_5O^+$ contribute to the observed ion signal at m/z = 45.

$$I_{C_2H_5O^+} = C_1'\exp(-k_1' f_{neut}) + C_2'\exp(-k_2' f_{neut}) \qquad \textbf{(3.18)}$$

Reactant	Products	Branching ratio	k_{obs} /10^{-9} cm^3 s^{-1}	k_{coll}[a] /10^{-9} cm^3 s^{-1}	PA[b] /kJ mol^{-1}
CH_3CHOH^+					
C_7H_7F[c]	adduct	1.0	0.45	2.3	763.8
CH_3OH	adduct	1.0	0.44	2.1	754.3
c-C_6H_6	adduct	1.0	0.13	1.4	750.4
C_2H_5Br	adduct	1.0	0.058	2.1	696.2
C_2H_2	adduct	1.0	<0.001	1.1	641.4
$CH_3OCH_2^+$					
C_7H_7F[c]	$C_8H_8F^+ + CH_3OH$	>0.90	0.26	2.3	763.8
	adduct	<0.10			
CD_3OD	adduct	>0.90	0.02	2.1	754.3
	$CD_3OCH_2^+ + CH_3OD$	<0.10			
c-C_6H_6	$C_7H_7^+ + CH_3OH$	1.0	0.5	1.4	750.4
C_2H_5Br	adduct	1.0	0.004	2.1	696.2
C_2H_2	NR		<0.0005	1.1	641.4
c-$CH_2(OH)CH_2^+$					
C_7H_7F[c]	$C_9H_{10}F^+ + H_2O$	0.9	0.63	2.3	763.8
	adduct	0.1			
CH_3OH	$C_3H_7O^+ + H_2O$	0.6	0.50	2.1	754.3
	adduct	0.4			
C_6H_6	$C_8H_9^+ + H_2O$	0.8	0.17	1.4	750.4
	adduct	0.2			
C_2H_5Br	adduct	1.0	0.065	2.1	696.2
C_2H_2	adduct		0.0036	1.1	641.4
	$C_4H_5O^+ + H_2$				

Table 3.1. Reaction rate coefficients and product ratios for the $C_2H_5O^+$ ions: protonated acetaldehyde, CH_3CHOH^+; methoxymethyl cation, $CH_3OCH_2^+$; and protonated oxirane, c-$CH_2(OH)CH_2^+$ with the specified reactant.

[a] Calculated using the method of Su and Chesnavich (ref. 161).
[b] Reactant neutral proton affinities are from ref. 164. [c] Reactant is 4-fluorotoluene.

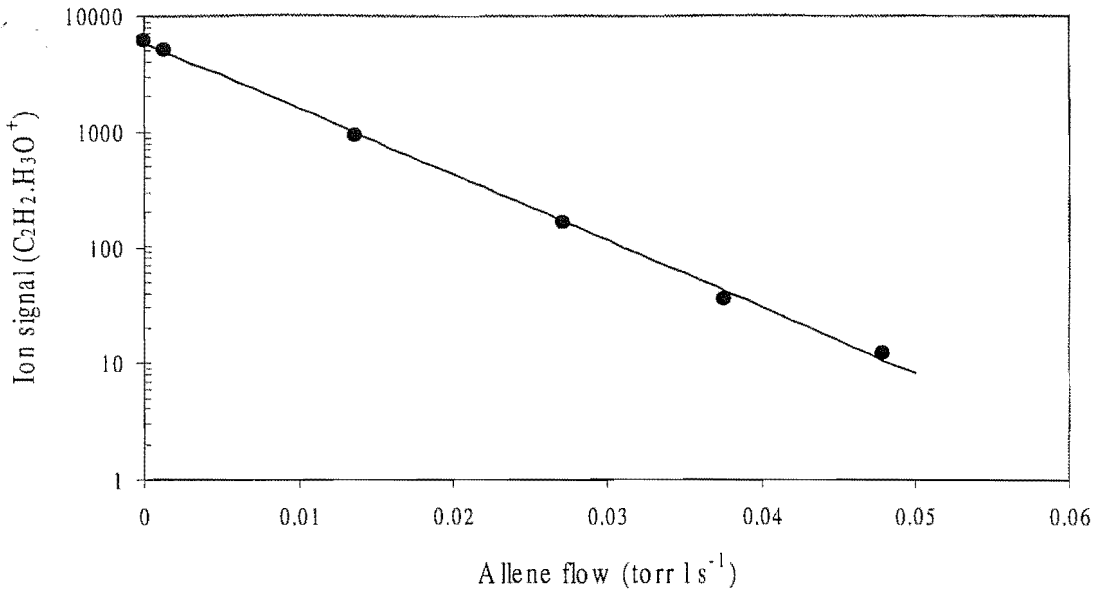

Figure 3.2. Semilogarithmic plot of the $C_2H_2.H_3O^+$ ion count rate versus allene flow. The linear fit is as expected for pseudo-first-order kinetics.

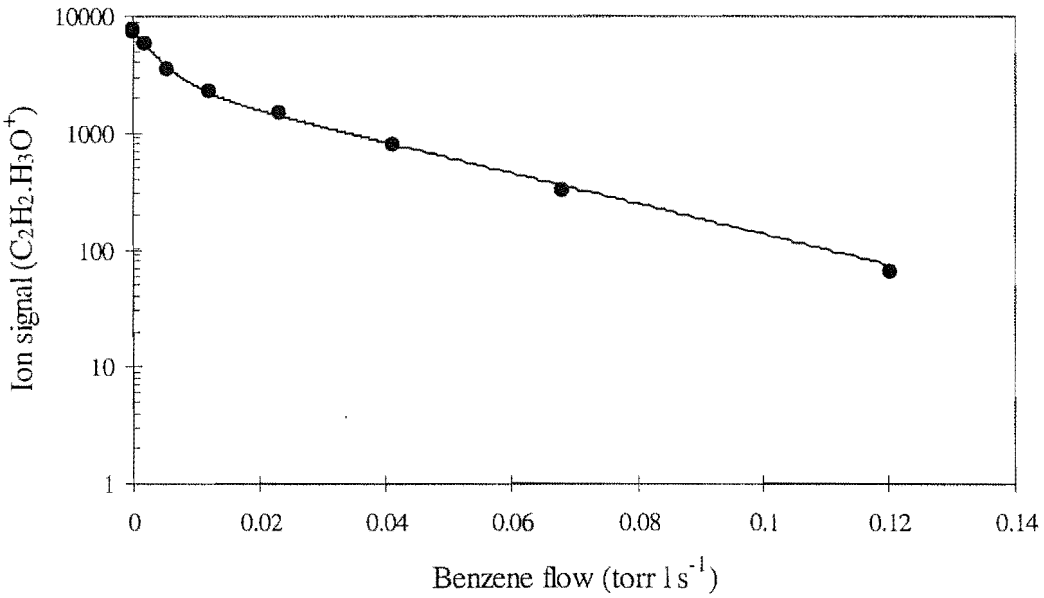

Figure 3.3. Semilogarithmic plot of the $C_2H_2.H_3O^+$ ion signal at m/z = 45 *vs.* benzene flow. The points are experimental and the curve is a computer-generated fit to the data using equation (3.18), with $k_1 = 1.2 \times 10^{-9}$ cm^3 s^{-1} and $k_2 = 1.5 \times 10^{-10}$ cm^3 s^{-1}. The plot indicates a ratio of fast to slow reacting isomers of 65:35.

The solid curve in Figure 3.3 is the computer-generated best fit modelled according to equation (3.18). C_1' and C_2' are the respective ion signals of the two isomeric $C_2H_5O^+$ species at zero neutral flow; k_1' and k_2' are directly proportional to the respective rate coefficients for the two isomeric ions and f_{neut} is the flow of the neutral reagent. Because of uncertainties in the curve-fitting procedure, the rate coefficients have larger uncertainties (± 50%) than rate coefficients usually obtained using the SIFT technique.

Reaction with 2-fluorotoluene

The reaction of $C_2H_2.H_3O^+$ with 2-fluorotoluene produced a linear semi-logarithmic decay which apparently corresponds to exothermic proton transfer from both isomeric $C_2H_5O^+$ species (proton transfer was the only observed product from $C_2H_2{\cdot}H_3O^+$), with a rate coefficient close to the collisional value.

$$C_2H_2.H_3O^+ + o\text{-}C_7H_7F \longrightarrow C_7H_7FH^+ + C_2H_4O \qquad \textbf{(3.19)}$$

$k_{3.19} = 1.6 \times 10^{-9}$ cm^3 s^{-1}

Reaction with C_2H_5Br

The reaction of $C_2H_2.H_3O^+$ with ethyl bromide yielded apparent product ion signals at m/z = 55 ($C_4H_7^+$), 153 and 155 (Br isotopomers of the adduct ion). A curved semilogarithmic decay was observed. The rate coefficient for the fast decay component was too high to be accounted for by the presence of CH_3CHOH^+, c-$C_2H_5O^+$ or $CH_3OCH_2^+$. The rate coefficient corresponding to the slow component is comparable to the rate coefficient observed in the reactions of CH_3CHOH^+ and c-$C_2H_5O^+$ with C_2H_5Br but not $CH_3OCH_2^+$.

$$C_2H_2.H_3O^+ + C_2H_5Br \longrightarrow \text{adduct} \qquad \textbf{(3.20a)}$$

$$\longrightarrow C_4H_7^+ + H_2O + HBr \qquad \textbf{(3.20b)}$$

$k_1 = 1.8 \times 10^{-9}$ cm^3 s^{-1}; $C_1 \geq 0.50$

$k_2 = 5.8 \times 10^{-11}$ cm^3 s^{-1}; $C_2 \leq 0.50$

Reaction with benzene

The only product ion signals observed in the reaction of $C_2H_2.H_3O^+$ with benzene correspond to proton transfer and adduct formation. Again, a curved semilogarithmic decay was obtained (Figure 3.3). The rate coefficient for the fast decay is inconsistent

with the rate coefficients observed in the reactions of CH_3CHOH^+, c-$C_2H_5O^+$ and $CH_3OCH_2^+$ with benzene.

$$C_2H_2.H_3O^+ + C_6H_6 \longrightarrow C_6H_7^+ + C_2H_4O \quad \textbf{(3.21a)}$$

$$\longrightarrow \text{adduct} \quad \textbf{(3.21b)}$$

$k_1 = 1.6 \times 10^{-9}$ cm^3 s^{-1}; $C_1 \geq 0.60$

$k_2 = 1.8 \times 10^{-10}$ cm^3 s^{-1}; $C_2 \leq 0.40$

Reaction with 4-fluorotoluene

Proton transfer and adduct formation were the only products identified in the reaction of $C_2H_2.H_3O^+$ with 4-fluorotoluene. Again, the fast initial decay is inconsistent with the rates observed in the reactions of CH_3CHOH^+, c-$C_2H_5O^+$ and $CH_3OCH_2^+$ with 4-fluorotoluene, although the lower rate coefficient is comparable to that observed in the reactions of CH_3CHOH^+ and c-$C_2H_5O^+$ with 4-fluorotoluene.

$$C_2H_2.H_3O^+ + \text{p-}C_7H_7F \longrightarrow C_7H_7FH^+ + C_2H_4O \quad \textbf{(3.22a)}$$

$$\longrightarrow \text{adduct} \quad \textbf{(3.22b)}$$

$k_1 = 2.6 \times 10^{-9}$ cm^3 s^{-1}; $C_1 \geq 0.60$

$k_2 = 5.1 \times 10^{-10}$ cm^3 s^{-1}; $C_2 \leq 0.40$

Reaction with CH_3OH

When this reaction was measured using the original SIFT apparatus a curved semilogarithmic decay was obtained (see Appendix II). A subsequent check of the measurement using the new FA-SIFT apparatus revealed a consistently linear semilogarthmic decay which yielded a rate coefficient of 5.5×10^{-10} cm^3 s^{-1}, which is also lower than the calculated collision rate. Measurements were performed at a range of acetylene flows added through the first neutral inlet, from 50% of the H_3O^+ signal removed to 100% of the H_3O^+ signal removed, yet the measured semilogarithmic decay was consistently linear. The reason for the disparity between the measurements using the two instruments is unclear. The major product observed was proton transfer, and the adduct was also identified. A possible minor product channel at m/z = 51, perhaps a product of a ligand exchange reaction (see the discussion below), $H_3O^+.HOCH_3$ was also identified.

$$C_2H_2.H_3O^+ + CH_3OH \longrightarrow \text{products} \quad \textbf{(3.23)}$$

Reaction with allene

$C_2H_2.H_3O^+ + C_3H_4 \longrightarrow$ products **(3.24)**

A disparity was also noted between the result obtained in the SIFT and that obtained in the FA-SIFT for the reaction of $C_2H_2.H_3O^+$ with allene. Although consistently linear semilogarithmic decays were observed using both instruments (Figure 3.2), the rate coefficient measured in the FA-SIFT of 6.7 x 10^{-10} cm^3 s^{-1}, is lower than the value of 1.0 x 10^{-9} cm^3 s^{-1} determined in the SIFT apparatus. The accuracy of the FA-SIFT measurement was verified by checking the rate coefficient for the reaction of H_3O^+ with allene, for which a value of 1.5 x 10^{-9} cm^3 s^{-1} was obtained in accord with the expected collisional value. Unequivocal identification of the products of reaction 3.24 was made difficult by the presence of excess acetylene in the flow tube. Upon addition of allene to the flow tube new peaks were observed at masses 43, 57, 59, 65, and 67. The peaks at m/z = 65 and 67 are almost certainly due to reaction of $C_3H_5^+$ (formed from unreacted $H_3O^+ + C_3H_4$) with excess acetylene, viz.

$C_3H_5^+ + C_2H_2 \longrightarrow C_5H_7^+$ **(3.25a)**

$\longrightarrow C_5H_5^+ + H_2$ **(3.25b)**

Of the three remaining peaks, m/z = 43 and 59 were the major signals. The signal at m/z = 59 must correspond to an ion of formula $C_3H_7O^+$, and possibly represents a simple ligand exchange process.

$C_2H_2.H_3O^+ + C_3H_4 \longrightarrow C_3H_7O^+ + C_2H_2$ **(3.26)**

The signal at m/z = 43 could be either $C_3H_7^+$ or $C_2H_3O^+$.

$C_2H_2.H_3O^+ + C_3H_4 \longrightarrow C_3H_7^+ + C_2H_2O$ **(3.27)**

or $\longrightarrow C_2H_3O^+ + C_3H_6$ **(3.28)**

Exothermic processes can be written for both reactions (3.27) and (3.28) if no particular structure is assumed for the $C_2H_5O^+$ reactant, so neither channel can be discounted on thermodynamic grounds.

C_1 and C_2 are the fractions of isomer 1 and 2 present in the mixture (see equation 3.18). The rate coefficient k_1 is the rate constant for the "fast reacting" isomer and corresponds to the initial rapid decay component in Figure 3.3. The rate coefficient k_2 is the rate constant for the slower reacting isomer. A summary of all the measurements of

designated $C_2H_5O^+$ isomer reactions is presented in Table 3.1 and the reactions of $C_2H_2.H_3O^+$ in Table 3.2.

If the two isomeric species react at different rates with acetylene then the isomeric distribution will exhibit a dependence on the flow of acetylene and should be extrapolated to zero C_2H_2 flow to obtain the "true" isomeric ratio at the time of formation (see the discussion in section 7.5 of Wilson's thesis [18]). Although an approximate ratio of 1:1 is suggested by the results detailed above, experiments in which the isomeric ratio was determined via reaction with benzene at various flows of acetylene suggest that the true ratio could be as high as 3:1 in favour of the fast reacting isomer.

3.3.5 H_3O^+ Reactions.

In the course of this work a number of reactions of H_3O^+ were measured. The neutral reagents investigated were 4-fluorotoluene, ethyl bromide, allene, and benzene. The reaction of HCO^+ with 4-fluorotoluene was also measured. The results were as follows:

4-fluorotoluene

Proton transfer only was observed occurring at the collision rate in keeping with the known proton affinities of H_2O and 4-fluorotoluene.

$$H_3O^+ + p\text{-}C_7H_7F \longrightarrow C_7H_7FH^+ + H_2O \qquad \textbf{(3.29)}$$

$k_{3.29} = 2.9 \times 10^{-9}$ cm^3 s^{-1}

Ethyl bromide

The observed rate coefficient for reaction 3.30 is approximately half the calculated collision rate of 2.9×10^{-9} cm^3 s^{-1} and a second bimolecular channel (producing $C_2H_7O^+$) is observed to compete with proton transfer, which accounts for ~ 30% of the total products. This result suggests that proton transfer from H_3O^+ to ethyl bromide may be slightly endothermic, rather than slightly exothermic as suggested by the values of $PA(H_2O) = 691$ kJ mol^{-1} and $PA(C_2H_5Br) = 696.2$ kJ mol^{-1} tabulated in reference 164.

$$H_3O^+ + C_2H_5Br \xrightarrow{\sim 0.6} C_2H_7O^+ + HBr \qquad \textbf{(3.30a)}$$

$$\xrightarrow{\sim 0.3} C_2H_5BrH^+ + H_2O \qquad \textbf{(3.30b)}$$

$$\xrightarrow{\sim 0.1} \text{adduct} \qquad \textbf{(3.30c)}$$

$k_{3.30} = 1.3 \times 10^{-9}$ cm^3 s^{-1}

Reactant	Products	PA[a] /kJ mol^{-1}	k_1[b] /10^{-9} cm^3 s^{-1}	k_2[c] /10^{-9} cm^3 s^{-1}	C_1[d]	k_{coll}[e] /10^{-9} cm^3 s^{-1}
C_2H_5Br	$C_4H_7^+ + H_2O + HBr$ adduct	696.2	1.8	0.058	>0.50	2.1
p-C_7H_7F[f]	$C_7H_7FH^+ + C_2H_4O$ adduct	763.8	2.6	0.51	>0.60	2.3
C_6H_6	$C_6H_7^+ + C_2H_4O$ adduct	750.4	1.6	0.18	>0.60	1.4
CH_3OH	$CH_3OH_2^+ + C_2H_4O$ adduct $H_3O^+.HOCH_3$ (?)	754.3	0.55	-	-	2.1
CH_2CCH_2	$C_3H_7O^+ + C_2H_2$ $C_3H_5O^+ + C_2H_4$ $C_3H_7^+ + C_2H_2O$, or $C_2H_3O^+ + C_3H_6$	775.3[g]	0.67	-	-	1.2
o-C_7H_7F[h]	$C_7H_8F^+ + C_2H_4O$	773.3		-	-	1.9

Table 3.2. Reaction rate coefficients and isomer ratio for the $C_2H_5O^+$ species, $C_2H_2.H_3O^+$, formed in the association reaction between H_3O^+ and C_2H_2, and the specified reagent.

Allene

Proton transfer only was observed. The reaction of H_3O^+ with allene has been shown to generate exclusively the 2-propenyl $C_3H_5^+$ structure (see chapter 4).

---

[a] Reference 164.
[b] Observed rate coefficient for the more reactive isomer. Uncertainty (± 50%).
[c] Observed rate coefficient for the less reactive isomer. Uncertainty (± 50%).
[d] Estimated proportion of the more reactive isomer.
[e] Collision rate calculated using the method of Su and Chesnavich (ref. 161).
[f] 4-fluorotoluene.
[g] The protonation site in allene is dependent on the proton affinity of the base from which proton transfer is occuring (see chapter 4.4).
[h] 2-fluorotoluene.

$H_3O^+ + C_3H_4 \longrightarrow C_3H_5^+ + H_2O$ **(3.31)**

$k_{3.31} = 1.5 \times 10^{-9}$ cm^3 s^{-1}

Benzene

Proton transfer only was observed, occurring at the collision rate, in keeping with the known proton affinities of H_2O and benzene.

$H_3O^+ + C_6H_6 \longrightarrow C_6H_7^+ + H_2O$ **(3.32)**

$k_{3.32} = 1.5 \times 10^{-9}$ cm^3 s^{-1}

HCO^+ + 4-fluorotoluene

Proton transfer was the only reaction channel observed for this reaction.

$HCO^+ + p\text{-}C_7H_7F \longrightarrow C_7H_7FH^+ + CO$ **(3.33)**

$k_{3.33} = 2.9 \times 10^{-9}$ cm^3 s^{-1}

The reactions of H_3O^+ and HCO^+ are summarised in Table 3.3.

3.3.6 Attempts to generate $CH_2CHOH_2^+$.

Burgers et al [169] report that electron impact ionisation of either n-butanol or propane-1,3-diol generates predominantly the vinyloxonium cation, $CH_2CHOH_2^+$. Their conclusion was based on the observation of quite different collisional activation and charge stripping mass spectra for the $C_2H_5O^+$ ions derived from these two neutral precursors compared to those observed for CH_3CHOH^+, $CH_3OCH_2^+$ and c-$CH_2(OH)CH_2^+$. Both n-butanol and propane-1,3-diol were subjected to electron impact in the SIFT ion source at a pressure of ~ 10^{-3} Torr and the resultant ion at m/z = 45 was injected into the flow tube following mass selection. Based on the calculated proton affinity of vinyl alcohol (see Table 3.7) one might expect to observe collision rate proton transfer from the vinyloxonium cation to 4-fluorotoluene. However this was not the case. The rate coefficient observed for the ion formed via electron impact on n-butanol or 1,3-propanediol in reaction with 4-fluorotoluene and methanol ($k \leq 5 \times 10^{-10}$ cm^3 s^{-1}) was faster than the rate coefficient observed for $CH_3OCH_2^+$ with methanol ($k = 2 \times 10^{-11}$ cm^3 s^{-1}), so the ion is not $CH_3OCH_2^+$. The observed rate is not consistent with that observed for the fast reacting $C_2H_5O^+$ isomer with 4-fluorotoluene. It was therefore concluded that the ion formed in these experiments was either CH_3CHOH^+ or c-$CH_2(OH)CH_2^+$. This is perhaps not surprising given the very different conditions of our SIFT experiment from

those of the mass spectral measurements of Burgers et al. [169] Very high repeller energies were required in order to generate sufficient $C_2H_5O^+$ ion signal to measure a rate coefficient. The observed break-up of the ions upon injection into the helium carrier suggests sufficient energy was available to induce isomeric interconversion.

	Products	Branching ratio	k_{obs} /10^{-9} cm^3 s^{-1}	k_{coll}[a] /10^{-9} cm^3 s^{-1}	PA[b] /kJ mol^{-1}
H_3O^+ reactions					
C_7H_7F[c]	$C_7H_7FH^+ + H_2O$	1.0	2.9	3.2	763.8
C_2H_5Br	$C_2H_7O^+ + HBr$	~0.6	1.3	2.9	696.2
	$C_2H_5BrH^+ + H_2O$	~0.3			
	adduct	~0.1			
allene	$C_3H_5^+ + H_2O$	1.0	1.5	1.6	775.3[d]
c-C_6H_6	$C_6H_7^+ + H_2O$	1.0	1.5	1.9	750.4
HCO^+ reactions					
C_7H_7F	$C_7H_7FH^+ + CO$	1.0	2.9	2.7	763.8

Table 3.3. Reaction rate coefficients and product ratios for the reactions of H_3O^+ and HCO^+ with the specified reactants.

3.4 Ab initio studies.

An earlier investigation of the $C_2H_5O^+$ potential surface found four low-lying stable isomers, corresponding to local minima on the surface. [172,173] These isomers are CH_3CHOH^+ (protonated acetaldehyde), $CH_2CHOH_2^+$ (protonated vinyl alcohol), $CH_3OCH_2^+$ (methoxymethyl cation) and c-$CH_2(OH)CH_2^+$ (protonated oxirane). A re-examination of these structures and relevant neutral C_2H_5O isomers was reported by Curtiss et al. [174] A theoretical study of hydronium ion complexes with electron donors [175] also identified the existence of a hydronium ion/acetylene complex, $H_3O^+.C_2H_2$, which occupies an energy minimum on the $C_2H_5O^+$ potential energy surface. The present study

[a] Calculated using the method of Su and Chesnavich (ref. 161).
[b] Proton affinities are from ref. 164. [c] 4-fluorotoluene. [d] See section 4.4 for discussion.

aimed to re-examine the calculations of Nobes et al [172,173] at a higher level of theory and explore further reaction pathways for interconversion between $C_2H_5O^+$ isomers. All calculations were performed using the Gaussian 90 [176], Gaussian 92 [177] and Gaussian 94 [178] programs and followed the procedure detailed in the original description of the G2 procedure. [158] The structures of relevant $C_2H_5O^+$ species and transition states with geometric parameters calculated at the MP2/6-31G* level of theory are illustrated in Figures 3.4 and 3.5 respectively. The structures of C_2H_4O species and transition states are illustrated in Figure 3.6. The calculated energies of these structures are given in Tables 3.4 – 3.6. The calculated enthalpies of formation and proton affinities of the relevant C_2H_4O neutral species are listed in Table 3.7. The energies of the different $C_2H_5O^+$ isomers relative to $H_3O^+ + C_2H_2$ are shown in Figure 3.7.

3.4.1 A note about proton affinities.

The proton affinity (PA) of a neutral species, B, is defined as the negative of the enthalpy change for the process:

$$B + H^+ \longrightarrow BH^+; \Delta H^o = - x \text{ kJ mol}^{-1} \quad (3.34)$$

i.e. PA(B) = + x kJ mol^{-1}.

A G2 proton affinity at 0 K is determined simply as the difference between the G2 energies of the neutral B and the ion BH^+, viz.

$$PA_{0K}(B) = E_{G2,\,0K}(BH^+) - E_{G2,\,0K}(B) \quad (3.35)$$

At 298 K one must apply a correction of $\frac{5}{2}$ RT, which is comprised of the thermal energy of the proton at 298K ($\frac{3}{2}$ RT) plus ΔnRT, the work term, since the proton affinity represents an enthalpy change.

$$PA_{298K}(B) = E_{G2,\,298K}(BH^+) - E_{G2,\,298K}(B) + \tfrac{5}{2}RT \quad (3.36)$$

3.4.2 A note about enthalpies of formation.

The enthalpy of formation of a species, C, is calculated by adopting an equation for the formation of C, of

$$A + B \longrightarrow C \quad (3.37)$$

and utilising tabulated literature values for the enthalpies of formation of A and B, i.e.

$$E_{G2}(C) - E_{G2}(B) - E_{G2}(A) = \Delta_f H^o(C) - \Delta_f H^o(B) - \Delta_f H^o(A) \quad (3.38)$$

Substitution of the calculated G2 energies of C, B and A, and literature values for the enthalpies of formation of A and B into equation (3.38) yields $\Delta_f H^o(C)$.

3.4.3 $C_2H_5O^+$ radical cations.

1. CH_3CHOH^+ (I)

The 1-hydroxyethyl cation (protonated acetaldehyde) has a C_s structure with the methyl group eclipsed with respect to the C-O bond and HOCC trans. The MP2/6-31G* optimised structure is identical to that calculated by Bock et al [179] at the same level of theory, and is very similar to that calculated by Curtiss et al [174] at the MP2(FULL)/6-31G* level. The 1-hydroxyethyl cation is the most stable of the $C_2H_5O^+$ isomers considered here, in accord with the findings of Curtiss et al [174] and Nobes et al. [172] At the G2 level (0 K) this cation lies 237 kJ mol^{-1} below $H_3O^+ + C_2H_2$. Smith and Radom [180-183] have previously reported a G2 energy for CH_3CHOH^+.

2. $CH_3OCH_2^+$ (II)

The methoxymethyl cation has C_s symmetry and lies 72.4 kJ mol^{-1} higher in energy than protonated acetaldehyde, in excellent agreement with the value reported by Curtiss et al. [174]

3. $CH_2CHOH_2^+$ (III)

The vinyloxonium cation (protonated vinyl alcohol) has C_s symmetry and is very similar to the structures described by Curtiss et al [174] and by Nobes and Radom. [173] It is calculated to lie 97.8 kJ mol^{-1} higher in energy than protonated acetaldehyde, which is consistent with the value reported by Curtiss et al. [174] This structure was also studied theoretically by Marcoccia et al. [184]

4. c-$CH_2(OH)CH_2^+$ (IV)

Protonated oxirane (protonated ethylene oxide) has C_s symmetry and is identical to the structure identified by Bock et al. [179] At the G2 level this cation lies 116.4 kJ mol^{-1} above protonated acetaldehyde, in excellent agreement with the value reported by Curtiss et al. [174] If the O-H bond in protonated oxirane is constrained to lie in the plane of the ring, the resulting structure with C_{2v} symmetry represents the transition state for inversion

in protonated oxirane and the energy of TS IV/IV' relative to IV measures the inversion barrier. At the G2 level the inversion barrier is 64.0 kJ mol^{-1}, which is consistent with the value of 58.1 kJ mol^{-1} reported by Nobes et al. [172]

5. $H_3O^+.C_2H_2$ (V)

Formation of this π complex with C_s symmetry involves approach of the oxygen atom of H_3O^+ perpendicularly to the mid-point of the C-C triple bond in acetylene, with the formation of a hydrogen bond at the most basic site (i.e. at the centre of the double bond). This picture is in accord with the conclusions of an earlier study based on STO-3G calculations. [175] This structure is calculated to lie 78.7 kJ mol^{-1} below $H_3O^+ + C_2H_2$ and 158.3 kJ mol^{-1} above protonated acetaldehyde at the G2 level. The diagonalised Hessian matrix for this structure possesses all positive eigenvalues as is required for a genuine energy minimum. The calculations failed to identify any local minima corresponding to a structure possessing bifurcated geometry (i.e. with the H_3O^+ moiety straddling the C-C triple bond and forming two hydrogen bonds to acetylene). This conclusion is in agreement with the conclusions of Jones et al [175], who predicted that linear geometry is favoured over bifurcated.

3.4.4 $C_2H_5O^+$ transition states.

1. TS I/III

This structure represents a transition state for the rearrangement of protonated vinyl alcohol to protonated acetaldehyde and has C_1 symmetry. It is similar to the structure identified by Nobes et al. [172] The barrier to rearrangement lies 272.4 kJ mol^{-1} higher in energy than protonated acetaldehyde, which is somewhat lower than the value of 321 kJ mol^{-1} calculated by Nobes et al at the MP3/6-31G^{++}//RHF/4-31G level of theory. This transition state lies 35.4 kJ mol^{-1} above the energy of $H_3O^+ + C_2H_2$ at the G2 level.

2. TS II/IV

The saddle point linking protonated oxirane and the methoxymethyl cation has a C···O edge protonated oxirane structure, similar to that identified by Nobes et al. [172] This structure lies 238.1 kJ mol^{-1} above protonated oxirane at the G2 level of theory, which is in reasonable agreement with the best calculated barrier of Nobes et al (262 kJ mol^{-1}). [172]

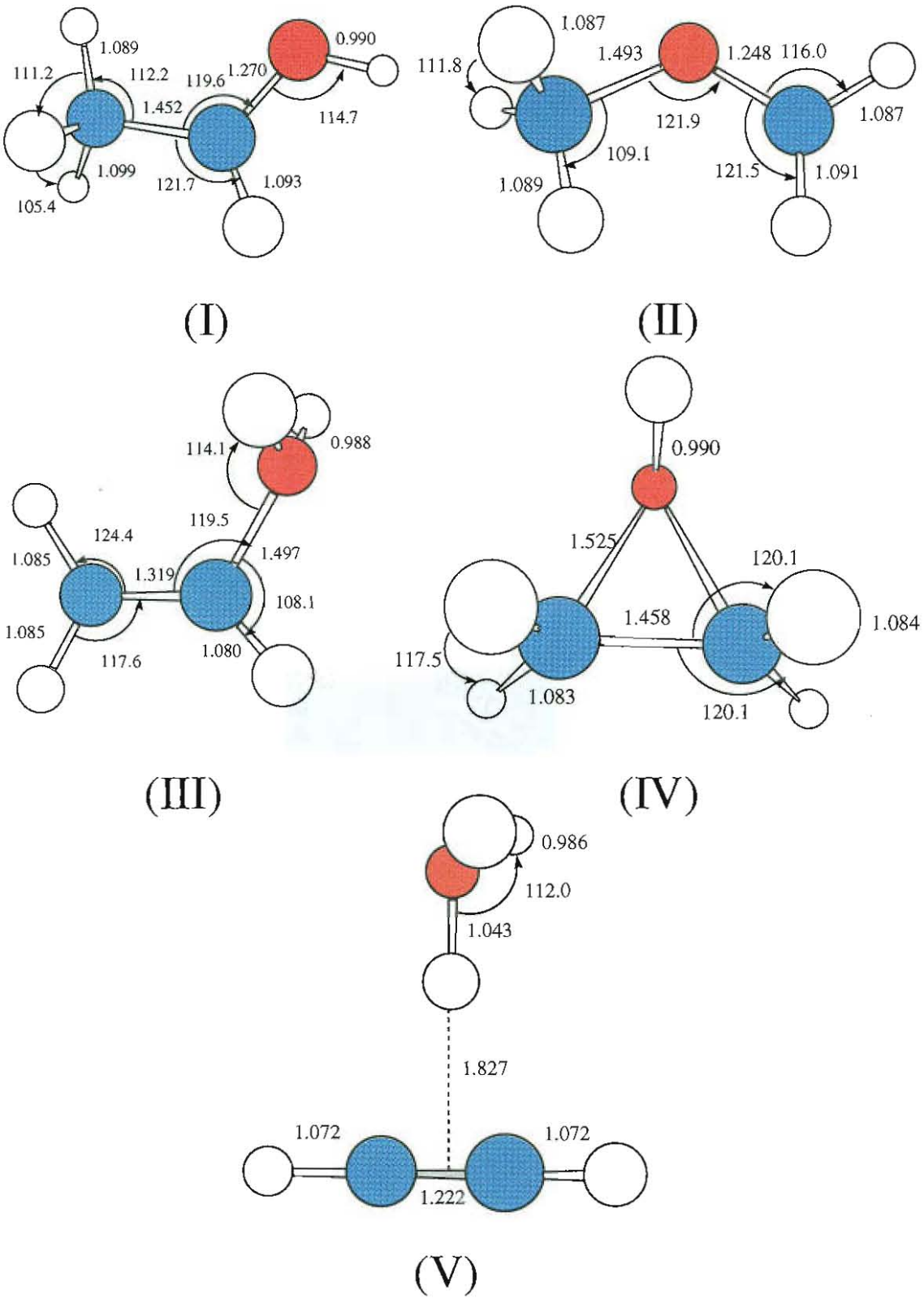

Figure 3.4. MP2/6-31G* optimised geometries of $C_2H_5O^+$ species with bond lengths in Å and bond angles in degrees.

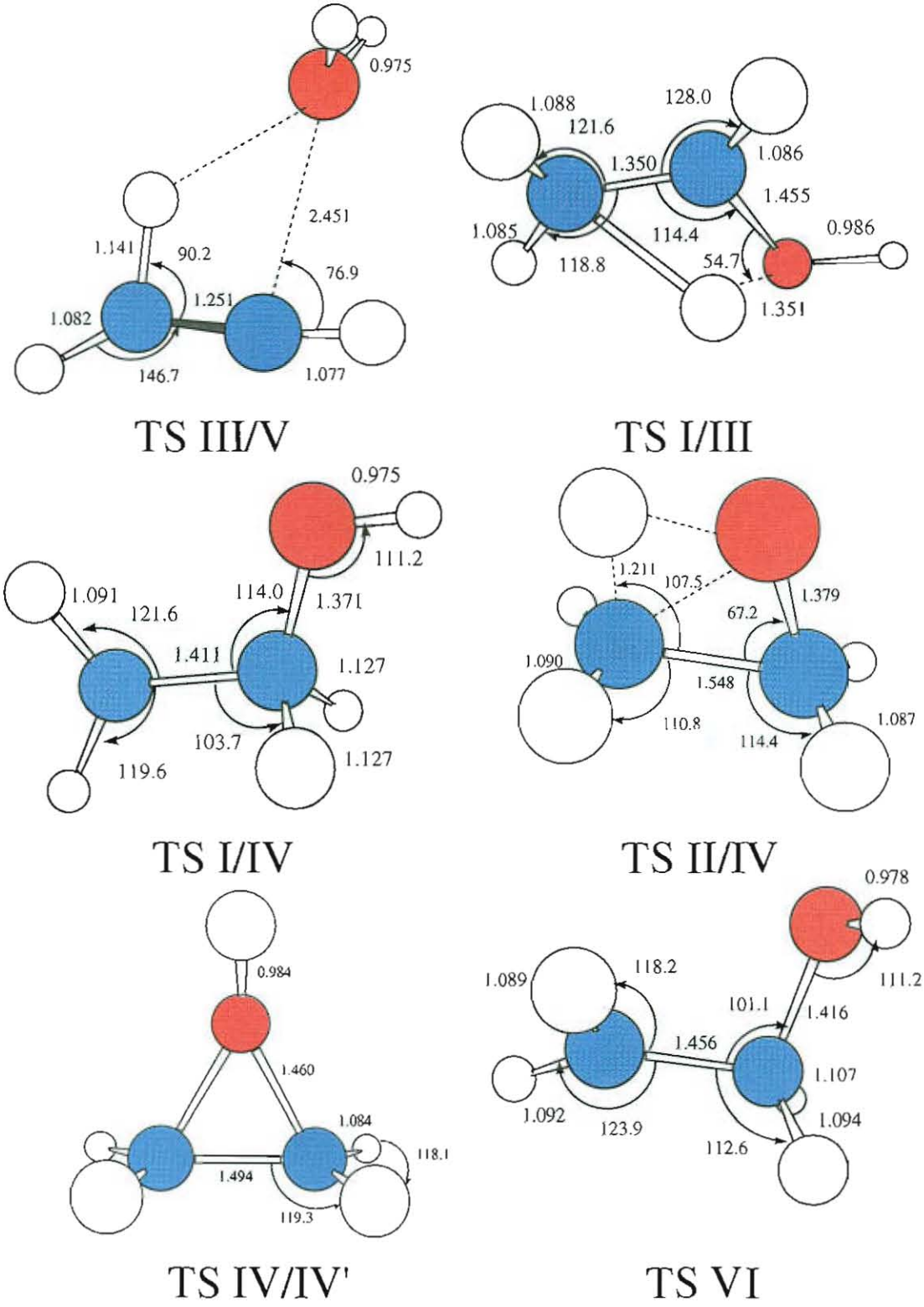

Figure 3.5. MP2/6-31G* optimised geometries of $C_2H_5O^+$ transtion states with bond lengths in Å and bond angles in degrees.

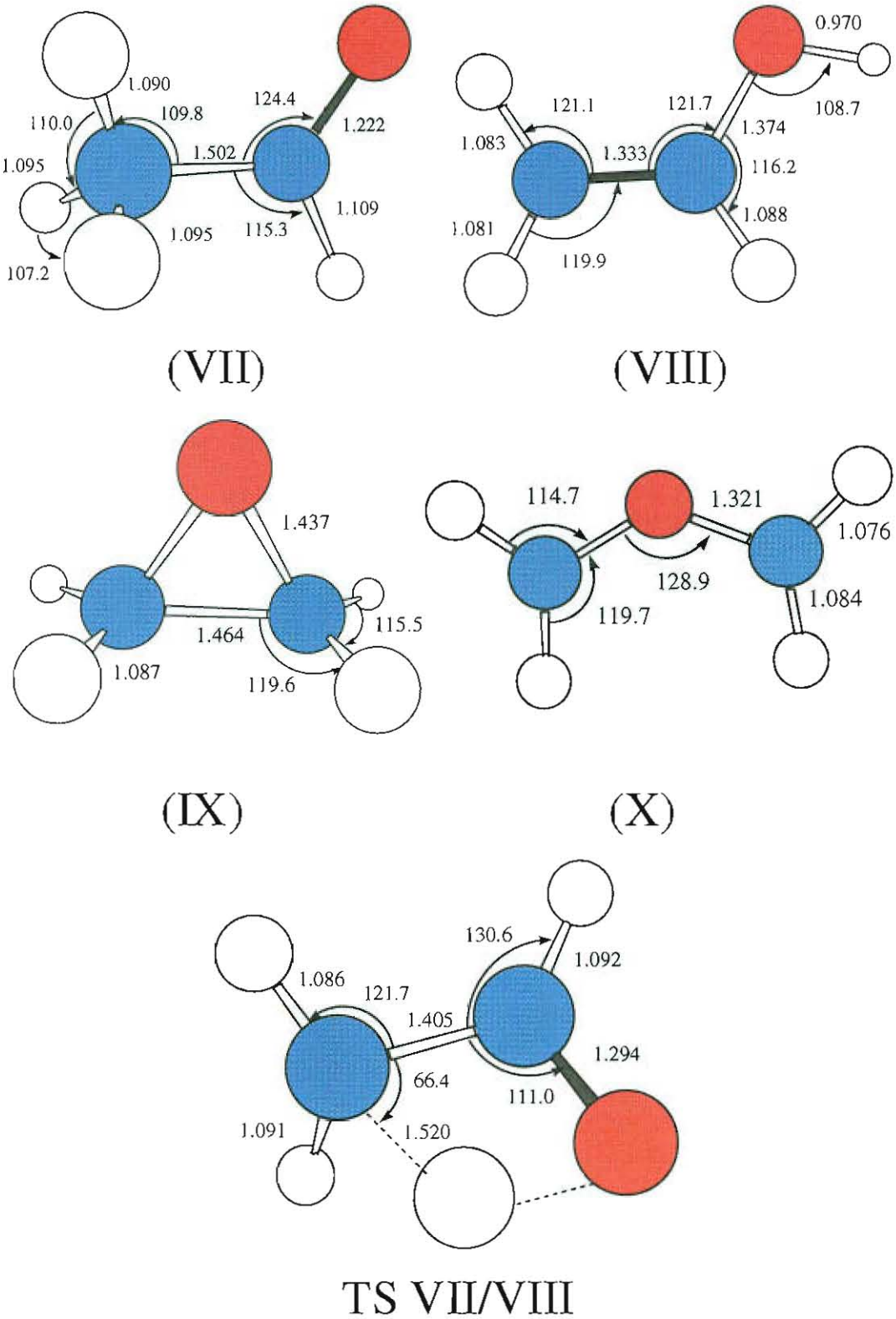

Figure 3.6. MP2/6-31G* optimised geometries of C_2H_4O isomers with bond lengths in Å and bond angles in degrees.

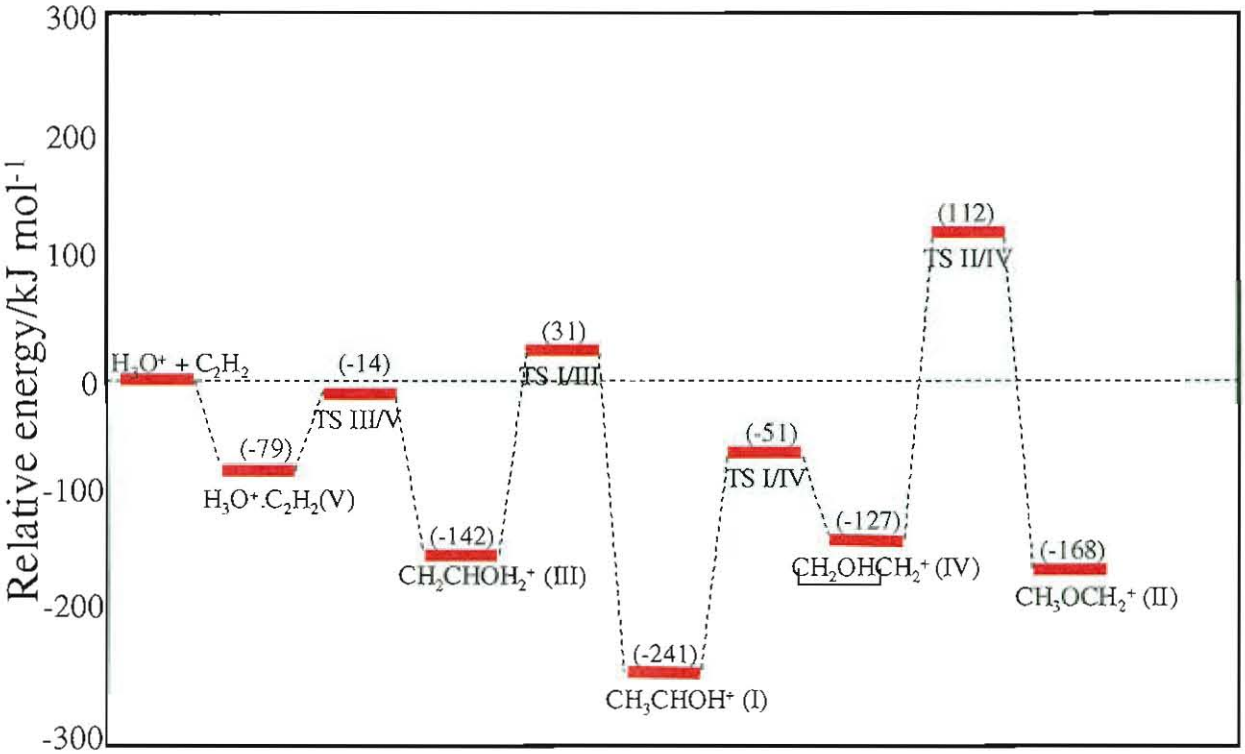

Figure 3.7. $C_2H_5O^+$ potential energy surface calculated using the G2 procedure. The energies are expressed in kJ mol^{-1} relative to $H_3O^+ + C_2H_2$ and are corrected to 298 K and for zero-point energy.

3. TS I/IV

The 1980 study by Nobes et al [172] identified the 2-hydroxyethyl cation as a genuine minimum on the STO-3G and 4-31G potential surfaces, although this was shown not to be the case at higher levels of theory. The present calculations indicate that this structure in fact represents a saddle point linking protonated acetaldehyde and protonated oxirane, in accord with the findings of Ford and Smith [185], Bock et al [179] and Curtiss et al. [174] This structure is identical to that identified by Bock et al [179] and is calculated to lie 47 kJ mol^{-1} below $H_3O^+ + C_2H_2$ and 190 kJ mol^{-1} above protonated acetaldehyde at the G2 level.

4. TS III/V

The transition state III/V resembles a loose association between a $C_2H_3^+$ cation and a water molecule which lies 15.6 kJ mol^{-1} below the energy of $H_3O^+ + C_2H_2$ at 0 K.

5. TS VI

The transition structure identified as a saddle point linking the 2-hydroxyethyl cation and protonated oxirane in the study of Nobes et al [172] (structure 20) was also identified as a transition state in the present work. The HF/6-31G* and MP2/6-31G* optimised geometries for structure VI both possess one imaginary vibrational frequency, indicating the structure represents a genuine saddle point on the $C_2H_5O^+$ hypersurface. Structure VI lies just 5.8 kJ mol^{-1} below the energy of $H_3O^+ + C_2H_2$ at the G2 level of theory.

3.4.5 C_2H_4O neutral structures.

The MP2/6-31G* optimised structures of neutral acetaldehyde, vinyl alcohol (anti conformation, the syn conformation is expected to be more stable by a few kJ mol^{-1} [186-190]) and oxirane are illustrated in Figure 3.5. Vinyl alcohol and oxirane are respectively 50.2 and 115.4 kJ mol^{-1} above the energy of acetaldehyde. The energy separation between vinyl alcohol and acetaldehyde is in good agreement with that determined by Smith et al [189] (47 kJ mol^{-1}), Bouma et al [187] (45 kJ mol^{-1}) and an experimental value of 41 ± 8 kJ mol^{-1}. [191] Similarly, the energy difference between acetaldehyde and oxirane is in good agreement with the value of 114 kJ mol^{-1} reported by Bouma et al. [187] A planar CH_2OCH_2 structure possessing C_{2v} symmetry was also identified as a minimum on the C_2H_4O potential surface (all positive eigenvalues in the force constant matrix). This is in contrast with the findings of Yamaguchi et al [192] who identified the planar CH_2OCH_2 structure as a higher order stationary point possessing a Hessian index of 2 in a combined TCSCF/CISD study of the ring opening reaction of oxirane. The C_{2v} CH_2OCH_2 structure has a calculated proton affinity with respect to the methoxymethyl cation of 992 kJ mol^{-1}. This may explain the non-observation of proton transfer to trimethyl amine (PA = 942 kJ mol^{-1}) in a SIFT study of $CH_3OCH_2^+$ reactions. [171] Okada et al [193] have proposed, however, that proton transfer from $CH_3OCH_2^+$ will lead to the formation of the cyclic neutral oxirane, a process which is predicted to possess a sizeable barrier associated with the closure of the ring. The saddle point linking acetaldehyde and vinyl alcohol is calculated to lie 283 kJ mol^{-1} above acetaldehyde at the G2 level (our G1 value of 282 kJ mol^{-1} agrees exactly with that determined by Smith et al [189]).

3.5 Discussion.

The flow tube measurements show that the $C_2H_5O^+$ species formed in the association reaction between H_3O^+ and C_2H_2 (reaction 3.4) is a mixture of $C_2H_5O^+$ isomers. The more reactive isomer accounts for up to 75% of the total $C_2H_5O^+$ signal. Furthermore the rate coefficient observed for the reaction of the fast reacting isomer with ethyl bromide, benzene and 4-fluorotoluene is significantly faster than that observed for the reactions of CH_3CHOH^+, c-$C_2H_5O^+$ and $CH_3OCH_2^+$ with the same neutrals. Some of our earlier observations (Appendix II) regarding the H_3O^+/C_2H_2 association reaction appear to be erroneous, and, in the light of a careful re-examination of the system in the FA-SIFT, our conclusions should be reconsidered. What is apparent is that a mixture of $C_2H_5O^+$ isomers ***is*** produced in the association reaction (3.4). Furthermore, the rate coefficients obtained from double exponential fits to the curved decays observed in the reactions of $C_2H_2.H_3O^+$ with C_2H_5Br, C_6H_6 (see Figure 3.3) and 4-fluorotoluene indicate that the ***fast reacting species*** is an isomer different from CH_3CHOH^+, c-$C_2H_5O^+$ and $CH_3OCH_2^+$. The consistent linearity observed in the semilogarithmic decays for the reactions of $H_3O^+.C_2H_2$ with CH_3OH, allene and 2-fluorotoluene indicates that the observed curvature is not an artifact due to an extended source of $C_2H_5O^+$ in the flow tube. Both of the $C_2H_5O^+$ species formed in reaction (3.4) appear to undergo collision rate proton transfer to 2-fluorotoluene (PA = 773.3 kJ mol^{-1}). Only the fast reacting isomer undergoes collision rate proton transfer to 4-fluorotoluene (PA = 763.8 kJ mol^{-1}). The observed rate coefficients obtained from the linear semilogarithmic decays for the reactions of $C_2H_2.H_3O^+$ with allene and methanol are not consistent with exothermic proton transfer, which should proceed at the collision rate, remembering that low energy proton transfer to allene generates the 2-propenyl cation (chapter 4.4). Thus the proton affinity of the fast reacting $C_2H_5O^+$ isomer is bracketed between that of 4-fluorotoluene (763.8 kJ mol^{-1}) and methanol (754.3 kJ mol^{-1}). This range is consistent with the proton affinity calculated for the electrostatic $H_3O^+.C_2H_2$ complex (763.5 kJ mol^{-1}, Table 3.7). Further, the product ion observed at m/z = 59 in the reaction of $C_2H_2.H_3O^+$ with allene is consistent with a simple ligand switch ($H_3O^+.C_2H_2 \longrightarrow H_3O^+.C_3H_4$), favouring the electrostatic complex structure.

Species	MP4/6-311G**	ΔE(+)	ΔE(2df)	ΔE(QCI)	ΔE(HLC)	ΔE(ZPE)	E(G1)
H_3O^+	-76.56181	-1.46	-33.42	-0.20	-24.56	32.80	-76.58865
C_2H_2	-77.13994	-1.92	-39.92	+0.18	-30.70	26.29	-77.18601
I	-153.79470	-3.14	-76.13	-0.21	-55.26	65.76	-153.86368
II	-153.76753	-3.17	-75.99	-0.07	-55.26	66.22	-153.83580
III	-153.75565	-3.68	-75.87	-1.34	-55.26	64.86	-153.82694
IV	-153.75140	-3.51	-76.55	+0.22	-55.26	67.77	-153.81873
V	-153.73167	-3.60	-74.64	+0.33	-55.26	60.75	-153.80408
TS I/III	-153.68234	-4.31	-78.25	-0.10	-55.26	60.10	-153.75995
TS I/IV	-153.71179	-6.16	-77.64	-2.94	-55.26	62.12	-153.79166
TS II/IV	-153.65473	-4.00	-77.34	+1.00	-55.26	61.83	-153.72851
TS IV/IV'	-153.72337	-4.31	-76.90	-0.19	-55.26	65.26	-153.79478
TS III/V	-153.70004	-7.01	-73.74	-2.02	-55.26	57.34	-153.78074
TS VI	-153.69806	-5.80	-75.97	-3.84	-55.26	63.66	-153.77527
VII	-153.48768	-7.13	-79.31	+1.79	-55.26	53.51	-153.57408
VIII	-153.46287	-8.82	-81.35	-0.37	-55.26	54.00	-153.55466
IX	-153.44089	-8.33	-81.92	+1.01	-55.26	55.62	-153.52977
X	-153.36703	-6.94	-82.50	+1.57	-55.26	51.45	-153.45871
TS VII/VIII	-153.37325	-7.69	-81.58	+2.74	-55.26	48.40	-153.46664

Table 3.4. G1 energies and corrections.[‡]

[‡] Energies in hartrees, corrections in millihartrees.

Structure	Δ	Σ thermal energies	E(G2) 298 K /hartrees	ΔE(G2) 298 K /kJ mol^{-1}
H_3O^+	-7.84	39.62	-76.58905	
C_2H_2	-5.42	32.08	-77.18310	
$H_3O^+ + C_2H_2$			-153.77215	0.0
$H_3O^+.C_2H_2$ (V)	-13.82	73.54	-153.80214	-78.8
CH_3CHOH^+ (I)	-14.52	77.63	-153.86396	-241.0
$CH_3OCH_2^+$ (II)	-14.83	78.21	-153.83632	-168.5
$CH_2CHOH_2^+$ (III)	-14.02	76.96	-153.82637	-142.4
c-$C_2H_5O^+$ (IV)	-15.17	79.12	-153.82041	-126.7
TS III/V	-13.13	70.46	-153.77737	-13.7
TS I/III	-14.49	71.00	-153.76049	+30.6
TS I/IV	-14.17	73.34	-153.79181	-51.6
TS II/IV	-14.69	72.56	-153.72962	+111.6
TS V/V'	-14.73	76.32	-153.79600	-62.6
TS VI	-14.85	74.93	-153.77624	-10.7

Table 3.5. G2 energies and corrections for $C_2H_5O^+$ species.[‡]

Structure	Δ	Σ thermal energies	E(G2) 298 K /hartrees
CH_3CHO (VII)	-13.03	63.75	-153.57303
CH_2CHOH (VIII)	-13.29	64.32	-153.55386
c-C_2H_4O (IX)	-13.37	65.33	-153.52984
CH_2OCH_2 (X)	-13.95	61.43	-153.45859
TS VII/VIII	-12.57	57.48	-153.46568

Table 3.6. G2 energies and corrections for C_2H_4O species.[‡]

[‡] Energies in hartrees, corrections in millihartrees.

Structure	ΔH_f^o (kJ mol^{-1})		Proton affinity (kJ mol^{-1})	
	calculated	experiment[a]	calculated[b]	experiment
CH_3CHO	-173.2	-165.8	770.0	768.5[a], ≥769[c], 768[d]
CH_2CHOH	-122.9	-125	721.7	
oxirane	-59.8	-52.6	769.1	774.2[a]
CH_2OCH_2	127.3		998.0	
$H_2O + C_2H_2$			763.5	

Table 3.7. Calculated enthalpies of formation and proton affinities of C_2H_4O isomers in kJ mol^{-1}.

If our calculated value for the proton affinity of vinyl alcohol is significantly in error (i.e. low by ~30 kJ mol^{-1}) then the vinyloxonium cation cannot be dismissed as a possibility for the fast reacting isomer either. We earlier concluded that the fast reacting isomer ***is*** the vinyloxonium cation. However, this was based on apparently erroneous rate determinations for the reactions of $C_2H_2.H_3O^+$ with CH_3OH and allene and the assumption that the fast reacting isomer underwent collision rate proton transfer to C_2H_5Br (which was also incorrectly assumed to possess a proton affinity of ~ 715 kJ mol^{-1}). Efforts to form the vinyloxonium cation, and probe its reactivity directly, proved unsuccessful (see section 3.3.5). The question of the less reactive isomer present in the mixture of isomers formed in reaction (3.4), identified by its slower reactivity with the neutral reagents C_2H_5Br, C_6H_6 (see Figure 3.3) and 4-fluorotoluene, is not so easily answered. Clearly, $CH_3OCH_2^+$ can be eliminated based on its much slower reaction with methanol ($k = 2 \times 10^{-11}$ cm^3 s^{-1}) than that observed for the isomeric ions formed in reaction (3.4). This is entirely consistent with the calculated potential energy surface (Figure 3.7). Formation of $CH_3OCH_2^+$ would require rearrangement via the cyclic protonated oxirane structure and the transition state linking protonated oxirane and the

[a] Experimental values are from ref. 163.
[b] Calculated proton affinities at 298K at the G2 level of theory.
[c] Value from ref. 194.
[d] Value from ref. 195.

methoxymethyl cation lies well above the energy of $H_3O^+ + C_2H_2$. Similarly the transition state linking protonated vinyl alcohol and protonated acetaldehyde lies above the energy of $H_3O^+ + C_2H_2$, which would suggest that CH_3CHOH^+ is unlikely to be energetically accessible from the reactants. Therefore protonated oxirane is also unlikely to be energetically accessible from $H_3O^+ + C_2H_2$, since, as Figure (3.7) shows, the formation of protonated oxirane requires rearrangement via CH_3CHOH^+. A low energy pathway directly linking the vinyloxonium cation and protonated oxirane may exist, however efforts to find one computationally proved unsuccessful. Also, as described above, protonated oxirane exhibits a very distinct reaction chemistry, with elimination of a water molecule occurring as the major reaction channel in reaction with the three neutral reagents: methanol, benzene and 4-fluorotoluene. Product ions corresponding to the loss of a water molecule were not observed in the reactions of $H_3O^+.C_2H_2$ with these three reagents despite careful adjustment of the acetylene and neutral reagent flow rates. However, if the fast reacting isomer is indeed the electrostatic complex then the slower reacting isomer is unlikely to be the vinyloxonium cation since this isomer should undergo collision rate proton transfer to methanol and allene based on the calculated proton affinity of vinyl alcohol, which was not observed.

This interpretation would therefore favour identification of the slow reacting isomer as protonated oxirane or protonated acetaldehyde, and suggest that there ***is*** a low energy barrier for the rearrangement to one of these isomers. Indeed protonated oxirane undergoes a similar reaction with acetylene to that observed from one or both of the $C_2H_2.H_3O^+$ isomers with C_2H_2. If the faster reacting isomer is the vinyloxonium cation then the calculated potential surface would tend to favour identification of the slower reacting isomer as the electrostatic complex. Let us compare this with the analogous reaction of H_3O^+ with C_2H_4 discussed in the next section. In both reactions linear $H_3O^+\cdots X$ ($X = C_2H_2$ or C_2H_4) complexes are formed which have similar stabilities with respect to reactants. These complexes can rearrange via analogous transition states to $CH_2CHOH_2^+$ and $C_2H_5OH_2^+$ respectively. The barrier between reactants and $CH_2CHOH_2^+$ or $C_2H_5OH_2^+$ is calculated to lie 14 kJ mol^{-1} below reactants in the H_3O^+/C_2H_2 system and 52 kJ mol^{-1} below reactants in the H_3O^+/C_2H_4 system. Provided

interconversion across the isomerisation barrier is rapid compared to the timescale for collisional relaxation the isomeric ratio would be expected to be determined by the density of states ratio at the energy of the isomerisation barrier (see the discussion in chapter 4 of Petrie's thesis [140]). This ratio will favour the ion-neutral complex to a greater extent in the H_3O^+/C_2H_2 system than in the H_3O^+/C_2H_4 system given the larger barrier height in the former. The difference in calculated barrier heights of ~ 40 kJ mol^{-1} could conceivably lead to a large difference in the density of states ratio at the height of the barrier in the two systems. This difference could also explain the observation of a single isomer in the H_3O^+/C_2H_4 system (see the discussion in the following section) but a mixture of isomers in the H_3O^+/C_2H_2 system.

3.6 Conclusions.

The results of this study clearly demonstrate that at least two isomeric species are formed in the association reaction between H_3O^+ and C_2H_2. The two species undergo reaction with the neutral reagents: ethyl bromide, benzene and 4-fluorotoluene at distinctly different rates. Further the observed rate coefficient for the faster reacting species allows us to conclude that it is an isomer different from protonated acetaldehyde (CH_3CHOH^+), protonated oxirane (c-$C_2H_5O^+$), or the methoxymethyl cation ($CH_3OCH_2^+$) which all react more slowly (see Table 3.1). The two candidate structures for the faster reacting species formed in reaction 3.4 are the vinyloxonium cation (protonated vinyl alcohol, $CH_2CHOH_2^+$) or the electrostatic complex, $H_3O^+.C_2H_2$. If the faster reacting isomer is the former then calculations performed on the $C_2H_5O^+$ potential energy surface favour identification of the slower reacting isomer as the electrostatic complex, since the barrier to rearrangement of the electrostatic complex to the vinyloxonium cation lies below the energy of the reactants ($H_3O^+ + C_2H_2$). If the faster reacting isomer is the electrostatic complex, then the slower reacting isomer is likely to be either protonated acetaldehyde or protonated oxirane. This conclusion is not supported by the ab initio calculations as no pathways below the energy of the reactants were identified between the $H_3O^+.C_2H_2$ complex and either protonated acetaldehyde or protonated oxirane. Either way, our results differ from the conclusions of Jarrold et al [166] who examined the product of the association reaction (3.4) using the technique of CID. They concluded that the

likely product of the association was either CH_3CHOH^+ or c-$C_2H_5O^+$. Their conclusions must now be modified, however, as they did not consider protonated vinyl alcohol as a possible structure, or consider the possibility of an ion-neutral complex.

In the SIFT experiments the $C_2H_5O^+$ product ions of the H_3O^+/C_2H_2 association reaction are stabilised by collision with the bath gas. At interstellar cloud pressures, however, the $(C_2H_5O^+)^*$ complex formed in the association process is stabilised by photon emission. Although these two stabilising mechanisms differ, it is unlikely that the outcomes of the different stabilising mechanisms will result in different structures. If reaction 3.1 followed by dissociative electron-ion recombination is responsible (at least in part) for the formation of vinyl alcohol in the interstellar medium, then efforts to detect vinyl alcohol in dense interstellar clouds may prove worthwhile. Indeed, the large calculated barrier separating vinyl alcohol and acetaldehyde had earlier prompted suggestions that vinyl alcohol may be an observable interstellar molecule. [188]

3.7 Ion-molecule association of H_3O^+ and C_2H_4: Interstellar ethanol

Ethanol, like acetaldehyde has been observed in interstellar clouds, and although it is not observed in cold, dark clouds, it is present in appreciable abundances, in, or near, so-called hot molecular cores, the regions where new stars are formed. [196-199] There are at least two such regions in the giant molecular cloud Sagittarius B2, SgrB2(M) and SgrB2(N). Studies have shown that both SgrB2(M) and SgrB2(N) contain regions of high molecular hydrogen column density ($>10^{24}$ cm^{-2}), high gas temperature (>150 K) and high density ($>10^6$ cm^{-3}). [200] Ethanol was first detected in SgrB2 by Zuckerman et al. [201] Recent detection of interstellar ethanol has been made by Ohishi et al [202] towards Orion KL, where rotational transitions from the gauche substates of ethanol have also been observed. [199]

Model calculations have used both gas-phase and heterogeneous reactions on grain surfaces, as sources of C_2H_5OH in the ISM. [167,198,203,204] Among the gas phase reactions considered in the models are the ion-molecule association reactions:

$$CH_3^+ + CH_3OH \longrightarrow (CH_3)_2OH^+ + h\nu \qquad \textbf{(3.39a)}$$

$$\longrightarrow C_2H_5OH_2^+ + h\nu \qquad \textbf{(3.39b)}$$

$H_3O^+ + C_2H_4 \longrightarrow C_2H_5OH_2^+ + h\nu$ **(3.40)**

C_2H_5OH has been assumed in the models to be formed from $C_2H_5OH_2^+$ via a dissociative electron-ion recombination reaction step.

$C_2H_5OH_2^+ + e \longrightarrow C_2H_5OH + H$ **(3.41)**

As in the reaction of H_3O^+ with C_2H_2, the possibility of several isomeric structures for the association product exists and again it is not immediately obvious which structure will be formed in the association reaction. Stable isomers corresponding to minima on the $C_2H_7O^+$ potential energy surface include the well characterised ions $C_2H_5OH_2^+$ (protonated ethanol) and $(CH_3)_2OH^+$ (protonated dimethyl ether), plus the possibility also exists of electrostatic-type complexes ($C_2H_4\cdots H\cdots OH_2^+$ and $CH_3^+\cdots HOCH_3$) being formed. Jarrold et al [166] examined the collision-induced dissociation (CID) spectra of $C_2H_5OH_2^+$ and $(CH_3)_2OH^+$ and concluded that the association product of reaction 3.39 has predominantly the $(CH_3)_2OH^+$ structure while the product of reaction 3.40 produces predominantly the $C_2H_5OH_2^+$ structure. In this study we investigated the structure of the ion formed in the termolecular analogue of reaction (3.40) by comparing the proton transfer behavior of the association ion with that of $C_2H_5OH_2^+$ and $(CH_3)_2OH^+$ using the neutral reagents 2-fluorotoluene and acrylonitrile, which were selected on the basis of their known proton affinities. An ab initio study of the $C_2H_7O^+$ potential energy surface was also performed to assist in the interpretation of the experiments.

3.7.1. Experimental.

The experiments were performed in a helium bath gas using the SIFT apparatus operating at (300 ± 5) K. The $C_2H_7O^+$ ions investigated in this work were formed in the following ways. The product of the association reaction 3.42b, which is designated $H_3O^+.C_2H_4$, was formed in the flow tube by introducing H_3O^+ (formed via electron impact on water vapour in a high pressure ion source) into a stream of C_2H_4 added at the first inlet port.

$H_3O^+ + C_2H_4 \longrightarrow C_2H_5^+ + H_2O$ **(3.42a)**

$\longrightarrow H_3O^+.C_2H_4$ **(3.42b)**

The association reaction occurs in parallel with the slightly endothermic bimolecular proton transfer channel. Sufficient C_2H_4 was added to remove >99% of the H_3O^+ ion

signal. At this flow of ethylene $C_2H_5^+$ reacts further to produce predominantly $(C_2H_4)_2H^+$ and $C_5H_9^+$, via the reactions:

$$C_2H_5^+ + C_2H_4 \longrightarrow (C_2H_4)_2H^+ \quad \textbf{(3.43a)}$$

$$\longrightarrow C_3H_5^+ + CH_4 \quad \textbf{(3.43b)}$$

$$C_3H_5^+ + C_2H_4 \longrightarrow C_5H_9^+ \quad \textbf{(3.44)}$$

Neither of the two ions ($C_4H_9^+$ or $C_5H_9^+$) reacted at significant rates with acrylonitrile or 2-fluorotoluene. The rate coefficient measured for reaction (3.42) was 8.4 x 10^{-11} cm^3 s^{-1} with a branching ratio of 30% $H_3O^+.C_2H_4$ and 70% $C_2H_5^+$, which is in fair agreement with the results of Bohme and Mackay [205] (k = 9 x 10^{-11} cm^3 s^{-1}, 40% $H_3O^+.C_2H_4$ in a H_2 bath gas at 0.5 Torr) and Matthews et al [206] (k = 7.8 x 10^{-11} cm^3 s^{-1}, 35% $H_3O^+.C_2H_4$). The agreement with the results of McIntosh et al [207] is less good (k = 1 x 10^{-10} cm^3 s^{-1}, 60% $H_3O^+.C_2H_4$ at 0.45 Torr He). Their quoted branching ratio suggests an effective termolecular association rate coefficient of 4.1 x 10^{-27} cm^6 s^{-1} which is nearly twice the value determined in the present work ($k_3eff = k_2/[He]$ = 2.2 x 10^{-27} cm^6 s^{-1}). It should be noted however that McIntosh et al [168] re-examined the termolecular association of H_3O^+ with C_2H_4 in a later study obtaining a k_3 value of 2 x 10^{-27} cm^6 s^{-1} in a He bath gas at 300 K which is in excellent agreement with the present determination.

The $C_2H_5OH_2^+$ ion was formed via electron impact on pure ethanol vapour in a high pressure ion source. Alternatively the ion was formed in the flow tube by injecting $HCNH^+$(from HCN in a high pressure source) into a stream of ethanol vapour added at the first neutral inlet. This technique circumvented the problem of collision-induced dissociation of $C_2H_5OH_2^+$ (to $H_3O^+ + C_2H_4$) following injection into the He bath gas which was observed even at relatively low injection energies. $(CH_3)_2OH^+$ was formed similarly via electron impact on $(CH_3)_2O$ in a high pressure ion source.

3.8 Results.

The reactions of $H_3O^+.C_2H_4$, $C_2H_5OH_2^+$ and $(CH_3)_2OH^+$ were examined with the neutral reagents 2-fluorotoluene (C_7H_7F) and acrylonitrile (CH_2CHCN). These reagents were selected on the basis of their known proton affinities, which are: C_7H_7F

(PA = 773.3 kJ mol^{-1}); CH_2CHCN (PA = 784.7 kJ mol^{-1}). Both reagents have proton affinities which are close to or intermediate between that of ethanol (PA = 776.4 kJ mol^{-1}) and dimethyl ether (PA = 792.0 kJ mol^{-1}).

3.8.1 $H_3O^+.C_2H_4$ reactions.

The $H_3O^+.C_2H_4$ association ion underwent proton transfer to both 2-fluorotoluene and acrylonitrile in competition with a termolecular association channel in each case. Termolecular association is often observed to compete with proton transfer when proton transfer is close to thermoneutral.

$$H_3O^+.C_2H_4 + C_7H_7F \xrightarrow{0.65} C_7H_8F^+ + C_2H_6O \quad \textbf{(3.45a)}$$

$$\xrightarrow{0.35} \text{adduct} \quad \textbf{(3.45b)}$$

$k_{3,45} = 5.4 \times 10^{-10}$ cm^3 s^{-1}

$$H_3O^+.C_2H_4 + CH_2CHCN \xrightarrow{0.40} CH_2CHCNH^+ + C_2H_6O \quad \textbf{(3.46a)}$$

$$\xrightarrow{0.60} \text{adduct} \quad \textbf{(3.46b)}$$

$k_{3,46} = 3.2 \times 10^{-9}$ cm^3 s^{-1}

$H_3O^+.C_2H_4$ was also reacted with the neutral methanol; the only product channel observed was termolecular association.

$$H_3O^+.C_2H_4 + CH_3OH \xrightarrow{1.0} \text{adduct} \quad \textbf{(3.47)}$$

$k_{3,47} = 6.9 \times 10^{-10}$ cm^3 s^{-1}

Matthews et al [206] report a value of $k_{3,47} = 8.1 \times 10^{-10}$ cm^3 s^{-1}, measured at a helium pressure of 0.5 Torr.

3.8.2 $C_2H_5OH_2^+$ reactions.

$C_2H_5OH_2^+$ was also observed to undergo both proton transfer and termolecular association with 2-fluorotoluene and acrylonitrile.

$$C_2H_5OH_2^+ + C_7H_7F \xrightarrow{0.70} C_7H_8F^+ + C_2H_5OH \quad \textbf{(3.48a)}$$

$$\xrightarrow{0.30} \text{adduct} \quad \textbf{(3.48b)}$$

$k_{3,48} = 4.3 \times 10^{-10}$ cm^3 s^{-1}

$$C_2H_5OH_2^+ + CH_2CHCN \xrightarrow{0.50} CH_2CHCNH^+ + C_2H_5OH \quad \textbf{(3.49a)}$$

$$\xrightarrow{0.50} \text{adduct} \quad \textbf{(3.49b)}$$

$k_{3,49} = 3.2 \times 10^{-9}$ cm^3 s^{-1}

3.8.3 $(CH_3)_2OH^+$ reactions.

The only product channel observed in both of the reactions of $(CH_3)_2OH^+$ was termolecular association.

$(CH_3)_2OH^+ + C_7H_7F \xrightarrow{1.0}$ adduct **(3.50)**

$k_{3.50} = 1.9 \times 10^{-10}$ cm^3 s^{-1}

$(CH_3)_2OH^+ + CH_2CHCN \xrightarrow{1.0}$ adduct **(3.51)**

$k_{3.51} = 2.3 \times 10^{-9}$ cm^3 s^{-1}

A summary of the experimental results is presented in Table 3.8.

Reactant	Products	Branching ratio	k_{obs} /10^{-9} cm^3 s^{-1}	k_{coll}[a] /10^{-9} cm^3 s^{-1}
		$H_3O^+.C_2H_4$		
CH_3OH	adduct	1.0	0.69	2.1
C_7H_7F[b]	$C_7H_8F^+ + C_2H_5OH$[c]	0.65	0.54	1.9
	adduct	0.35		
CH_2CHCN	$CH_2CHCNH^+ + C_2H_5OH$[c]	0.40	3.2	3.8
	adduct	0.60		
		$C_2H_5OH_2^+$		
C_7H_7F[b]	$C_7H_8F^+ + C_2H_5OH$	~0.70	0.43	1.9
	adduct	~0.30		
CH_2CHCN	$CH_2CHCNH^+ + C_2H_5OH$	0.50	3.2	3.8
	adduct	0.50		
		$(CH_3)_2OH^+$		
C_7H_7F	adduct	1.0	0.19	1.9
CH_2CHCN	adduct	1.0	2.3	3.8

Table 3.8 Reaction rate coefficients and product ratios with the specified reagent for the three $C_2H_7O^+$ ions: $H_3O^+.C_2H_4$, protonated ethanol, $C_2H_5OH_2^+$, and protonated dimethyl ether, $(CH_3)_2OH^+$.

[a] Calculated using the method of Su and Chesnavich (ref. 161). [b] 2-fluorotoluene. [c] See text for discussion.

3.8 Ab initio studies.

Two isomers of $C_2H_7O^+$, protonated ethanol, $C_2H_5OH_2^+$, and protonated dimethyl ether, $(CH_3)_2OH^+$, have been well characterised and identified experimentally as distinct isomeric species that retain their identities under a wide range of conditions. Their enthalpies of formation have been determined. [163,164] The $C_2H_7O^+$ potential surface was estimated by Jarrold et al [166] in their CID study. The potential surface has been partially calculated by Herbst [167] and by Radom [208]. Bouchoux and Hoppilliard [209] in an ab initio study characterised an electrostatic complex $C_2H_4\cdots H\cdots OH_2^+$ that is readily accessible from $C_2H_5OH_2^+$. Recently Audier et al [210] also identified an electrostatic complex $CH_3^+\cdots HOCH_3$ formed from the association of CH_3^+ and CH_3OH , which they predicted to be separated by a small potential barrier from $(CH_3)_2OH^+$. Previous ab initio studies of the proton affinities of dimethyl ether [180,181,183,211] and ethanol [212] have been reported.

Four stable $C_2H_7O^+$ species corresponding to minima on the potential energy surface were identified in the present study using the G2 procedure. These structures, in order of decreasing stability are: protonated ethanol, protonated dimethyl ether, and the electrostatic complexes $C_2H_4\cdots H\cdots OH_2^+$ and $CH_3^+\cdots HOCH_3$.

Formation of the $H_3O^+.C_2H_4$ electrostatic π complex involves approach of the oxygen atom of H_3O^+ towards the midpoint of the C-C double bond with the formation of a single hydrogen bond directed toward the centre of the double bond (i.e. the most basic site). The calculations failed to identify any local minima corresponding to a hydrogen-bonded complex possessing bifurcated geometry. Jones et al [213] also concluded that linear geometry is favoured over bifurcated.

The transition state resembles a loose association between a classical $C_2H_5^+$ ion and a water molecule. Collision complexes with sufficient excitation may dissociate to $C_2H_5^+ + H_2O$ (reaction 3.42a); this proton transfer is calculated to be 7 kJ mol^{-1} endothermic. Complexes below this threshold can either dissociate back to reactants or be stabilized to form $C_2H_5OH_2^+$, which lies 136 kJ mol^{-1} below the reactants, $H_3O^+ + C_2H_4$. This mechanism supports the intuitive assumption that formation of $C_2H_5OH_2^+$ is more likely than $(CH_3)_2OH^+$ since the latter requires significantly more rearrangement.

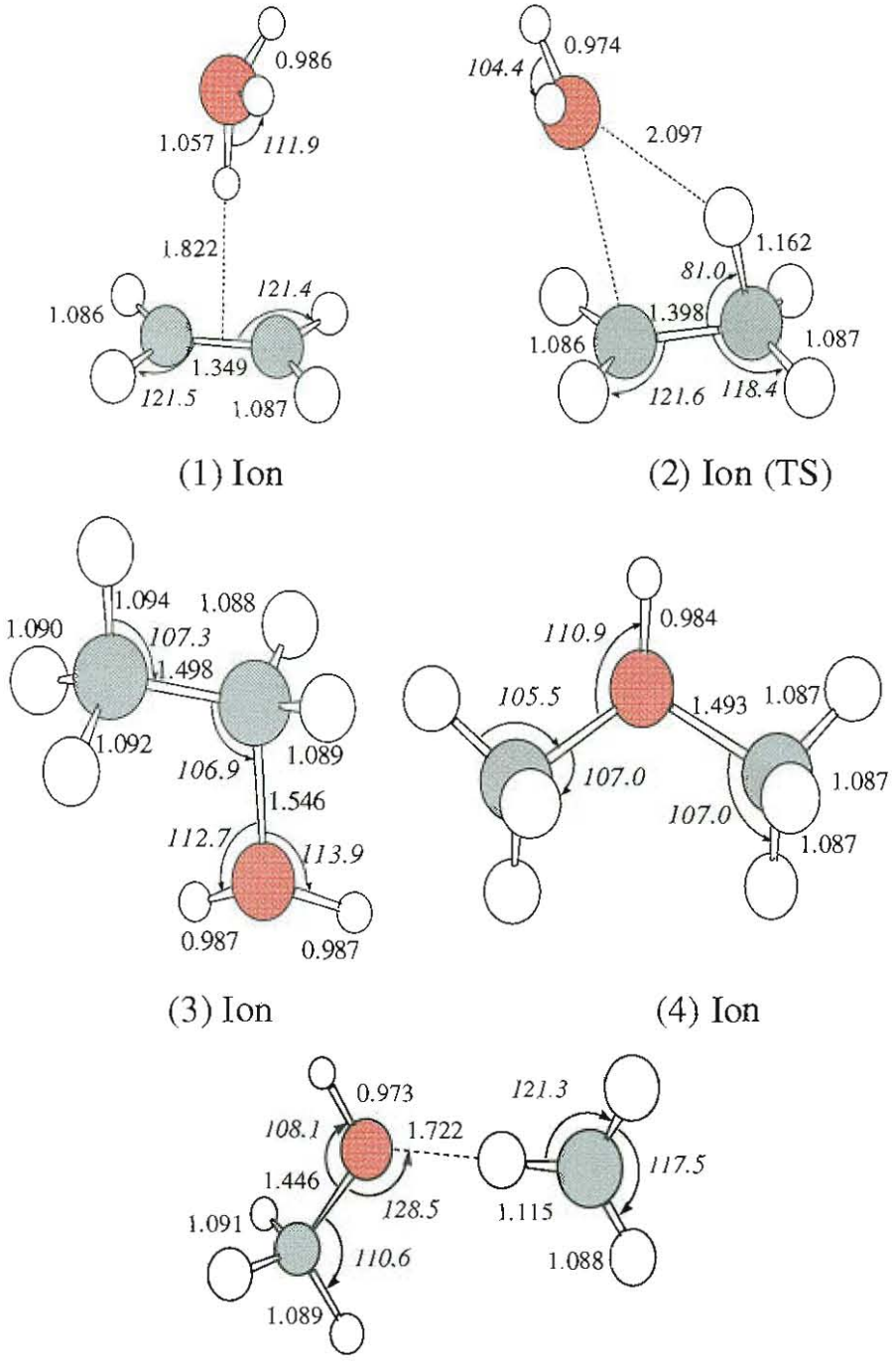

Figure 3.8. MP2/6-31G* optimised geometries for the designated $C_2H_7O^+$ species with bond lengths in Å and bond angles in degrees.

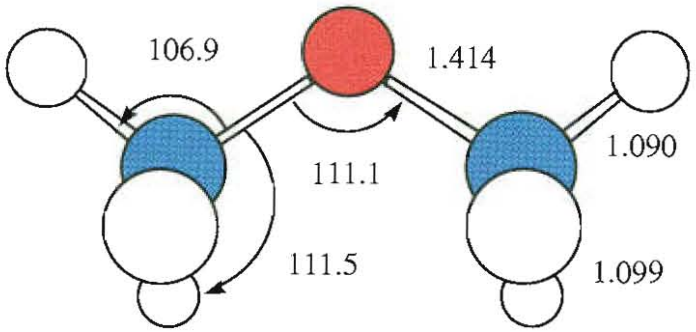

(6) $(CH_3)_2O$

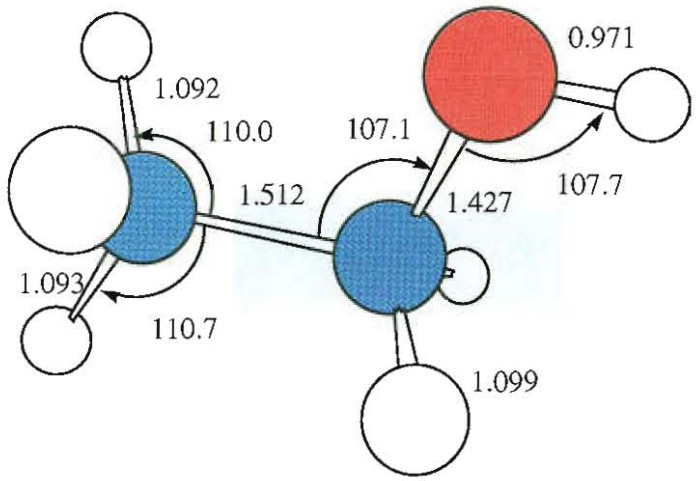

(7) C_2H_5OH

Figure 3.9. MP2/6-31G* optimised geometries for the designated C_2H_6O species with bond lengths in Å and bond angles in degrees.

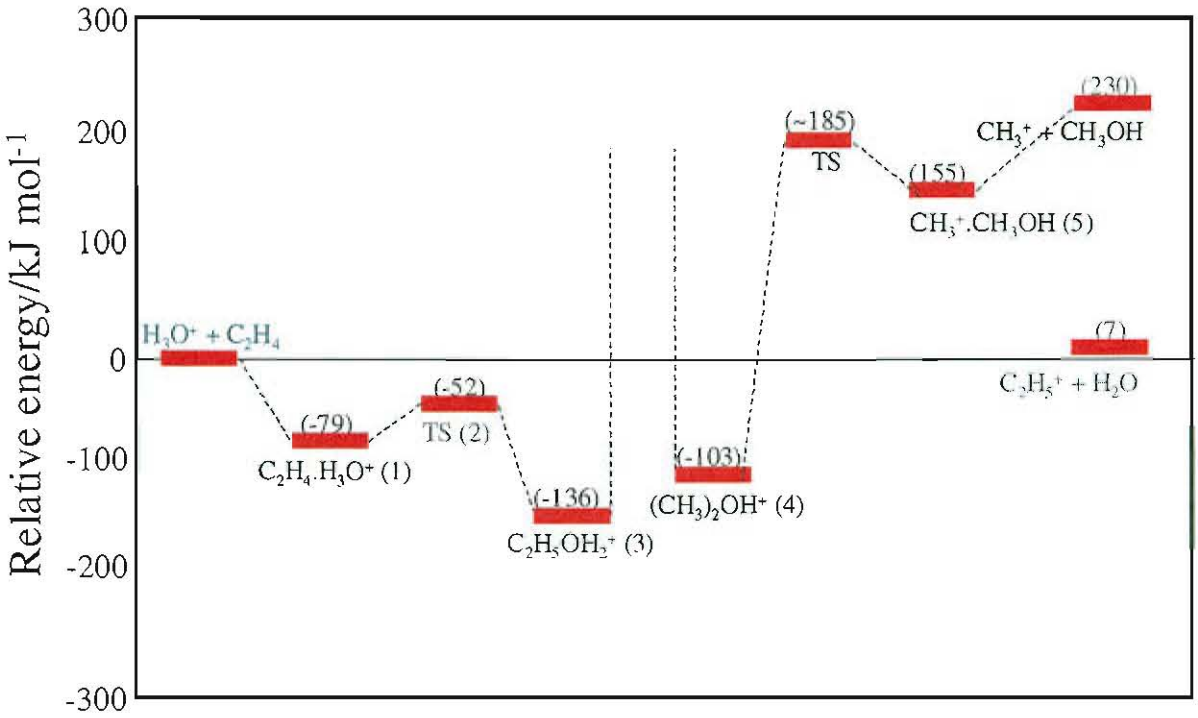

Figure 3.10. $C_2H_7O^+$ potential energy surface calculated using the G2 procedure. The energies are expressed in kJ mol^{-1} relative to $H_3O^+ + C_2H_4$ and are corrected to 298 K and for zero-point energy.

In the reaction of $CH_3^+ + CH_3OH$, an electrostatic complex is formed with the CH_3^+ moiety attached by an H atom to the O atom of CH_3OH, with a binding energy of 75 kJ mol^{-1}. If the C-O bond distance is decreased, the energy of the system is raised until, at approximately R(C-O) = 2.6 Å the CH_3^+ moiety is flipped to allow bonding between the C atom of CH_3^+ and the O atom of CH_3OH. The barrier between the $CH_3^+\cdots HOCH_3$ electrostatic complex and $(CH_3)_2OH^+$ is about 30 kJ mol^{-1}. The barrier was estimated by performing a series of single point calculations on the $CH_3^+\cdots HOCH_3$ complex in which the C-O bond distance was systematically decreased. Failure to directly locate a saddle point linking the ion-neutral complex and protonated dimethyl ether is probably a reflection of the very flat nature of the potential energy surface in this

region as noted by Audier et al. [210] An experimental investigation of the $CH_3^+ + CH_3OH$ reaction has been performed by Matthews et al. [206]

3.9 Discussion.

The reaction chemistry summarised in Table 3.8 distinguishes clearly between the isomeric species, $C_2H_5OH_2^+$ and $(CH_3)_2OH^+$, on the basis of the different proton affinities of C_2H_5OH and $(CH_3)_2O$. Both ions exhibited near collision rate reactions with CH_2CHCN (PA = 784.7 kJ mol^{-1}), but protonated ethanol $C_2H_5OH_2^+$, yielded a 50% proton transfer channel whereas protonated dimethyl ether, $(CH_3)_2OH^+$, yielded only termolecular adduct formation. Both ions underwent slower reactions with 2-fluorotoluene (PA = 773.3 kJ mol^{-1}), but whereas $C_2H_5OH_2^+$ yielded a 70% proton transfer product channel and a faster reaction, no proton transfer was found for

Species[a]	MP4/6-311G**	ΔE(+)	ΔE(2df)	ΔE(QCI)	ΔE(HLC)	ΔE(ZPE)	E(G1)
H_3O^+	-76.56181	-1.46	-33.42	-0.20	-24.56	32.80	-76.58865
C_2H_4	-78.38239	-1.86	-40.07	-1.75	-36.84	48.91	-78.41401
$C_2H_5^+$	-78.65343	-0.62	-36.17	-1.31	-36.84	58.21	-78.67016
H_2O	-76.27607	-10.83	-37.39	-0.07	-24.56	20.51	-76.32834
(1) Ion	-154.97564	-3.44	-74.55	-1.24	-61.40	83.88	-155.03238
(3) Ion	-155.00029	-3.72	-74.12	-0.98	-61.40	88.28	-155.05223
(2) TS Ion	-154.95697	-7.44	-73.30	-1.60	-61.40	77.18	-155.02353
(4) Ion	-154.98737	-3.79	-75.10	-0.93	-61.40	88.95	-155.03963
(5) Ion	-154.88204	-7.22	-72.74	-1.73	-61.40	81.43	-154.94370
(6) Neut.	-154.68637	-8.93	-78.64	-0.45	-61.40	76.81	-154.75898
(7) Neut.	-154.66774	-7.87	-81.21	-0.30	-61.40	76.93	-154.74161

Table 3.9. G1 energies and corrections.[‡]

[a] The numbered species refer to the structures illustrated in Figs. 3.8 and 3.9.
[‡] Energies in hartrees, corrections in millihartrees.

$(CH_3)_2OH^+$. These findings are in accord with the established proton affinities of C_2H_5OH (PA = 776.4 kJ mol^{-1}) and $(CH_3)_2O$ (PA = 792 kJ mol^{-1}). [164]

What is also evident from the experimental studies is that the product of the termolecular association reaction (3.42b), $H_3O^+.C_2H_4$, is indistinguishable in our experiments from $C_2H_5OH_2^+$. The rate coefficients and product distributions of the reactions of $H_3O^+.C_2H_4$ with 2-fluorotoluene and acrylonitrile are identical (within the experimental uncertainty) with those of $C_2H_5OH_2^+$ giving strong support to the identification of the product of reaction (3.42b) as $C_2H_5OH_2^+$. The transition state barrier between the two structures is only 27 kJ mol^{-1} above the energy of $C_2H_4.H_3O^+$ (Figure 3.10), and it is apparent that at the entrance level of $H_3O^+ + C_2H_4$ at room temperature there is ample energy to overcome this small barrier and sample the surface above the $C_2H_5OH_2^+$ global minimum.

It is concluded, therefore, that the experimental evidence supports the contention that the structure of the ion formed in reaction (3.42b) is that of $C_2H_5OH_2^+$. Matthews et al [206] cite evidence that a fraction of the $C_2H_7O^+$ ions formed in reaction (3.42b) exists in the electrostatic form based on the observation of different product channels for $H_3O^+.C_2H_4$ versus $C_2H_5OH_2^+$ with some neutral reactants. The present work does not of course rule out this possibility. It is likely, however, that at the energy of the reactants $H_3O^+ + C_2H_4$, the density of states ratio will favour formation of $C_2H_5OH_2^+$ over $H_3O^+.C_2H_4$. Also, given the closeness of the proton affinities calculated for the two species, it is difficult to find a neutral reagent that reacts at appreciably different rates with the two ions, which is also the situation for protonated propyne and allene (see the discussion in chapter 4). Consequently, observation of curvature in a semilogarithmic decay plot as a means of distinction between the isomers is difficult to achieve. Indeed linear decays were observed for both $C_2H_5OH_2^+$ and $H_3O^+.C_2H_4$ with the ten neutral reagents employed by Matthews et al [206] and the three reagents employed in the present study. Any distinction of isomeric species therefore rests on a difference in observed product branching ratios which may be complicated by virtue of the method employed to form $H_3O^+.C_2H_4$ (i.e. adding excess C_2H_4 to a H_3O^+ ion swarm, with resultant secondary

Structure	Δ /millihartrees	Σ thermal energies /millihartrees	E(G2) 298 K /hartrees	ΔE(G2) 298 K /kJ mol^{-1}
$C_2H_7O^+$ species				
H_3O^+	-7.84	39.62	-76.58905	
C_2H_4	-8.76	57.75	-78.41295	
CH_3^+	-5.61	36.58	-39.38272	
CH_3OH	-12.27	58.60	-115.53162	
$H_3O^+ + C_2H_4$			-155.00200	0.0
$H_3O^+.C_2H_4$	-17.12	99.92	-155.03212	-79.1
$C_2H_5OH_2^+$	-17.58	103.43	-155.05385	-136.1
TS (2)	-16.57	93.19	-155.02195	-52.4
$(CH_3)_2OH^+$	-17.94	104.39	-155.04141	-103.5
$C_2H_5^+ + H_2O$			-154.99953	6.5
$CH_3^+.HOCH_3$	-17.57	98.18	-154.94289	155.2
$CH_3^+ + CH_3OH$			-154.91435	230.1
C_2H_6O species				
C_2H_5OH	-17.58	91.51	-154.75897	
CH_3OCH_3	-16.46	90.36	-154.74246	

Table 3.10. G2 energies and corrections.

Structure	ΔH_f° (kJ mol^{-1})		Proton affinity(kJ mol^{-1})	
	calculated	experiment[a]	calculated[b]	experiment
CH_3CH_2OH	-233.6	-234.7	780.4	776.4
$(CH_3)_2O$	-190.2	-184.0	791.1	792.0
$H_2O + C_2H_4$	-180.2	-189.5	767.5	

Table 3.11. Calculated enthalpies of formation and proton affinities of C_2H_6O isomers.

[a] Experimental values are from ref. 163. [b] Calculated proton affinities at 298 K at the G2 level of theory.

ion chemistry). It therefore remains an open question as to whether a mixture of electrostatically and covalently bonded species are formed in reaction (3.42).
Two earlier studies also favour $C_2H_5OH_2^+$ as the structure of the $H_3O^+.C_2H_4$ adduct. Jarrold et al [166] found supporting evidence from CID studies. Herbst et al [168] compared the measured ternary reaction rate coefficient of reaction (3.42) with a calculated value that was based on a designated structure of the $C_2H_7O^+$ product ion. They obtained satisfactory agreement between theory and experiment when they assumed a structure of $C_2H_5OH_2^+$ for the adduct. It should be noted however that neither of these methods would necessarily be sensitive to the presence of a fractional contribution from an electrostatic complex.

3.11 Conclusions.

We have utilised ab initio calculations of the $C_2H_7O^+$ energy surface and experimental observations of the proton transfer reactivity of the $C_2H_7O^+$ isomers, $C_2H_5OH_2^+$ and $(CH_3)_2OH^+$, to identify the $H_3O^+.C_2H_4$ product of reaction (3.42b) as $C_2H_5OH_2^+$. Thus sources of C_2H_5OH in interstellar models utilising the ion-molecule association reaction (3.40) remain valid although it should be noted that the products of the subsequent ion-electron recombination reaction (3.41) have yet to be determined. Indeed, experimental measurements [214] of the electron-ion recombination of H_3O^+ indicate that loss of a single H-atom to yield H_2O represents only a very minor (~5%) channel.[‡] If this behaviour can be extrapolated to the electron ion recombination of $C_2H_5OH_2^+$, then the importance of reactions (3.40) and (3.41) will be diminished significantly. Indeed, the observation of ethanol specifically in hot molecular cores points to a dominant role of grain surface chemistry in its formation. [199,217]

The observation of the endothermic proton transfer channel in reaction 3.42a ($C_2H_5^+ + H_2O$, $\Delta H^o = +10.5$ kJ mol^{-1}) [164], which competes with formation of the $H_3O^+.C_2H_4$ adduct, shows that the exit channel from the ($H_3O^+.C_2H_4$) complex to $C_2H_5^+$

[‡] The precise branching ratio for the dissociative recombination of H_3O^+ is still subject to considerable uncertainty. Andersen et al [215,216] report a branching ratio for H_2O formation of 0.33 based on heavy-ion storage ring experiments.

+ H_2O is found before collisional stabilisation can occur. In this work our measurement of the rate coefficient for endothermic proton transfer is 5.9 x 10^{-11} cm^3 s^{-1} at 0.35 Torr of helium. At 0.5 Torr of helium, Matthews et al [206] report a rate coefficient for proton transfer of 5.1 x 10^{-11} cm^3 s^{-1} and Bohme and Mackay [205] report a value of 6.3 x 10^{-11} cm^3 s^{-1} in a hydrogen carrier gas. The slight variation in rate coefficient in these three measurements is within the experimental uncertainty. We conclude that the proton transfer channel takes place on a time scale that is much shorter than the time between collisions (<125 ns), and proceeds independently of complex stabilisation. The branching ratio is therefore expected to vary with pressure because of the variation in the termolecular rate.

3.12 Ion-molecule association of $CH_2NH_2^+$ + HCOOH: Interstellar glycine.

Glycine is the simplest α-amino acid, and one of the most important biological molecules. Tremendous interest in the prebiotic synthesis of glycine (and other amino acids) was spurred by the pioneering experiments of Miller [218,219] over 40 years ago. Studies of the Murchison meteorite, which fell in Australia in 1969 and belongs to a class of carbonaceous chondrites containing 2-3 % carbon by weight mostly in the form of organic materials, identified amino acids as constituents of the organic component. [220,221] Large amounts of apparently extraterrestrial amino acids were also found recently in rocks at the Cretaceous/Tertiary boundary in Denmark. [220] These observations together with the large amounts of extraterrestrial dust accreted annually on Earth has led to the suggestion that the organic matter on our planet may have its main origins in interplanetary, or even interstellar, space. [220,222] Astronomical searches for interstellar biomolecules such as glycine are of enormous interest. [223,224] Detection of interstellar glycine is at present tentative. Snyder [223] has reviewed the progress in the interstellar search for this molecule.

Given the facile nature of ion-molecule reaction processes even under interstellar conditions, the potential role of ion-molecule chemistry in the synthesis of extraterrestrial

prebiotic material is evident. This has led some ion-molecule chemists to investigate potential synthetic ion-molecule routes to the formation of amino acids. Meot-Ner et al [225] investigated the association of ammonium (protonated amine) ions with carbon dioxide in a pulsed ionization high-pressure mass spectrometer.

$$CH_3NH_3^+ + CO_2 \longrightarrow CH_3NH_3^+.CO_2 \qquad \textbf{(3.52)}$$

$$C_2H_5NH_3^+ + CO_2 \longrightarrow C_2H_5NH_3^+.CO_2 \qquad \textbf{(3.53)}$$

The empirical formulae of the product ions in (3.52) and (3.53) are identical with those of protonated glycine and protonated alanine respectively, which could result from the formation of new covalent bonds in the adduct ions. However, it was concluded [225] that the products of the two association reactions did not correspond to protonated glycine and protonated alanine, but rather to hydrogen-bonded cluster ions. By studying the equilibrium constant for the two association reactions as a function of temperature Meot-Ner et al [225] were able to derive enthalpies of formation for the product ions from van't Hoff plots. The values so obtained for $CH_3NH_3^+.CO_2$ (175.7 kJ mol^{-1}) and $C_2H_5NH_3^+.CO_2$ (146.4 kJ mol^{-1}) do not agree with the known heats of formation of protonated glycine (255.2 kJ mol^{-1}) and protonated alanine (217.6 kJ mol^{-1}).

The association reaction between $CH_2NH_2^+$ and HCOOH was observed to occur rapidly at 0.35 Torr of helium in a SIFT apparatus by Bohme and co-workers. [226] This reaction also produces an ion with an empirical formula identical to that of protonated glycine. Elucidation of the structure of the product ion produced in the association reaction between $CH_2NH_2^+$ with HCOOH forms the major focus of this section. It has also been suggested [223,227] that the reaction of NH_2^+ with CH_3COOH may provide a route to the formation of protonated glycine. The reactions of NH_n^+ (n = 2-4) with acetic acid, were also investigated in the course of this work.

3.12.1 Experimental.

Most of the reaction chemistry described in this section was investigated initially using the SIFT apparatus, and subsequently re-examined with the FA-SIFT apparatus. NH_n^+ (n = 2-4) ions were generated via electron impact on ammonia in the SIFT ion source and by adding ammonia to a helium carrier subjected to microwave discharge in the FA-SIFT apparatus. $CH_2NH_2^+$ and $CH_3NH_3^+$ were formed similarly from

methylamine (CH_3NH_2). As discussed below, rate coefficients for the reactions of acetic acid and formic acid were determined using the undiluted vapour from the respective liquids. The exothermic proton transfer reactions of H_3O^+ with CH_3COOH and HCOOH were measured and assumed to proceed at the collision rate. All other rate coefficients were scaled accordingly. The justification of this approach has been discussed by Spanel and Smith [228] who routinely employ this method in their SIFT trace gas analysis technique.

3.13 Results.

3.13.1 CH_3COOH reactions.

Acetic acid, like formic acid, exists in equilibrium with a dimer at room temperature and vapour pressure (11.4 Torr at 20°C), which means that one must take account of this when measuring flow rates of the vapour. To circumvent this problem, the exothermic proton transfer reaction from H_3O^+ to CH_3COOH was measured and assumed to proceed at the collision rate, making the reasonable assumption that following expansion into the flow tube any acetic acid dimers dissociate rapidly to the monomer. All subsequently measured reaction rate coefficients were scaled accordingly.

$$H_3O^+ + CH_3COOH \longrightarrow CH_3COOH_2^+ + H_2O \qquad \textbf{(3.54)}$$

$k_{3.54} = k_c = 2.6 \times 10^{-9}\ cm^3\ s^{-1}$

A number of reactions of acetic acid with nitrogen-containing ions were considered as potential routes to protonated glycine based on calculated reaction enthalpies.

$CH_3NH_3^+ + CH_3COOH$

Formation of protonated glycine from the reaction of protonated methylamine with acetic acid is calculated to be close to thermoneutral.

$$CH_3NH_3^+ + CH_3COOH \longrightarrow Gly\text{-}H^+ + CH_4 \qquad \textbf{(3.55)}$$

$\Delta H^\circ_{3.55} = +2.0\ kJ\ mol^{-1}$

The only product observed from the reaction of these precursors, however, was a termolecular association adduct.

$CH_3NH_3^+ + CH_3COOH \longrightarrow CH_3NH_3^+.CH_3COOH$ **(3.56)**

$k_{3.56} = 6.0 \times 10^{-10}$ cm^3 s^{-1} at 0.48 Torr

$CH_2NH_2^+ + CH_3COOH$

Similarly, the reaction of protonated methanimine with acetic acid led to the formation of a termolecular adduct only.

$CH_2NH_2^+ + CH_3COOH \longrightarrow CH_2NH_2^+.CH_3COOH$ **(3.57)**

$k_{3.57} = 4.6 \times 10^{-10}$ cm^3 s^{-1} at 0.48 Torr

$NH_n^+ + CH_3COOH$

The reactions of NH_2^+, NH_3^+ and NH_4^+ with acetic acid were investigated. The reaction of NH_2^+ with acetic acid was proposed as one of the simplest potential bimolecular pathways to protonated glycine. [223,227] The reactions of the three ammonia derived ions proceeded as follows:

$NH_4^+ + CH_3COOH \longrightarrow NH_4^+.CH_3COOH$ **(3.58)**

$k_{3.58} = 6.5 \times 10^{-10}$ cm^3 s^{-1} at 0.48 Torr

$NH_3^+ + CH_3COOH \longrightarrow NH_4^+ + CH_3CO_2$ **(3.59)**

$k_{3.59} = 2.7 \times 10^{-9}$ cm^3 s^{-1}

The reaction of NH_3^+ with acetic acid represents an H-atom abstraction reaction and proceeds at the collision rate as is typical of many, but by no means all, such reactions (see chapter 5).

$NH_2^+ + CH_3COOH \longrightarrow CH_3COOH_2^+ + NH$ **(3.60)**

$\Delta H^o_{3.60} = -141.1$ kJ mol^{-1}; $k_{3.58} = 2.8 \times 10^{-9}$ cm^3 s^{-1}

The only product observed in the reaction between NH_2^+ and acetic acid was proton transfer, and the reaction proceeded at the collision rate as expected for exothermic proton transfer.

3.13.2 HCOOH reactions.

At 298K formic acid has a vapour pressure of 40 Torr and exists almost exclusively as a dimer, $(HCOOH)_2$, at this pressure. [229] One must therefore take account of this when measuring flow rates of formic acid as was discussed earlier by Freeman et al. [229] Following expansion into the flow tube complete dissociation of formic acid dimer to monomer is assumed to occur rapidly. [229] In the present work formic acid was used

without dilution and all measured rate coefficients were determined by assuming that the exothermic proton transfer reaction between H_3O^+ and HCOOH proceeds at the collision rate and scaling all other rate coefficients accordingly.

$H_3O^+ + HCOOH \longrightarrow HCOOH_2^+ + H_2O$ **(3.61)**

$k_{3.61} = k_c = 2.2 \times 10^{-9}$ cm^3 s^{-1}

$CH_2NH_2^+ + HCOOH$

Protonated methanimine, $CH_2NH_2^+$, underwent termolecular association only with formic acid. Although the pressure dependence of the effective bimolecular rate coefficient was not determined, it appears the reaction has not yet reached pressure saturation at 0.48 Torr.

$CH_2NH_2^+ + HCOOH \longrightarrow CH_2NH_2^+.HCOOH$ **(3.62)**

$k_{3.62} = 1.0 \times 10^{-10}$ cm^3 s^{-1} (0.48 Torr)

$CH_3NH_3^+ + HCOOH$

The reaction of protonated methylamine with formic acid was measured. Formation of protonated glycine is calculated to be slightly endothermic.

$CH_3NH_3^+ + HCOOH \longrightarrow Gly\text{-}H^+ + H_2$ **(3.63)**

$\Delta H^o_{3.63} = +23$ kJ mol^{-1};

The only product observed was the termolecular association adduct, which forms with an efficiency similar to that of the $CH_2NH_2^+$/HCOOH product, viz.

$CH_3NH_3^+ + HCOOH \longrightarrow CH_3NH_3^+.HCOOH$ **(3.64)**

$k_{3.64} = 1.1 \times 10^{-10}$ cm^3 s^{-1} (0.48 Torr)

Reactivity of $CH_2NH_2^+.HCOOH$

Glycine has a proton affinity, PA(Gly), of 886.5 kJ mol^{-1}, relative to the proton affinity of ammonia, PA(NH_3) = 853.5 kJ mol^{-1}. PA(Gly) has been established via proton transfer equilibria between glycine and appropriate reference bases, and is in accord with proton affinity orders established from unimolecular dissociation of proton-bound heterodimers containing glycine and other amino acids. [230] The value is also in excellent agreement with recent high level calculations of PA(Gly). [231]

If the association ion, $CH_2NH_2^+.HCOOH$, has the protonated glycine structure it would therefore be expected to undergo facile proton transfer to bases having a proton

affinity > 887 kJ mol^{-1}. The bases methylamine, CH_3NH_2, and ethylamine, $C_2H_5NH_2$, were selected on the basis of their known proton affinities, viz. PA(CH_3NH_2) = 899 kJ mol^{-1} and PA($C_2H_5NH_2$) = 912 kJ mol^{-1}. The reaction of $CH_2NH_2^+$.HCOOH with NH_3 was also measured.

Methodology

The $CH_2NH_2^+$.HCOOH association ion was formed in the flow tube by injecting $CH_2NH_2^+$ from the FA source and adding formic acid vapour at the upstream neutral inlet. The resultant $CH_2NH_2^+$.HCOOH ion was subsequently reacted with the bases NH_3, CH_3NH_2 and $C_2H_5NH_2$ at the downstream neutral inlet.

$CH_2NH_2^+$.HCOOH + NH_3

The major product of the reaction between $CH_2NH_2^+$.HCOOH and NH_3 was observed at m/z = 47. The observation was rationalised in terms of a ligand exchange reaction in which formic acid is exchanged for ammonia.

$$CH_2NH_2^+.HCOOH + NH_3 \xrightarrow{0.75} CH_2NH_2^+.NH_3 + HCOOH \quad \textbf{(3.65a)}$$

$$\xrightarrow{0.25} \text{adduct} \quad \textbf{(3.65b)}$$

$k_{3.65} = 1.6 \times 10^{-9}$ cm^3 s^{-1}

At higher flows of ammonia, ion products were observed at m/z = 64, m/z = 35 and m/z = 52. These products were attributed to the following reaction sequence:

$$CH_2NH_2^+.NH_3 + NH_3 \longrightarrow CH_2NH_2^+(NH_3)_2;\ m/z = 64 \quad \textbf{(3.66a)}$$

$$\longrightarrow NH_4^+.NH_3 + CH_2NH;\ m/z = 35 \quad \textbf{(3.66b)}$$

$$NH_4^+.NH_3 + NH_3 \longrightarrow NH_4^+(NH_3)_2;\ m/z = 52 \quad \textbf{(3.67)}$$

The tabulated proton affinity of methanimine, CH_2NH, is very close to that of ammonia, viz. PA(CH_2NH) = 852.9 kJ mol^{-1}.

$CH_2NH_2^+$.HCOOH + CH_3NH_2

$$CH_2NH_2^+.HCOOH + CH_3NH_2 \xrightarrow{>0.9} CH_2NH_2^+.CH_3NH_2 + HCOOH \quad \textbf{(3.68a)}$$

$$\xrightarrow{<0.1} \text{adduct} \quad \textbf{(3.68b)}$$

$k_{3.68} = 1.5 \times 10^{-9}$ cm^3 s^{-1}

An analogous reaction to that with ammonia was observed between the $CH_2NH_2^+$.HCOOH association ion and methylamine, the reaction proceeding almost exclusively via ligand exchange. Again no proton transfer was observed.

At higher flows of methylamine, major products were observed at m/z = 63 and m/z =94.

$CH_2NH_2^+.CH_3NH_2 + CH_3NH_2 \longrightarrow CH_3NH_3^+.CH_3NH_2$; m/z =63 **(3.69)**

$CH_3NH_3^+.CH_3NH_2 + CH_3NH_2 \longrightarrow CH_3NH_3^+(CH_3NH_2)_2$; m/z =94 **(3.70)**

$CH_2NH_2^+.HCOOH + C_2H_5NH_2$

The major product of the reaction between the $CH_2NH_2^+$.HCOOH association ion and ethylamine also produced, almost exclusively, a product corresponding to ligand exchange.

$CH_2NH_2^+.HCOOH + C_2H_5NH_2 \longrightarrow CH_2NH_2^+.C_2H_5NH_2 + HCOOH$ **(3.72)**

$k_{3.72} = 1.1 \times 10^{-9}$ cm^3 s^{-1}

Again, at high neutral flows a further ligand exchange was observed to occur, viz.

$CH_2NH_2^+.C_2H_5NH_2 + C_2H_5NH_2 \longrightarrow C_2H_5NH_3^+.C_2H_5NH_2 + CH_2NH$ **(3.73)**

3.14 Discussion.

The results described above suggest that the termolecular association reaction which occurs between $CH_2NH_2^+$ and HCOOH does not produce an ion with the structure of protonated glycine. If protonated glycine was formed in reaction 3.62 then facile, exothermic proton transfer would be expected to occur to both CH_3NH_2 and $C_2H_5NH_2$, however none was observed. Further the observation of apparent ligand exchange reactions from the $CH_2NH_2^+$.HCOOH association ion with ammonia, methylamine and ethylamine tends to suggest that the ion is an electrostatic, hydrogen-bonded adduct, rather than a covalently bound adduct. Formation of protonated glycine in the ISM from an association reaction between $CH_2NH_2^+$ and HCOOH would require the reaction not to possess an activation barrier, and as such the reverse dissociation would be expected to occur at threshold. Experiments which have examined the dissociation of protonated glycine and other protonated amino acids suggest that ion-molecule association of protonated imines with formic acid to yield protonated amino acids must occur over a substantial activation barrier. [230,232]

Reactant	Products	Branching ratio	k_{obs} /10^{-9} cm^3 s^{-1}	k_{coll}[a] /10^{-9} cm^3 s^{-1}
H_3O^+ reactions				
CH_3COOH	$CH_3COOH_2^+ + H_2O$	1.0	[2.6]	2.6
HCOOH	$HCOOH_2^+ + H_2O$	1.0	[2.2]	2.2
$CH_3NH_3^+$ reactions				
CH_3COOH	adduct	1.0	0.60	2.2
HCOOH	adduct	1.0	0.11	1.9
$CH_2NH_2^+$ reactions				
CH_3COOH	adduct	1.0	0.46	2.2
HCOOH	adduct	1.0	0.10	1.9
NH_4^+ reactions				
CH_3COOH	adduct	1.0	0.65	2.6
NH_3^+ reactions				
CH_3COOH	$NH_4^+ + CH_3CO_2$	1.0	2.7	2.7
NH_2^+ reactions				
CH_3COOH	$CH_3COOH_2^+ + NH$	1.0	2.8	2.8
$CH_2NH_2^+$.HCOOH reactions				
NH_3	$CH_2NH_2^+.NH_3$ +		1.6	2.1
	HCOOH	0.75		
	adduct	0.25		
CH_3NH_2	$CH_2NH_2^+.CH_3NH_2$ +		1.5	1.7
	HCOOH	>0.90		
	adduct	<0.10		
$C_2H_5NH_2$	$CH_2NH_2^+.C_2H_5NH_2$ +	1.0	1.1	1.6
	HCOOH			

Table 3.12. Rate coefficients and branching ratios for the designated ions with the specified neutrals.

[a] Calculated using the method of Su and Chesnavich (ref. 161).

3.14.1 Corroborating evidence.

Beranová et al [230] examined fragmentation reactions of protonated glycine by a combination of metastable ion (MI) characteristics, collisionally activated dissociation (CAD) and neutralization-reionization mass spectrometry (NRMS). Although m/z = 30, $CH_2NH_2^+$, was observed as a minor fragment in the MI spectrum and as the major peak in the CAD spectrum of protonated glycine, direct loss of HCOOH (or dihydroxycarbene, $:C(OH)_2$) would have been expected to produce a sizeable peak at m/z = 46 in the N_fR (neutral fragment-reionization) spectrum. However, m/z = 46 was virtually non-existent in the N_fR spectrum of protonated glycine, suggesting that there is a substantial barrier associated with loss of HCOOH from protonated glycine and, by inference, a large barrier to the reverse association reaction of $CH_2NH_2^+$ with HCOOH. A combined theoretical and experimental study of the mechanism by which CH_2O_2 is eliminated from protonated leucine and isoleucine was performed by Bouchoux et al. [232] Their study demonstrated that elimination of intact $:C(OH)_2$ or HCOOH proceeds over a much higher barrier than consecutive losses of H_2O + CO. Similarly, Beranová et al [230] demonstrated that sequential elimination of H_2O + CO from protonated glycine to form $CH_2NH_2^+$ represents a lower energy pathway than direct elimination of HCOOH.

3.15 Conclusions.

The termolecular association reaction of $CH_2NH_2^+$ with HCOOH produces an electrostatic complex rather than protonated glycine. The product of reaction (3.62) undergoes facile ligand exchange with ammonia, methylamine and ethylamine, switching formic acid for the respective amines. Exothermic proton transfer would be expected from protonated glycine to CH_3NH_2 and $C_2H_5NH_2$, but is not observed. The failure of reaction (3.62) to generate protonated glycine is in accord with the results of metastable ion, collisionally activated dissociation and neutralisation-reionisation mass spectrometry experiments performed on protonated glycine. Results from these experiments indicate a sizeable barrier exists to the loss of HCOOH (or its dihydroxycarbene isomer $:C(OH)_2$) from protonated glycine, suggesting also a large reverse activation energy to the association reaction.

CHAPTER 4.

SIFT STUDIES OF THE ISOMERS OF $C_6H_5^+$, $C_7H_7^+$ AND $C_3H_5^+$

4.1 Introduction.

Reactivity studies have been used to distinguish between isomers of $C_6H_5^+$, $C_7H_7^+$ and $C_3H_5^+$.

Electron impact on bromobenzene is shown to produce a mixture of linear and cyclic $C_6H_5^+$ isomers in accord with earlier work. Reaction with acetylene or O_2 is used as a diagnostic for distinguishing between the linear and cyclic species. By selectively forming c- $C_6H_5^+$ via reactions of X^+ with chlorobenzene (X = Kr, CO, CO_2), c- $C_6H_5^+$ is shown to be more reactive with acetylene than the acyclic isomer(s), in accord with the findings of an earlier ICR study. [233] The rates and product distributions are reported for the reactions of several ions with halobenzenes.

Similarly, electron impact on bromotoluene is shown to produce a mixture of $C_7H_7^+$ isomers, which exhibit differing reactivities towards benzene. Low energy chemi-ionisation of cycloheptatriene and benzyl bromide is used to selectively form the tropylium and benzyl isomers of $C_7H_7^+$ respectively, and it is shown that the benzyl structure is generally more reactive than the tropylium structure. Using benzene as the diagnostic reagent, the $C_7H_7^+$ structure(s) formed in a number of bimolecular and termolecular ion-molecule reactions are identified.

The allyl, $CH_2CHCH_2^+$, and 2-propenyl, $CH_3CCH_2^+$ isomers of $C_3H_5^+$ have been observed as distinct isomeric species in the FA-SIFDT apparatus. Methanol is used as the diagnostic reagent for distinguishing between the two isomers. The isomeric ratio of allyl:2-propenyl formed via protonation of allene or propyne by a protonated base, BH^+, is shown to be dependent on the proton affinity of the base B. Proton transfer from H_3O^+ to allene produces the 2-propenyl cation exclusively, whereas proton transfer from SO_2H^+ to allene generates a mixture of allyl and 2-propenyl cations, enabling an estimate to be made of the barrier height for the rearrangement allyl $\longrightarrow$ 2 propenyl. The barrier

height estimated from experiment is in excellent agreement with ab initio calculations performed at the G2(MP2) level of theory. The $C_3H_5^+$ product of the reaction between $C_2H_4^+$ and C_2H_4 is identified as the 2-propenyl cation. Rate coefficients are also reported for reactions of the allyl and 2-propenyl cations with several neutrals.

4.2 $C_6H_5^+$

Although $C_6H_5^+$ ions are common fragments in the electron impact induced fragmentation of molecular hydrocarbon ions, and are observed as products of reactions between ions and neutrals, some considerable uncertainty has existed in the past as to the structures and reactivities of these ions. [233] It is generally accepted, however, and has been confirmed by theory, [234-236] that the lowest energy $C_6H_5^+$ isomer is the singlet phenylium ion (Figure 4.1), and that the acyclic isomeric species have considerably higher heats of formation. [234]

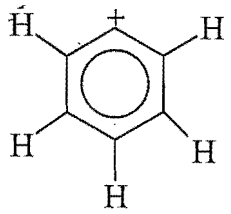

Figure 4.1. The phenylium cation.

Several groups have identified the existence of more than one $C_6H_5^+$ isomer experimentally. [139,233,237-241] Following on from previous work performed in this laboratory [18,139,240], different structures of $C_6H_5^+$ are distinguished by their differing reactivities with neutral molecules. The methods of forming $C_6H_5^+$ previously employed by Wilson [18] in this laboratory, viz. electron impact on benzene and acetylene and dissociative chemi-ionization of bromobenzene by Ar^+ and Kr^+, all produced mixtures of $C_6H_5^+$ isomers, and the unequivocal identification of the isomers formed remained unresolved by his work. He tentatively suggested, however, that the reactive isomer was likely to be the lower energy isomer, which is the cyclic phenylium structure. The aim of the present work was to resolve any remaining doubt as to the identity of the "reactive" and "unreactive" $C_6H_5^+$ isomers, by employing techniques to exclusively form the phenylium ion and probe its reactivity in the absence of other $C_6H_5^+$ isomers. Theoretical

calculations [234] indicate that the acyclic isomers are on the order of 60 kJ mol^{-1} higher in energy than the cyclic structure and predict a sizeable barrier to ring opening (~ 250 kJ mol^{-1}). Therefore, careful variation in the internal energy of the precursor ion should give information about whether the reactive or unreactive $C_6H_5^+$ ion(s) produced in the fragmentation of aromatic compounds has the ring structure.

4.2.1 $C_6H_5^+$ Experimental.

The following experiments related to the chemistry of $C_6H_5^+$ were performed using the Canterbury SIFT apparatus. Rate coefficients and product ratios were measured using the downstream neutral inlet to add the neutral reagent. In situations where $C_6H_5^+$ was generated in the flow tube and subsequently probed for its reactivity, both the upstream and downstream neutral inlets were employed.

4.2.2 Results.

Electron impact on C_6H_5Br

Bromobenzene was subjected to ~70eV electron impact in the ion source and the resultant $C_6H_5^+$ ion was mass selected at m/z = 77 and injected into the flow tube. Sufficiently low injection energies could be achieved to prevent fragmentation of the ions upon injection, a problem experienced in the earlier studies performed by Wilson. [18] Subsequent reaction with acetylene at the downstream neutral inlet clearly illustrates the presence of at least two isomeric species, one reactive and one relatively unreactive with C_2H_2 (Figure 4.2). This is in accord with the observations of Ausloos et al [233] who showed that 40 eV electron impact on bromobenzene also produced a mixture of $C_6H_5^+$ isomers, as evidenced by distinctly different reactivities with bromobenzene. Knight et al [240] observed similar behaviour when $C_6H_5^+$ was formed via 70 eV electron impact on benzene.

Kr^+ + fluorobenzene

The reaction of Kr^+ (I.P. = 13.99 eV) with fluorobenzene was investigated as a potential route to the formation of (predominantly cyclic) $C_6H_5^+$, however the only product observed was due to the charge transfer reaction:

$$Kr^+ + C_6H_5F \xrightarrow{1.0} C_6H_5F^+ + Kr \qquad (4.1)$$

$k_{4.1} = 1.5 \times 10^{-9}$ cm^3 s^{-1}

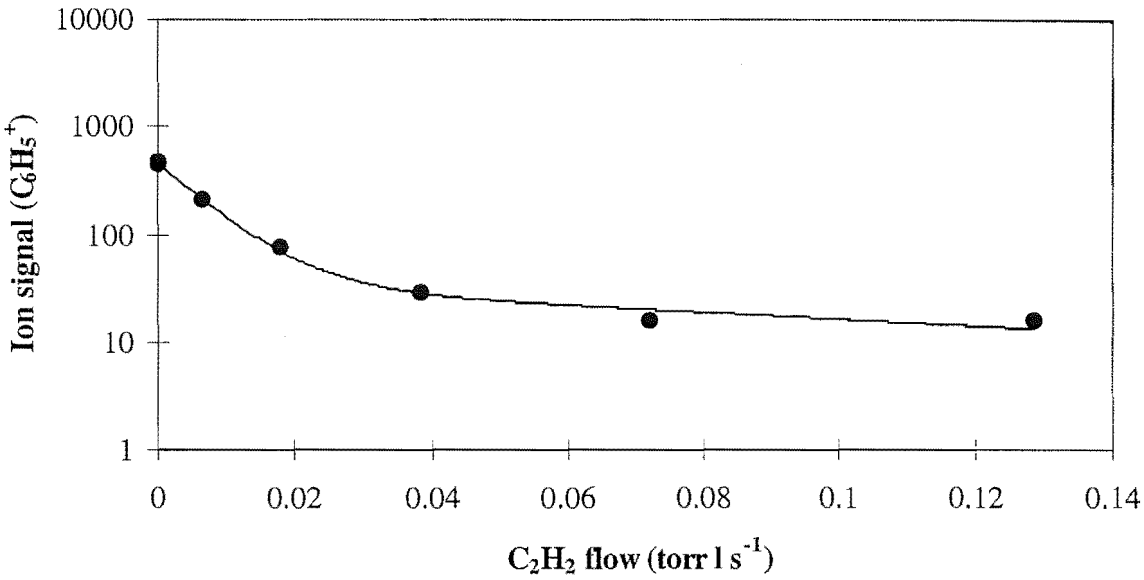

Figure 4.2. Semilogarithmic plot of the $C_6H_5^+$ ion signal (derived from electron impact on C_6H_5Br) versus acetylene flow rate. The points are experimental and the curve has been fitted according to equation (3.18) with $k_1 = 5.2 \times 10^{-10}$ cm^3 s^{-1} and $k_2 = 2.9 \times 10^{-11}$ cm^3 s^{-1} in excellent accord with the results of Knight et al for the $C_6H_5^+$ species derived from electron impact on benzene. [240] The curve indicates an isomeric ratio of 90:10 in favour of the faster reacting $C_6H_5^+$ isomer.

Ar^+ + fluorobenzene

Multiple products were observed in the reaction of Ar^+ (I.P. = 15.76 eV) with fluorobenzene, of which $C_6H_5^+$ was only a minor component. Because of the large C-F bond strength in fluorobenzene, other fragmentation pathways are favoured over rupture of the C-F bond.

$$Ar^+ + C_6H_5F \xrightarrow{0.07} C_4H_2^+ + C_2H_3F + Ar \quad \textbf{(4.2a)}$$

$$\xrightarrow{0.03} H_2C_3F^+ + C_3H_3 + Ar \quad \textbf{(4.2b)}$$

$$\xrightarrow{0.03} C_5H_3^+ + H_2 + F + Ar \quad \textbf{(4.2c)}$$

$$\xrightarrow{0.50} C_4H_3F^+ + C_2H_2 + Ar \quad \textbf{(4.2d)}$$

$$\xrightarrow{0.07} C_6H_4^+ + HF + Ar \quad \textbf{(4.2e)}$$

$$\xrightarrow{0.06} C_6H_5^+ + F + Ar \quad \textbf{(4.2f)}$$

$$\xrightarrow{0.02} C_6H_3F^+ + H_2 + Ar \quad \textbf{(4.2g)}$$

$$\xrightarrow{0.10} C_6H_4F^+ + H + Ar \quad \textbf{(4.2h)}$$

$$\xrightarrow{0.13} C_6H_5F^+ + Ar \quad \textbf{(4.2i)}$$

$k_{4.2} = 1.8 \times 10^{-9}$ cm^3 s^{-1}

This situation is analogous to that observed in a study of the fluorinated toluenes. [242] Again, in contrast to other halogenated toluenes, the C-F bond does not break in the fragmentation of the parent ion.

Kr^+ + benzene

The reaction of Kr^+ with benzene produced almost exclusively non-dissociative charge transfer, yielding $C_6H_6^+$. Although a rate coefficient was not measured for this reaction, it is almost certainly close to the Langevin value as were the rate coefficients for all of the other charge transfer reactions studied. Ausloos [243,244] has noted that the rate constants for charge transfer from X^+ (X = Ar, Kr and Xe) to a range of organic compounds are typically within 20% of the collision rate.

$$Kr^+ + C_6H_6 \xrightarrow{>0.95} C_6H_6^+ + Kr \quad \textbf{(4.3a)}$$

$$\xrightarrow{<0.05} C_6H_5^+ + Kr + H \quad \textbf{(4.3b)}$$

$k_{4.3} \sim k_L = 1.2 \times 10^{-9}$ cm^3 s^{-1}

C_6H_5Cl reactions

The reactions of Kr^+ (I.P. = 13.99 eV), CO_2^+ (I.P. = 13.78 eV) and CO^+ (I.P. = 14.01 eV) with chlorobenzene were all investigated as sources of $C_6H_5^+$. All three reactions produced significant signals of $C_6H_5^+$, which could be probed for isomeric structure by reaction at the downstream neutral inlet.

$$Kr^+ + C_6H_5Cl \xrightarrow{0.80} C_6H_5^+ + Kr + Cl \quad \textbf{(4.4a)}$$

$$\xrightarrow{0.20} C_6H_5Cl^+ + Kr \quad \textbf{(4.4b)}$$

$k_{4.4} = 1.6 \times 10^{-9}$ cm^3 s^{-1}

$$CO_2^+ + C_6H_5Cl \xrightarrow{0.20} C_6H_5^+ + CO_2 + Cl \quad \textbf{(4.5a)}$$

$$\xrightarrow{0.80} C_6H_5Cl^+ + CO_2 \quad \textbf{(4.5b)}$$

$k_{4.5} = 1.7 \times 10^{-9}$ cm^3 s^{-1}

$$CO^+ + C_6H_5Cl \xrightarrow{0.50} C_6H_5^+ + CO + Cl \quad \textbf{(4.6a)}$$

$$\xrightarrow{0.50} C_6H_5Cl^+ + CO \quad \textbf{(4.6b)}$$

$k_{4.6} = 1.8 \times 10^{-9}$ cm^3 s^{-1}

The reactivity of the resultant $C_6H_5^+$ ion was probed by subsequent addition of acetylene or oxygen at the downstream neutral inlet. Oxygen was selected as a neutral reagent because addition of acetylene to the ion swarm containing unreacted CO_2^+ (or CO^+) resulted in an increase in ion signal at m/z = 77 as a result of the following reaction sequence of reactions:

$$CO_2^+ + C_2H_2 \longrightarrow C_2H_2^+ + CO_2 \quad \textbf{(4.7)}$$

$k_{4.7} = 7.3 \times 10^{-10}$ cm^3 s^{-1} [245]

$$C_2H_2^+ + C_2H_2 \xrightarrow{0.32} C_4H_2^+ + H_2 \quad \textbf{(4.8a)}$$

$$\xrightarrow{0.68} C_4H_3^+ + H \quad \textbf{(4.8b)}$$

$k_{4.8} = 1.4 \times 10^{-9}$ cm^3 s^{-1} [156]

$$C_4H_3^+ + C_2H_2 \xrightarrow{M} C_6H_5^+ \quad \textbf{(4.9)}$$

$k_{4.9} = 1.14 \times 10^{-23}$ cm^3 s^{-1} (M = C_2H_2) [18]

The $C_6H_5^+$ ion formed via the reaction of $Kr^+ + C_6H_5Cl$, when reacted subsequently with acetylene, yielded a rate coefficient of 4×10^{-10} cm^3 s^{-1} at 0.35 Torr. This is in acceptable agreement with the value measured by Knight et al [240] at 0.30 Torr, for the fast reacting $C_6H_5^+$ isomer formed by electron impact on benzene. Similarly, it is in reasonable accord with the rate coefficients reported by Wilson [18] for the reaction of the fast reacting $C_6H_5^+$ component, formed via dissociative charge transfer of bromobenzene by Ar^+ and Kr^+, with acetylene, given the uncertainty involved in the simplex fitting procedure used. [18] The rate coefficient measured using O_2 as the neutral reagent was 3.2×10^{-11} cm^3 s^{-1} at 0.35 Torr.

$$C_6H_5^+ + C_2H_2 \longrightarrow C_8H_7^+ \quad \textbf{(4.10)}$$

$k_{4.10} = 4.0 \times 10^{-10}$ cm^3 s^{-1} @ 0.35 Torr

$$C_6H_5^+ + O_2 \longrightarrow C_6H_5^+.O_2 \quad \textbf{(4.11)}$$

$k_{4.11} = 3.2 \times 10^{-11}$ cm^3 s^{-1} @ 0.35 Torr

All three reactions (i.e. $Kr^+/CO^+/CO_2^+ + C_6H_5Cl$) generated $C_6H_5^+$ ions which yielded linear decays upon subsequent reaction with (O_2 or C_2H_2) at the downstream neutral inlet. It is therefore concluded, in accord with the findings of Ausloos et al, [233] that the reaction

of Kr^+ (as well as CO^+ and CO_2^+) with C_6H_5Cl yields, conservatively, > 98% of ions possessing the phenylium structure.

The reaction chemistry discussed above is summarised in Table 4.1.

4.2.3 Discussion.

The present results indicate that the faster reacting $C_6H_5^+$ isomer formed via the electron impact induced fragmentation of benzene and halobenzenes, has the phenylium structure. Low energy dissociative charge transfer to chlorobenzene from CO^+, CO_2^+ or Kr^+ generates almost exclusively the phenylium cation, c-$C_6H_5^+$. The measured rate coefficient for the reaction of this species with acetylene suggests that the fast reacting isomer formed via sequential ion-molecule reactions of ionised and neutral acetylene also has the phenylium structure, in contrast to the conclusions of two earlier studies, [238,240] but in accord with the findings of Ausloos et al. [233] Considering that the thermodynamic threshold for the formation of phenylium ions from chlorobenzene is 12.4 eV, the present findings also confirm the conclusion of Ausloos et al [233] that an appreciable barrier exists (> 1.4 eV) to the ring opening of the phenylium ion. Further, the observation of an unreactive $C_6H_5^+$ component formed in reaction (4.12) by Ausloos et al [233] and Wilson [18] places an upper limit of 2.2 eV on this energy barrier.

$$Kr^+ + C_6H_5Br \longrightarrow C_6H_5^+ + Br + Kr \qquad \textbf{(4.12)}$$

Ausloos et al [233] also examined the laser induced dissociation of $C_6H_5Cl^+$ ions formed by electron impact within 0.5 eV of threshold and were able to assign a value of 2.0 ± 0.3 eV to the barrier for the ring opening process. This is in reasonable accord with the ab initio value calculated by Tasaka et al (2.7 eV). [234]

4.2.4 Mobility of $C_6H_5^+$.

Given that it was possible to generate a source of pure phenylium cations, via the reaction of X^+ (X = CO, CO_2, Kr) with C_6H_5Cl, it was considered that it may be possible to distinguish the linear and cyclic $C_6H_5^+$ ions via their mobilities. The proposed methodology was similar to that employed by Rowe et al [104] who distinguished $O^+(^4S)$ and $O^{+*}(^2D, ^2P)$ in a SIFDT apparatus employing a difference method.

Reaction	Products	Branching ratio	k_{obs} 10^{-9} cm^3 s^{-1}	k_{coll}[a] 10^{-9} cm^3 s^{-1}	ΔH^o_r[b] (kJ mol^{-1})
$Kr^+ + C_6H_5F$	$C_6H_5F^+ + Kr$	1.0	1.5	1.6	-463.2
$Ar^+ + C_6H_5F$	$C_4H_2^+ + C_2H_3F + Ar$	0.07	1.8	2.0	-121.1[c]
	$H_2C_3F^+ + C_3H_3 + Ar$	0.03			-
	$C_5H_3^+ + H_2 + F + Ar$	0.03			-
	$C_4H_3F^+ + C_2H_2 + Ar$	0.50			-
	$C_6H_4^+ + HF + Ar$	0.07			-367.5[d]
	$C_6H_5^+ + F + Ar$	0.06			-198.4
	$C_6H_3F^+ + H_2 + Ar$	0.02			-
	$C_6H_4F^+ + H + Ar$	0.10			-
	$C_6H_5F^+ + Ar$	0.13			-633.2
$Kr^+ + C_6H_6$	$C_6H_6^+ + Kr$	>0.95	~ 1.2	1.2	-457.7
	$C_6H_5^+ + H + Kr$	<0.05			-88.6
$Kr^+ + C_6H_5Cl$	$C_6H_5Cl^+ + Kr$	0.20	1.6	1.7	-476.2
	$C_6H_5^+ + Cl + Kr$	0.80			-156.9
$CO_2^+ + C_6H_5Cl$	$C_6H_5Cl^+ + CO_2$	0.80	1.7	2.0	-454.6
	$C_6H_5^+ + Cl + CO_2$	0.20			-135.3
$CO^+ + C_6H_5Cl$	$C_6H_5Cl^+ + CO$	0.50	1.8	2.5	-477.7
	$C_6H_5^+ + Cl + CO$	0.50			-158.4
c-$C_6H_5^+ + C_2H_2$	adduct	1.0	0.4	1.0	-354.8[e]
c-$C_6H_5^+ + O_2$	adduct	1.0	0.032	0.62	-

Table 4.1. Rate coefficients and branching ratios for the specified reactions.

[a] Calculated using the method of Su and Chesnavich [161].
[b] Based on ΔH^o values presented in ref. 163.
[c] Calculated assuming diacetylene ion and vinyl fluoride neutral structures.
[d] Calculated assuming the benzyne ion structure.
[e] Calculated assuming the c-$C_6H_5C{\equiv}CH_2^+$ structure.

The method involved measuring the arrival time distribution of a mixture of O^+ and O^+* ions (which exhibited a significant late-time skew) and then measuring the arrival time distribution of ground state O^+ ions only (by quenching O^+*). The difference between the two arrival time spectra (normalised to the same peak height) yielded an arrival time distribution for O^+* which had a 7 – 11 % lower mobility than ground state O^+. [104] It was envisaged that it may be possible to similarly measure an arrival time distribution for linear $C_6H_5^+$ by subtracting the arrival time spectrum for pure c-$C_6H_5^+$ (formed via reaction of Kr^+, CO^+ or CO_2^+ with chlorobenzene) from the arrival time spectrum measured for a mixture of linear and cyclic $C_6H_5^+$ (formed, for example, by electron impact on C_6H_5Br in the ion source). The SIFDT apparatus used by Rowe et al [104] possessed ion shutters for gating the ion signal and measuring an arrival time distribution, with the result that the measured arrival time spectra appeared as raised peaks on a zero count background. In contrast, the pulsed ion depletion technique (see the discussion in chapter 2) yields an arrival time distribution that consists of a negative-going dip in a roughly constant background. To improve signal to noise and facilitate ease of data analysis it was decided to employ an ion gating technique for measuring ion arrival time distributions. A power supply and pulsing circuit were constructed to enable a gating voltage to be "stacked" on a desired drift ring. The voltage could be adjusted to a value just sufficient to reduce the transmitted ion signal to zero. The ion gate was opened by pulsing the gating voltage briefly ($\leq$ 20 μs) to zero, enabling ions to enter the drift region. The set-up employed is illustrated schematically in Figure 4.3. This technique suffered from the problem that quite large gating voltages were required to reduce the transmitted ion signal to zero, as the gating voltage was only applied to a drift ring and not, for example, to a grid across the entire diameter of the drift ring. As a consequence, measuring a suitable arrival time distribution was a time consuming process, taking typically twenty minutes or so. Preliminary measurements suggested that it might indeed be possible to distinguish linear from cyclic $C_6H_5^+$ based on mobility. The spectra obtained for a mixture of linear and cyclic $C_6H_5^+$ showed significantly more late-time skew than the spectra obtained for pure c-$C_6H_5^+$, indicative of a linear species possessing a mobility *lower* than the cyclic isomer by a few percent.

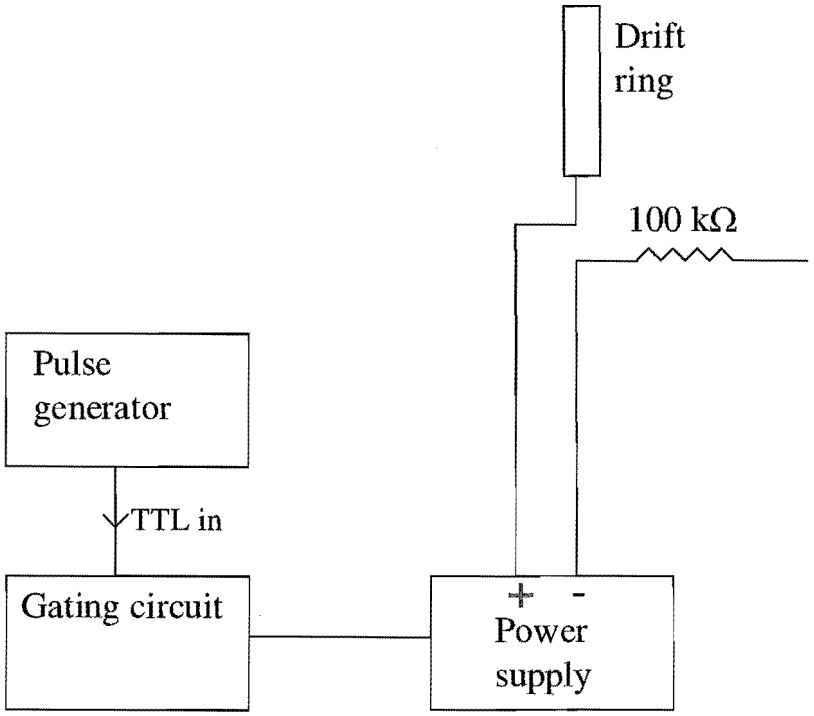

Figure 4.3. Block diagram of the ion gating circuit.

The results were, however, not consistent enough to be unequivocal. Interestingly, a study of the mobility of $C_nH_x^+$ ions ($9 \leq n \leq 22$ and $0 \leq x \leq 5$) indicates that the mobilities of linear isomers are consistently measurably *lower* than those of the monocyclic or bicyclic isomers. [246] Whether or not these results can be extrapolated to $C_6H_5^+$ is uncertain. This question could possibly be resolved by comparing the hard sphere collision integrals calculated for the linear and cyclic $C_6H_5^+$ isomers.

4.3 $C_7H_7^+$

In 1957 Meyerson's group [247] suggested that $C_7H_7^+$, generated by electron impact on toluene and some other alkylbenzenes, was the tropylium ion (Tr^+), with a symmetrical seven membered ring structure, rather than the benzyl ion (Bz^+). Their deduction was based on the observation of hydrogen scrambling in deuterated toluenes, which tended to indicate that hydrogens in $C_7X_7^+$ (X = H or D) lose positional identity and become equivalent. Following the pioneering work of Meyerson et al, numerous research groups,

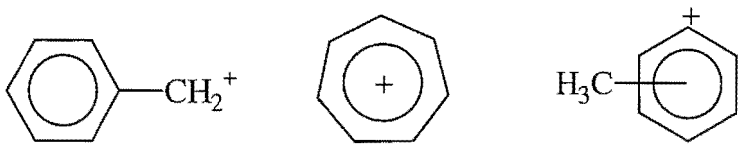

Bz^+ Tr^+ $tolyl^+$

Figure 4.4. The benzyl cation (Bz^+), tropylium cation (Tr^+) and tolyl ion structures.

applying a variety of experimental techniques [242,243,248-272], and coupled with theoretical studies [273-279], have endeavored to understand the structures and energetics of $C_7H_7^+$ ions.[‡] By examining the collisional activation spectra of $C_7H_7^+$, generated from various organic compounds, McLafferty and co-workers [248,249] reported that up to six different isomeric structures of $C_7H_7^+$, including tropylium, benzyl, and tolyl, were observable and could be retained for 10^{-5} seconds without isomerising. In a photoelectron photoion coincidence (PEPICO) study to determine the heats of formation of $C_7H_7^+$ isomers, Baer et al [260] reported that p- and m-tolyl cations were observed as unique structures on the microsecond time scale. Similarly, Cacace et al [258] have reported evidence for the stability of o-, m- and p- tolyl cations in a gas and liquid phase study of the radiolysis of tritiated toluenes. Heath et al [262] have reported selective detection of the tolyl cation among other $C_7H_7^+$ isomers using ion-molecule reactions with dimethyl ether as a diagnostic. Using ICR spectrometry, Dunbar et al [250,251] and Ausloos et al [242] identified benzyl and tropylium structures based on their reactivity, and observed that both structures were stable without interconversion for at least seconds. They also surmised that tolyl ions, known to be higher energy ions, rearrange exclusively to the more stable benzyl structure within 10^{-3} seconds.

In the present work, various methods of forming $C_7H_7^+$ were investigated with the aim of achieving selective formation of a single isomer and estimating the barrier to isomerisation between the benzyl and tropylium structures. Also, it was hoped this would provide a means of distinguishing the isomeric form(s) of $C_7H_7^+$ produced in different bimolecular and termolecular ion-molecule reactions.

[‡] The list of cited references is by no means exhaustive or comprehensive, but is rather intended to give an introduction to the wealth of literature pertaining to the isomers of $C_7H_7^+$. The recent review by Lifshitz [267] is highly recommended.

4.3.1 $C_7H_7^+$ Experimental.

The measurements described below relating to the isomers of $C_7H_7^+$ were performed using the Canterbury SIFT. Rate coefficients and product ratios were measured using the downstream neutral inlet. In situations where $C_7H_7^+$ was formed in the flow tube and subsequently probed for its reactivity, both the upstream and downstream neutral inlets were used.

Thermochemistry of c-$C_7H_7^+$

Some considerable uncertainty has existed as to the enthalpy of formation of the tropylium cation (see, for example, the discussion in references 261 and 267). The value for $\Delta_fH^\circ(Tr^+)$ = 849.4 kJ mol^{-1} tabulated in the 1988 NIST database of Lias and co-workers [163] is apparently too low. In what follows, values of $\Delta_fH^\circ(Tr^+)$ = 871 kJ mol^{-1} and $\Delta_fH^\circ(Bz^+)$ = 916 kJ mol^{-1}, as given in reference 267, have been adopted.

Electron impact on p-fluorotoluene

It was not possible to obtain a workable ion signal at m/z = 91 ($C_7H_7^+$) by subjecting p-fluorotoluene to ~70 eV electron impact. This is entirely in accord with mass spectral data reported for o-, m-, and p-fluorotoluene [280] which shows the major peak derived from the electron impact induced fragmentation of all three isomers is at m/z = 109, $C_7H_6F^+$, as a result of the strength of the C-F bond relative to C-H. Electron impact on the isomers of fluorotoluene was therefore rejected as a convenient source of $C_7H_7^+$. Jackson et al [242] report that electron impact on fluorotoluenes generates a mixture of reactive and unreactive $C_7H_6F^+$ isomers, by direct analogy to the case of unsubstituted toluene.

Electron impact on m-bromotoluene

$C_7H_7^+$ was formed in the ion source via 70 eV impact on m-bromotoluene, mass selected at m/z = 91 and injected into the flow tube. The resultant $C_7H_7^+$ isomer(s) did not react with O_2 added at the downstream neutral inlet, viz. $k_{m/z=91} < 5 \times 10^{-13}$ cm^3 s^{-1}. Subsequent reaction with benzene at the downstream neutral inlet yielded a curved semilogarithmic decay of ln (ion counts) versus neutral flow, indicating the presence of a mixture of at least two isomers, one reactive, the other relatively unreactive with benzene (Figure 4.5). The two isomers produced are believed to be the benzyl (reactive) and tropylium

(unreactive) structures respectively. This conclusion is based on the results of previous reactivity studies which demonstrated that the benzyl cation is generally more reactive than the tropylium structure and also on the results of reaction chemistry described below in which the benzyl and tropylium structures are formed selectively.

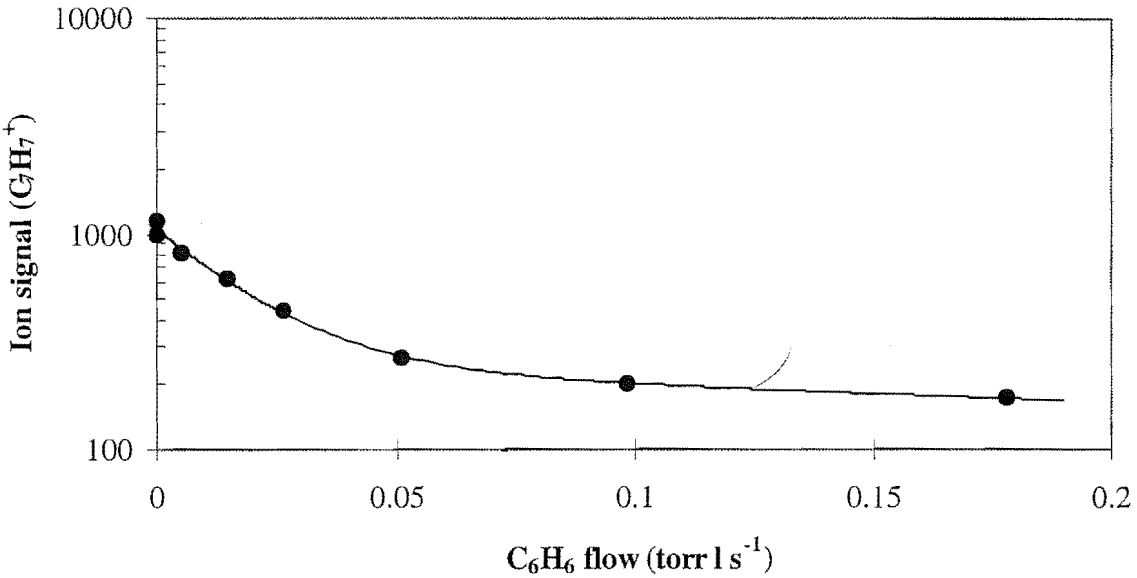

Figure 4.5 Semilogarithmic plot of the $C_7H_7^+$ ion signal (generated via electron impact on m-bromotoluene) versus benzene flow rate. The points are experimental and the curve has been fitted according to equation (3.18) with $k_1 = 2.1 \times 10^{-10}$ cm^3 s^{-1} and $k_2 = 7 \times 10^{-12}$ cm^3 s^{-1}. The curve indicates an isomeric ratio of 78:22 in favour of the fast reacting $C_7H_7^+$ isomer.

Kr^+ + cycloheptatriene

Kr^+ was injected into the flow tube and reacted with cycloheptatriene at the downstream neutral inlet. $C_7H_7^+$ was the major product ion.

$$Kr^+ + c\text{-}C_7H_8 \xrightarrow{0.95} C_7H_7^+ + H + Kr \qquad \textbf{(4.13a)}$$

$$\xrightarrow{0.05} C_5H_5^+ + CH_2 + Kr \qquad \textbf{(4.13b)}$$

$k_{4.13} = 1.4 \times 10^{-9}$ cm^3 s^{-1}

By injecting Kr^+ and adding cycloheptatriene at the upstream neutral inlet it was possible to probe the reactivity of the resultant $C_7H_7^+$ ions via subsequent reaction with benzene at

the downstream neutral inlet. The observation of curvature in the resultant semilogarithmic decay indicated that the reaction of Kr^+ with cycloheptatriene is sufficiently exothermic to produce a mixture of $C_7H_7^+$ isomers. The thermochemical threshold for formation of the tropylium ion, c-$C_7H_7^+$, from cycloheptatriene is 9.4 eV. Given that I.P.(Kr) = 13.99 eV, we can infer that the barrier for interconversion between the tropylium and benzyl cations lies < 3.6 eV above the energy of the tropylium cation.

C^+ + cycloheptatriene

C^+ was produced by subjecting a 5% mixture of CO in He to electron impact in the ion source and was injected into the flow tube following mass-selection at m/z = 12. The reaction of C^+ with cycloheptatriene yielded multiple products, $C_7H_7^+$ being the major product.

$$C^+ + \text{c-}C_7H_8 \xrightarrow{0.20} C_7H_8^+ + C \qquad \textbf{(4.14a)}$$

$$\xrightarrow{0.35} C_7H_7^+ + H + C \qquad \textbf{(4.14b)}$$

$$\xrightarrow{0.21} C_6H_5^+ + CH_3 + C \qquad \textbf{(4.14c)}$$

$$\xrightarrow{0.05} C_5H_5^+ + C_2H_3 + C \qquad \textbf{(4.14d)}$$

$$\xrightarrow{0.03} C_5H_3^+ + C_2H_5 + C \qquad \textbf{(4.14e)}$$

$$\xrightarrow{0.07} C_4H_4^+ + C_3H_4 + C \qquad \textbf{(4.14f)}$$

$$\xrightarrow{0.09} C_3H_3^+ + C_4H_5 + C \qquad \textbf{(4.14g)}$$

$k_{4.14} = 2.6 \times 10^{-9}$ cm^3 s^{-1}

Subsequent reaction of the $C_7H_7^+$ ion with benzene at the downstream neutral inlet indicated that the m/z = 91 signal was comprised of a mixture of $C_7H_7^+$ isomers. Given that I.P.(C) = 11.26 eV, we can infer that the barrier to the isomerisation tropylium $\rightleftharpoons$ benzyl lies $\leq$ 1.8 eV above the energy of the tropylium cation, provided the injected C^+ signal was comprised solely of ground state ions. This assumption may not be justified (see the discussion which follows).

SO^+ + cycloheptatriene

SO^+ was formed via electron impact on a ~10% mixture of SO_2 in He, mass-selected at m/z = 48 and injected into the flow tube. The only primary product ion observed following reaction of the injected SO^+ with cycloheptatriene resulted from charge transfer.

$SO^+ + c\text{-}C_7H_8 \xrightarrow{\geq 0.98} C_7H_8^+ + SO$ **(4.15a)**

$\xrightarrow{\leq 0.02} C_7H_7^+ + H + SO$ **(4.15b)**

$k_{4.15} = 1.6 \times 10^{-9}$ cm^3 s^{-1}

An upper limit of 2% has been placed on the $C_7H_7^+$ channel since, at high flows of cycloheptatriene, m/z = 91 appeared as a secondary product.

$c\text{-}C_7H_8^+ + c\text{-}C_7H_8 \longrightarrow C_7H_7^+ + C_7H_9$ **(4.16a)**

$\longrightarrow$ adduct **(4.16b)**

Reaction (4.16a) was also noted by Ausloos [243] in an ICR study of the $C_7H_7^+$ ions formed in the charge transfer induced fragmentation of ethylbenzene, toluene and norbornadiene. Ausloos noted that the growth of $C_7H_7^+$ as a function of time made it impossible to monitor the formation of $C_7H_7^+$ formed via charge transfer induced fragmentation of cycloheptatriene.

The $C_7H_7^+$ species formed in reaction (4.16) was observed to be unreactive with benzene ($k < 5 \times 10^{-13}$ cm^3 s^{-1}) and the tropylium structure was therefore assigned to this ion. Given that reaction (4.16a) yields the tropylium structure exclusively, the thermochemistry of this reaction should yield information concerning the barrier height for the tropylium $\longrightarrow$ benzyl rearrangement. Unfortunately, the structure of the neutral fragment or fragments formed in reaction (4.16a) is unknown. A channel known to be exothermic is:

$c\text{-}C_7H_8^+ + c\text{-}C_7H_8 \longrightarrow c\text{-}C_7H_7^+ + c\text{-}C_7H_7 + H_2$ **(4.17)**

however any suggestion that reaction (4.17) occurs is purely speculative.

C^+ + benzyl bromide

The reaction of C^+ with benzyl bromide was difficult to measure as a result of the very low vapour pressure of benzyl bromide at room temperature, however the reaction was shown to proceed at close to the collision rate. Determination of an accurate branching ratio was also made difficult by the low neutral vapour pressure, however $C_7H_7^+$ was verified as the major reaction product.

$C^+ + C_7H_7Br \xrightarrow{\sim 0.80} C_7H_7^+ + Br + C$ (or CBr) **(4.18a)**

$\xrightarrow{\sim 0.20} C_6H_5^+ + (CH_2Br + C\ ?)$ **(4.18b)**

$$\xrightarrow{\leq 0.05} C_7H_7Br^+ + C \qquad \textbf{(4.18c)}$$

$k_{4.18} = 3.0 \times 10^{-9}$ cm^3 s^{-1}

$C_6H_5^+$ is not energetically accessible from ground state C^+ and as such the observation of this product probably indicates the presence of some metastable $C^+(^4P)$ in the reactant ion swarm. The $C_7H_7^+$ ion product of this reaction produced a linear decay when reacted subsequently with benzene at the downstream neutral inlet, with a rate coefficient of k = 1.6×10^{-10} cm^3 s^{-1}. The observed reactivity suggests that the $C_7H_7^+$ ion formed in reaction (4.18a) has the Bz^+ structure. The reaction chemistry described above is summarised in Tables 4.2 and 4.3.

4.3.2 Discussion.

Traeger and Kompe [261] in a photoionisation study of benzyl halides proposed that photoionisation of $C_6H_5CH_2X$ (X = Cl, Br, I) produces the tropylium structure at threshold. This conclusion was based on the fact that the 298 K heats of formation for $C_7H_7^+$ derived from the $C_7H_7^+$ threshold appearance energies for $C_6H_5CH_2X$ were 31 – 36 kJ mol^{-1} lower than the well established heat of formation of the benzyl cation. Although this was contrary to the results obtained from low electron energy collisional activation mass spectra for benzyl bromide [259], it was proposed that the threshold formation of tropylium is rapidly overtaken, and subsequently dominated, by the production of benzyl cation at ionising energies 30 – 40 kJ mol^{-1} in excess of threshold. The apparent disparity between the photoionisation and collisional activation results can be understood in terms of the parallel behaviour exhibited in the toluene ($TOL^{\bullet+}$)/cycloheptatriene ($CHT^{\bullet+}$) radical cation system. [267]

$TOL^{\bullet+}$ $CHT^{\bullet+}$

Figure 4.6. The toluene ($TOL^{\bullet+}$) and cycloheptatriene ($CHT^{\bullet+}$) radical cations.

Reaction	Products	Branching ratio	k_{obs} /10^{-9} cm^3 s^{-1}	$\Delta H^{o\,a}_r$ /kJ mol^{-1}
$Kr^+ + c\text{-}C_7H_8$[b]	$C_7H_7^+ + H + Kr$	0.95	1.4	-444.4[c]
	$C_5H_5^+ + CH_2 + Kr$	0.05		-131.8[d]
$SO^+ + c\text{-}C_7H_8$	$c\text{-}C_7H_8^+ + SO$	≥ 0.98		-195.4
	$C_7H_7^+ + H + SO$	≤ 0.02		-89.6[c]
$C^{+e} + c\text{-}C_7H_8$	$c\text{-}C_7H_8^+ + C$	0.20	2.6	-286.2
	$C_7H_7^+ + H + C$	0.35		-180.4[c]
	$C_6H_5^+ + CH_3 + C$	0.21		+3.0
	$C_5H_5^+ + C_2H_3 + C$	0.05		+8.4[d]
	$C_5H_3^+ + C_2H_5 + C$	0.03		-
	$C_4H_4^+ + C_3H_4 + C$	0.07		+151.4[f]
	$C_3H_3^+ + C_4H_5^+ + C$	0.09		+94.3[g]
$C^+ + C_7H_7Br$[h]	$C_7H_7^+ + Br + C$	~ 0.80	3.0	-125.9[i]
	$C_6H_5^+ + CH_2Br + C$	~ 0.20		+33.1
	$C_7H_7Br^+ + C$	≤ 0.05		-216.4

Table 4.2. Rate coefficients and branching ratios for the specified reactions.

[a] Based on ΔH^o values presented in refs 163 and 164.
[b] cycloheptatriene
[c] Calculated assuming $C_7H_7^+$ ion has the tropylium structure (see text for note on thermochemistry).
[d] Calculated assuming vinylcyclopropenyl cation structure for $C_5H_5^+$.
[e] Probably comprised of a mixture of ground state C^+ (^2P) and metastable C^+ (^4P).
[f] Calculated assuming $CH_2{=}C{=}C{=}CH_2^+$ structure for $C_4H_4^+$.
[g] Calculated assuming cyclic $C_3H_3^+$ structure.
[h] benzyl bromide.
[i] Calculated assuming $C_7H_7^+$ ion has the benzyl structure (see text for note on thermochemistry).

Source of $C_7H_7^+$	k_1[a] (10^{-9} cm^3 s^{-1})	k_2[b] (10^{-9} cm^3 s^{-1})	C_1[c]
$Kr^+ + c\text{-}C_7H_8$	0.25	< 0.001	0.61
$C^+ + c\text{-}C_7H_8$	0.23	< 0.0005	0.25
$c\text{-}C_7H_8^+ + c\text{-}C_7H_8$	< 0.0005[d]		1.0
$C^+ + C_7H_7Br$	0.16[d]		1.0

Table 4.3. Reaction rate coefficients with benzene and isomer ratio for the $C_7H_7^+$ isomer(s) formed in the specified reactions.

At low ionising energies, equilibration occurs between the toluene and cycloheptatriene radical cations, below their respective dissociation thresholds to Bz^+ and Tr^+. At higher energies, direct dissociation becomes favoured relative to the isomerisation of $TOL^{\bullet+}$ to $CHT^{\bullet+}$. After formation of Bz^+, provided sufficient energy is available, Bz^+ and Tr^+ can interconvert across a potential barrier. Formation of Tr^+ from toluene therefore proceeds via two parallel routes: (1) isomerisation to $CHT^{\bullet+}$ followed by loss of $H^\bullet$ and (2) C-H cleavage forming Bz^+ followed by isomerisation to Tr^+. The following reaction scheme is appropriate:

$$TOL^{\bullet+} \xrightarrow{k_1} Bz^+ + H^\bullet \qquad \textbf{(4.19a)}$$

$$TOL^{\bullet+} \underset{k_3}{\overset{k_2}{\rightleftharpoons}} CHT^{\bullet+} \qquad \textbf{(4.19b)}$$

$$CHT^{\bullet+} \xrightarrow{k_4} Tr^+ + H^\bullet \qquad \textbf{(4.19c)}$$

The details of this mechanism are discussed fully in reference 267 and references cited therein. Evidence that the benzyl bromide and benzyl chloride radical cations undergo rearrangement to the respective halogenated cycloheptatrienes prior to dissociation (in contrast to the halogenated toluenes) has been given by Fu et al. [252]

In the present experiments, by systematically varying the internal energy content of the $C_7H_8^+$ or $C_7H_7Br^+$ precursor, it has been possible to form the tropylium or benzyl

[a] Observed rate coefficient for the more reactive isomer (uncertainty ± 50%) with benzene.
[b] Observed rate coefficient for the less reactive isomer (uncertainty ± 50%) with benzene.
[c] Estimated proportion of the more reactive isomer.
[d] Linear semilogarithmic decay observed (see text for discussion).

cations selectively. The reaction of C^+ with benzyl bromide yielded the benzyl cation only. Since this reaction is exothermic by 1.3 eV we conclude that the barrier to isomerisation must lie > 1.3 eV above the energy of the benzyl cation, or > 1.8 eV above the tropylium cation, since benzyl is less stable than tropylium by 0.5 eV. The reaction of C^+ with cycloheptatriene produced a mixture of benzyl and tropylium cations, however the proportion of metastable $C^+(^4P)$ present in the injected ion swarm was not determined. $C^+(^4P)$ ions possess an additional 5.3 eV of excitation energy which would undoubtedly be sufficient energy to promote isomerisation of tropylium to benzyl. It should be noted that no evidence for isomerisation of Bz^+ to Tr^+ was observed when $C_7H_7^+$ was formed via the reaction of C^+ with benzyl bromide, although the same source of C^+ was used, viz. electron impact on a 5% mixture of CO in He. Regardless of the uncertainty concerning what fraction of C^+ was in an excited electronic state in the present experiments, the barrier to the $Tr^+ \rightleftharpoons Bz^+$ isomerisation almost certainly lies within 2.7 ± 0.9 eV of the energy of Tr^+, based on the observation that reaction (4.18) yields the benzyl cation exclusively and reaction (4.13) yields a mixture of Tr^+ and Bz^+. This conclusion is in accord with MINDO/3 calculations of the $C_7H_7^+$ potential energy surface which predict the barrier to isomerisation to lie 57.5 kcal mol^{-1} (2.5 eV) above the tropylium structure. [274] It is also in reasonable agreement with the value (2.0 eV) estimated by McLafferty and Bockhoff [253] based on collisional activation mass spectra. Ausloos [243] concluded from an ICR study that the internal energy at which $C_7H_7^+$ undergoes isomerisation is in the region of 3 – 4 eV above the energy of Tr^+, which is significantly higher than that derived from the collisional activation study, but is in accord with the present results within the combined uncertainties. A recent high level re-investigation of the $C_7H_7^+$ potential energy surface by Smith and Hall [278] suggests that the barrier to the $Bz^+ \rightleftharpoons Tr^+$ isomerisation lies 301.5 kJ mol^{-1} (3.1 eV) above the energy of Tr^+. The matrix isolation study of Andrews and Keelan [255] suggests a value for the barrier height in the region of 2.0 – 3.6 eV above the energy of Bz^+ based on the observation that photolysis with 340 – 600 nm light promoted isomerisation of Bz^+ to Tr^+.

4.3.3 Determining the isomeric product distribution of ion-molecule reactions.

Several ion-molecule reactions have been reported in the literature, which lead to the formation of ions with molecular formula $C_7H_7^+$. It was decided to examine the isomeric distributions of $C_7H_7^+$ ions formed as products in these reactions.

Methodology

In each case the $C_7H_7^+$ ions probed for structure were formed in the flow reactor tube by injecting the respective mass-selected reactant ions into the helium carrier flow and adding the appropriate reagent at the first neutral inlet. Benzene was then added at the downstream neutral inlet to facilitate identification of the $C_7H_7^+$ structure or structures formed in the respective reactions. In order to determine the rates and product ratios of each reaction producing $C_7H_7^+$, the mass-selected primary ions were reacted with the appropriate neutrals at the downstream neutral inlet in a separate experiment.

$C_3H_3^+ + C_6H_6$

The reaction of $C_3H_3^+$ with benzene was measured by Ausloos et al [244,281] in an ICR spectrometer. They report a rate coefficient for the reaction of 1.4×10^{-9} cm^3 s^{-1} and observed two product ions, $C_7H_7^+$ and $C_9H_7^+$, although they did not report a branching ratio for each channel.

In the present work $C_3H_3^+$ was formed via electron impact on ethylene in a high pressure ion source, producing a mixture (~ 50:50) of both linear and cyclic $C_3H_3^+$. Upon subsequent reaction with benzene vapour at the downstream neutral inlet, a curved semilogarithmic decay of ln (ion counts) versus neutral flow was observed. A double exponential expression was fitted to the curve yielding a rate coefficient of 1.9×10^{-9} cm^3 s^{-1} for l- $C_3H_3^+$ and 9.5×10^{-12} cm^3 s^{-1} for c- $C_3H_3^+$ respectively. Previous studies have identified the linear isomer as generally more reactive. [282] The major reaction product was the termolecular adduct at m/z = 117, accounting for 70% of the total reaction products.

$$\text{l-}C_3H_3^+ + C_6H_6 \xrightarrow{0.70} \text{adduct} \qquad \textbf{(4.20a)}$$

$$\xrightarrow{0.25} C_9H_7^+ + H_2 \qquad \textbf{(4.20b)}$$

$$\xrightarrow{0.05} C_7H_7^+ + C_2H_2 \qquad \textbf{(4.20c)}$$

$C_9H_7^+$ and $C_7H_7^+$ were both observed as minor products, however the fact that $C_7H_7^+$ constituted a 5% channel only, made determination of the $C_7H_7^+$ structure impractical. Ausloos and Lias [244] earlier concluded that the $C_7H_7^+$ product of reaction (4.20c) was > 80% benzyl cation.

$C_3H_5^+ + C_6H_6$

Houriet et al [283] examined the reaction of $C_3H_5^+$ with benzene, also in an ICR spectrometer. They report a rate coefficient of 1.15 x 10^{-9} cm^3 s^{-1} and a 91% product channel to $C_7H_7^+$, with a 9% channel producing $C_6H_7^+$. In the present work, $C_3H_5^+$ was formed via electron impact on ethylene in a high-pressure ion source, mass selected at m/z = 41 and injected into the flow tube. Some concomitant breakup to $C_3H_3^+$ was observed, but since the reaction of $C_3H_3^+$ with benzene had been measured previously it was possible to clearly identify the products arising from the reaction of $C_3H_5^+$ with benzene.

$$C_3H_5^+ + C_6H_6 \xrightarrow{0.60} C_3H_5^+.C_6H_6 \quad \textbf{(4.21a)}$$

$$\xrightarrow{0.40} C_7H_7^+ + C_2H_4 \quad \textbf{(4.21b)}$$

$$\xrightarrow{<0.05} C_6H_7^+ + C_3H_4 \quad \textbf{(4.21c)}$$

$k_{4.21}$ = 1.4 x 10^{-9} cm^3 s^{-1}

The measured rate and product distribution for this reaction is in excellent agreement with that measured for the reaction of the allyl cation with benzene in the new FA-SIFDT apparatus (section 4.4). When the $C_7H_7^+$ product of reaction (4.21b) was subsequently reacted with benzene at the downstream neutral inlet, a linear semilogarithmic decay was obtained with a rate coefficient of 1.6 x 10^{-10} cm^3 s^{-1}. The $C_7H_7^+$ ion formed in reaction (4.21b) is therefore believed to be the benzyl cation.

$C_6H_5^+ + C_3H_6$

Ausloos et al [233] reported that the reaction of c-$C_6H_5^+$ with propene produced $C_7H_7^+$ exclusively, with a rate coefficient of 3.4 x 10^{-10} cm^3 s^{-1}. $C_6H_5^+$ was formed in the ion source via electron impact on bromobenzene. A curved semilogarithmic decay of ln (ion counts) versus neutral flow was observed when this ion was reacted with propene as a result of the presence of a mixture of linear and cyclic isomers. The rate coefficient determined for the reaction of c-$C_6H_5^+$ with propene from a double exponential fit to the

data was 6.2 x 10^{-10} cm^3 s^{-1}. The linear isomer was shown to be relatively unreactive, $k_{linear} \leq 10^{-12}$ cm^3 s^{-1}. Subsequent reaction of the $C_7H_7^+$ product of reaction (4.22) with benzene at the downstream neutral inlet indicated that the ion again has the benzyl structure.

$$c\text{-}C_6H_5^+ + C_3H_6 \xrightarrow{1.0} C_7H_7^+ + C_2H_4 \qquad \textbf{(4.22)}$$

$C_6H_5^+ + CH_4$

Ausloos et al [233] also reported that reaction of $c\text{-}C_6H_5^+$ with methane generates $C_7H_7^+$ with concomitant loss of H_2. No appreciable $C_7H_7^+$ was observed in the present work, the only observed product of reaction (4.23) appearing at m/z = 93, $C_6H_5^+.CH_4$, with a rate coefficient of 3.9 x 10^{-10} cm^3 s^{-1} at 0.35 Torr. Linear $C_6H_5^+$ was again observed to be unreactive, with $k < 10^{-12}$ cm^3 s^{-1}. The rate coefficient reported by Ausloos et al [233], for the formation of $C_7H_7^+$, 7.5 x 10^{-11} cm^3 s^{-1}, corresponds to only 8 % of the Langevin rate. The difference between the present *higher pressure* results and the low pressure results of Ausloos et al may reflect different $(C_6H_5^+ \cdot CH_4)^*$ complex lifetimes in the two systems. In the present study the intermediate complex exists for ~ 160 ns prior to a collision with a helium bath gas atom. At the much lower pressure of the ICR experiment (< 10^{-6} Torr) the intermediate collision complex has a much longer time to access the channel to bimolecular products.

$$c\text{-}C_6H_5^+ + CH_4 \xrightarrow{1.0} C_6H_5^+.CH_4 \qquad \textbf{(4.23)}$$

$k_{4.23}$ = 3.9 x 10^{-10} cm^3 s^{-1} at 0.35 Torr

$C_5H_5^+ + C_2H_2$

Ozturk et al [284,285] identified a $C_7H_7^+$ product formed via radiative association of $C_5H_5^+$ with C_2H_2 in an FT-ICR spectrometer at 373 K. $C_5H_5^+$ was formed in the SIFT ion source via electron impact on a ~10% mixture of propyne in C_2H_2 or alternatively via electron impact on cycloheptatriene. The first method was employed because linear $C_3H_3^+$, a major fragment ion from propyne, is known to associate rapidly with C_2H_2 to form $C_5H_5^+$. [282]

$$C_3H_4 \longrightarrow l\text{-}C_3H_3^+ \xrightarrow{C_2H_2} C_5H_5^+ \qquad \textbf{(4.24)}$$

$$c\text{-}C_7H_8 \longrightarrow C_7H_7^+ \longrightarrow C_5H_5^+ \qquad \textbf{(4.25)}$$

Subsequent reaction of the injected $C_5H_5^+$ with acetylene at the downstream neutral inlet yielded a rate coefficient of $k < 1 \times 10^{-12}$ cm^3 s^{-1} indicating that the association reaction (4.26) is relatively inefficient at 0.35 Torr.

$$C_5H_5^+ + C_2H_2 \longrightarrow C_7H_7^+ \qquad \textbf{(4.26)}$$

Since the isomeric form of the reactant $C_5H_5^+$ ion(s) was unknown in each case it is possible that the observed reaction arose due the presence of a small amount (< 10%) of a reactive $C_5H_5^+$ isomer in a mostly unreactive ion swarm. The observation by Ozturk et al [284,285] of a much faster association reaction between $C_5H_5^+$ and acetylene ($k = 3.1 \times 10^{-11}$ cm^3 s^{-1}) may indicate that the isomeric form of $C_5H_5^+$ was different in their FT-ICR experiment. It should be noted that Ausloos [243] identified the presence of at least two isomeric $C_5H_5^+$ structures formed upon dissociation of Bz^+ and Tr^+.

$C_3H_5^+ + C_4H_2$

$C_3H_5^+$ had previously been shown to associate rapidly with diacetylene (see chapter 4.4) and it was therefore decided to identify the $C_7H_7^+$ ion(s) formed in reaction (4.27).

$$C_3H_5^+ + C_4H_2 \xrightarrow{0.70} C_7H_7^+ \qquad \textbf{(4.27a)}$$

$$\xrightarrow{0.30} C_5H_5^+ + C_2H_2 \qquad \textbf{(4.27b)}$$

$k_{4.27} = 1.3 \times 10^{-9}$ cm^3 s^{-1}; $\Delta H^\circ_{4.27a} = -514$ kJ mol^{-1} (Tr^+); - 469 kJ mol^{-1} (Bz^+)

Subsequent reaction of the $C_7H_7^+$ ions produced in reaction (4.27a) with benzene at the downstream neutral inlet produced a curved semilogarithmic decay of ln (ion counts) versus neutral flow, indicating the presence of a mixture of $C_7H_7^+$ isomers. The rate coefficients determined from the curved decay are consistent with a mixture of benzyl and tropylium cations. This is perhaps not surprising, given the large exothermicity of reaction (4.27a). The energy of the reactants, $C_3H_5^+ + C_4H_2$, lies above the dissociation threshold for $C_5H_5^+$ formation and hence well above the $Tr^+ \rightleftharpoons Bz^+$ isomerisation barrier. The observation of $C_5H_5^+$ as a product of reaction (4.27) is consistent with the threshold for dissociation of $C_7H_7^+$ to $C_5H_5^+$ determined by Ausloos. [243]

Reaction	Products	Branching ratio	k_{obs} 10^{-9} cm^3 s^{-1}	k_{coll}[a] 10^{-9} cm^3 s^{-1}	ΔH^o_r[b] (kJ mol^{-1})
1-$C_3H_3^+$ + C_6H_6	adduct	0.70	1.9	1.5	-
	$C_9H_7^+$ + H_2	0.25			-
	$C_7H_7^+$ + C_2H_2	0.05			-118.7[c]
$C_3H_5^+$[d] + C_6H_6	adduct	0.60	1.4	1.4	-
	$C_7H_7^+$ + C_2H_4	0.40			-60.1[c]
	$C_6H_7^+$ + C_3H_4	<0.05			+24.6
c-$C_6H_5^+$ + C_3H_6	$C_7H_7^+$ + C_2H_4	1.0	0.62	1.1	-178.5
$C_5H_5^+$[e] + C_2H_2	$C_7H_7^+$	1.0	<0.001	1.0	-
$C_3H_5^+$[d] + C_4H_2	$C_7H_7^+$	0.70	1.3	1.2	-513.9[f]
	$C_5H_5^+$ + C_2H_2	0.30			-143.9[g]

Table 4.4. Rate coefficients and branching ratios for reactions which produce $C_7H_7^+$.

4.4 $C_3H_5^+$

4.4.1 Introduction.

$C_3H_5^+$ carbocations are commonly produced as fragments in the mass spectra of many organic compounds and the structure of these cations has been the focus of continued interest. Many studies, both theoretical and experimental, have been reported. [286-306] Quite early on it was recognised that different isomeric structures of $C_3H_5^+$ exist. This recognition was based on the existence of several minima on the $C_3H_5^+$ potential surface. Two of the structures identified in theoretical investigations, [287-289] the allyl and 2-propenyl cations, were also characterised in the laboratory. [291,294,295]

---

[a] Calculated using the method of Su and Chesnavich. [161]
[b] Based on ΔH^o values presented in refs 163 and 164.
[c] Calculated assuming $C_7H_7^+$ has the benzyl ion structure (see text for discussion).
[d] Allyl cation (see text for discussion).
[e] Structure unknown (see text for discussion).
[f] Calculated assuming $C_7H_7^+$ has the tropylium ion structure (see text for discussion).
[g] Calculated assuming vinylcyclopropenyl cation structure for $C_5H_5^+$.

Aue et al [291], in an ICR equilibrium study in which they examined the equilibrium system:

$$H_3S^+ + C_3H_4 \rightleftharpoons C_3H_5^+ + H_2S \qquad \textbf{(4.28)}$$

reported a proton affinity for propyne of 728 kJ mol^{-1} assuming PA(H_2S) = 720 kJ mol^{-1}. Further, the $C_3H_5^+$ structure arising from the protonation of propyne was found to have the 2-propenyl structure (2, Figure 4.7). Proton transfer from H_3S^+ to allene was also found to produce the 2-propenyl structure. [291] Other measurements based on ionisation energies [286], photoelectron spectroscopy [307] and photoionisation mass spectrometry [308], in combination with contributions from theory [288], have clearly identified the allyl structure (1, Figure 4.7) as the lowest energy structure and global minimum on the $C_3H_5^+$ surface. [288,293,296,303] Collision induced dissociation studies [294,295,297] and proton transfer reactions [291,298,302] have also distinguished between the allyl and 2-propenyl structures.

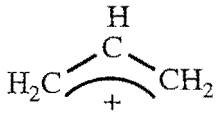

1

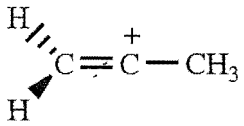

2

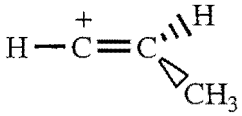

3

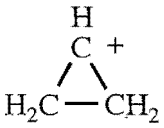

4

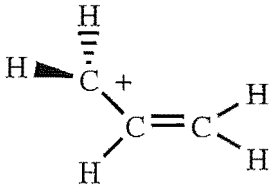

5

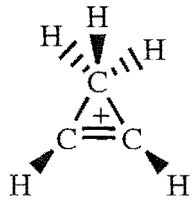

6

Figure 4.7. Possible $C_3H_5^+$ ion structures: allyl cation (1), 2-propenyl cation (2), 1-propenyl cation (3), cyclopropyl cation (4), perpendicular allyl ion (5), corner protonated cyclopropene (6).

Two other structures, 1-propenyl and cyclopropyl (3,4 respectively, Figure 4.7) have not been unequivocally identified and some doubt remains as to whether they retain their identity under the conditions existing in most mass spectrometer systems, or whether they collapse to the more stable 2-propenyl and allyl structures. Some evidence has been found for a stable cyclopropyl ion (4, Figure 4.7). Aue et al [291] proposed that proton transfer from $(CH_3)_2OH^+$ to cyclopropene produces the cyclopropyl structure. Further, bands arising from the photoionisation of the c-C_3H_5 radical have been attributed to the cyclopropyl cation structure. [309]

A study was made of the proton transfer reactions of $C_3H_5^+$ made from propyne, allene, ethylene and cyclopropane in the FA/SIFDT apparatus. Ab initio calculations of the proton affinities of propyne and allene were also performed.

4.4.2 $C_3H_5^+$ Experimental.

All of the following measurements pertinent to the chemistry of $C_3H_5^+$ were carried out using the new FA-SIFDT apparatus. Two techniques were used to form $C_3H_5^+$ ions. In the first method, $C_3H_5^+$ was generated in the FA source region by addition of cyclopropane or ethylene to a helium carrier subjected to microwave discharge. $C_3H_5^+$ was mass selected from the ions in the afterglow and injected into the flow tube. In the second method a suitable base, B (e.g. H_2O), was protonated, mass selected and then injected into the flow tube. Proton transfer then occurred from HB^+ to propyne or allene added at the first inlet port of the flow reactor tube. The structure of the resultant $C_3H_5^+$ ions was then probed using a diagnostic reagent added at the second inlet port.

4.4.3 Results and discussion.

Theoretical calculations

All calculations were performed using the Gaussian 94 programs. [178] The calculations follow the prescription detailed in the original description of the G2(MP2) procedure. [160]

Previous theoretical studies have shown that protonation of allene at the C_2 position cannot occur directly. Originally it was proposed that protonation and CH_2 rotation occurred in a concerted fashion [291] but Foresman et al [304] found the necessary perpendicular allyl structure (5, Figure 4.7) did not represent a true saddle point on the

potential surface. Instead, low energy protonation of allene occurs via the terminal carbon atom forming the 2-propenyl structure and not the allyl structure. In the present work a structure corresponding to the perpendicular allyl cation was identified at the HF/6-31G* level of theory, which collapses at the higher MP2/6-31G* level to the 2-propenyl species, in accordance with the calculations of Foresman et al. [304] It was also determined that the cyclopropyl ion represents a transition state for the disrotatory stereomutation of the allyl cation, again in accord with earlier calculations. [288,293]

The G2(MP2) energies and relative energies from the calculations are given in Table 4.5. The calculated proton affinities of both allene and propyne are given in Table 4.6. It is interesting to note that the 2-propenyl structure may give rise to either propyne or allene on deprotonation. A schematic diagram of a section of the $C_3H_5^+$ potential surface is illustrated in Figure 4.8.

Species[a]	E(G2(MP2)) /hartree	ΔE (0 K) /kJ mol^{-1}
I H_2CCCH_2	-116.41565	
II H_3CCCH	-116.41506	
III $H_2CCHCH_2^+$	-116.70624	0.0
IV $H_3CCCH_2^+$	-116.69354	+33.4
V c-$H_2CCHCH_2^+$ (TS)	-116.65260	+140.9
VI TS (III – IV)	-116.66478	+108.9
VII TS ($H_2CCHCH_2^+$) Twist – HF geom.	-116.65377	+137.8
VIII c-C_3H_4[b]	-116.37906	

Table 4.5. G2(MP2) energies of $C_3H_5^+$ species.

[a] The species listed here correspond to structures shown in Fig. 4.7 as follows: III = 1; IV = 2; V = 4; VII =5.
[b] cyclopropene

Species	Proton Affinity (298 K) /kJ mol^{-1}	Expt [164]
H_2CCCH_2 C1	733.6	-
H_2CCCH_2 C2	769.1	775
H_3CCCH C1	735.4	747.6
c-C_3H_4[a]	828.5[b]	818.5

Table 4.6. Proton affinities of C_3H_4 species from G2(MP2) calculations.

Measurements

A knowledge of the structure of $C_3H_5^+$ is crucial to an understanding of the reactivity of each individual isomer. It was therefore necessary to develop a method for distinguishing between the allyl (1, Figure 4.7) and 2-propenyl (2, Figure 4.7) isomers. Of all the reactions examined in this work, the only reaction found that distinguishes clearly between the structures was the reaction with methanol.

CH_3OH Reactions (PA = 754 kJ mol^{-1})

The 2-propenyl $C_3H_5^+$ structure was formed by injecting H_3O^+ from the source region into the flow tube and adding propyne at the first inlet port as discussed in the experimental section. As the difference in PA (propyne-H_2O) is small (57 kJ mol^{-1}) and the barrier calculated for the rearrangement to the more stable allyl structure is larger than this (see Figure 4.8) then the resulting $C_3H_5^+$ should have the 2-propenyl structure, designated hereafter as $CH_3CCH_2^+$.

$$CH_3CCH_2^+ + CH_3OH \xrightarrow{\sim 0.70} CH_3OH_2^+ + C_3H_4 \qquad \textbf{(4.29a)}$$

$$\xrightarrow{\sim 0.30} C_3H_5^+.CH_3OH \qquad \textbf{(4.29b)}$$

$k_{4.29} = 1.7 \times 10^{-9}$ cm^3 s^{-1}

The semilogarithmic decay for this reaction is shown in Figure 4.9a.

The allyl structure, designated hereafter as $CH_2CHCH_2^+$, was prepared by injecting any $C_3H_5^+$ ion formed in the FA source section into the flow tube. All sources of $C_3H_5^+$ (proton transfer and fragmentation) produced a common $C_3H_5^+$ structure after

[a] cyclopropene.
[b] Calculated with respect to the 2-propenyl cation, $CH_3CCH_2^+$ (see text for discussion).

injection into the flow tube. Even though the injection energies were relatively small (ion energies were typically 20 eV, or < 2eV in the centre of mass frame) the very process of injecting the ion into the helium carrier gas flow of the reactor tube was sufficient to cause rearrangement to the allyl structure, $CH_2CHCH_2^+$.

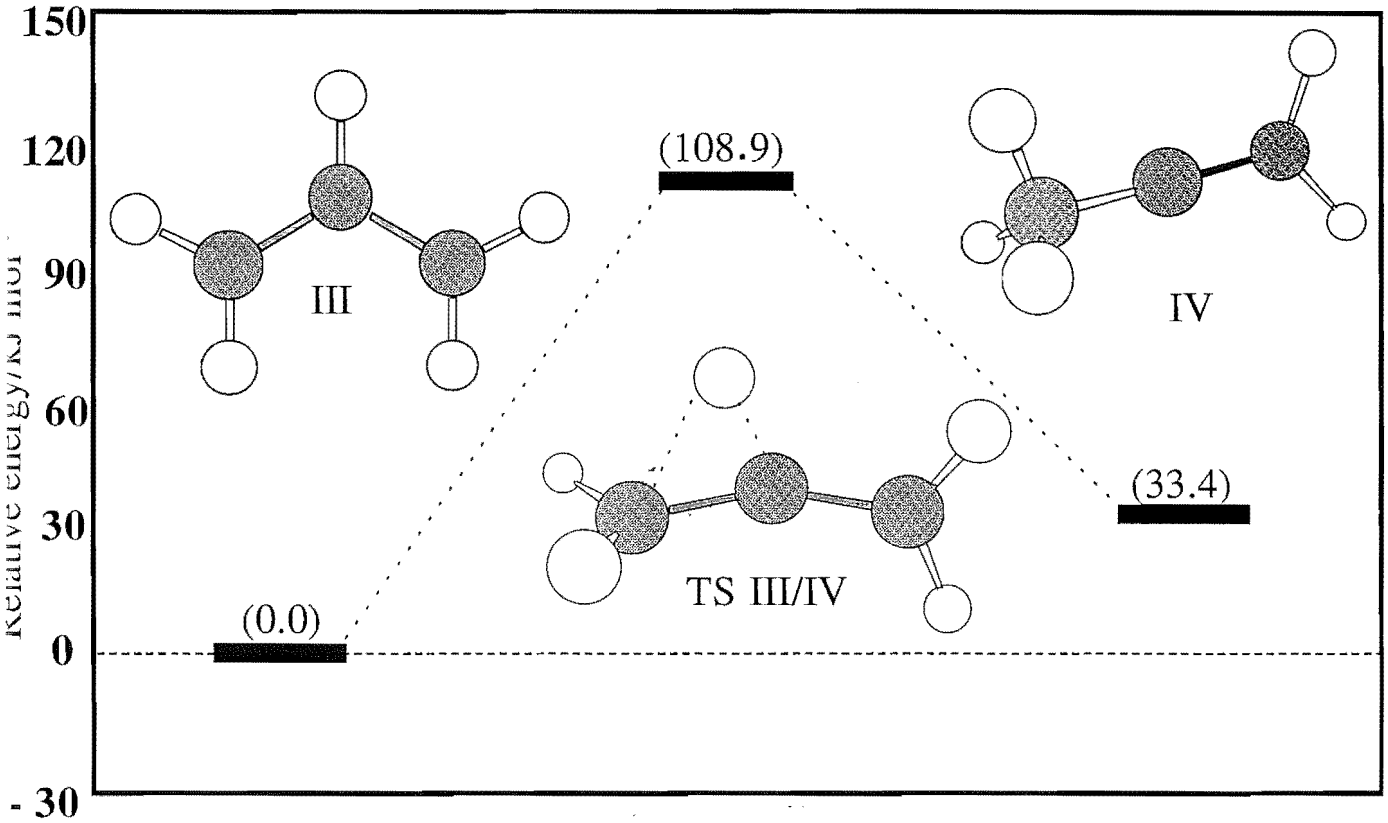

Figure 4.8. Schematic diagram of a section of the $C_3H_5^+$ potential energy surface showing the allyl and 2-propenyl structures and the transition state between them (bridge protonated allene). The energies are expressed in kJ mol^{-1} relative to the allyl cation at 0 K.

$$CH_2CHCH_2^+ + CH_3OH \xrightarrow{0.35} C_3H_7^+ + CH_2O \quad \textbf{(4.30a)}$$

$$\xrightarrow{0.55} CH_3OH_2^+ + C_3H_4 \quad \textbf{(4.30b)}$$

$$\xrightarrow{\sim 0.05} C_4H_7^+ + H_2O \quad \textbf{(4.30c)}$$

$$\xrightarrow{\sim 0.05} C_3H_5^+.CH_3OH \quad \textbf{(4.30d)}$$

$k_{4.30} = 7.3 \times 10^{-10}$ cm^3 s^{-1}

The semilogarithmic decay for this reaction is shown in Figure 4.9b. The rate coefficients and product distributions observed for the two isomers $CH_2CHCH_2^+$ and $CH_3CCH_2^+$ are thus sufficiently different to enable ready characterisation of the ion structure. Recently Riveros and Zhu [302] also noted a difference in reactivity with CH_3OH for each structure using the FT-ICR technique. However they concluded that $CH_3CCH_2^+$ reacted seven times faster than $CH_2CHCH_2^+$ with CH_3OH while the present results show a difference in rate coefficients of a factor of 2.3. They also did not report product channels. Proton transfer from $CH_2CHCH_2^+$, reaction 4.30b, was not reported by Aue et al [291] in their study. The fact that it occurs at all, although being apparently endothermic (ΔH^o = +21 kJ mol^{-1} for allyl structure), may indicate that tabulated PA's [164] are slightly in error.

C_6H_6 Reactions (PA = 750 kJ mol^{-1}).

Both $CH_2CHCH_2^+$ and $CH_3CCH_2^+$ reactions with benzene were examined.

$$CH_3CCH_2^+ + C_6H_6 \longrightarrow \text{products} \qquad \textbf{(4.31)}$$

$k_{4.31} = 1.1 \times 10^{-9}$ cm^3 s^{-1}

The products of reaction could not be unequivocally determined because of a mass overlap at m/z = 79 arising from the presence of $C_6H_7^+$ formed via secondary reaction of protonated propyne, viz.

$$CH_3CCH_2^+ + C_3H_4 \longrightarrow C_6H_7^+ + H_2 \qquad \textbf{(4.32a)}$$

$$\longrightarrow \text{adduct} \qquad \textbf{(4.32b)}$$

However, proton transfer is likely to be the major process. No proton transfer to benzene was observed from $CH_2CHCH_2^+$.

$$CH_2CHCH_2^+ + C_6H_6 \xrightarrow{0.35} C_7H_7^+ + C_2H_4 \qquad \textbf{(4.33a)}$$

$$\xrightarrow{0.65} C_3H_5^+.C_6H_6 \qquad \textbf{(4.33b)}$$

$k_{4.33} = 1.35 \times 10^{-9}$ cm^3 s^{-1}

C_6F_6 Reactions (PA = 648 kJ mol^{-1})

Both structures, $CH_2CHCH_2^+$ and $CH_3CCH_2^+$, exhibited identical rate coefficients (k = 2.0×10^{-11} cm^3 s^{-1}) with C_6F_6. The products were not determined but there is some evidence for the cluster ion, and possibly a product at m/z = 59, $C_3H_4F^+$.

4-fluorotoluene Reactions (PA = 764 kJ mol^{-1})

Both $CH_2CHCH_2^+$ and $CH_3CCH_2^+$ exhibited near collision-rate reactions with p-C_7H_7F. Proton transfer was a major product of reaction from $CH_3CCH_2^+$.

$$CH_3CCH_2^+ + p\text{-}C_7H_7F \longrightarrow C_7H_7FH^+ + C_3H_4 \quad \textbf{(4.34a)}$$

$$\longrightarrow C_3H_5^+.C_7H_7F \quad \textbf{(4.34b)}$$

$k_{4.34} = 1.5 \times 10^{-9}$ cm^3 s^{-1}

No proton transfer was observed from $CH_2CHCH_2^+$.

$$CH_2CHCH_2^+ + p\text{-}C_7H_7F \longrightarrow C_3H_5^+.C_7H_7F \quad \textbf{(4.35)}$$

$k_{4.35} = 1.8 \times 10^{-9}$ cm^3 s^{-1}

Other Allyl Cation Reactions

In addition to these reactions, in which the reactivity of both $CH_2CHCH_2^+$ and $CH_3CCH_2^+$ were examined, a number of reactions of the allyl ion only were investigated. The allyl $C_3H_5^+$ ion was formed via electron impact on cyclopropane in the FA source and injected, following mass selection, into the flow tube. The structure of this ion was confirmed as the allyl structure by examining its reactivity with CH_3OH.

Reaction with CNBr

$$CH_2CHCH_2^+ + CNBr \xrightarrow{0.50} CNBrH^+ + C_3H_4 \quad \textbf{(4.36a)}$$

$$\xrightarrow{0.50} C_3H_5^+.CNBr \quad \textbf{(4.36b)}$$

$k_{4.36} = 6.6 \times 10^{-10}$ cm^3 s^{-1}

Both proton transfer and adduct formation were observed in the reaction with CNBr. The measured rate coefficient for proton transfer, $k = 3.3 \times 10^{-10}$ cm^3 s^{-1}, suggests a reaction endothermicity for reaction (4.36a) of 5 kJ mol^{-1} (calculated by assuming Arrhenius behaviour and a pre-exponential factor equal to the collision rate). This is apparently at odds with the tabulated thermochemical data [164], which predicts reaction (4.36a) to be endothermic by 25 kJ mol^{-1}. Again this may indicate that the tabulated proton affinities are in error.

Reaction with HCN

$$CH_2CHCH_2^+ + HCN \longrightarrow C_3H_5^+.HCN \quad \textbf{(4.37)}$$

$k_{4.37} = 1.1 \times 10^{-10}$ cm^3 s^{-1}

The allyl cation was observed to react with HCN via a termolecular association channel only. The effective bimolecular rate coefficient for reaction 4.37 was measured at 0.34 Torr.

Reaction with C_2H_5I

$$CH_2CHCH_2^+ + C_2H_5I \longrightarrow C_3H_5^+.C_2H_5I \qquad \textbf{(4.38)}$$

The observed reaction between the allyl cation and ethyl iodide also proceeded via termolecular association. The measured effective bimolecular rate coefficient suggests that this reaction is close to pressure saturation at 0.34 Torr.

Reaction with C_4H_2

$$CH_2CHCH_2^+ + C_4H_2 \xrightarrow{0.70} C_7H_7^+ \qquad \textbf{(4.39a)}$$

$$\xrightarrow{0.30} C_5H_5^+ + C_2H_2 \qquad \textbf{(4.39b)}$$

$k_{4.39} = 1.3 \times 10^{-9}$ cm^3 s^{-1}

The allyl cation also undergoes rapid termolecular association with diacetylene. $C_5H_5^+$ was also identified as a reaction product.

The $C_7H_7^+$ product of reaction 4.39a was shown to consist of a mixture of benzyl and tropylium cations (see the section on $C_7H_7^+$ above).

Proton transfer Reactions

The reactions of several protonated bases, HB^+, with propyne and allene were examined. The bases, B, were selected on the basis of their known proton affinities, viz. H_2O (PA = 691 kJ mol^{-1}), SO_2 (PA = 636 kJ mol^{-1})[‡] and CO (PA at C = 594 kJ mol^{-1}). The HB^+ ions were produced in the FA source region of the FA/SIFDT instrument, mass selected, and injected into the flow reactor tube. Propyne and allene were added at the upstream inlet of the flow tube and the resulting $C_3H_5^+$ product ions then identified via subsequent reaction with methanol at the downstream reactant neutral inlet.

(a) H_3O^+ Reactions

$$H_3O^+ + C_3H_4 \text{ (propyne)} \longrightarrow CH_3CCH_2^+ + H_2O \qquad \textbf{(4.40)}$$

$\Delta H^o = -57$ kJ mol^{-1} (2-propenyl)

[‡] A value of PA(SO_2) = 636 kJ mol^{-1} was assumed based on a re-examination of the proton affinity of cyanogen performed in this laboratory [310], which showed that the value of PA(SO_2) = 672 kJ mol^{-1} tabulated at ref 164 is too high (see also the footnote in chapter 5).

$H_3O^+ + C_3H_4$ (allene) $\longrightarrow$ $CH_3CCH_2^+ + H_2O$ **(4.41)**

$\Delta H^o = -84$ kJ mol^{-1} (allyl)

It was found that protonation of allene via low energy proton transfer produces the 2-propenyl structure exclusively. This finding is consistent with the earlier studies of Aue et al [291] who also observed that proton transfer from H_3O^+ to allene produced the 2-propenyl structure. It should be noted, however, that Aue et al reported that the allyl cation does not undergo proton transfer to methanol, whereas the 2-propenyl cation does. The present study indicates that ***both ions*** proton transfer to methanol (reactions 4.28 and 4.29), although the 2-propenyl cation undergoes much faster, apparently exothermic, proton transfer than the allyl cation. Proton transfer from the allyl cation to methanol is deduced to be endothermic, based on the magnitude of the rate coefficient for this process.

(b) SO_2H^+ Reactions

SO_2 was protonated via addition of SO_2 to a hydrogen carrier gas subjected to microwave discharge in the FA source. The resultant SO_2H^+ ion was mass-selected, injected into the flow tube and allowed to undergo proton transfer to propyne or allene, added at the first neutral inlet.

$SO_2H^+ + C_3H_4$ (propyne) $\longrightarrow$ $C_3H_5^+ + SO_2$ **(4.42)**

$\Delta H^o = -112$ kJ mol^{-1} (2-propenyl)

$SO_2H^+ + C_3H_4$ (allene) $\longrightarrow$ $C_3H_5^+ + SO_2$ **(4.43)**

$\Delta H^o = -139$ kJ mol^{-1} (allyl)

The $C_3H_5^+$ ions formed in reaction 4.42 were examined for structure by measuring their reaction with CH_3OH.

$C_3H_5^+ + CH_3OH$ $\longrightarrow$ products **(4.44)**

The resulting semilogarithmic plot of $C_3H_5^+$ signal against CH_3OH flow is ***curved*** indicating that two $C_3H_5^+$ structures are present. The curve was fitted using a double exponential expression, which showed that ~20% of the $C_3H_5^+$ had the 2-propenyl structure and ~80% had the allyl structure.

The $C_3H_5^+$ ion formed in reaction 4.43 from allene was examined for structure by its reaction with methanol as above. The resulting semilogarithmic decay of $C_3H_5^+$ signal

versus CH_3OH flow is also curved (Figure 4.9c) and indicates a 2-propenyl to allyl ratio of 35:65.

(c) HCO^+ Reactions

Protonated CO, HCO^+, was made by adding CO to a hydrogen carrier in the FA source. After mass selection and injection into the flow tube, the resultant HCO^+ ion underwent proton transfer to propyne or allene at the first inlet.

Following subsequent reaction with methanol it was found that proton transfer from HCO^+ to both allene and propyne produces predominantly the allyl structure.

$HCO^+ + C_3H_4$ (propyne) $\longrightarrow C_3H_5^+ + CO$ **(4.45)**

$\Delta H^o = -154$ kJ mol^{-1} (2-propenyl)

$HCO^+ + C_3H_4$ (allene) $\longrightarrow C_3H_5^+ + CO$ **(4.46)**

$\Delta H^o = -181$ kJ mol^{-1} (allyl)

These results indicate that in the proton transfer reactions of HCO^+ and SO_2H^+ sufficient energy is available within the complex to overcome the transition barrier between the 2-propenyl and allyl structures, whereas this energy is not available in the proton transfer reaction of H_3O^+ with allene. From these results we estimate the height of the transition state barrier between the 2-propenyl and allyl structures as 110 ± 30 kJ mol^{-1} (1.2 ± 0.3 eV) above the allyl structure. This is in excellent agreement with our calculated value of 109 kJ mol^{-1}.

$C_2H_4^+ + C_2H_4$ Reaction

$C_2H_4^+$ was formed in the FA source from ethylene, mass selected at m/z = 28 and injected into the flow tube. Addition of C_2H_4 at the first neutral inlet produced $C_3H_5^+$ via reaction 4.47.

$C_2H_4^+ + C_2H_4 \longrightarrow C_3H_5^+ + CH_3$ **(4.47)**

$k_{4.46} = 7.2 \times 10^{-10}$ cm^3 s^{-1}; $\Delta H^o = -6$ kJ mol^{-1} (2-propenyl); $\Delta H^o = -27$ kJ mol^{-1} (allyl)

Subsequent reaction with CH_3OH at the second neutral inlet identified the product of reaction 4.47 as the 2-propenyl cation only. This is in conflict with the findings of Bowers et al [295] who, on the basis of CID experiments, identified the $C_3H_5^+$ product of reaction 4.47 as the allyl cation only. Interestingly, formation of both the allyl and 2-propenyl ions in 4.47 is close to thermoneutral.

Reactant	Products	Branching ratio	k_{obs} /10^{-9} cm^3 s^{-1}	k_{coll}[a] /10^{-9} cm^3 s^{-1}	$-\Delta H^o$ /kJ mol^{-1} [b]
$CH_2CHCH_2^+$ (1)					
CH_3OH	$C_3H_7^+ + CH_2O$	0.35	0.73	2.2	53.7[c]
	$CH_3OH_2^+ + C_3H_4$	0.55			-21.0
	$C_4H_7^+ + H_2O$	~ 0.05			140.7[d]
	$C_3H_5^+.CH_3OH$	~ 0.05			
C_6H_6	$C_7H_7^+ + C_2H_4$	0.35	1.35	1.4	76.5[e]
	$C_3H_5^+.C_6H_6$	0.65			
C_7H_7F[f]	$C_3H_5^+.C_7H_7F$	1.0	1.8	2.3	
CNBr	$CNBrH^+ + C_3H_4$	0.5	0.66	2.0	-25.5
	$C_3H_5^+.CNBr$	0.5			
HCN	$C_3H_5^+.HCN$	1.0	0.11	3.4	
C_2H_5I	$C_3H_5^+.C_2H_5I$	1.0	1.2	2.1	
C_4H_2	$C_5H_5^+ + C_2H_2$	0.3	1.3	1.2	144.0[g]
	$C_3H_5^+.C_4H_2$	0.7			
$CH_3CCH_2^+$ (2)					
CH_3OH	$CH_3OH_2^+ + C_3H_4$	~ 0.7	1.7	2.2	6.3
	adduct	~ 0.3			
C_6H_6	products		1.1	1.4	
C_7H_7F	$C_7H_8F^+ + C_3H_4$		1.5	2.3	15.8
	$C_3H_5^+.C_7H_7F$				

Table 4.7. Reaction rate coefficients and product ratios with the specified reagent for the $C_3H_5^+$ ions: allyl, $CH_2CHCH_2^+$ (1), and 2-propenyl, $CH_3CCH_2^+$ (2).

[a] Calculated using the method of Su and Chesnavich [161].
[b] Based on ΔH^o values presented in ref. 163.
[c] Calculated assuming the iso-$C_3H_7^+$ structure.
[d] Calculated assuming the $CH_3CHCH{=}CH_2^+$ structure.
[e] Calculated assuming the benzyl $C_7H_7^+$ structure.
[f] 4-fluorotoluene.
[g] Calculated assuming the vinyl cyclopropenyl structure.

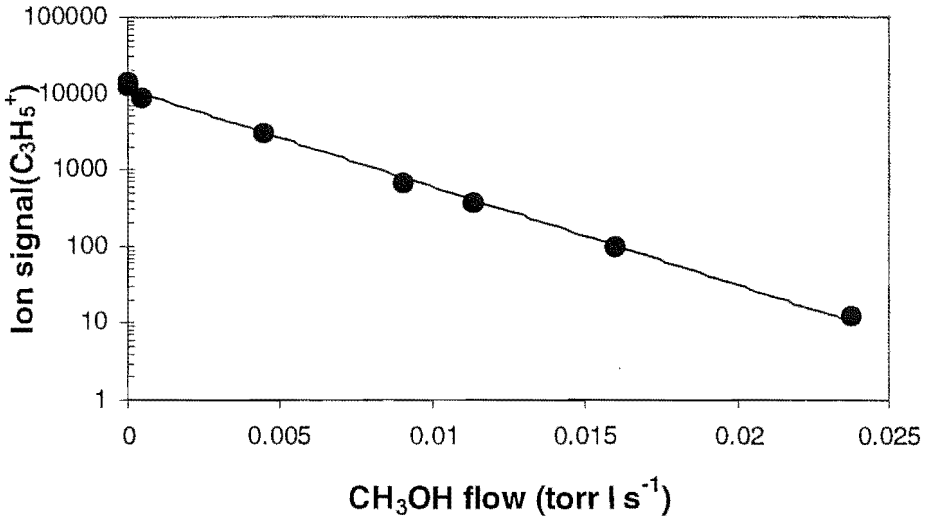

Figure 4.9a. Semi-logarithmic decay of the 2-propenyl $C_3H_5^+$ ion signal versus CH_3OH flow. The linear fit yields a rate coefficient of k = 1.7 x 10^{-9} cm^3 s^{-1}.

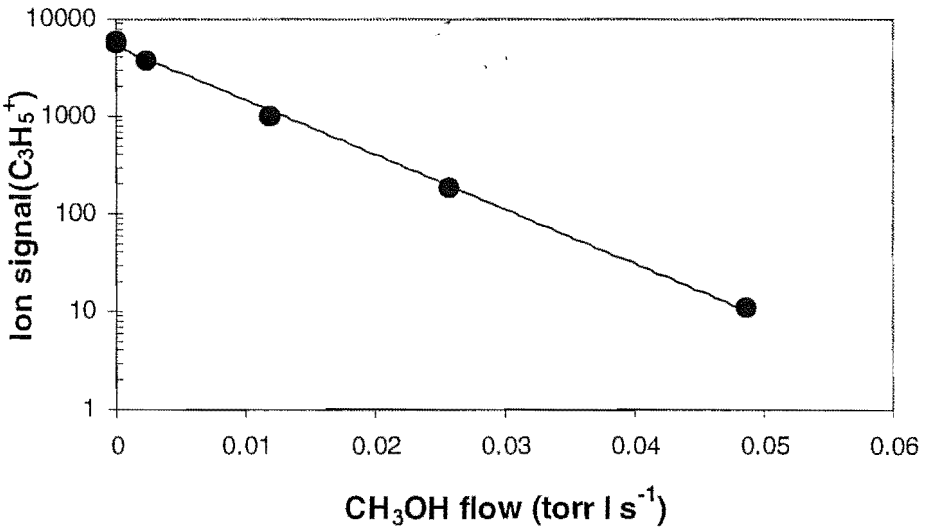

Figure 4.9b. Semi-logarithmic decay of the allyl $C_3H_5^+$ ion signal versus CH_3OH flow. The linear fit yields a rate coefficient of 7.3 x 10^{-10} cm^3 s^{-1}.

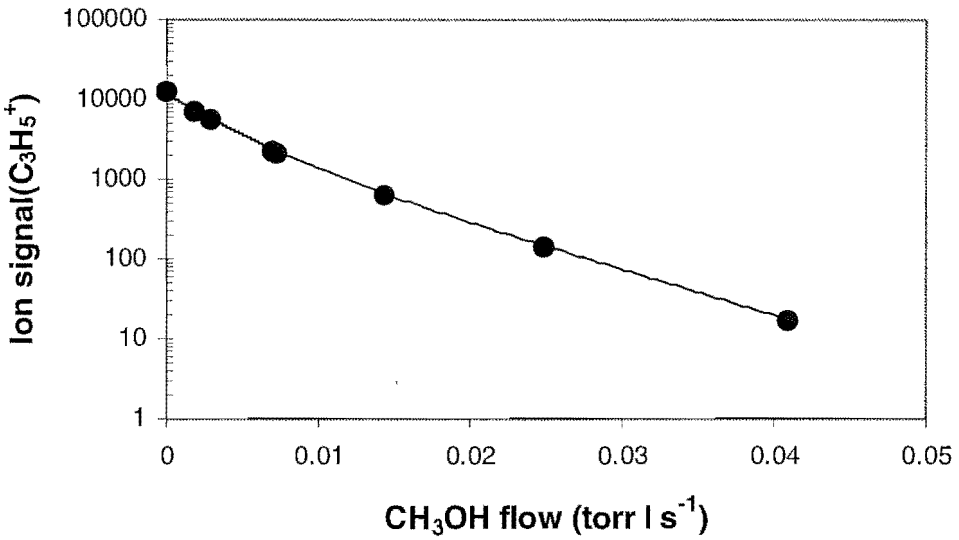

Figure 4.9c. Semi-logarithmic decay of the $C_3H_5^+$ ion signal, formed via the reaction of SO_2H^+ with allene, versus CH_3OH flow. The curve is a double-exponential fit with $k_1 = 1.7 \times 10^{-9}$ cm^3 s^{-1} and $k_2 = 7.3 \times 10^{-10}$ cm^3 s^{-1} and yields an allyl:2-propenyl ratio of 65:35.

Cyclopropyl Cation

Attempts to generate the cyclopropyl cation, c-$C_3H_5^+$ (4, Figure 4.7), via Penning ionisation of cyclopropane by metastable excited helium, He*(2^3S), in the FA source, resulted in only the allyl structure being present after injection into the flow tube. Using ion cyclotron double resonance techniques Aue et al [291] found that cyclopropene forms a $C_3H_5^+$ ion by proton transfer from $(CH_3)_2OH^+$ but not $(C_2H_5)_2OH^+$. From this they deduced a heat of formation for the $C_3H_5^+$ ion formed of 996 kJ mol^{-1}, which is not consistent with the allyl cation. They suggested that either a cyclopropyl structure is formed or that there is a barrier associated with concerted protonation and rearrangement to the allyl structure. Köhler and Lischka [293] offered an alternative explanation of the experimental results of Aue et al based on MINDO/3 and CEPA calculations of the $C_3H_5^+$ hypersurface. They proposed that the most favourable approach of a proton towards cyclopropene will be towards the CH_2 group producing corner-protonated cyclopropene (6, Figure 4.7). The resulting structure undergoes facile ring opening and rearranges to the 2-propenyl cation. Their calculated proton affinity of cyclopropene with respect to the

2-propenyl cation, and calculated ΔH^{o}_{f} for the 2-propenyl cation were in excellent agreement with the values determined for the $C_3H_5^+$ species observed experimentally by Aue et al. [291] Similarly, the proton affinity of cyclopropene with respect to the 2-propenyl cation, calculated in the present work, is in good agreement with the revised PA (cyclopropene) listed in reference 164, lending credence to the conclusions of Köhler and Lischka. [293]

CHAPTER 5.

SIFDT STUDY OF THE SO_2^+/H_2 H-ATOM ABSTRACTION REACTION

5.1 Introduction.

Molecular hydrogen is the most abundant molecular species present in the interstellar medium. Hydrogen atom abstraction reactions (equation 5.1) are, therefore, an important step in the formation of many of the complex molecules observed in dense interstellar clouds. [204] These objects consist mainly of H_2 and He at densities of ~ 10^4 – 10^6 cm^{-3} and temperatures of < 100K, together with dust grains, at greater concentrations than exist in the so-called diffuse clouds (densities ~ 10^2 cm^{-3} and T ~ 100-200 K). [311] H-atom abstraction reactions (HAARs) have been the focus of considerable attention from modellers and ion-molecule experimentalists. [156]

$$X^+ + H_2 \longrightarrow XH^+ + H \qquad (5.1)$$

The role of H-atom abstraction (hydrogenation) reactions in the sequences leading to OH_n^+ (n = 1-3), NH_n^+ (n = 1-4) and CH_n^+ (n = 1-3) in interstellar clouds is well understood, and detailed reaction schemes involving sequential hydrogenation reactions have been developed. [311] Sequential addition of H atoms via abstraction reactions may be interrupted for two main reasons: (1) endothermicity of the reaction, or (2) the existence of a barrier on the potential energy surfaces leading to hydrogen atom abstraction. [226] In the interstellar medium ***non-reactivity*** with molecular hydrogen has implications for further synthesis, in that such ions will be available to react with other species that are less abundant than molecular hydrogen. [226]

Exothermic, but kinetically unfavorable HAARs form the topic of this chapter, and in particular the reaction between SO_2^+ and H_2. It is instructive to consider first some previous drift tube studies of HAARs.

5.1.1 Drift tube studies of H-atom abstraction.

Twiddy et al [105] investigated the endothermic reactions of ground state C^+ with molecular hydrogen and deuterium. The $C^+ + H_2$ reaction has become a model system for experimental and theoretical studies of the kinetics, dynamics and energy requirements of endothermic ion-molecule reactions. [9]

$$C^+(^2P) + H_2 \rightarrow CH^+ + H - 0.398\ eV \qquad (5.2)$$

$$C^+(^2P) + D_2 \rightarrow CD^+ + D - 0.430\ eV \qquad (5.3)$$

By constructing pseudo-Arrhenius plots of the logarithm of the observed rate coefficient versus reciprocal ion-neutral centre-of-mass energy (E_r^{-1}) Twiddy et al obtained values of 0.47 ± 0.07 eV and 0.50 ± 0.07 eV for the thermochemical endoergicities of reactions (5.2) and (5.3) respectively, in good accord with the "expected" values. These reactions were recently re-examined by Hierl et al [9] in a high temperature flowing afterglow (HTFA) apparatus under truly thermal conditions. The rate coefficients measured in the HTFA experiment showed excellent agreement, particularly at the lower end of the temperature range studied, with the drift tube data of Twiddy et al at the same value of the average *total* energy (rotational plus translational). This was despite the fact that the relative proportions of translational and rotational energy are different in the HTFA and drift tube experiments. The reason for the difference is that the translational temperature of the H_2 reactant is identical to that of the C^+ reactant ion in the HTFA experiment but remains at room temperature in the drift tube experiment. The HTFA results of Hierl et al clearly demonstrate that reactant rotational and translational energy are equally efficient at overcoming the endothermicity of this reaction. The agreement between the HTFA data and the drift tube data of Twiddy et al [105] is not as good at the higher end of the temperature range studied. The poorer agreement was attributed to the onset of a vibrational contribution to the internal energy of H_2.

$$C^+ + H_2(v=1) \longrightarrow CH^+ + H \qquad (5.4)$$

Since reaction (5.4) is exothermic, it was suggested that a small percentage of vibrationally excited H_2 could measurably enhance the overall rate coefficient. [9]

It has been suggested that reaction (5.2) may be responsible for the formation of CH^+ in shocked regions of interstellar gas. [94,312] It has also been proposed that the excess kinetic energy imparted to C^+ in the reaction

$$He^+ + CO \longrightarrow C^+ + O + He + 2.2\ eV \qquad (5.5)$$

may drive reaction (5.2) in diffuse (and dense) interstellar clouds. [311] Both of these mechanisms may help explain the apparent overabundance of CH^+ observed in diffuse interstellar clouds, compared to that predicted theoretically from gas-phase ion-chemical reaction models.

The flow drift tube techniques have been used in the evaluation of rate coefficients appropriate to shocked regions of the interstellar gas. [94] The conditions of a flow drift tube experiment simulate the conditions of a magneto-hydrodynamic (MHD) shock in which kinetically "hot" ions stream through the cold ambient gas of an interstellar cloud.

Millar et al, [313] using the Innsbruck selected ion drift tube (SIDT), studied the endothermic reactions (5.6), (5.7) and (5.8) which are potentially important for the synthesis of H_2S in shocked regions of interstellar clouds.

$$S^+ + H_2 \longrightarrow SH^+ + H \qquad (5.6)$$

$$SH^+ + H_2 \longrightarrow SH_2^+ + H \qquad (5.7)$$

$$SH_2^+ + H_2 \longrightarrow SH_3^+ + H \qquad (5.8)$$

From an Arrhenius plot of ln k versus E_r^{-1} they obtained a value of 0.7eV for the endothermicity of reaction (5.6) which is in reasonable agreement with the thermochemical data. Non-linear Arrhenius plots for the other two reactions were taken as an indication that vibrational excitation of the reactant SH^+ and SH_2^+ ions was occurring at the higher values of E_r.

The reaction of N^+ with H_2 was observed to proceed very slowly at 11K [314], k = 3.5×10^{-11} $cm^3\ s^{-1}$, compared to the rate measured at 300K by Adams, Smith and Paulson [315], k = $4.8 \times 10^{-10} cm^3\ s^{-1}$, indicating a reaction endothermicity of ~ 8meV.

$$N^+ + H_2 \longrightarrow NH^+ + H \qquad (5.9)$$

This prompted Adams and Smith [312,316] to study the reaction in their SIFDT apparatus at 300K. Again the data was analysed according to the Arrhenius law and yielded a value of 11 ± 3 meV for the endothermicity. Adams et al [312] later proposed that reaction (5.9) may be driven at interstellar cloud temperatures by the excess kinetic energy imparted to N^+ via the reaction:

$$He^+ + N_2 \rightarrow He + N + N^+ + 0.28eV \quad \textbf{(5.10)}$$

The H-atom abstraction reaction of C_3H^+ with H_2 has also been investigated in a variable temperature selected ion flow drift tube (VT-SIFDT) instrument. [317,318]

$$C_3H^+ + H_2 \rightarrow c\text{-}C_3H_2^+ + H \quad \textbf{(5.11)}$$

The variation of the rate coefficient with temperature was used to infer a reaction endothermicity of ~ 4 kJ mol^{-1}, and an enthalpy of formation for c-$C_3H_2^+$ of 1377 ± 21 kJ mol^{-1}.

The H-atom abstraction reaction (5.12) was studied in the presence of a drift field, and an endothermicity of ~ 17 kJ mol^{-1} was deduced for the reaction.

$$C_3H_2^+ + H_2 \longrightarrow C_3H_3^+ + H \quad \textbf{(5.12)}$$

This apparent endothermicity was subsequently shown [319] to actually represent a kinetic barrier to the formation of c-$C_3H_3^+$ from c-$C_3H_2^+$, and a value of 4 kJ mol^{-1} for the barrier height was obtained theoretically. [319]

An investigation of the H-atom abstraction reaction:

$$c\text{-}C_3H_2^+ + H_2O \rightarrow C_3H_3^+ + OH \quad \textbf{(5.13)}$$

led Prodnuk et al [320] to propose that reaction (5.11) was actually ***exothermic*** by 24 kJ mol^{-1}, based on the assumption that since reaction (5.13) was slow it was ***endothermic***. Their basis for this assumption was that HAARs, if exothermic, are generally fast except when the neutral reactant is molecular hydrogen. This apparent discrepancy was later resolved by Wong and Radom [319] who showed via theoretical calculations that reaction (5.11) ***is*** in fact endothermic by 4 kJ mol^{-1}. The reason for the slow HAAR between c-$C_3H_2^+$ and H_2O is due to a 23 kJ mol^{-1} barrier between reactants and products on the potential energy surface. Wong and Radom [319] also recommended a value of Δ_fH°(c-$C_3H_2^+$) = 1389 kJ mol^{-1} be adopted based on a re-analysis of the data obtained by Smith and Adams. [317,318]

The HAAR between NH_3^+ and H_2 (reaction 5.14) has been the subject of numerous experimental investigations, principally because of its importance to interstellar cloud chemistry. [314,315,321-329]

$$NH_3^+ + H_2 \longrightarrow NH_4^+ + H \quad \textbf{(5.14)}$$

$k_{5.14} = 4.4 \times 10^{-13}$ cm^3 s^{-1}; $\Delta H^\circ_{5.14}$ = -84.1 kJ mol^{-1}

Original studies by Schiff et al [321] and Kim et al [322] showed the reaction to be slow at room temperature ($k \sim 5 \times 10^{-13}$ cm^3 s^{-1}). This observation was confirmed by Fehsenfeld et al, [323] who also investigated the temperature dependence of reaction (5.14) in a variable temperature flowing afterglow and the kinetic energy dependence in a flow drift tube apparatus. The observed variation in rate coefficient with temperature indicated the system possesses an activation energy of approximately 9 kJ mol^{-1}. Subsequent work by Smith and Adams [324,325] indicated that the rate coefficient for reaction (5.14) does not obey typical Arrhenius behaviour at temperatures significantly below 300 K, but rather levels off at temperatures near 80 – 100 K. Work by Luine and Dunn [314] and Böhringer [327] showed that the rate coefficient actually increases at still lower temperatures. These authors also proposed that the mechanism for reaction (5.14) involves initial formation of a complex, from which tunneling occurs under a small transition state barrier. Studies by Barlow and Dunn [328] on the effects of deuterium substitution on the rate of reaction (5.14) at low temperatures strongly supported the tunneling hypothesis. The proposed tunneling mechanism gained further credence from a theoretical study by Herbst et al. [330] The theoretical study also satisfactorily reproduced the interesting experimental results of Böhringer [327], who showed that in addition to the binary mechanism for reaction (5.14), there is a pressure dependent three-body process,

$$NH_3^+ + H_2 + He \longrightarrow NH_4^+ + H + He \qquad \textbf{(5.15)}$$

which is observable at temperatures below ~ 150 K. This process can be pictured as a normal three-body association to form a stabilised $NH_3^+ \cdot H_2$ complex which, although lower in energy than reactants and hence stable with respect to redissociation, still manages to tunnel under the transition state barrier on a time scale shorter than the observation time of the experiment. The potential role of tunneling in hydrocarbon radical/molecular hydrogen reactions at low temperatures has also been considered. [331]

5.1.2 Kinetic barriers to H-atom abstraction.

For H-atom abstraction reactions that are unquestionably exothermic yet proceed slowly at room temperature (i.e. at a small fraction of the Langevin rate) one can infer the existence of a potential barrier to the reaction. This situation has been observed, for example, in the reactions of HC_3N^+ [332-334], CH_2CHCN^+ [335], c-$C_3H_2^+$ [317-319], NH_3^+ [314,315,321-329], C_6H^+ [241] and $CHCl^+$ [336] with H_2, and in the reaction of c-$C_3H_2^+ + H_2O$. [319,320] Table

5.1 lists these reactions with the corresponding reaction barrier either calculated from experiment or inferred by assuming that the reaction exhibits Arrhenius behavior with a pre-exponential factor equal to the corresponding collision (Langevin) rate coefficient.

Reaction	ΔH^{o}_{r} (kJ mol^{-1})	k_{obs} (T ~ 300 K)	Inferred barrier /kJ mol^{-1}	Calculated barrier /kJ mol^{-1}
$HC_3N^+ + H_2 \longrightarrow H_2C_3N^+ + H$	-129.3	2.8×10^{-12} [156]	15.6	-
$CH_2CHCN^+ + H_2 \longrightarrow CH_2CHCNH^+ + H$	-100.0	1.2×10^{-12} [335]	17.7	-
$c\text{-}C_3H_2^+ + H_2 \longrightarrow c\text{-}C_3H_3^+ + H$	-90.9	$<5 \times 10^{-14}$ [317]	>20	~ 17 [317]; 4‡ [319]
$NH_3^+ + H_2 \longrightarrow NH_4^+ + H$	-84.1	4.4×10^{-13} [156]	20.3	~ 9
$C_6H^+ + H_2 \longrightarrow C_6H_2^+ + H$	-	1.3×10^{-12} [241]	17.5	≤ 4
$CHCl^+ + H_2 \longrightarrow CH_2Cl^+ + H$	-69.8	6.0×10^{-12} [336]	13.7	-
$c\text{-}C_3H_2^+ + H_2O \longrightarrow c\text{-}C_3H_3^+ + OH$	-25.6	NR [320]	> 20	23‡

Table 5.1 Exothermic H-atom abstraction reactions for which a kinetic barrier has been inferred. The inferred barrier assumes Arrhenius behaviour with a pre-exponential factor equal to the Langevin collision rate. The calculated barrier is obtained directly from experiment or theory.

‡ Value obtained from theoretical calculations (reference 319).

5.2 The exothermic SO_2^+/H_2 H-atom abstraction reaction.

The H-atom abstraction reaction between SO_2^+ and H_2 is calculated to be exothermic by 75 kJ mol^{-1} and one would therefore expect the reaction to occur with close to unit efficiency ($k_L = 1.5 \times 10^{-9}$ cm^3 s^{-1}). However, Scott et al [337] measured a rate coefficient for (5.16) of $k \sim 5 \times 10^{-12}$ cm^3 s^{-1}.

$$SO_2^+ + H_2 \longrightarrow SO_2H^+ + H \qquad \textbf{(5.16)}$$

$\Delta H^\circ_{5.16} = -75$ kJ mol^{-1}

One other measurement of $k = 1.7 \times 10^{-11}$ cm^3 s^{-1}, obtained using the ICR technique, has been reported. [156] The low observed reaction efficiency implies the existence of a kinetic barrier to reaction (5.16). Again, assuming Arrhenius behavior one can estimate the size of the barrier as $E_a = -RT \ln(k/A)$, where k is the observed rate coefficient and A is the calculated Langevin rate. This yields a value of ~ 14 kJ mol^{-1}. SO_2 is an observed interstellar molecule [311], and although SO_2^+ has not been directly observed it will almost certainly be present in the interstellar medium, and therefore reaction (5.16) is of potential relevance to the chemistry occurring in interstellar clouds. SO_2 and H_2 are also major species observed on Io, one of the Galilean satellites of Jupiter. To gain further insight into the potential energy surface for the reaction of SO_2^+ with H_2, the reaction was examined using the SIFDT apparatus.

5.2.1 Experimental details.

All measurements were made at (300 ± 5 K) in a helium bath gas. SO_2^+ ions were formed by subjecting a 10% mixture of SO_2 in argon to ~70eV electron impact in a high pressure ion source. A mixture in argon was used in order to minimise instability in the SO_2^+ signal that occurred when pure SO_2 was used in the ion source.

5.2.2 Results and discussion.

Rate coefficients for reaction (5.16) were measured at different values of E/N between 0 and 60 Td. The energy range covered was restricted in part by the occurrence of electrical breakdown inside the flow tube upon addition of H_2 to the helium carrier flow at E/N > 60 Td. Evidence that breakdown had occurred was provided by a concomitant rapid loss of all ion signals. Recovery of the ion signal took several hours and was aided by venting the flow tube to atmospheric pressure. The exact reason for this phenomenon is not well understood, but it has been observed in other laboratories

when investigating reactions of molecular hydrogen in a drift tube. [338] SO_2H^+ was the only product ion observed over the energy range covered. Drift velocities were obtained by fitting a tenth order polynomial to the mobility data of Böhringer et al [339] and interpolating as required. Drift velocities were also measured at selected values of E/N and were found to agree with those of Böhringer et al to within ± 5% (see Figure 5.1). At zero field (E_r = ½ kT = 0.038eV) and a pressure of 0.35 Torr, the measured rate coefficient for reaction (5.16) was 4.2 x 10^{-12} cm^3 s^{-1}. The variation in the measured rate coefficient is plotted in Figure (5.2) as a function of E_r, as is conventional for drift tube studies.

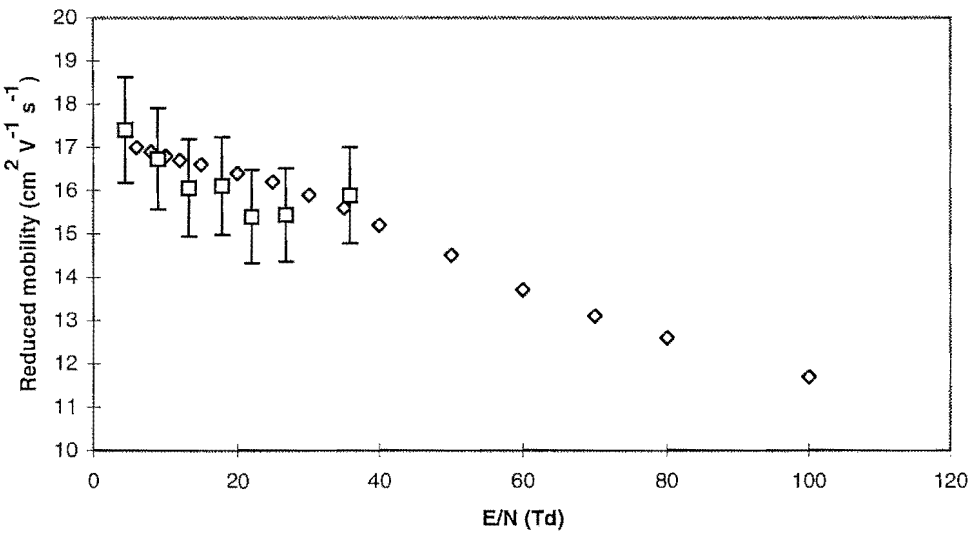

Figure 5.1 Reduced mobility of SO_2^+ in He as a function of E/N (□) present work and (◇) from Böhringer et al [339].

For reactions which are predicted to be endothermic or possess an activation barrier it is usual to plot ln k vs E_r^{-1} to test for Arrhenius behaviour, assuming k may be expressed by the Arrhenius equation (5.17):

$$k = A\exp(-E_a / RT) \qquad \textbf{(5.17)}$$

Implicit in this procedure is the assumption that the effective reaction temperature is equilibrated on E_r, i.e. E_r = ½ R"T_{eff}". Substitution into (5.17) yields

$$k = A\exp(-\tfrac{3}{2}(E_a / E_r)) \qquad \textbf{(5.18)}$$

The validity of this approach is discussed fully in chapter 1.

The plot of ln k versus E_r^{-1} is shown in Figure (5.3b) and from this an Arrhenius activation energy of 6.0 kJ mol^{-1} was calculated from a linear least squares fit to the data. It was suggested by Smith et al [340], in their investigation of the endothermic HAAR of $C_2H_2^+$ with H_2 (reaction 5.19), that a plot of ln k versus E_c^{-1} is more reasonable.

$$C_2H_2^+ + H_2 \longrightarrow C_2H_3^+ + H \qquad \textbf{(5.19)}$$

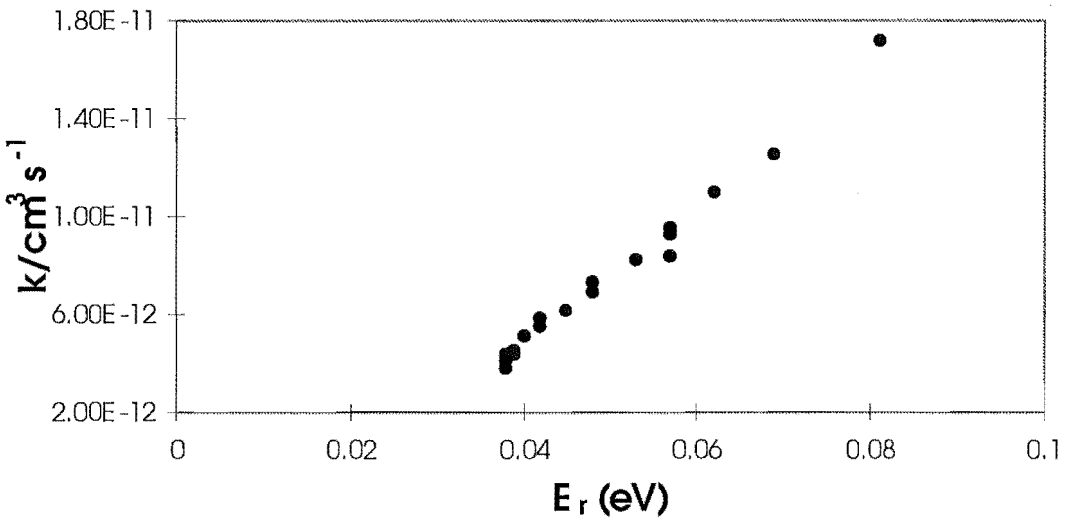

Figure 5.2. Variation in the rate coefficient k for the H-atom abstraction reaction $SO_2^+ + H_2$ with E_r.

Their conclusion was based on the argument that since collisions of the reactant ion are more frequent with the He bath gas than with the reactant H_2 molecules, the internal energy state of the ions is described by E_c rather than E_r. Since the energy E_r in the ion-neutral centre-of-mass frame is distributed amongst the several modes of the ion-reactant gas complex, then the energy input from E_r is effectively smaller than E_c, and hence E_c will have the dominant influence on the reaction. With this in mind a plot of ln k versus E_c^{-1} was also constructed (Figure 5.3a). The Arrhenius activation energy calculated from this plot was 4.3 kJ mol^{-1}. The excellent linearity of the two Arrhenius plots would tend to suggest that significant vibrational excitation of SO_2^+ in collisions with He does not

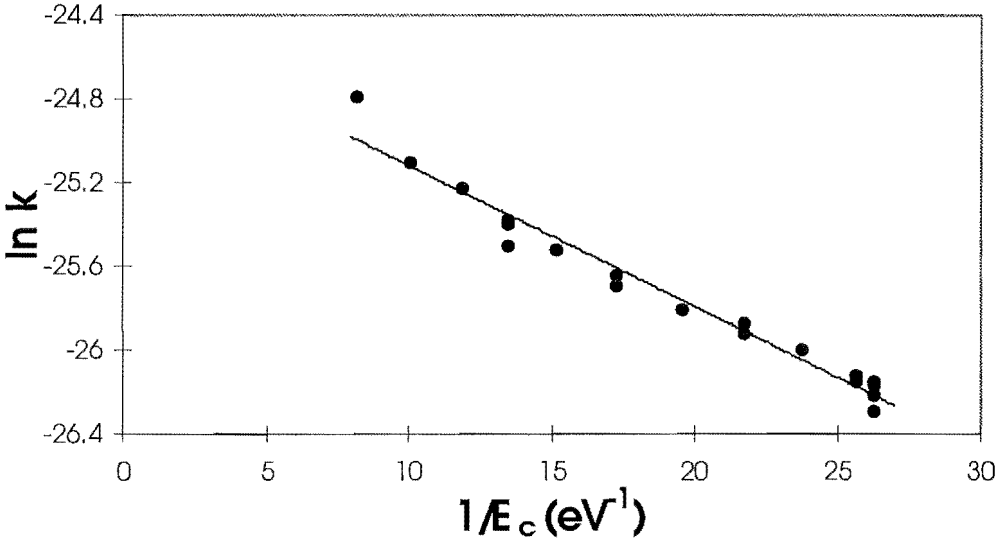

(a)

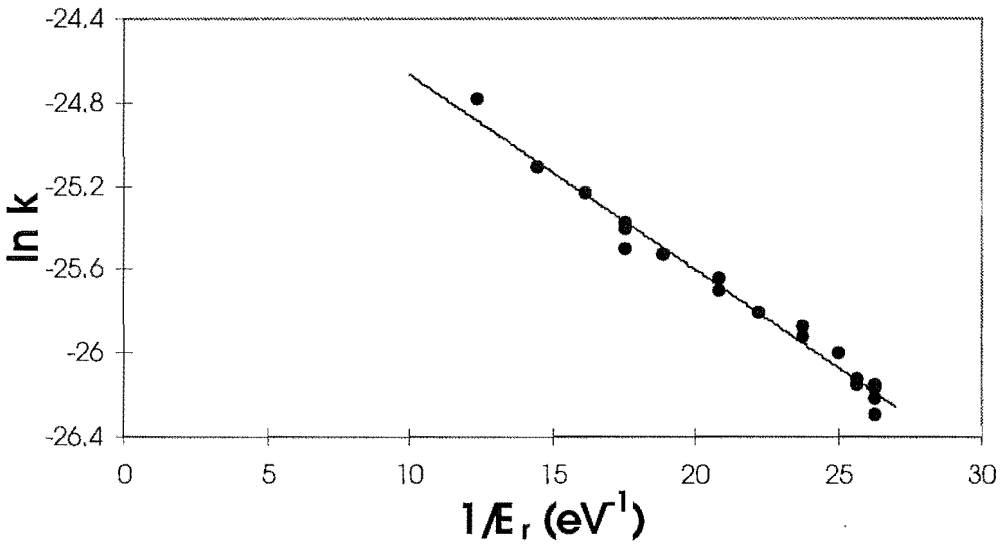

(b)

Figure 5.3. SIFDT data for the reaction $SO_2^+ + H_2$, plotted in the form of an Arrhenius plot of ln k against (a) $E_c^{-1}/(eV^{-1})$ and (b) $E_r^{-1}/(eV^{-1})$.

occur at centre-of-mass energies below ~ 0.1 eV (9.6 kJ mol^{-1}). This is consistent with the findings of Durup-Ferguson et al who examined reactions of N_2O^+, NO_2^+, SO_2^+, H_2O^+ and CO_2^+ in He, Ne and Ar buffer gases. [53,66] Their quenching experiments showed that

little or no vibrational excitation of N_2O^+ occurred at energies over three times the threshold for vibrational excitation. Support is also given to this conclusion by the results of Smith et al [340] who observed curvature in their Arrhenius plot for the reaction of $C_2H_2^+$ with H_2 at the higher values of E_c. From the observed curvature they deduced that the C=C stretching mode of the $C_2H_2^+$ ions was becoming significantly populated and were able to derive a value of 0.22eV for the energy of this state from their experimental data. No evidence for a departure from linearity in either of the Arrhenius plots constructed in the present work, over the energy range covered, was observed.

Thus the drift tube studies indicate a barrier to H-atom abstraction is present in reaction (5.16). In order to gain some insight into the reasons for a barrier to H-atom abstraction in the SO_2^+/H_2 reaction, an ab initio study of the $SO_2H_2^+$ potential energy surface was conducted.

5.3 Ab initio calculations.

Calculations were performed using the Gaussian 94 program [178], and followed the prescription detailed in the original description of the G2 (MP2) procedure. [160] The structures of the reactants, possible products and transition states with geometric parameters calculated at the MP2=FU/6-31G* level of theory are illustrated in Fig. 5.4. The calculated energies of these structures are given in Table 5.2. Two stable $OSOH_2^+$ complexes were identified (cis and trans) which lead to the formation of a cis or trans $OSOH^+$ product ion respectively. In the $OSOH_2^+$ structures there is a long (2.022 Å trans, 2.008 Å cis) H-H bond. In the $OSOH_2^+$ transition state structures there is a long O-H bond (1.686Å trans, 1.896 Å cis) with the H-H bond only slightly elongated (0.738 Å trans and 0.752 Å cis). The weak interaction between SO_2^+ and H_2 means that considerable H-H bonding energy is lost before a gain in O-H bonding occurs with a barrier to H-atom abstraction resulting. Formation of S-protonated HSO_2^+ is calculated to be endothermic by >100 kJ mol^{-1}. The energies of the various $H_2SO_2^+$ species relative to $SO_2^+ + H_2$ are given in Table 5.3. The calculated proton affinities for SO_2 at 0K are: 627 kJ mol^{-1} (trans $OSOH^+$), 636 kJ mol^{-1} (cis $OSOH^+$) and 456 kJ mol^{-1} (S-protonated HSO_2^+). The experimentally determined proton affinity for SO_2 at room temperature is

636 kJ mol^{-1} in good agreement with the calculated value. ‡ Figure (5.5) illustrates the calculated minimum energy pathway for reaction (5.16) at 298K (including zero-point energies). The pathway presumably proceeds through a weakly bound entrance channel complex in analogy to the NH_3^+/H_2 reaction although such a species was not identified directly in the calculations as a consequence of the very shallow well. The pathway then rises to a transition state structure, corresponding to the barrier height for H-atom abstraction, which is calculated to lie 19.9 kJ mol^{-1} above the energy of the reactants at 298 K (23.2 kJ mol^{-1} at 0K). The potential energy of the system then drops towards the strongly exothermic products via a weakly-bound exit channel complex, $SO_2H^+\cdots H$.

Structure	Species	HF/6-31G*	MP2=FU/6-31G*	G2(MP2)
I	H_2	-1.14414	-1.16832	-1.16832
II	H	-0.49823	-0.49823	-0.50000
III	SO_2^+	-546.73386	-547.25021	-547.36248
IV	SO_2	-547.16901	-547.70010	-548.00709
V	trans $OSOH^+$	-547.42155	-547.94340	-548.24605
VI	cis $OSOH^+$	-547.42762	-547.94950	-548.24933
VII	HSO_2^+	-547.33948	-547.87562	-548.18073
VIII	trans $OSOH_2^+$	-547.92090	-548.44339	-548.74855
IX	cis OSOH2$^+$	-547.92697	-548.44950	-548.75157
X	trans $OSOH_2^+$ TS	-547.87288	-548.36509	-548.71152
XI	cis $OSOH_2^+$ TS	-547.87765	-548.38512	-548.71170

Table 5.2. Calculated energies at 0 K (in hartrees) for the designated structures.

5.4 Comparison between experiment and theory.

The agreement between theory (19.9 kJ mol^{-1}) and experiment (6.0 kJ mol^{-1} (E_r) and 4.3 kJ mol^{-1} (E_c) for the barrier height is reasonable given the uncertainties inherent in calculating the energies of transition states. [341-343] In the study of Herbst et al, [330] the

‡ $PA(SO_2)$ = 636 kJ mol^{-1} is taken from the 1988 NIST database. [163] A recent re-examination of the proton affinity of cyanogen, ref. 310, has shown, in accord with ref. 344, that the value of $PA(SO_2)$ = 672 kJ mol^{-1} tabulated at ref. 164 is too high.

calculated barrier height of 20.1 kJ mol^{-1} for the reaction between NH_3^+ and H_2 was also significantly larger than that determined experimentally (8.8 kJ mol^{-1}). [323] Smith et al [340] in a SIFDT study of the H-atom abstraction reaction between $C_2H_2^+$ and H_2 found that better agreement was obtained with truly thermal SIFT and ion-trap data when they

Structure	0 K	298 K
$SO_2^+ + H_2$	0.0	0.0
trans $OSOH_2^+$	-73.5	-73.8
cis $OSOH_2^+$	-81.5	-82.0
trans $OSOH_2^+$ TS	23.7	20.3
cis $OHOH_2^+$ TS	23.2	19.9
trans $OSOH^+ + H$	-67.0	-69.0
cis $OSOH^+ + H$	-75.6	-77.7
$HSO_2^+ + H$	+104.5	+102.1

Table 5.3. Energies of the stated structures relative to $SO_2^+ + H_2$ at 0 K and 298 K in kJ mol^{-1}.

plotted their measured rate coefficients against E_c, rather than E_r. Given the lack of similar, truly thermal, data for the reaction between SO_2^+ and H_2, it is not possible to say whether E_r or E_c best describes the effective reaction temperature in the SO_2^+/H_2 reaction. It should be noted, however, that the activation barriers calculated from the two Arrhenius-type plots (Fig. 5.3) agree within the experimental uncertainty anyway, given the similar masses of the H_2 reactant and the He carrier gas. As discussed above, we take the linearity of the two Arrhenius plots as evidence that significant vibrational excitation of SO_2^+ does not occur at ion-carrier gas centre-of-mass energies, $E_c < 0.1$ eV. This satisfies the criterion that in order to obtain accurate thermodynamic data from drift tube measurements, one must work in a regime where vibrational excitation will not affect the measured rate constants. [62]

5.5 Conclusions.

A kinetic barrier has been identified from both experiment and theory, between the reactants and products in the exothermic H-atom abstraction between SO_2^+ and H_2. This barrier accounts for the small rate coefficient observed at 300K. It is apparent from this and other studies that kinetic barriers occur in several H-atom abstraction reactions with H_2, including NH_3^+ [330], c-$C_3H_2^+$ [319], C_6H^+ [241] and a barrier has been inferred for $C_2H_2^+$. [340] Inspection of the literature [156] demonstrates that many exothermic H-atom abstraction reactions proceed with rate coefficients that are less than half of the Langevin collision rate. There is therefore a marked contrast between H-atom abstraction reactions and exothermic proton transfer reactions, which are invariably fast. [345] H-atom abstraction from H_2 requires the H_2 molecule to be bound to the ion before eventual H-atom loss rather than exchange of a proton. It is this binding process and subsequent loss of H that may result in a barrier. The presence of kinetic barriers has important implications for interstellar cloud chemistry, which, for the most part, takes place at temperatures < 50K. [226] HAARs possessing kinetic barriers may not be important at the low temperatures of the interstellar environment unless a new mechanism takes over as quantum tunneling is believed to in the $NH_3^+ + H_2$ reaction. [330] A similar tunneling mechanism has also been invoked to explain the apparent inverse temperature dependence of reaction (5.19) between $C_2H_2^+$ and H_2 [329,346], although it should be noted that some doubt exists as to the rate coefficients appropriate to this reaction at temperatures below 15 K (see ref. 340 and references cited therein). Indeed, such a tunneling mechanism may be important in the reaction of SO_2^+ with H_2 at very low temperatures, such as those prevalent in the interstellar medium, given the obvious qualitative similarities between the NH_3^+/H_2 and SO_2^+/H_2 potential energy surfaces.

One must always bear in mind that the SIFDT technique is not a truly thermal technique. In all of the present experiments, the translational/internal temperature of the H_2 reactant is equilibrated to that of the He carrier gas (300 K), whilst the internal temperature of the SO_2^+ reactant is expected to be equilibrated to E_c. Under truly thermal conditions at an equivalent temperature to the effective temperature of the SIFDT experiment, the contributions from internal and translational energy to the total energy

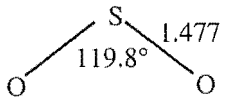

III

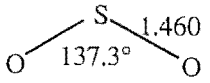

IV

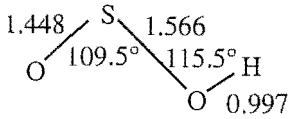

V

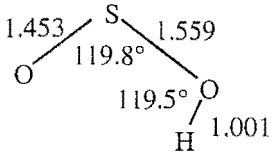

VI

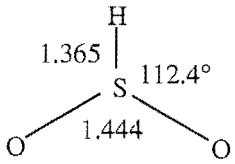

VII

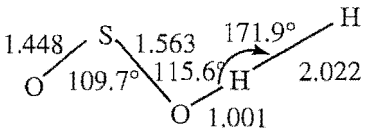

VIII

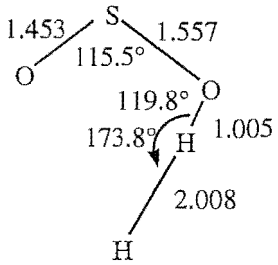

IX

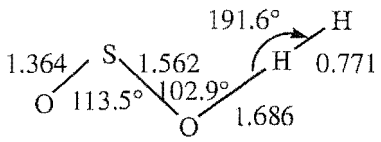

X

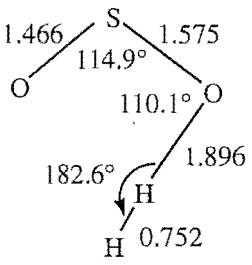

XI

Figure 5.4. MP2=FU/6-31G* optimised structures of transition states, reactants and products in the reaction $SO_2^+ + H_2 \longrightarrow OSOH^+ + H$.

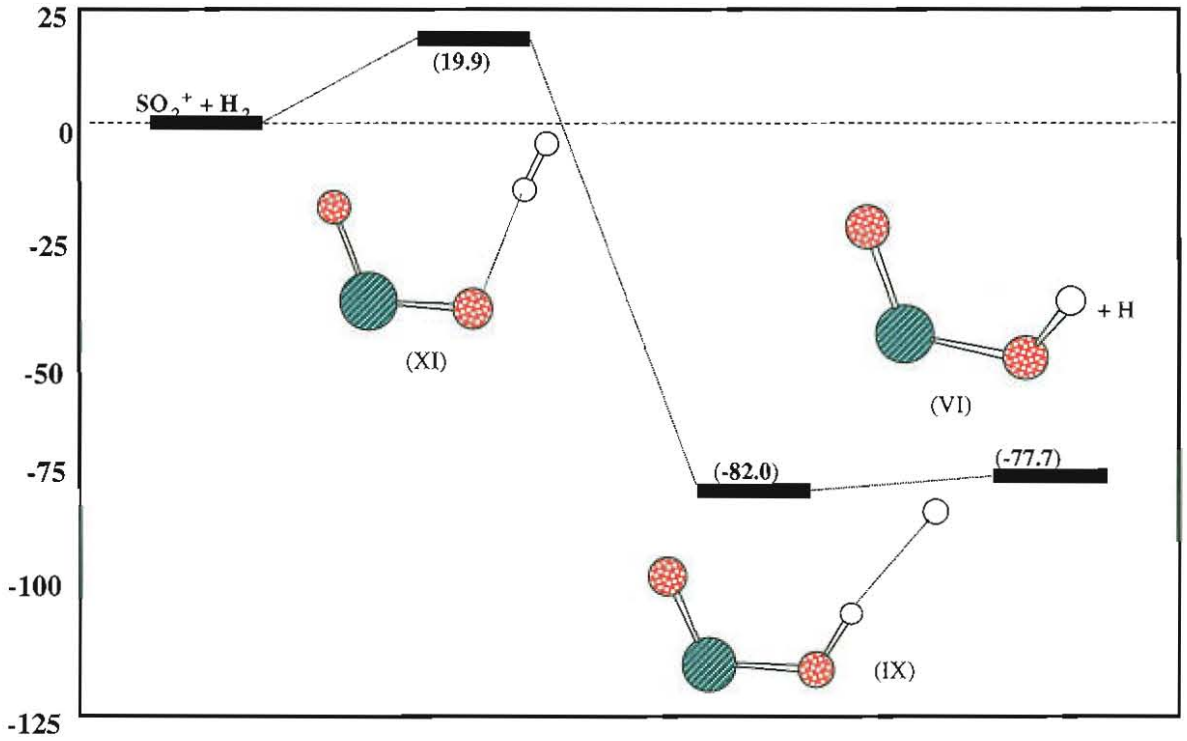

Figure 5.5. $H_2SO_2^+$ energy surface calculated using the G2 procedure. The energies are expressed in kJ mol^{-1} relative to $SO_2^+ + H_2$ and are corrected to 298 K and for zero-point energy.

are expected to be different, since rotational (and vibrational) excitation of the H_2 reactant will occur under truly thermal conditions. Sufficient endothermic reactions have been studied via the VT-SIFDT technique, however, to expect translational and internal energy to both be effective in overcoming the endothermicity of the reaction. [65] Thus the *total* energy (translational plus internal) is expected to be the important parameter, regardless of the relative contribution from each. The present results suggest that a SO_2^+/H_2 centre of mass energy of ~ 0.08 eV is appropriate to the one previous ICR measurement of this reaction. [156]

It should also be noted that not all HAARs possessing rate coefficients considerably less than their respective capture rates have kinetic barriers. Of the five HAARs of $C_nH_m^+$ ions with H_2 investigated by Giles et al [241], only one, $C_6H^+ + H_2$ has a rate coefficient that is less at 80 K than it is at 300 K indicating a kinetic barrier. The

remaining four reactions have rate coefficients that are substantially less than the collision rate at 300 K yet all show noticeable increases in rate coefficient at 80 K. In these cases the lifetime of the $(C_nH_m^+.H_2)^*$ complex (which is greater at 80 K than it is at 300 K) may be the major factor contributing to the low efficiency of the reaction. Alternatively, a change in reaction mechanism may explain the observed increase in the rate coefficients at low temperatures. As discussed previously, the rate coefficient for the HAAR between NH_3^+ and H_2 levels off at temperatures near 80-100 K and increases at still lower temperatures due to a tunneling mechanism. A similar mechanism may occur at low temperatures in the $C_nH_m^+/H_2$ reactions.

CHAPTER 6.

SIFDT STUDIES OF TERMOLECULAR ASSOCIATION AND THE COMPETITION BETWEEN BIMOLECULAR AND TERMOLECULAR REACTION PROCESSES

6.1. Association and charge transfer: NO^+ + ketones.

6.1.1 Introduction.

In recent years a great deal of interest has focussed on the potential of the trace gas analysis of breath as a non-invasive technique for medical diagnosis. [347] The SIFT technique has recently entered this exciting new area of applied science, with the development of the SIFT trace gas analysis technique. [348-350] Trace gas analysis via the SIFT technique utilises chemi-ionisation[‡] of the trace species by the ions H_3O^+, NO^+ and O_2^+ (derived from air) [348-350] and NH_4^+ [351]. The technique enables trace gases to be measured quantitatively down to the parts per billion (ppb) level (or even lower) provided the relevant ion chemistry is well understood. [349] The technique is not only limited to the analysis of human breath, but has potential application to the trace gas analysis of flatus (bowel gas), environmental air, vehicle exhaust emissions, the vapours emitted from fruits and even the head spaces above liquids. The major advantages of the SIFT technique over the gas chromatographic techniques employed for trace gas analysis are: (1) partial pressures of multiple components can be measured down to the ppb level in a few seconds from a single exhalation of breath; (2) no pre-concentration using cryogenic or adsorption traps is necessary and (3) samples do not need to be stored in bags with the attendant risk of selective adsorption of specific compounds onto the bag surface. [348]

An essential point to note is that the precursor ions used to ionise the trace gases in a mixture under study must be relatively unreactive with the major components of the air sample (N_2, O_2, H_2O, Ar and CO_2) compared with their reactivity with the trace

[‡] See ref. 351 and references cited therein for a discussion of the development of chemi-ionisation as a technique for the identification and quantification of mixtures of organic compounds.

species to be quantified. [349] If this were not the case the precursor ions would be consumed immediately in reaction with the major air components. This is a major reason for the choice of the precursor ions H_3O^+, NO^+ and O_2^+. H_3O^+, for example, undergoes bimolecular proton transfer to many volatile organic compounds without fragmentation, facilitating quantitative analysis of multi-component mixtures. [348,349] One complicating factor is that H_3O^+ undergoes termolecular association with water molecules forming the hydrates, $H_3O^+(H_2O)_n$, with n = 1,2,3 depending on the partial pressure of water in the air sample being analysed. These hydrates may subsequently undergo ligand-switching reactions with the trace species to be quantified and this must be accounted for in the analysis. [349] Neither of the two ions, NO^+ or O_2^+, undergoes bimolecular reactions with the major air components at significant rates, making them ideal precursor ions for trace gas analysis. [348,349] O_2^+ (I.P. (O_2) = 12.07 eV) either undergoes direct charge transfer reactions with organic molecules, or dissociative charge transfer, resulting in two (or three) fragments of the parent ion. [348] The relatively high recombination energy of O_2^+ ensures that it reacts with most molecules, including, significantly, many that do not react with H_3O^+, so the value of O_2^+ for trace gas analysis is evident. NO^+ has a much lower recombination energy (9.26 eV) than O_2^+ and hence only molecules possessing an ionisation potential lower than 9.26 eV can be ionised in collisions with ground state NO^+ to produce their respective parent ions. Charge transfer, when energetically accessible, is usually non-dissociative. [348] When charge transfer from NO^+ is endothermic, other processes may occur. One such process is hydride ion transfer (which generates the neutral species HNO) which has been observed in the reactions of NO^+ with several alcohols [352], ethers [353], amines [354] and aldehydes [355]. Termolecular ion-molecule association is another likely process when charge transfer is endothermic. [348]

It is clear that in order to analyse complex mixtures of trace gases, an extensive database of rate coefficients and product ions of the reactions of the selected precursor ions with a large range of compounds is required. Smith and Spanel have begun to establish such a database. To date they have examined the reactions of H_3O^+, O_2^+ and NO^+ with seventeen alcohols [352], nine carboxylic acids and eight esters [228], ten ethers [353], eight organosulfur molecules [356], fifteen amines and other nitrogen-containing compounds [354], plus eleven aldehydes and nine ketones [355].

6.1.2 NO^+ + ketones.

Spanel, Ji and Smith examined the reactions of NO^+ with nine ketones [355]. Ketones are ubiquitous compounds in nature. Indeed, the simplest aliphatic ketone, acetone, a metabolite of glucose, is present in human breath. [347] The dominant process observed in most of the NO^+/ketone reactions is ion-molecule collisional association resulting in ions of the type $NO^+.RCOR'$, where RCOR' is a ketone molecule. [355]

$$NO^+ + RCOR' \xrightarrow{He} NO^+.RCOR' \qquad (6.1)$$

These reactions proceed (see e.g. ref. 357) via the formation of a long-lived $(NO^+.RCOR')^*$ complex, which survives long enough to collide with a carrier gas atom. A fraction of the excitation energy is removed in the collision thus preventing dissociation back to reactants,viz.

$$NO^+ + RCOR' \underset{k_r}{\overset{k_f}{\rightleftharpoons}} (NO^+.RCOR')^* \qquad (6.2)$$

$$(NO^+.RCOR')^* + He \xrightarrow{\beta k_c} NO^+.RCOR' + He \qquad (6.3)$$

Association was the only process observed by Spanel et al in the reactions of NO^+ with acetone, butanone, 2- and 3-pentanone and 2-hexanone. [355] Termolecular association was also observed in the reactions of NO^+ with some carboxylic acids and esters [228] and in the reactions of NO^+ with acetonitrile and benzonitrile [354]. In the 3-hexanone and acetophenone reactions, charge transfer occurred in parallel with association. [355] This indicates that the ionisation energies of 3-hexanone and acetophenone are close to or slightly lower than that of NO (9.26 eV). Charge transfer was the only channel observed in the reaction of NO^+ with menthone, which indicates that the ionisation potential of menthone is appreciably lower than that of NO. Parallel charge transfer and association was also observed by Spanel and Smith in the reaction of NO^+ with pyridine, which also has an ionisation energy close to that of NO. [354]

Reents and Freiser [358] had earlier noted that the NO^+ affinity (i.e. the binding energy of a NO^+·neutral complex) of a particular compound correlates with the proton affinity and first ionisation potential of the compound (within a specific class of compounds, e.g. ketones, aldehydes etc.). This trend shows excellent qualitative agreement with the findings of Spanel and Smith. [228,354,355] Their results suggest that as

charge transfer becomes increasingly endothermic there is a corresponding decrease in the efficiency of ion-molecule association, presumably as a consequence of the concomitant decrease in the binding energy of the intermediate (NO^+·neutral)* complex. For example, the association of NO^+ with acetonitrile (I.P. = 12.2 eV) is relatively slow, whereas association with benzonitrile (I.P. = 9.7 eV) is facile. [354] Similarly, association of NO^+ with formic acid (I.P. = 11.3 eV) occurs at less than 5% of the collision rate, whereas association with acetic acid (I.P. = 10.7 eV) occurs at close to 50% of the collision rate. [228] The difference in association rates is probably a reflection of the larger binding energy of the excited transient complex (NO^+·CH_3COOH)*, relative to that of the analogous (NO^+·HCOOH)* complex, which increases its lifetime against unimolecular dissociation back to $NO^+ + CH_3COOH$. It should be noted that the observation of parallel charge transfer and association, when charge transfer is close to thermoneutral, is in some respects analogous to near-thermoneutral proton transfer, where association often occurs in parallel with proton transfer.

A number of Fourier transform-ion cyclotron resonance (FT-ICR) studies at much lower pressures have been reported by the Dunbar group [359-363], in which they examined association reactions of NO^+ with a series of ketones. They attributed the observed association reactions at ~ 10^{-7} Torr in their ICR cell to radiative stabilisation of the (NO^+·RCOR')* complex rather than collisional stabilisation, since no pressure variation was evident in the observed rate coefficient over the pressure range accessed. They also report a parallel charge transfer channel in the reaction of NO^+ with 3-pentanone, which they note is slightly endothermic. [360]

The present study aimed to examine the competition between charge transfer and association in the reactions of NO^+ with ketones (specifically acetone, butanone and 3-pentanone) by examining the kinetic energy dependence of the rates and product distributions in the FA-SIFDT apparatus. Very few studies have been made of the competition between termolecular and bimolecular reaction channels using drift tubes. In 1987 the Innsbruck group of Lindinger and co-workers reported a study of the competition between binary ion-molecule reactions and ternary association reactions of CH_3^+ and NH_3 (reaction 6.4) using a selected ion drift tube (SIDT) over the wide pressure

range from 0.2 – 1.7 Torr, and in the centre-of-mass energy (E_r) range from 0.047 – 0.2 eV. [364] The product channels for the reaction were:

$$CH_3^+ + NH_3 \longrightarrow CH_2NH_2^+ + H_2 \quad \textbf{(6.4a)}$$

$$\longrightarrow NH_4^+ + CH_2 \quad \textbf{(6.4b)}$$

$$\xrightarrow{He} CH_3NH_3^+ \quad \textbf{(6.4c)}$$

The rate for the ternary association channel (6.4c) was observed to decline from 4 x 10^{-26} cm^6 s^{-1} at 0.047 eV to 6 x 10^{-27} cm^6 s^{-1} at 0.2 eV. The bimolecular rate for channel (6.4a) was also observed to decline over the studied energy regime, while the rate coefficient for channel (6.4b) increased slightly. An analysis of the pressure dependence of the effective bimolecular rate coefficient as a function of E_r led to estimates of the $(CH_3^+ \cdot NH_3)^*$ collision complex lifetime in the range of ~10^{-7} s to ~10^{-8} s.

More recently Lindinger's group investigated the competition between association and binary reactions in the reaction of $SF_5^+ + H_2S$ in the centre-of-mass energy (E_r) range from 0.052 to 1.7 eV (reaction 6.5). [365] At low energies a slow binary reaction channel producing SF_4HS^+ (+ HF) occurs in parallel with a medium-fast association reaction. The rate coefficients for both processes decline from 3 x 10^{-11} cm^3 s^{-1} and 3 x 10^{-27} cm^6 s^{-1} respectively at 0.052 eV to < 5 x 10^{-12} cm^3 s^{-1} and < 5 x 10^{-28} cm^6 s^{-1} respectively at E_r = 0.3 eV. Above 0.3 eV the effective bimolecular rate coefficient increases again due to the onset of the endothermic charge transfer channel (6.5c).

$$SF_5^+ + H_2S \xrightarrow{He} SF_5^+ \cdot H_2S \quad \textbf{(6.5a)}$$

$$\longrightarrow SF_4HS^+ + HF \quad \textbf{(6.5b)}$$

$$\longrightarrow H_2S^+ + SF_5 \quad \textbf{(6.5c)}$$

6.1.3 Experimental.

The following experiments relevant to the NO^+/ketone association reactions were all performed using the FA-SIFDT apparatus. Initially, NO^+ was formed by addition of a flow of nitric oxide to a helium carrier subjected to microwave discharge in the flowing afterglow source. One difficulty with the production of NO^+ from NO is that metastable $NO^+(a^3\Sigma^+)$ and vibrationally excited $NO^+(X\ ^1\Sigma^+, v>0)$ may be produced, in addition to ground state $NO^+(X\ ^1\Sigma^+, v=0)$. [77] Indeed, as the NO flow diminished (NO was stored in a glass bulb at ~ 760 Torr pressure and was rapidly depleted) it became apparent that

excited state species, $(NO^+)^*$, were being produced and transmitted into the flow tube. This behaviour was probably a consequence of the less efficient quenching of $(NO^+)^*$ at low flows of NO. The presence of $(NO^+)^*$ was apparent from the observation of dissociative charge transfer reactions with the ketones with no applied drift field. Dissociative charge transfer is not thermodynamically possible from ground state NO^+. Penning ionisation of NO by $He^*(2\ ^3S)$ was therefore rejected as the best means of forming ground state NO^+. Similar observations were made when N_2O or laboratory air was added to the FA source. Two subsequent methods were used to form NO^+. In the first, zero grade nitrogen was subjected to microwave discharge in the FA source and a flow of laboratory air was added to the nitrogen carrier, generating NO^+, predominantly via the reaction:

$$N^+ + O_2 \longrightarrow NO^+ + O \qquad \textbf{(6.6)}$$

In the second method (which was most often used in this study) direct microwave discharge of dry air yielded good signals of NO^+. Metastable and vibrationally excited NO^+ are known to be quenched by N_2, [366,367] keeping the fraction of excited state species down to a minimum level.

The ketones were purified via multiple freeze-pump-thaw cycles and the vapour was used without dilution. Absolute flow rates of the ketones (acetone, butanone and 3-pentanone) were measured via the pressure drop from a calibrated volume. This should be compared with the method employed by Spanel et al [355], who prepared the ketones as a dilute mixture in air and measured the relative decay rates of H_3O^+, NO^+ and O_2^+ ion signals (injected simultaneously from their ion source) versus the flow rate of the air/ketone mixture. The H_3O^+/ketone reactions were assumed (with justification [345]) to proceed at their respective collision rates and the rate coefficients for the O_2^+ and NO^+ reactions were scaled accordingly. Dipole moments, μ, for the ketones butanone and 3-pentanone were estimated by Spanel et al from the known value of μ(acetone) by assuming that μ does not change significantly with the number of carbon atoms in the ketones. [355] A value for the dipole moment of butanone (μ = 2.78 D) has been published [162] which is negligibly different from the value (μ = 2.8 D) assumed by Spanel et al. [355]

6.2 Results and discussion.

The reactions of NO^+ with the three ketones acetone, butanone and 3-pentanone were all examined in the ion-neutral centre-of-mass energy (E_r) range from thermal (0.038 eV) to ~ 1 eV. NO^+ mobility data were taken from reference 37. The measured effective bimolecular rate coefficients at E_r = 0.038 eV and 0.44 Torr are listed in Table 6.1 together with the earlier results of Spanel et al [355] (obtained at 0.5 Torr) for comparison. The present measurements agree with the earlier results within the experimental uncertainty. The only observed product in the reactions of NO^+ with acetone and butanone at E_r = 0.038 eV was the ternary association ion $NO^+.M$ (M = acetone, butanone), in accord with the findings of Spanel et al. [355] The NO^+ affinities of acetone, butanone and 3-pentanone are listed in Table 6.2. A (minor) parallel charge transfer channel (4% at 0.44 Torr of He) was observed in the reaction of NO^+ with 3-pentanone. The endothermicity of charge transfer to 3-pentanone from NO^+ is only 0.05 eV (~ 2kT at room temperature) so a small fraction of reactants possess sufficient energy to overcome the reaction endothermicity. As the kinetic energy of the NO^+ ions is increased, more energy becomes available for charge transfer. The kinetic energy dependence of each of the NO^+/ketone reactions is discussed next, in the order 3-pentanone, butanone and acetone.

Ketone	Product ratio	Products	k_{obs}[a] /10^{-9} cm^3 s^{-1}	k_{prev}[b] /10^{-9} cm^3 s^{-1}	k_{coll} /10^{-9} cm^3 s^{-1}	Δ I.P. (eV)[c]
acetone	1.0	adduct	1.3	1.2	3.3	0.44
butanone	1.0	adduct	2.1	2.8	3.2	0.26
3-pentanone	0.96	adduct	2.6	3.4	3.3	0.05
	0.04	C.T.[d]				

Table 6.1. Rate coefficients and branching ratios at zero field for the reactions of $NO^+(X\ ^1\Sigma^+)$ with the designated ketones.

[a] At a pressure of 0.44 Torr of helium.
[b] At a pressure of ~ 0.5 Torr of helium. Association only was reported for all three reactions.
[c] Δ I.P. = I.P.(ketone) – I.P.(NO) in eV.
[d] Denotes charge transfer.

Ketone	acetone	butanone	3-pentanone
NO^+ affinity (eV)	1.77	1.82	1.85

Table 6.2. Binding energies of NO^+·ketone complexes (NO^+ affinities) for the designated ketones (taken from ref. 360).

6.2.1 $NO^+ + (C_2H_5)_2CO$ (I.P. = 9.31 eV).

The reaction between NO^+ and 3-pentanone (diethylketone) proceeds over the energy range investigated thus:

$$NO^+ + (C_2H_5)_2CO \xrightarrow{He} NO^+\cdot(C_2H_5)_2CO \quad \textbf{(6.7a)}$$

$$\longrightarrow (C_2H_5)_2CO^+ + NO \quad \textbf{(6.7b)}$$

$$\longrightarrow C_2H_5CO^+ + C_2H_5 + NO \quad \textbf{(6.7c)}$$

$$\longrightarrow C_2H_4CO^+ + C_2H_6 + NO \quad \textbf{(6.7d)}$$

Charge transfer and dissociative charge transfer yielding $C_2H_5CO^+$ and $C_2H_4CO^+$ are also observed in the reaction of O_2^+ with 3-pentanone.[355] The measured variation in the effective bimolecular rate coefficient with E_r is illustrated in Figure 6.1. As the dominant channel at low energies is association, occurring at essentially the collision rate, then the association reaction is close to the pressure saturation regime. In this regime every complex formed is stabilised by collision before it can dissociate back to reactants. The measured branching ratio as a function of E_r is illustrated in Figure 6.2. The effective bimolecular rate coefficient shows little (< 5%) variation from E_r = 0.038 eV (at 0.44 Torr) to E_r ~ 0.13 eV (at 0.44 Torr) indicating that the reaction remains close to pressure saturation at low energies. As the ion-reactant centre-of-mass energy is increased further, the effective bimolecular rate coefficient begins to decline reaching a value of 9.7 x 10^{-10} cm^3 s^{-1} at E_r = 0.93 eV at a helium carrier gas pressure of 0.25 Torr. Figure 6.2 clearly illustrates the strong decline in the termolecular channel as E_r increases. The termolecular rate coefficient decreases from > 1.7 x 10^{-25} cm^6 s^{-1} at E_r = 0.038 eV to ~ 1.5 x 10^{-26} cm^6 s^{-1} at E_r = 0.93 eV. This decrease is entirely in accord with expectation, because ternary association depends on the lifetime of the intermediate collision complex, $(NO^+\cdot(C_2H_5)_2CO)^*$, which decreases markedly with increasing E_r.

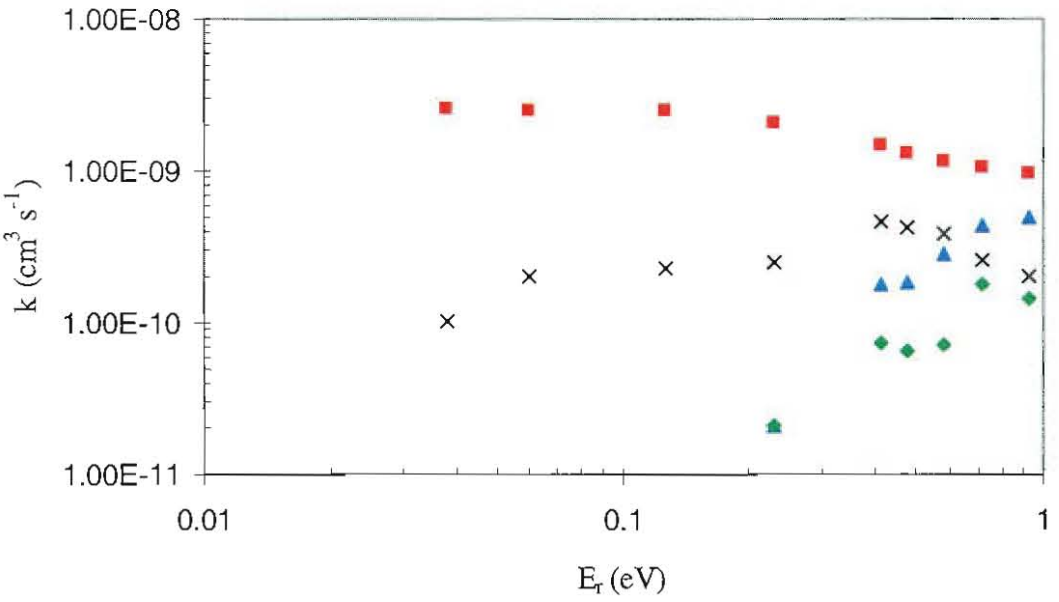

Figure 6.1. Variation in the effective bimolecular rate coefficient for reaction 6.7 (■). Also plotted are the bimolecular rate coefficients for channel 6.7b (x); channel 6.7c (◆); and channel 6.7d (▲).

Although the pressure dependence of the effective bimolecular rate was not measured the rate will surely exhibit a pressure dependence as the reaction exits the pressure saturation regime at higher values of E_r (see the discussion of the NO^+/acetone reaction which follows). The rate coefficient for the charge transfer channel increases from 1.0×10^{-10} cm^3 s^{-1} at $E_r = 0.038$ eV, rises to a maximum of ~ 4.3×10^{-10} cm^3 s^{-1} at E_r ~ 0.5 eV and begins to decline again at still higher energies ($k = 2.0 \times 10^{-10}$ cm^3 s^{-1} at E_r = 0.93 eV), as the dissociative charge transfer channels begin to dominate. Following onset of the dissociative charge transfer channels (6.7c) and (6.7d), the rate coefficients for both processes increase with increasing E_r reaching 1.5×10^{-10} cm^3 s^{-1} and 4.9×10^{-10} cm^3 s^{-1} respectively at $E_r = 0.93$ eV. The observed increase in rate coefficient with increasing kinetic energy ("temperature") is as expected for an endothermic reaction. Such enhancements in the rate of endothermic charge transfer with increasing kinetic energy have been noted before in the reactions of O_2^+ with CH_4, SO_2 and H_2O. [368]

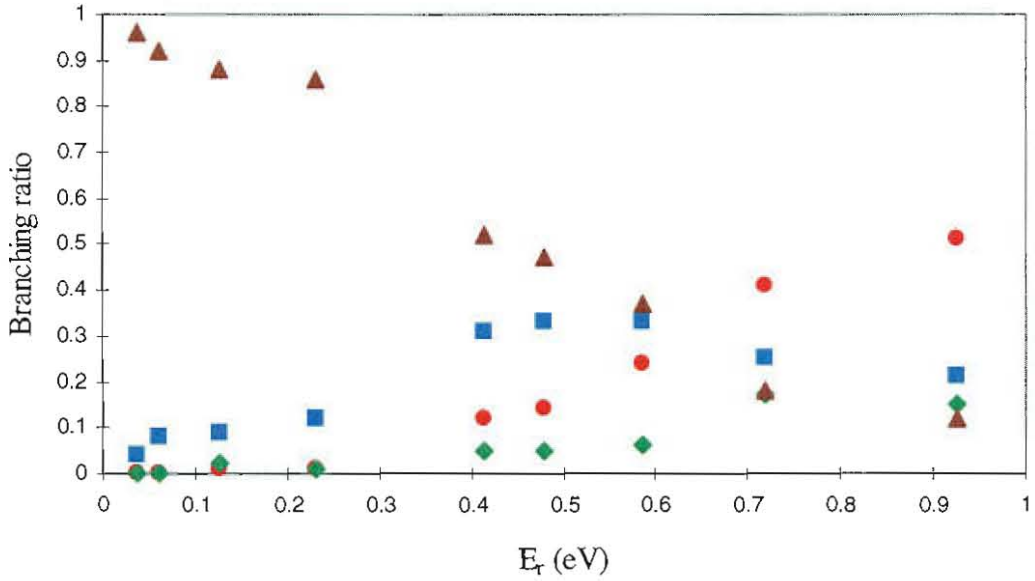

Figure 6.2. Measured branching ratio for reaction 6.7 as a function of E_r. The points correspond to the products (▲) $NO^+ \cdot (C_2H_5)_2CO$; (■) $(C_2H_5)_2CO^+$; (●) $C_2H_4CO^+$; and (◆) $C_2H_5CO^+$. The four highest E_r values correspond to He pressures of 0.40, 0.35, 0.30 and 0.25 Torr respectively. All other measurements were made at a helium pressure of 0.44 Torr.

Assuming Arrhenius behaviour for the endothermic charge transfer and dissociative charge transfer channels, pseudo-Arrhenius plots of ln k_2 versus E_r^{-1} were constructed and are presented in Figure 6.3. The endothermicity derived from Fig. 6.3a for reaction 6.7b of 0.027 eV is in reasonable accord with the thermochemical value of 0.05 eV. The endothermicities derived from Fig. 6.3b are 0.41 eV for reaction 6.7c and 0.66 eV for reaction 6.7d. Possible isomeric structures for the ions at m/z = 57 and m/z = 56 derived from the reaction of NO^+ with 3-pentanone are $CH_3CH_2C{=}O^+$ and $CH_3CH{=}C{=}O^+$ respectively. Indeed both of these products require minimal rearrangement within the intermediate species $(C_5H_{10}O^+)^*$ and might therefore be expected to form at or near the thermochemical threshold. However, the endothermicities calculated from the available thermochemical data, [163] assuming the $CH_3CH_2C{=}O^+$ and $CH_3CH{=}C{=}O^+$ structures for the products at m/z = 57 and m/z =56 respectively, are 0.74 eV (reaction 6.7c) and 0.39 eV (reaction 6.7d), which are respectively ~40% higher and ~40% lower than the values

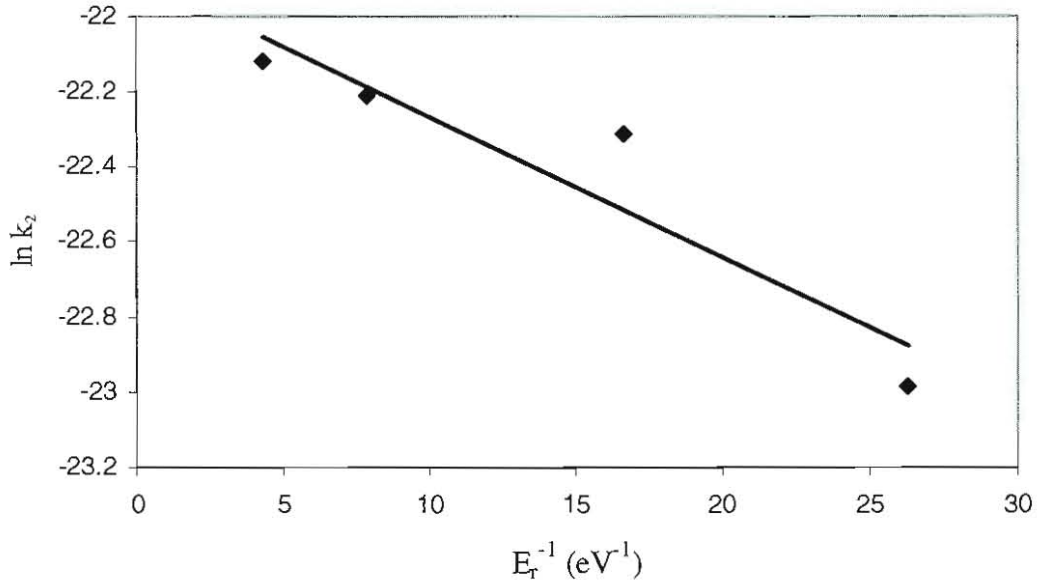

Figure 6.3a. Pseudo-Arrhenius plot of ln k_2 versus E_r^{-1} for reaction 6.7b. The derived endothermicity is 0.027 eV.

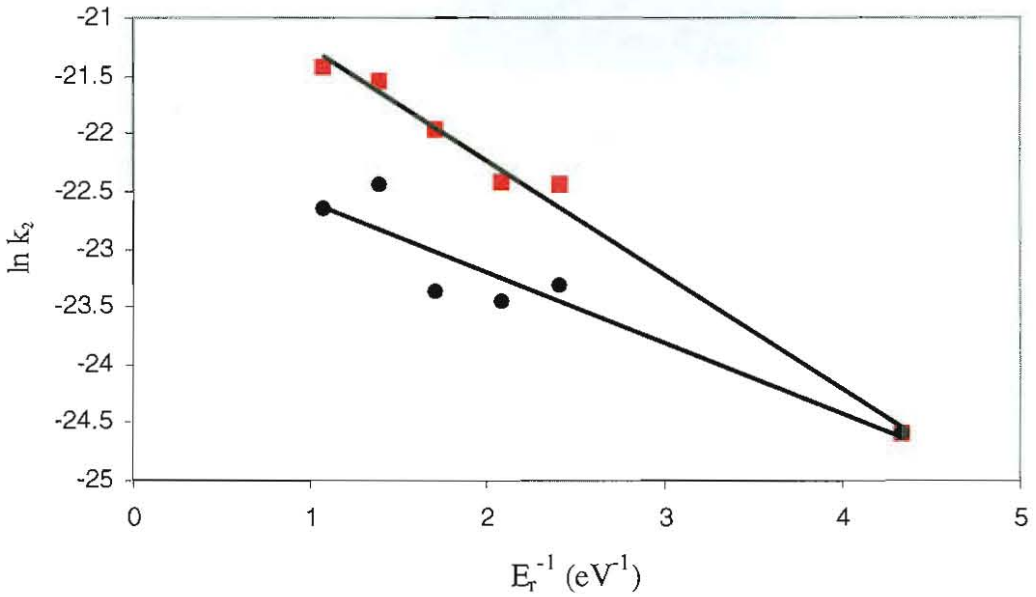

Figure 6.3b. Pseudo-Arrhenius plots of ln k_2 versus E_r^{-1} for reaction 6.7c (●) and reaction 6.7d (■). The derived endothermicities are 0.41 eV and 0.66 eV respectively.

derived from the pseudo-Arrhenius plots. This discrepancy may indicate that other structures are formed in reactions (6.7c) and (6.7d) or simply reflect the uncertainty in the Arrhenius plots due to the presence of competing channels. It is also not clear why channel (6.7d) should dominate over channel (6.7c), over the energy range accessed in the present measurements, given the apparently larger endothermicity for channel (6.7d) and the observation by Spanel et al [355] that charge transfer from O_2^+ to 3-pentanone yields predominantly (70%) m/z = 57 ($C_3H_5O^+$) relative to $C_3H_4O^+$ (15%).

The simple model developed by Adams and Smith [74] (discussed in chapter 1.6) predicts the ternary association rate coefficient, for reaction (6.7a), to vary as $E_c^{-1.0}$ (since NO^+ is a diatomic ion, and hence possesses only two rotational degrees of freedom). A log-log plot of the effective termolecular rate coefficient (= k_2/[He]) versus E_c (and E_r) is presented in Figure 6.4.

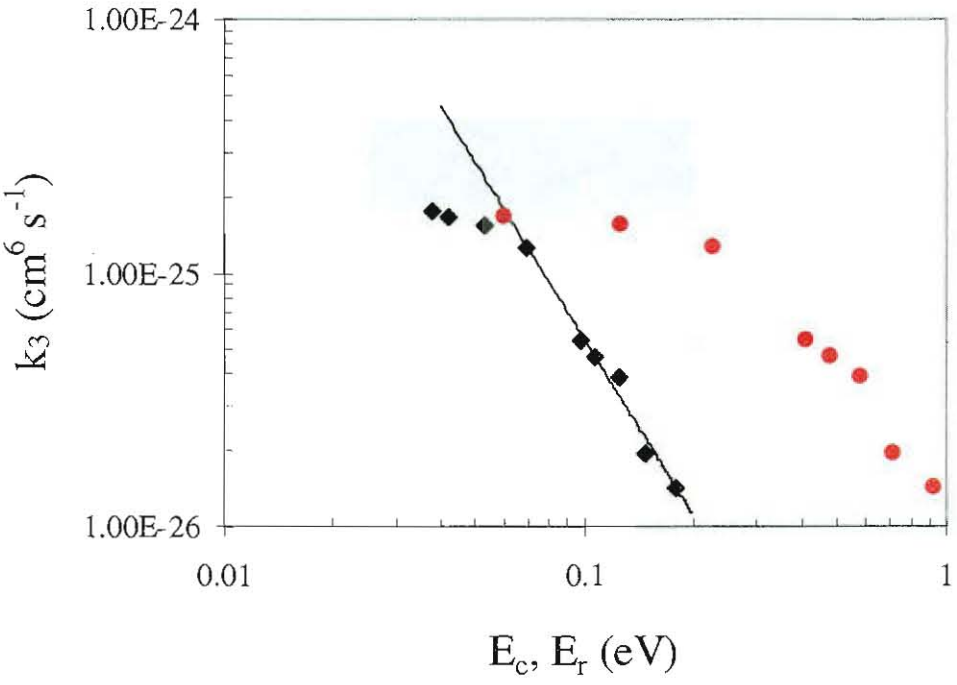

Figure 6.4. The effective ternary rate coefficient, k_3, for the reaction of NO^+ with 3-pentanone in a helium carrier gas at 300 K plotted in log-log form against E_c (◆) and E_r (●). A linear least squares fit to the E_c data yields a slope of –2.3 (see the text for discussion).

The curvature of the plot at low E_c further indicates that the reaction is close to pressure saturation at near thermal energies. At higher E_c the plot does become linear however, suggesting a power law relationship between k_3 and E_c, i.e. $k_3 \alpha E_c^{-m}$. No such power law relationship describes the variation of k_3 with E_r, except at higher values of E_r where the two curves become parallel in accord with expectation. [74] A linear least squares fit to the linear section of the data indicates a slope of –2.3, which is significantly larger than the value of –1.0 predicted by the model of Adams and Smith. The steeper observed E_c dependence of the ternary rate coefficient than predicted by the model is unlikely to be due to the excitation of vibrations in the NO^+ reactant ions (see the discussion which follows). The observed $E_c^{-2.3}$ dependence might therefore reflect an increase in the index in the power law which describes the ***"temperature"*** dependence of k_3, due to the involvement of internal rotations and low energy vibrations in the 3-pentanone reactant. Bass and Jennings [369] commented earlier that divergence from a simple T^{-n} variation in k_3 tends to be greatest for complexes with large well depths and a large number of low frequency vibrations and internal rotations. They also suggest that the influence of these effects will be described by an increase in the power index of the power law. Thus, the –2.3 index observed in the plot of k_3 versus E_c for the NO^+/3-pentanone reaction presumably constitutes a –1.0 contribution for rotations and a –1.3 contribution for vibrations (and internal rotations) in the 3-pentanone reactant, i.e. $k_3 \approx E_c^{-1.0} \cdot E_c^{-1.3}$.

6.2.2 $NO^+ + CH_3COC_2H_5$ (I.P. = 9.52 eV).

The reaction between NO^+ and butanone accesses the following product channels over the energy range investigated:

$$NO^+ + CH_3(CO)C_2H_5 \xrightarrow{He} NO^+.CH_3COC_2H_5 \quad \textbf{(6.8a)}$$

$$\longrightarrow CH_3COC_2H_5^+ + NO \quad \textbf{(6.8b)}$$

$$\longrightarrow CH_3CO^+ + C_2H_5 + NO \quad \textbf{(6.8c)}$$

$$\longrightarrow C_2H_5CO^+ + CH_3 + NO \quad \textbf{(6.8d)}$$

Charge transfer and dissociative charge transfer yielding CH_3CO^+ and $C_2H_5CO^+$ are also observed in the reaction of O_2^+ with butanone. [355] The observed variation in the effective bimolecular rate coefficient with E_r is illustrated in Figure 6.5. The measured branching ratio as a function of E_r is illustrated in Figure 6.6. At thermal energies (E_r = 0.038 eV) the only product is the association adduct at m/z = 102, as charge transfer from ground

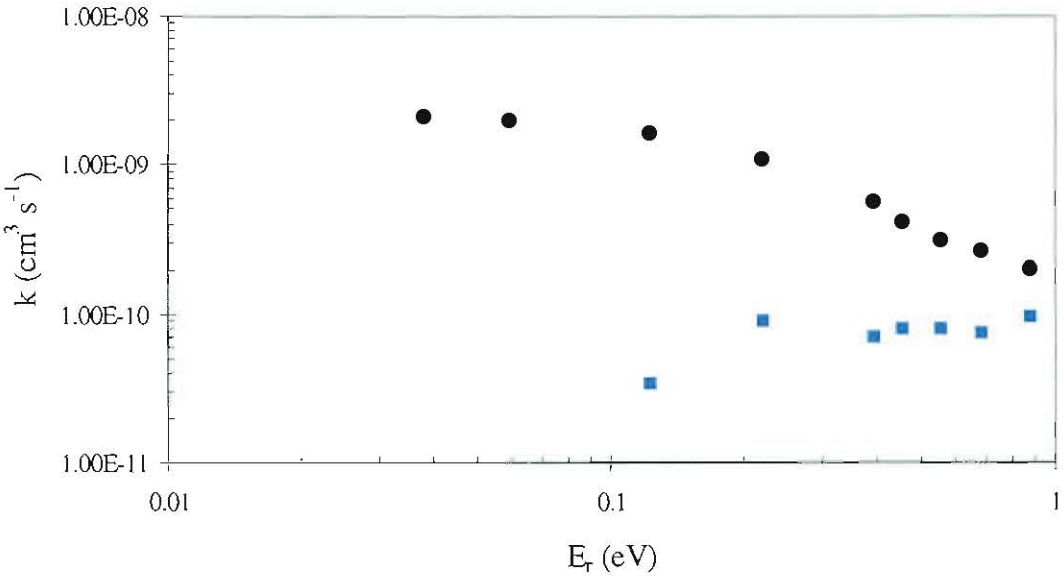

Figure 6.5. Variation in the effective bimolecular rate coefficient, k, for reaction 6.8 (●) and the effective bimolecular rate coefficient for channel 6.8b (■).

state NO^+ is endothermic by 0.26 eV. Again, the reaction is apparently at, or approaching pressure saturation at low energies. The termolecular rate coefficient for reaction (6.8a) decreases from > 1.8×10^{-25} cm^6 s^{-1} at E_r = 0.038 eV to 7.6×10^{-27} cm^6 s^{-1} at E_r = 0.89 eV. The onset of charge transfer is observed close to threshold and charge transfer becomes the dominant product channel at 0.89 eV (Figure 6.6), with a bimolecular rate coefficient of 1.0×10^{-10} cm^3 s^{-1}. The bimolecular rate coefficients for channels (6.8c) and (6.8d) are 2.0×10^{-11} cm^3 s^{-1} and 3.0×10^{-11} cm^3 s^{-1} respectively at E_r = 0.89 eV. A log-log plot of the effective termolecular rate coefficient (= k_2/[He]) versus E_c (Figure 6.7) was constructed and a linear least-squares fit to the data yields a slope of –2.3, which is significantly larger than the –1.0 predicted by the model of Smith and Adams [74]. Again this may indicate the involvement of low frequency vibrations and internal rotations in the butanone reactant. Curvature is also evident in the plot at low values of E_c, which again probably indicates an approach to pressure saturation at near-thermal energies.

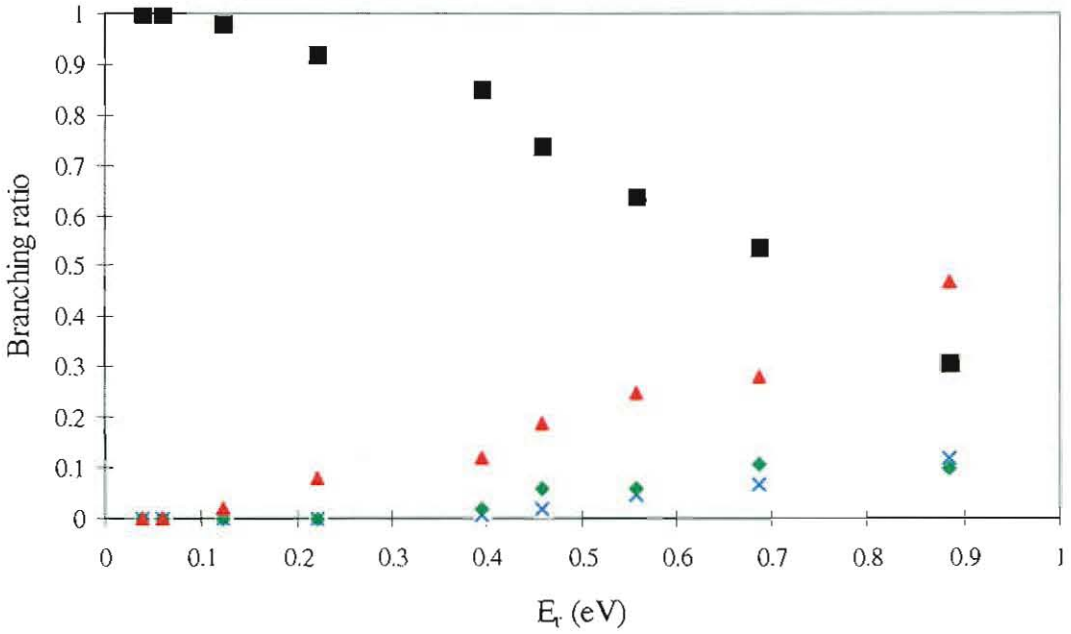

Figure 6.6. Measured branching ratio for reaction 6.8 as a function of E_r. The points correspond to the products (■) $NO^+ \cdot C_4H_8O$; (▲) $C_4H_8O^+$; (◆) $C_2H_5CO^+$; and (x) CH_3CO^+. The four highest E_r values correspond to He pressures of 0.40, 0.35, 0.30 and 0.25 Torr respectively. All other measurements were made at a helium pressure of 0.44 Torr.

6.2.3 $NO^+ + (CH_3)_2CO$ (I.P. = 9.70 eV).

$$NO^+ + (CH_3)_2CO \xrightarrow{He} NO^+ \cdot (CH_3)_2CO \qquad \textbf{(6.9a)}$$

$$\longrightarrow (CH_3)_2CO^+ + NO \qquad \textbf{(6.9b)}$$

The measured effective bimolecular rate coefficient for the association reaction between NO^+ and acetone was 1.3 x 10^{-9} cm^3 s^{-1} (~ 40% of the calculated collision rate) at a pressure of 0.44 Torr. Further, no variation in the rate coefficient was observed in the pressure range from 0.25 to 0.70 Torr. This may indicate a very shallow rise in the pressure fall-off curve in this pressure regime (i.e. less than the precision of the individual rate measurements, or ~ 15%) towards the gas kinetic rate at pressures far in excess of 1 Torr. Alternatively, it may indicate that the termolecular association of NO^+ with acetone is governed by a more complex mechanism than that described by equations (6.2) and

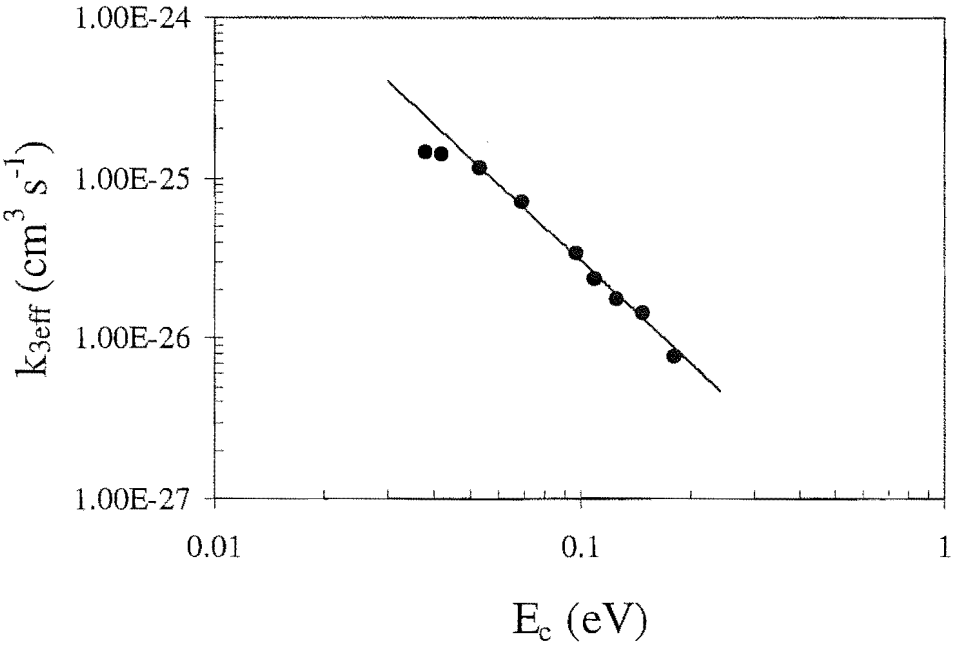

Figure 6.7. The effective ternary rate coefficient, k_3, for the reaction of NO^+ with butanone in a helium carrier gas at 300 K plotted in log-log form against E_c. A linear least squares fit to the E_c data yields a slope of –2.3 (see the text for discussion).

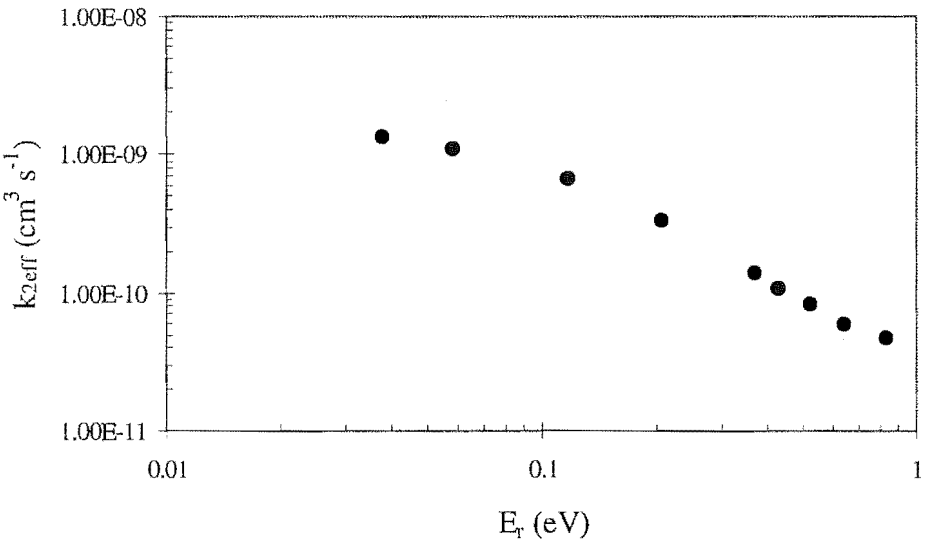

Figure 6.8. Variation in the effective bimolecular rate coefficient for reaction 6.9 as a function of E_r.

(6.3). A mechanism which would account for a high pressure limiting rate constant that is less than the collision rate has been proposed by Meot-Ner (equation 3.10). [357] The mechanism involves reaction on a double-minimum potential surface. Formation of a loose orbiting complex precedes rearrangement to a tight complex that can be collisionally stabilised. The scheme predicts second order kinetics at high pressures, however the high pressure limiting rate constant can be significantly smaller than the collision rate. This will happen when dissociation of the loose complex is competitive with rearrangement to the tight complex (i.e. when $k_r > k_1$).

$$A^+ + B \underset{k_r}{\overset{k_f}{\rightleftharpoons}} (A^+\cdot B)^*_{loose} \underset{k_2}{\overset{k_1}{\rightleftharpoons}} (A^+\cdot B)^*_{tight} \xrightarrow{M} AB^+ \qquad \textbf{(6.10)}$$

The measured ternary rate coefficient for reaction (6.9a) declines from > 9.1 x 10^{-26} cm^6 s^{-1} at E_r = 0.038 eV to < 5.7 x 10^{-27} cm^6 s^{-1} at E_r = 0.83 eV. Figure 6.9 is a plot of k_{2eff} versus [He] at E_r = 0.43 eV and depicts the observed pressure variation in the effective bimolecular rate coefficient for reaction (6.9a). The effective bimolecular rate coefficient is linearly dependent on the helium pressure, indicating that the reaction exhibits true third-order kinetics at E_r = 0.43 eV, i.e. that the reaction is no longer in the pressure saturation regime. A linear least-squares fit to the data yields a termolecular rate coefficient of 1.2 x 10^{-26} cm^6 s^{-1}.

Two problems were encountered in the measurements of the NO^+ + acetone reaction. At higher values of E_r, where the effective bimolecular rate coefficient had dropped to less than 10^{-10} cm^3 s^{-1}, distinct downward curvature was noted in the semilogarithmic decays at high acetone flows. The curvature was attributed to rapid variation in the flow rate of acetone, which is limited by the available partial pressure of acetone vapour (185 Torr at 20°C). Also, at the higher values of E_r, the product distributions were complicated by the presence of a small (≤ 3%) population of NO^+* (probably NO^+ ($a\ ^3\Sigma^+$) injected from the source, but some $NO^+(v>0)$ either injected from the source or formed in the drift tube cannot be excluded. The likelihood of vibrational excitation of NO^+ occurring in the drift field region at the E_c values accessed in the present experiments is discussed below. The available data suggests that, at the highest centre-of-mass energy accessed, E_r = 0.83 eV, the charge transfer channel (6.9b) possesses a rate coefficient of ~ 9.0 x 10^{-12} cm^3 s^{-1}, which means the ternary association

reaction (6.9a) is the dominant process over entire energy range accessed in the experiment.

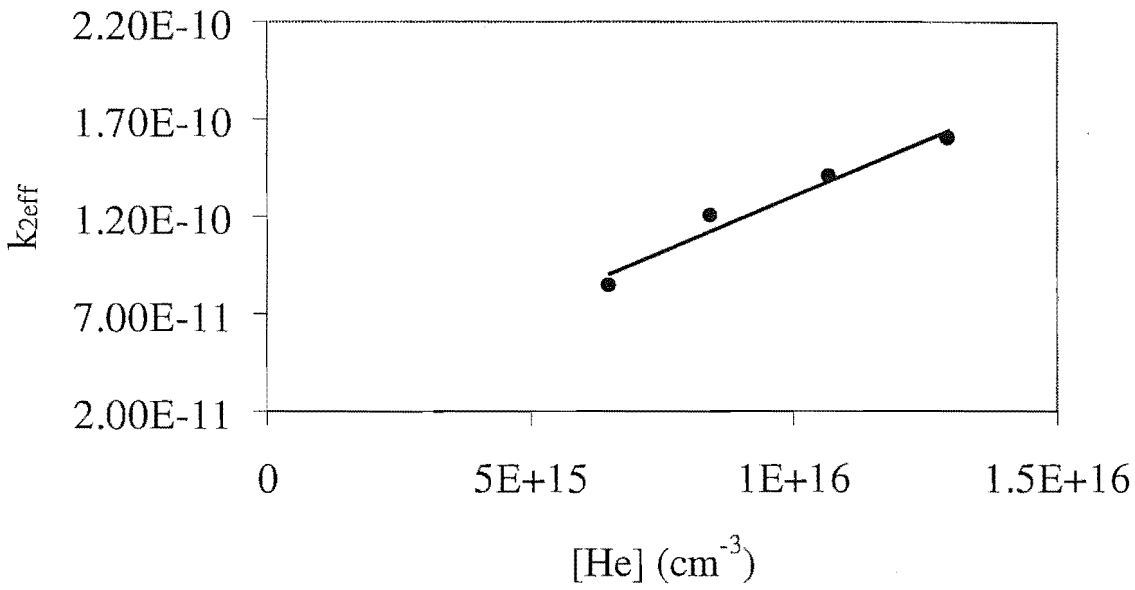

Figure 6.9. Plot of k_{2eff} versus [M], where [M] equals the helium carrier gas density, for the reaction of NO^+ with acetone at E_r = 0.43 eV. The linear fit yields a rate coefficient for termolecular association of 1.2 x 10^{-26} cm^3 s^{-1}.

A log-log plot of the effective ternary rate coefficient versus E_c was constructed. A linear least squares fit to the data yields a slope of –2.5, which is again significantly larger than the –1.0 predicted by the model of Adams and Smith. [74]

6.2.4 Does vibrational excitation of NO^+ play a role?

It is believed that the preceding results are appropriate to ground vibrational state NO^+ over the entire accessed energy range (with the exception of the small quantity of vibrationally excited or metastable NO^+ injected from the ion source). Pogrebnya et al [77] measured quenching rate coefficients for $NO^+(v \geq 1)$ and $NO^+(v \geq 4)$ in collision with a helium bath gas as a function of E_c in a SIFDT apparatus. Using their results we can estimate the rates for vibrational excitation of $NO^+(v = 0)$ to $NO^+(v = 1)$ in the range of ion-neutral centre-of-mass energies (E_c) accessed in the present experiments. The

maximum value of E_c attained in the present measurements was ~ 0.2 eV. At E_c = 0.3 eV, Pogrebnya et al [77] report a rate coefficient for quenching, k_q, for the process:

$$NO^+(v \geq 1) + He \longrightarrow NO^+ (v = 0) + He \qquad \textbf{(6.11)}$$

of ~ 3 x 10^{-14} cm^3 s^{-1}. Detailed balance requires that

$$k_{ex} = k_q \exp(-h\nu/kT) \qquad \textbf{(6.12)}$$

where k_{ex} is the rate coefficient for vibrational excitation. Taking $h\nu$ = 0.29 eV, k_{ex} is calculated to be 3 x 10^{-19} cm^3 s^{-1} at E_c = 0.3 eV. The fraction of NO^+ (v = 1) formed can be estimated from equation (6.13):

$$[NO^+]_f = [NO^+]_i \exp(-k_{ex}[He]t) \qquad \textbf{(6.13)}$$

Assuming a helium pressure of 0.5 Torr and a reaction time of 1ms (both overestimate the values appropriate to the experiment) the amount of NO^+ (v=1) formed at E_c = 0.3 eV is negligible (<0.1%). Therefore, any vibrationally excited NO^+ present in the flow tube in the present experiments has to have originated in the ion source or to have been formed upon injection into the flow tube.

6.3 Conclusions.

The present results indicate, in accord with expectation, that the lifetime of the intermediate (NO^+·ketone)* complex, formed when NO^+ collides with a ketone molecule, is very sensitive to the centre-of-mass energy appropriate to the collision. In accord with the simple model developed by Adams and Smith [74] the ternary association rate exhibits an inverse power law relationship with E_c, the ion-carrier gas centre-of-mass energy. It should be noted, however, that the power law indices measured in the present experiments (all greater than –2.0) are significantly larger than the value of –1.0 predicted by the model of Adams and Smith. [74] It should also be noted that in the systems examined here, the number of atoms involved is significantly larger than in the CH_3^+/diatomic reactions examined by Adams and Smith. [74] The enhanced power law indices observed in the present measurements may reflect the involvement of internal rotations and low frequency vibrations in the ketone molecules or a simple failure of the model to describe the NO^+/ketone systems. Detailed phase space calculations [369], similar to those performed on the systems examined by Adams and Smith would help to resolve this question.

The rates of endothermic charge transfer (and dissociative charge transfer) are observed to increase with increasing energy, beyond their respective thresholds. The increase in rate coefficient with increasing energy is as expected for an endothermic reaction. Such enhancements in the rate coefficient with increasing kinetic energy have been noted before in endothermic charge transfer reactions of O_2^+ with SO_2 and H_2O. [368] Vibrational excitation of the NO^+ reactant ions is not believed to occur to any significant extent in the range of ion-carrier gas centre-of-mass energies (E_c) accessed in the present experiments. Rapid equilibration of the NO^+ rotational energy levels, to an effective temperature described by E_c, is expected. It is expected, although not confirmed, that rotational and translational energy will be equally efficient in overcoming the reaction endothermicity in the endothermic charge transfer processes. Another process which was not explicitly identified in the present experiments, but which cannot be dismissed as a possibility, is third-body assisted dissociation, as observed by Glosik et al. [137] The dissociative charge transfer channels may exhibit some pressure dependence if a process of the type:

$$NO^+ + RCOR' \longrightarrow (RCOR'^+)^* \xrightarrow{He} RCO^+ + R' \qquad \textbf{(6.14)}$$

competes with collisional stabilisation of the intermediate $(RCOR'^+)^*$ species.

6.4 Competition between binary ion-molecule reactions and ternary association in the reactions of CH_3^+ with C_2N_2 and CH_3CN.

6.4.1 Introduction.

Association reactions of CH_3^+ have attracted much attention from experimentalists.

$$CH_3^+ + X \xrightarrow{M} CH_3^+\cdot X \qquad \textbf{(6.15)}$$

Flow tube studies of reactions of type (6.15) where the association adduct is stabilised in collisions with the carrier gas molecules, have been used to estimate rate coefficients for the analogous radiative association reactions in which the excited intermediate complex is stabilised by the emission of a photon.

$$CH_3^+ + X \longrightarrow CH_3^+\cdot X + h\nu \qquad \textbf{(6.16)}$$

Such reactions have been implicated in the synthesis of some observed interstellar molecules. [74]

Ionic species of the type $CH_3^+ \cdot X$ are also of interest to thermodynamicists in the construction of a methyl cation affinity scale. [370] Alkyl (e.g. methyl) cation transfer reactions are also proposed to play a role in the chemistry of the interstellar medium. [217]

Experimental studies of the collisional association reactions of CH_3^+ ions have also received special attention from experimentalists as a valuable test of theoretical models of termolecular association. [74] In some reactions of CH_3^+ ions, association is observed to occur in parallel with binary channels. Such reactions often exhibit very different behaviour in the pressure regimes applicable to ICR (< ~10^{-4} Torr) and flow tube (~ 0.1 – 1 Torr) techniques. [371] One such example is the reaction between CH_3^+ and CH_3CN (acetonitrile).

$$CH_3^+ + CH_3CN \longrightarrow \text{products} \qquad \textbf{(6.17)}$$

In a SIFT study of reaction (6.17) the major product channel observed was termolecular association leading to the product ion at m/z = 56, $CH_3CNCH_3^+$, with a minor binary channel (12%) to $H_2CN^+ + C_2H_4$. [371] The measured rate coefficient was 5.5 x 10^{-9} cm^3 s^{-1} and showed little or no pressure variation in the range 0.2 – 0.4 Torr. In an ICR study [372] of the same reaction, three reaction channels were observed with a measured rate coefficient of 1.9 x 10^{-9} cm^3 s^{-1}. The branching ratio [$C_2H_5^+$ + HCN (37%), H_2CN^+ + C_2H_4 (58%) and $CH_3CNCH_3^+$ (5%)] was independent of pressure below ~10^{-6} Torr. At higher pressures the transition to termolecular association was observed:

$$CH_3^+ + CH_3CN \xrightarrow{M} CH_3CNCH_3^+ \qquad \textbf{(6.18)}$$

and termolecular rate coefficients, k_3 = 1.9 x 10^{-22} cm^6 s^{-1} (M = CH_3CN) and k_3 = 1.0 x 10^{-23} cm^6 s^{-1} (M = He), were determined. Smith et al [371] were able to satisfactorily account for all of the features of the experimental studies in an RRKM treatment of the CH_3^+/CH_3CN system.

In a SIFT study aimed at bracketing the proton affinity of C_2N_2, Petrie et al [373] noted a facile ternary association reaction between CH_3^+ and C_2N_2:

$$CH_3^+ + C_2N_2 \xrightarrow{He} CH_3^+ \cdot C_2N_2 \qquad \textbf{(6.19)}$$

The measured rate coefficient was equal to 1.5 x 10^{-9} cm^3 s^{-1}, close to the Langevin collision rate, k_c =1.9 x 10^{-9} cm^3 s^{-1}, indicating that the reaction is very close to pressure

saturation at a helium pressure of 0.3 Torr. A subsequent SIFT measurement [374] of reaction (6.19) yielded a rate coefficient of 1.7 x 10^{-9} cm^3 s^{-1} at 0.3 Torr, in excellent agreement with the earlier measurement. Quite different behaviour was observed in an ICR study of the same reaction. [374] Two product channels were observed [CH_2CN^+ + HCN (~80%) and the association channel product, $CH_3^+ \cdot C_2N_2$ (~20%) at P = 3 x 10^{-5} Torr].

$$CH_3^+ + C_2N_2 \xrightarrow{M} CH_3^+ \cdot C_2N_2 \qquad \textbf{(6.20a)}$$

$$\longrightarrow CH_2CN^+ + HCN \qquad \textbf{(6.20b)}$$

The measured pressure variation in the effective bimolecular rate for reaction (6.20) yielded a ternary rate coefficient, k_3 = 8.2 x 10^{-24} cm^6 s^{-1} (M =C_2N_2).

The CH_3^+/C_2N_2 and CH_3^+/CH_3CN systems were both investigated using the FA-SIFDT apparatus. The results of these two studies are discussed below.

6.4.2 Experimental.

CH_3^+ was formed in the FA source via addition of CH_3Br to a helium carrier subjected to microwave discharge. The off-axis discharge was used which eliminated the problem of photons from the discharge traversing the SIFT chamber and entering the flow reactor tube. The resultant CH_3^+ ions were mass selected at m/z = 15 and injected into the flow tube. Sufficiently low injection energies could be achieved, E_{lab} < 20 eV, to prevent significant collision-induced dissociation of the ions in collision with the helium carrier gas. Mobility data for CH_3^+ were taken from ref. 40. The reactants cyanogen and acetonitrile were added at the downstream neutral inlet.

6.4.3 $CH_3^+ + C_2N_2$.

At zero drift field the measured effective bimolecular rate coefficient was 1.5 x 10^{-9} cm^3 s^{-1}, in excellent agreement with the two earlier SIFT measurements. [373,374] The predominant product was the association adduct at m/z = 67. A small peak at m/z = 40 was observed and may constitute a ~1% product channel. This is consistent with the slow rate measured for the binary reaction channel (6.20a) in the earlier ICR study [374], k_2 ~ 7.2 x 10^{-11} cm^3 s^{-1}, which is < 5% of the effective bimolecular rate measured in the present work. The measured variation in the effective bimolecular rate coefficient with ion-neutral centre-of-mass energy, E_r, is illustrated in Figure 6.10. The dominant product

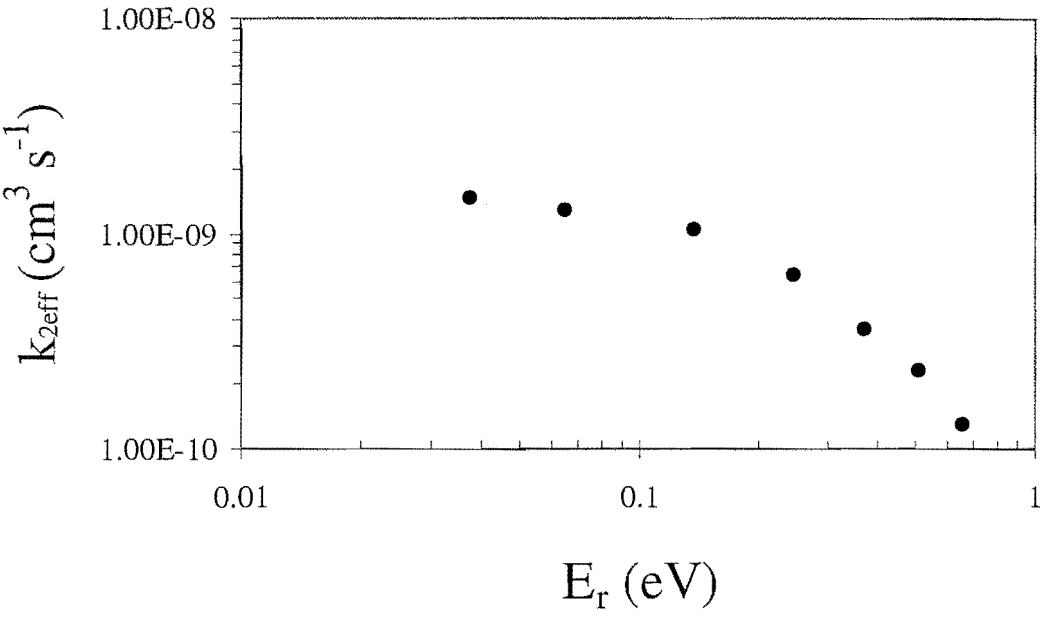

Figure 6.10. Measured variation in the effective bimolecular rate coefficient, k_{2eff}, for the reaction between CH_3^+ and C_2N_2.

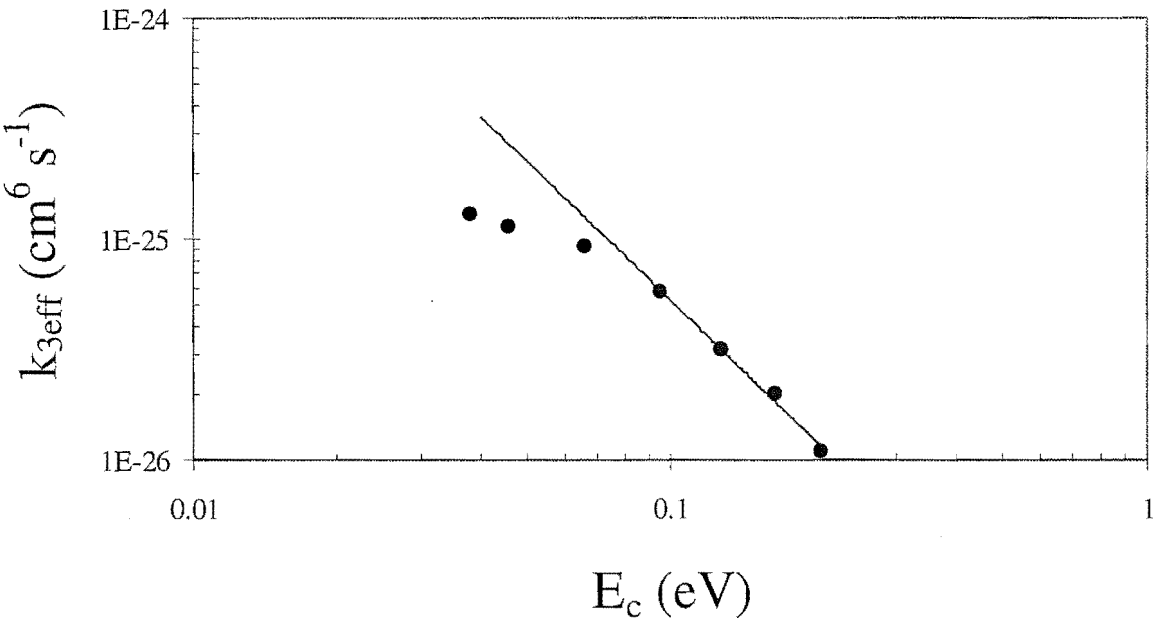

Figure 6.11. The termolecular rate coefficient, k_{3eff} (= k_2/[He]), for the reaction of CH_3^+ with C_2N_2 in a helium carrier gas at 300 K plotted in log-log form against E_c. A linear least squares fit to the data at high E_c yields a slope of –2.0 (see the text for discussion).

channel over the entire energy range covered is the ternary association adduct. The termolecular rate coefficient decreases from > 1.3 x 10^{-25} cm^6 s^{-1} at E_r = 0.038 eV to ~1.1 x 10^{-26} cm^6 s^{-1} at E_r = 0.66 eV. A log-log plot of the effective ternary rate coefficient, $k_{3eff} = k_2/[He]$, versus E_c, was again constructed to test the predictions of the model of Adams and Smith. [74] The plot is shown in Figure 6.11. Again, the curvature at low E_c suggests a transition to pressure saturation in the ternary association rate at near thermal energies. The Adams/Smith model predicts that the ternary rate coefficient should vary as $E_c^{-1.5}$, since CH_3^+ is a non-linear ion. A linear least squares fit to the linear section of the curve (i.e. the last four points) yields a slope of –2.0, in reasonable accord with the model prediction, but still noticeably larger. At 295 K and at values of E_c approaching 100meV, Adams and Smith [74] noted downward curvature in their plot of log k_3 versus log E_c for the reaction of CH_3^+ + CO. They attributed the observed curvature to the onset of vibrational excitation of the CH_3^+ ions, which are known to possess low-lying bending modes, the lowest of which has an energy of ~0.1 eV. This conclusion was supported by the observation that the reduction in k_3 with E_c was steeper in an argon carrier gas than in a helium carrier, due to facile vibrational excitation of CH_3^+ in collisions with the heavier argon atoms. Vibrational excitation of CH_3^+ in the drift field at the higher values of E_c might explain the steeper variation in the CH_3^+/C_2N_2 ternary rate coefficient with E_c than that predicted by the model of Adams and Smith. [74] It should also be noted that the bimolecular channel to CH_2CN^+ had a measured branching ratio of 7% at E_r = 0.66 eV, which corresponds to a rate coefficient of 9.1 x 10^{-12} cm^3 s^{-1} (the zero field rate was ~ 0.01 x 1.5 x 10^{-9} = 1.5 x 10^{-11} cm^3 s^{-1}). This may imply a role for vibrational excitation of CH_3^+ in promoting this channel, but what is clear is that the binary channel is accessed on a time scale shorter than the time required for collisional stabilisation.

6.4.4 $CH_3^+ + CH_3CN$.

The reaction of CH_3^+ with CH_3CN proceeds over the studied energy range thus:

$$CH_3^+ + CH_3CN \xrightarrow{He} CH_3CNCH_3^+ \quad \textbf{(6.21a)}$$

$$\longrightarrow HCNH^+ + C_2H_4 \quad \textbf{(6.21b)}$$

$$\longrightarrow C_2H_5^+ + HCN \quad \textbf{(6.21c)}$$

$$\longrightarrow CH_3CNH^+ + CH_2 \quad \textbf{(6.21d)}$$

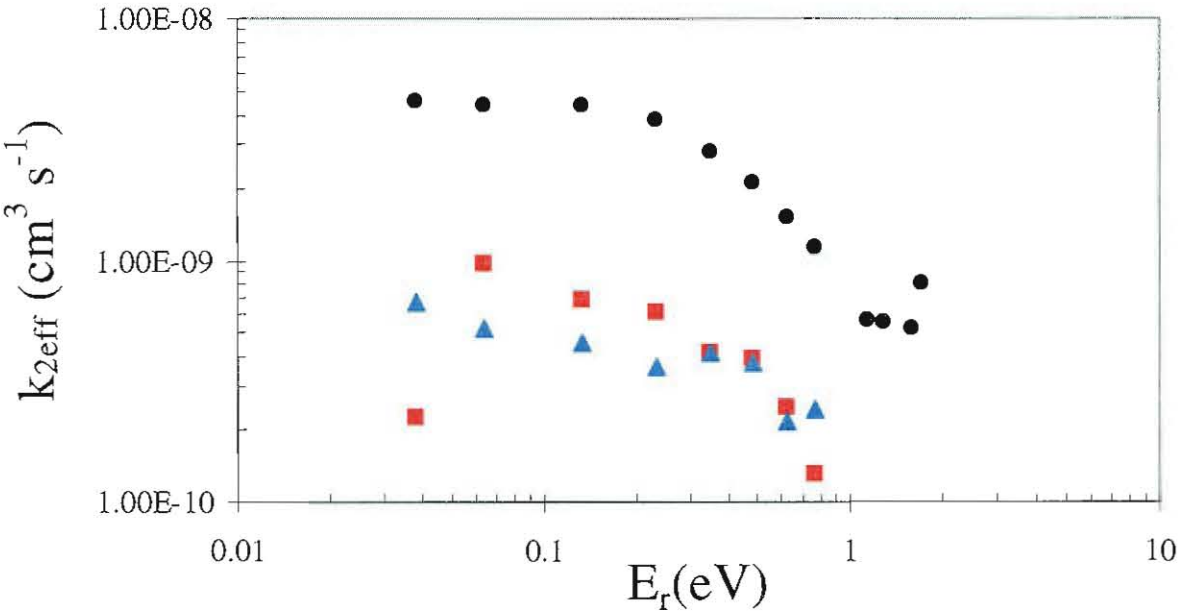

Figure 6.12. Measured variation in the effective bimolecular rate coefficient for reaction 6.21 (●) and the bimolecular rate coefficients for channels 6.21b (▲); and 6.21c (■).

At zero field and a pressure of 0.345 Torr of He a rate coefficient of 4.5 x 10^{-9} cm^3 s^{-1} was measured for reaction (6.21), which is somewhat lower than the value of 5.5 x 10^{-9} cm^3 s^{-1} at 0.2 – 0.4 Torr reported by Smith et al [371] (which is equal to the calculated collision rate), but well within the experimental uncertainty of the earlier measurement. The measured zero-field branching ratio at 0.345 Torr [$CH_3CNCH_3^+$ (80%), $HCNH^+$ + C_2H_4 (15%), $C_2H_5^+$ + HCN (5%)] is in excellent agreement with the earlier result of Smith et al [$CH_3CNCH_3^+$ (88%), $HCNH^+$ + C_2H_4 (12%)], although they did not report the minor channel to $C_2H_5^+$ + HCN. The observed variation in the total effective bimolecular rate coefficient and the rate coefficients for channels (6.21b) and (6.21c) with ion-neutral centre-of-mass energy, E_r, is plotted in Figure 6.12. The small variation in the total bimolecular rate coefficient at low E_r (< ~0.1eV) indicates that the reaction is close to pressure saturation at thermal energy and pressures near 0.3 Torr, in accord with the conclusions of Smith et al. [371] No measurements were made of the pressure variation of the effective bimolecular rate coefficient, however the binary rate coefficient is expected to be pressure dependent outside the pressure saturation regime. The effective

termolecular rate coefficient for channel (6.21a) declines from > 3.2 x 10^{-25} cm^6 s^{-1} at E_r = 0.038 eV to ~ 2 x 10^{-26} cm^6 s^{-1} at E_r = 1.1 eV.

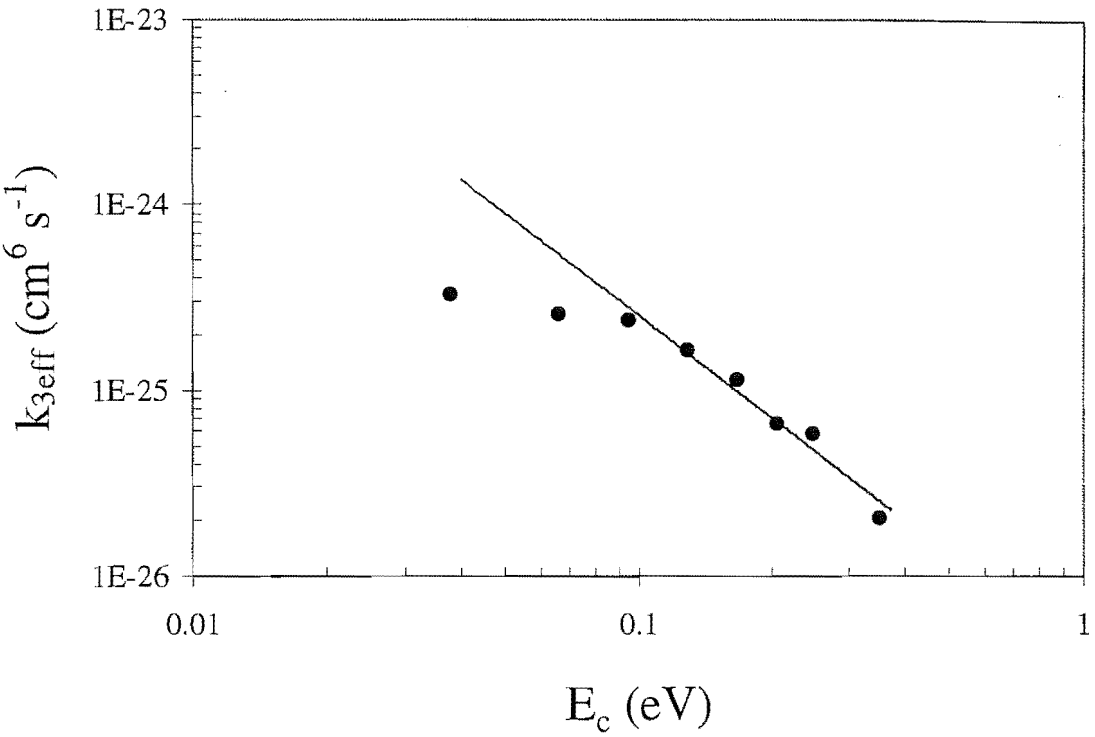

Figure 6.13. The termolecular rate coefficient, k_{3eff} (= k_2/[He]), for the reaction of CH_3^+ with CH_3CN in a helium carrier gas at 300 K plotted in log-log form against E_c. A linear least squares fit to the data at higher E_c yields a slope of –1.8 (see the text for discussion).

A log-log plot of k_3 versus E_c again indicates a power law variation in k_3 with E_c, with an index of –1.8 (fitted to the linear section of the plot), which is in reasonable accord with the –1.5 predicted by the Adams/Smith model. [74] The binary rate coefficient for reaction (6.21b) declines with increasing E_r, from 6.8 x 10^{-10} cm^3 s^{-1} at thermal energy to 2.4 x 10^{-10} cm^3 s^{-1} at E_r = 1.1 eV. The rate coefficient for channel (6.21c) first increases from 2.3 x 10^{-10} cm^3 s^{-1} at thermal energy to 9.7 x 10^{-10} cm^3 s^{-1} at E_r = 0.13 eV and then exhibits a pronounced decline with increasing E_r, dropping to 1.3 x 10^{-10} cm^3 s^{-1} at E_r = 1.1 eV. The observed energy dependence of the two binary channels is in accord with expectation. Both channels must depend strongly on the lifetime, τ, of the intermediate

collision complex. Since bonds are broken and new bonds formed, the reaction probability will decrease as τ decreases and hence the observed rate coefficient decreases. The observed increase in the effective bimolecular rate coefficient for reaction (6.21) at $E_r > 1$ eV is believed to be due to the increasing dominance of channel (6.21d) at energies in excess of 1 eV. This reaction involves simple transfer of a proton from CH_3^+ to CH_3CN, and requires less extensive rearrangement than channels (6.21b) and (6.21c) for example. It is therefore reasonable to suppose that the proton transfer channel will be less sensitive to the lifetime of the intermediate collision complex than reactions involving more extensive bond rearrangement. Indeed, Hansel et al [80] have shown that proton transfer from H_3O^+ to CH_2O, for example, occurs at the collision rate at centre-of-mass collision energies up to, and in excess of ~1 eV. The possibility that the proton transfer is promoted by vibrational excitation of the CH_3^+ ions cannot be dismissed.

CHAPTER 7.

A SUMMARY

In what follows I summarise the results presented in this thesis and offer some suggestions for future work that might augment the results discussed herein.

7.1. Conclusions.

The radiative association reaction of H_3O^+ with C_2H_2 has been suggested as a synthetic route to protonated acetaldehyde in dense interstellar clouds. [166,167] Earlier SIFT studies of the analogous termolecular association of H_3O^+ with C_2H_2, led to the conclusion that the ion formed in the ternary association reaction is a higher energy isomer of $C_2H_5O^+$. [168] The present work examined the reactivity of the ion formed in the termolecular association reaction of H_3O^+ with C_2H_2, plus the reactivity of the stable $C_2H_5O^+$ isomers, CH_3CHOH^+, c-$CH_2(OH)CH_2^+$ and $CH_3OCH_2^+$, for comparison. The experiments demonstrated that more than one isomer of $C_2H_5O^+$ is produced in the association reaction of H_3O^+ with C_2H_2. This conclusion is based on the observation of curved semilogarithmic decays of the $C_2H_2.H_3O^+$ ion signal in reaction with the neutrals: benzene, 4-fluorotoluene and ethyl bromide. Further, the experiments demonstrate that one of the isomers (which accounts for ~75% of the $C_2H_5O^+$ formed in the association reaction) is a structure other than protonated acetaldehyde, protonated oxirane or the methoxymethyl cation. This conclusion is based on the observation of a much faster reaction of the major isomer formed in the association reaction with benzene, 4-fluorotoluene and ethyl bromide, than was observed from any of the three stated isomers. The results of an ab initio study of the $C_2H_5O^+$ potential energy surface combined with the experimental results suggest that the most likely outcome of the association reaction between H_3O^+ and C_2H_2 is formation of a mixture comprised of the vinyloxonium cation and an electrostatic complex, $H_3O^+.C_2H_2$, although confirmation of this conclusion awaits efforts to directly probe the reactivity of the vinyloxonium cation.

In the course of this work several reactions of the three $C_2H_5O^+$ isomers: protonated acetaldehyde, protonated oxirane and the methoxymethyl cation were also examined. These three ions exhibit quite distinct reaction chemistry, enabling clear distinction between them. Protonated acetaldehyde was observed to undergo only termolecular association with a range of reagents possessing proton affinities lower than that of acetaldehyde. A major channel in the reaction of $CH_3OCH_2^+$ with 4-fluorotoluene and benzene was CH^+ transfer (with elimination of neutral CH_3OH), a process noted previously [171] in the reactions of the methoxymethyl cation with a number of oxygen and nitrogen-containing bases. Elimination of a water molecule as the neutral fragment was observed as a major process in three reactions of protonated oxirane (with the neutrals: benzene, 4-fluorotoluene and CH_3OH).

The $C_2H_7O^+$ ion formed in the termolecular association of H_3O^+ with C_2H_4 was identified as protonated ethanol, on the grounds that its reactivity with the neutrals 2-fluorotoluene and acrylonitrile was identical to the ion formed via direct protonation of ethanol. Parallel proton transfer and termolecular association were observed in both reactions. Protonated dimethylether is quite distinct from protonated ethanol, undergoing termolecular association only, with the neutrals 2-fluorotoluene and acrylonitrile. The observed chemistry is in excellent accord with the accepted values for the proton affinities of ethanol, dimethylether, 2-fluorotoluene and acrylonitrile. An ab initio study of the $C_2H_7O^+$ potential surface accounts well for the experimental observations. Formation of protonated ethanol proceeds through a hydrogen bonded $H_3O^+.C_2H_4$ complex which is separated from protonated ethanol by a barrier that lies well below the energy of the reactants.

The association reaction of $CH_2NH_2^+$ with HCOOH has been suggested as a synthetic route to protonated glycine. [226] The $C_2H_6NO_2^+$ ion formed in this reaction was shown to undergo simple ligand exchange reactions with the amines: NH_3, CH_3NH_2 and $C_2H_5NH_2$, in which HCOOH is swapped for an amine ligand. Proton transfer from protonated glycine to CH_3NH_2 and $C_2H_5NH_2$ is exothermic, however no proton transfer was observed from the $C_2H_6NO_2^+$ ion formed via association of $CH_2NH_2^+$ and HCOOH. It was therefore concluded that association of $CH_2NH_2^+$ with HCOOH yields an electrostatic-type complex rather than a covalently bonded $C_2H_6NO_2^+$ structure. This

conclusion agrees with the results of collision-induced dissociation studies [230] of protonated glycine which show that elimination of intact HCOOH occurs over a much larger barrier than sequential losses of CO and H_2O. The reaction of NH_2^+ with CH_3COOH, another proposed route to protonated glycine [223] was shown to yield protonated acetic acid only, in accord with the large exothermicity to proton transfer.

It was demonstrated that low energy dissociative charge transfer to chlorobenzene from CO^+, CO_2^+ or Kr^+ yields the phenylium cation exclusively, indicating a barrier of at least 1.4 eV to the ring opening of the phenylium ion, in agreement with the results of an earlier ICR study. [233] The measured rate coefficient for the reaction of the phenylium ion with C_2H_2 is identical to that seen in the reaction of the faster reacting $C_6H_5^+$ isomer (formed via sequential ion-molecule reactions of C_2H_2 or via electron impact on benzene or halobenzenes), and we therefore ascribe the phenylium structure to this isomer.

The isomeric tropylium and benzyl cations have been observed as species possessing distinctly different reactivities towards benzene in the SIFT apparatus. Further, by varying the energy content of the $C_7H_7^+$ ions formed in the dissociative charge transfer of cycloheptatriene and benzyl bromide, a value for the barrier to isomerisation of benzyl $\rightleftharpoons$ tropylium of 2.7 ± 0.9 eV was determined. Reaction with benzene was used as a convenient diagnostic for determining the structure(s) of the isomeric $C_7H_7^+$ ions formed in a number of ion-molecule reactions. The reaction of the allyl cation with benzene and the phenylium cation with propene were shown to produce the benzyl cation only. The facile termolecular association of $C_3H_5^+$ with C_4H_2 was shown to produce a mixture of benzyl and tropylium cations, in accord with the large reaction exothermicity.

The allyl, $CH_2CHCH_2^+$, and 2-propenyl, $CH_3CCH_2^+$ isomers of $C_3H_5^+$ have been observed as distinct isomeric species in the SIFT apparatus. Methanol was used as the diagnostic reagent for distinguishing between the two isomers. The isomeric ratio of allyl:2-propenyl formed via protonation of allene by a protonated base, BH^+, was shown to be dependent on the proton affinity of the base B. Proton transfer from H_3O^+ to allene produces the 2-propenyl cation exclusively, whereas proton transfer from SO_2H^+ to allene generates a mixture of allyl and 2-propenyl cations. These observations provided an estimate of the barrier height for the rearrangement allyl $\rightleftharpoons$ 2-propenyl of 110 ± 30 kJ

mol^{-1}, in excellent accord with ab initio calculations performed on the $C_3H_5^+$ potential energy surface. The $C_3H_5^+$ product of the reaction between $C_2H_4^+$ and C_2H_4 was identified as the 2-propenyl cation. Rate coefficients were also determined for reactions of the allyl and 2-propenyl cations with several neutrals.

The exothermic H-atom abstraction reaction of SO_2^+ with H_2 was investigated in a combined experimental (SIFDT) and theoretical study. The measured rate coefficient at 300 K was 4.2 x 10^{-12} cm^3 s^{-1}, which is very much less than the Langevin capture rate. The increase in rate coefficient with ion kinetic energy yielded a linear pseudo-Arrhenius plot with a slope that indicates a barrier to H-atom abstraction of ~ 5 kJ mol^{-1} exists on the potential energy surface. A G2(MP2) study of the $H_2SO_2^+$ potential surface identified an $(SO_2^+ \cdot H_2)^*$ transition state in the entrance channel, corresponding to the barrier found from experiments.

The competition between charge transfer and association was investigated in a SIFDT study of the reactions of NO^+ with the ketones: acetone, butanone and 3-pentanone. Association is the sole process observed in all three reactions at thermal energies (the 3-pentanone reaction possesses a minor channel to the slightly endothermic charge transfer product). As the ion-neutral centre-of-mass energy is increased the rate coefficient for termolecular association decreases markedly, as a result of the decreasing lifetime of the intermediate (NO^+·ketone) complex with increasing "temperature". Bimolecular charge transfer can compete with association once sufficient energy is available to overcome the endothermicity and at higher energies still, dissociative charge transfer channels open up. In accord with model predictions [74], the termolecular association rate coefficients exhibit a power law variation with the ion-carrier gas centre-of-mass energy, i.e. $k_3 \propto E_c^{-m}$. The measured power law indices for the three NO^+/ketone systems are, however, significantly larger than the –1.0 predicted by the model and it is proposed that this may reflect the involvement of internal rotations and low frequency vibrations in the ketone molecules.

The association reactions of CH_3^+ with CH_3CN and C_2N_2 were also investigated in the SIFDT as a natural extension of previous SIFT and ICR studies performed by previous workers in this laboratory. The CH_3^+/CH_3CN reaction exhibits competitive binary and ternary channels. The bimolecular channels to $C_2H_5^+$ + HCN and $HCNH^+$ +

C_2H_4 both involve extensive intramolecular rearrangement of the intermediate $(CH_3^+ \cdot CH_3CN)^*$ collision complex and the rate coefficients for both channels exhibit a marked (negative) dependence on the ion-neutral centre-of-mass energy.

7.2. Suggestions for further work.

The combined experimental and theoretical study of the termolecular association reaction between H_3O^+ and C_2H_2 did not unequivocally identify the mixture of $C_2H_5O^+$ isomers generated in the reaction. It seems almost certain that the major isomeric component produced in the reaction is either protonated vinyl alcohol, or an electrostatic-type $H_3O^+.C_2H_2$ complex. The ab initio calculations show that both of these species are readily accessible from the reactants, $H_3O^+ + C_2H_2$. No transition states linking the reactants directly to other $C_2H_5O^+$ isomers below the energy of the reactants were identified, favouring a mixture of protonated vinyl alcohol and the electrostatic adduct as the likely products of reaction. The only direct experimental evidence for the stability of the vinyloxonium cation (protonated vinyl alcohol) comes from the collisional activation and charge stripping experiments of Burgers et al. [169] Continued efforts to form this little studied ion and directly compare its reactivity with that of other $C_2H_5O^+$ isomers would be worthwhile. Potential routes to the formation of protonated vinyl alcohol include ionisation of n-butanol or 1,3-propanediol [169], or direct protonation of vinyl alcohol, which is formed, for example, upon low pressure pyrolysis of cyclobutanol [191] or 3-thietanol. [375] Further investigation of the $C_2H_5O^+$ potential energy surface and RRKM modeling of the $H_3O^+ + C_2H_2$ association reaction may provide additional insights into the likely outcome of reaction, e.g. the ratio of protonated vinyl alcohol to electrostatic adduct formed in the SIFT pressure regime, assuming no other rearrangement pathways exist.

As a result of the studies on the association reaction of H_3O^+ with C_2H_4 we concluded that the association product is protonated ethanol. Matthews et al [206] argued that the ion formed upon association of H_3O^+ with C_2H_4 has access to the more weakly bound electrostatic adduct, based on the observation of different products in some reactions of $C_2H_5OH_2^+$ compared to the H_3O^+/C_2H_4 association ion. Again RRKM modeling of the association reaction utilising the calculated potential surface would be

valuable in establishing the likely ratio of $C_2H_5OH_2^+$ to $H_3O^+ \cdot C_2H_4$ formed in the SIFT pressure regime.

It was concluded that the association reaction of $CH_2NH_2^+$ with HCOOH yields an electrostatic-type adduct rather than a covalently bound $C_2H_6NO_2^+$ species such as protonated glycine. Direct measurement of the reactions of protonated glycine with CH_3NH_2 and $C_2H_5NH_2$, which are exothermic to proton transfer, would serve as a useful confirmation of the present results. A heated insertion probe or Knudsen cell could be coupled to the FA source to generate sufficient vapour pressure of glycine to form protonated glycine. An ab initio investigation of the $C_2H_6NO_2^+$ potential surface would be useful in confirming the conclusion [230] that there is a substantial barrier associated with the loss of HCOOH from protonated glycine and hence a large reverse barrier to the association of $CH_2NH_2^+$ with HCOOH.

Continued efforts to distinguish the linear and cyclic isomers of $C_6H_5^+$ via a difference in mobility are recommended. Ideally grids need to be inserted into two or more drift rings to allow lower "gating voltages" to be applied to the rings for measuring arrival time distributions, as discussed in chapter 4. Such measurements could readily be extended to other isomeric ion systems.

One avenue not explored in the study of $C_7H_7^+$ isomers was the possibility that tolyl ions may be experimentally observable at typical SIFT pressures. Following dissociative charge transfer to substituted toluenes, the tolyl ions initially formed may be rapidly relaxed before isomerisation to the more stable benzyl and tropylium structures occurs, as has been observed in other high pressure studies. If they are relaxed before isomerisation then a comparison of the reactivity of tolyl ions with that of the benzyl and tropylium ions could be carried out.

The work on $C_3H_5^+$ isomers identified some apparent inconsistencies in the published proton affinity scale. [164] The allyl cation was observed to undergo proton transfer to CNBr and CH_3OH despite calculated endothermicities of 25.5 and 21.0 kJ mol^{-1} respectively for these processes. A recent accurate re-evaluation of the enthalpy of formation of the allyl cation [270] of 957.7 kJ mol^{-1}, together with the enthalpy of formation of allene (190.8 kJ mol^{-1}), yields a proton affinity for allene at C2 of 763.1 kJ mol^{-1}, somewhat lower than the currently accepted PA (allene) = 775 kJ mol^{-1}. The value is,

however, in better accord with the observation of slow (presumably endothermic) proton transfer to CH_3OH and CNBr. An experimental re-evaluation of the relative proton affinities of allene (at C2), CH_3OH and CNBr would therefore be worthwhile. It must be borne in mind when performing such experiments that low energy protonation of allene occurs on the terminal carbon (to produce the 2-propenyl cation) so traditional proton transfer equilibria experiments cannot be used to evaluate the C2 proton affinity of allene.

A truly thermal variable temperature flow tube investigation of the H-atom abstraction reaction between SO_2^+ and H_2 would be valuable in confirming the present conclusions that the reaction possesses a kinetic barrier. A variable temperature thermal study would also enable a comparison of the barrier heights calculated from truly thermal measurements and the present drift tube results. It would also be interesting to investigate whether the reaction rate exhibits a similar inverse temperature dependence at low temperatures to that observed in the analogous reaction of NH_3^+ with H_2, indicating a quantum tunneling mechanism is operative at low temperatures. As discussed in chapter 5, several other exothermic H-atom abstraction reactions proceed slowly at room temperature, implying the presence of a kinetic barrier on the potential surface. Theoretical or experimental investigations of these reactions would be useful in establishing whether or not these reactions exhibit analogous behaviour to the SO_2^+/H_2 and NH_3^+/H_2 systems.

Further SIFDT studies of the competition between termolecular and bimolecular reaction channels would be of value for establishing trends in the influence of reaction complex lifetime on the outcome of reaction and how internal energy in the reactants is coupled to the reaction coordinate. Theoretical modeling of the NO^+/ketone and CH_3^+/reactant systems could be used to compare experimental observations with model predictions of termolecular association rates and branching ratios to bimolecular channels. For example, it would be interesting to establish whether the observation of a larger power law variation (in the NO^+/ketone reactions with E_c) than the $E_c^{-1.0}$ dependence predicted by the model of Smith and Adams [74] is substantiated by theory. Any insight from a theoretical investigation may then be used to modify the existing models of the variation in termolecular association rate with kinetic energy in the drift tube. The association reaction of NO^+ with acetone is unusual since the effective

bimolecular rate coefficient apparently reaches "pressure saturation" at ~ 40% of the calculated collision rate. The scheme developed by Meot-Ner [357] involving formation of a loose collision complex prior to rearrangement to a tight complex would account for this observation. Theoretical calculations of the NO^+/acetone potential surface would offer valuable assistance in supporting or repudiating such a mechanism. Measurements of the NO^+/acetone association reaction over as large a pressure range as possible would also be valuable in modeling the association fall-off curve.

In Chapter 1 I briefly reviewed the scope of drift tube experiments, offering a feel for the tremendous utility of the SIFDT technique. The studies presented here have only skimmed the surface of what can be achieved with the SIFDT apparatus. All of the areas discussed in the review leave tremendous scope for further study. Rather than revisiting each of these areas in this concluding discussion, I offer one suggestion for a potentially interesting and profitable area of study. This thesis examined several isomeric ion systems and, in favourable circumstances, isomerisation barriers could be estimated from the experiments. The drift tube potentially offers an alternative method for studying isomerisation and deriving information on the height of isomerisation barriers. An increase in the kinetic energy of an ion in the drift field region increases the internal energy of the ion. The increased internal energy is then potentially available to overcome the barrier to intramolecular isomerisation. An ideal isomeric system for investigation would be one in which a single isomer of a molecular ion can be introduced into the drift region selectively, and which possesses an accessible isomerisation barrier below any dissociation thresholds. Using a monitor gas technique the isomeric ratio could then be measured as a function of ion-carrier gas centre-of-mass energy. Such an investigation may then yield information on the isomerisation barrier. Ideally the experiment would need to be performed under conditions where the drift voltage is applied over an initial section of the drift tube followed by a field-free region. This would allow any vibrational excitation in the ions to relax, ensuring that it is the ground vibrational state of the isomers that reacts with the monitor gas. Vibrational excitation in the ions could greatly confuse interpretation of the results.

REFERENCES

1. Ferguson, E.E., Fehsenfeld, F.C., Dunkin, D.B., Schmeltekopf, A.L., and Schiff, H.I., *Planet. Space Sci.* **12,** 1169 (1964).
2. Ferguson, E.E., Fehsenfeld, F.C., and Schmeltekopf, A.L., *Adv. At. Mol. Phys.* **5,** 1 (1969).
3. Ferguson, E.E., *J. Am. Soc. Mass Spectrom.*, **3**, 479 (1992).
4. Squires, R.R., *J. Mass Spectrom.*, **32**, 1271 (1997).
5. Dunkin, D.B., Fehsenfeld, F.C., Schmeltekopf, A.L., and Ferguson, E.E., *J. Chem. Phys.*, **49**, 1365 (1968).
6. Hierl, P.M., Friedman, J.F., Miller, T.M., Dotan, I., Menendez-Barreto, M., Seeley, J.V., Williamson, J.S., Dale, F., Mundis, P.L., Morris, R.A., Paulson, J.F., and Viggiano, A.A., *Rev. Sci. Instrum.*, **67**, 2142 (1996).
7. Hierl, P.M., Dotan, I., Seeley, J.V., Van Doren, J.M., Morris, R.A., and Viggiano, A.A., *J.Chem. Phys.*, **106**, 3540 (1997).
8. Dotan, I., Hierl, P.M., Morris, R.A., and Viggiano, A.A., *Int. J. Mass Spectrom. Ion Proc.*, **167/168**, 223 (1997).
9. Hierl, P.M., Morris, R.A., and Viggiano, A.A., *J.Chem. Phys.*, **106**, 10145 (1997).
10. Viggiano, A.A., Morris, R.A., Miller, T.M., Friedman, J.F., Menendez-Barreto, M., Paulson, J.F., Michels, H.H., Hobbs, R.H., and Montgomery, J.A. Jr, *J.Chem. Phys.*, **106**, 8455 (1997).
11. Adams, N.G., and Smith, D., *Int. J. Mass Spectrom. Ion Phys.*, **21**, 349 (1976).
12. Adams, N.G., and Smith, D., *J. Phys. B*, **9**, 1439 (1976).
13. McIver, R.T. Jr., *Rev. Sci. Instrum.*, **49**, 111 (1978).
14. McIver, R.T. Jr, in *Kinetics of Ion-Molecule Reactions*, edited by Ausloos, P., Plenum Press, New York, 1978, p. 255.
15. Aue, D.H. and Bowers, M.T., in *Gas Phase Ion Chemistry Vol. 2*, edited by Bowers, M.T., Academic Press, New York, 1979, p. 1.

16. Futrell, J.H., in *Gaseous Ion Chemistry and Mass Spectrometry*, edited by Futrell, J.H., Wiley, New York, 1986, p. 127.
17. Kemper, P.R. and Bowers, M.T., in *Techniques for the Study of Ion-Molecule Reactions*, edited by Farrar, J.M. and Saunders, W.H., Techniques of Chemistry, Vol.XX, Wiley, New York, 1988, p. 1.
18. Wilson, P.F., *Experimental Studies of Gas-Phase Ion-Molecule Reactions*, Ph.D. Thesis, University of Canterbury, New Zealand (1994).
19. Graul, S.T., and Squires, R.R., *Mass Spectrom. Rev.*, **7**, 263 (1988).
20. Smith, D., and Adams, N.G., in *Gas Phase Ion Chemistry Vol. 1*, edited by Bowers, M.T., Academic Press, New York, 1979, p. 1.
21. Smith, D., and Adams, N.G., *Adv. At. Mol. Phys.*, **24**, 1 (1988).
22. Adams, N.G., and Smith, D., in *Techniques for the Study of Ion-Molecule Reactions*, edited by Farrar, J.M., and Saunders, W.H., Techniques of Chemistry Vol XX, Wiley, New York, 1988, p. 165.
23. Ferguson, E.E., *Adv. At. Mol. Phys.*, **25**, 61 (1988).
24. Farrar, J.M., in *Techniques for the Study of Ion-Molecule Reactions*, edited by Farrar, J.M., and Saunders, W.H., Techniques of Chemistry Vol. XX, Wiley, New York, 1988, p. 325.
25. Gentry, W.R., in *Gas Phase Ion Chemistry Vol. 2*, edited by Bowers, M.T., Academic Press, New York, 1979, p. 221.
26. Futrell, J.H. in *Gaseous Ion Chemistry and Mass Spectrometry*, edited by Futrell, J.H., Wiley, New York, p. 155.
27. Gentry, W.R., McClure, D.J., and Douglas, C.H., *Rev. Sci. Instrum.*, **46**, 367 (1976).
28. Ervin, K.M., and Armentrout, P.B., *J. Chem. Phys.*, **83**, 166 (1985).
29. Armentrout, P.B., in *Advances in Gas Phase Ion Chemistry Vol. 1*, edited by Adams, N.G. and Babcock, L.M., JAI Press, Connecticut, 1992, p. 83.
30. McFarland, M., Albritton, D.L., Fehsenfeld, F.C., Ferguson, E.E., and Schmeltekopf, A.L., *J. Chem. Phys.*, **59**, 6610 (1973).
31. McFarland, M., Albritton, D.L., Fehsenfeld, F.C., Ferguson, E.E., and Schmeltekopf, A.L., *J. Chem. Phys.*, **59**, 6620 (1973).

32. McFarland, M., Albritton, D.L., Fehsenfeld, F.C., Ferguson, E.E., and Schmeltekopf, A.L., *J. Chem. Phys.*, **59**, 6629 (1973).

33. Mason, E.A., and McDaniel, E.W., *Transport Properties of Ions in Gases*, Wiley, New York, 1988.

34. McDaniel, E.W., Cermák, V., Dalgarno, A., Ferguson, E.E., and Friedman, L., *Ion-Molecule Reactions*, Wiley, New York, 1970, p. 64.

35. Howorka, F., Dotan, I., Fehsenfeld, F.C., and Albritton, D.L., *J. Chem. Phys.*, **73**, 758 (1980).

36. Lindinger, W., and Smith, D., in *Reactions of Small Transient Species*, edited by Fontijn, A., and Clyne, M.A.A., Academic Press, New York, 1983, p. 387.

37. Ellis, H.W., Pai, R.Y., McDaniel, E.W., Mason, E.A., and Viehland, L.A., *Atom. Data Nucl. Data Tables*, **17**, 177 (1976).

38. Ellis, H.W., McDaniel, E.W., Albritton, D.L., Viehland, L.A., Lin, S.L., and Mason, E.A., *Atom. Data Nucl. Data Tables*, **22**, 179 (1978).

39. Ellis, H.W., Thackston, M.G., McDaniel, E.W., and Mason, E.A., *Atom. Data Nucl. Data Tables*, **31**, 113 (1984).

40. Viehland, L.A., and Mason, E.A., *Atom. Data Nucl. Data Tables*, **60**, 37 (1995).

41. Wannier, G.H., *Bell Syst. Tech. J.*, **32**, 170 (1953).

42. Albritton, D.L., Dotan, I., Lindinger, W., McFarland, M., Tellinghausen, J., and Fehsenfeld, F.C., *J. Chem. Phys.*, **66**, 410 (1977).

43. Viehland, L.A. and Mason, E.A., *J. Chem. Phys.*, **66**, 422 (1977).

44. Lin, S.L. and Bardsley, *J. Chem. Phys.*, **66**, 435 (1977).

45. Dressler, R.A., Meyer, H., Langford, A.O., Bierbaum, V.M., and Leone, S.R., *J. Chem. Phys.*, **87**, 5578 (1987).

46. Dressler, R.A., Beijers, J.P.M., Meyer, H., Penn, S.M., Bierbaum, V.M., and Leone, S.R., *J. Chem. Phys.*, **89**, 4707 (1988).

47. Viehland, L.A., Viggiano, A.A., and Mason, E.A., *J. Chem. Phys.*, **95**, 7286 (1991).

48. Viehland, L.A., and Robson, R.E., *Int. J. Mass Spectrom. Ion Proc.*, **90**, 167 (1989).

49. Albritton, D.L., in *Kinetics of Ion-Molecule Reactions*, edited by Ausloos, P., Plenum, New York, 1979, p. 119.

50. Lindinger, W., in *Swarms of Ions and Electrons in Gases*, edited by Lindinger, W., Märk, T.D., and Howorka, F., Springer-Verlag, Wien, 1984, p. 146.
51. Ferguson, E.E., in *Swarms of Ions and Electrons in Gases*, edited by Lindinger, W., Märk, T.D., and Howorka, F., Springer-Verlag, Wien, 1984, p. 126.
52. Lindinger, W., in *Gaseous Ion Chemistry and Mass Spectrometry*, edited by Futrell, J.H., Wiley, New York, 1986, p. 141 & 237.
53. Ferguson, E.E., in *Structure/Reactivity and Thermochemistry of Ions*, edited by Ausloos, P. and Lias, S.G., NATO ASI Series, D. Reidel Publishing Co., 1987, p. 81.
54. Lindinger, W., *Int. J. Mass Spectrom. Ion Proc.*, **80**, 115 (1987).
55. Duncan, M.A., Bierbaum, V.M., Ellison, G.B., and Leone, S.R., *J. Chem. Phys.*, **79**, 5448 (1983).
56. Viehland, L.A. and Mason, E.A., *Ann. Phys. (N.Y.)*, **110**, 287 (1978).
57. Lin, S.L., Viehland, L.A., and Mason, E.A., *Chem. Phys.*, **37**, 411 (1979).
58. Viehland, L.A., Lin, S.L., and Mason, E.A., *Chem. Phys.*, **54**, 341 (1981).
59. Viehland, L.A. and Fahey, D.W., *J. Chem. Phys.*, **78**, 435 (1983).
60. Viehland , L.A., in *Swarms of Electrons and Ions in Gases*, edited by Lindinger, W., Märk, T.D., and Howorka, F., Springer-Verlag, Wien, 1984, p. 27.
61. Viehland, L.A., *Chem. Phys.*, **101**, 1 (1986).
62. Henchman, M.J., in *Fundamentals of Gas Phase Ion Chemistry*, edited by Jennings, K.R., Kluwer, Dordrecht, 1991, p. 267.
63. Federer, W., Ramler, H., Villinger, H. and Lindinger, W., *Phys. Rev. Lett.*, **54**, 540 (1985).
64. Kriegel, M., Richter, R., Lindinger, W., Barbier, L., and Ferguson, E.E., *J. Chem. Phys.*, **88**, 213 (1987).
65. Viggiano, A.A., and Morris, R.A., *J. Phys. Chem.*, **100**, 19227 (1996).
66. Durup-Ferguson, M., Böhringer, H., Fahey, D.W., and Ferguson, E.E., *J. Chem. Phys.*, **79**, 265 (1983).
67. Glosik, J., Freysinger, W., and Lindinger, W., *J. Chem. Phys.*, **95**, 3020 (1991).
68. Glosik, J., Freysinger, W., Hansel, A., Spanel, P., and Lindinger, W., *J. Chem.*

Phys., **98**, 6995 (1993).

69. Glosik, J., Smith, D., Spanel, P., Freysinger, W., and Lindinger, W., *Int. J. Mass Spectrom. Ion Proc.*, **129**, 131 (1993).
70. Glosik, J., Zakouril, P., Skalsky, V., and Lindinger, W., *Int. J. Mass Spectrom. Ion Proc.*, **149/150**, 499 (1995).
71. Zakouril, P., Glosik, J., Skalsky, V., and Lindinger, W., *J. Phys. Chem.*, **99**, 15890 (1995).
72. Glosik, J., Zakouril, P., and Lindinger, W., *J. Chem. Phys.*, **103**, 6490 (1995).
73. Smith, S.C., McEwan, M.J., Giles, K, Smith, D., and Adams, N.G., *Int. J. Mass Spectrom. Ion Proc.*, **96**, 77 (1990).
74. Adams, N.G. and Smith, D., *Int. J. Mass Spectrom. Ion Proc.*, **81**, 273 (1987).
75. Lindinger, W., McFarland, M., Fehsenfeld, F.C., Albritton, D.L., Schmeltekopf, A.L., and Ferguson, E.E., *J. Chem. Phys.*, **63**, 2175 (1975).
76. Ferguson, E.E., *J. Phys. Chem.*, **90**, 731 (1986).
77. Pogrebnya, S.K., Freysinger, W., Hansel, A., Kriegel, M. and Lindinger, W., *Int. J. Mass Spectrom. Ion Proc.*, **129**, 89 (1993).
78. Zenevich, V.A., Pogrebnya, S.K., Lindinger, W., and Cacciatore, M., *Int. J. Mass Spectrom. Ion Proc.*, **129**, 101 (1993).
79. Zenevich, V.A., Lindinger, W., Progrebnya, S.K., Cacciatore, M., and Billing, G.D., *J. Chem. Phys.*, **102**, 6669 (1995).
80. Hansel, A., Singer, W., Wisthaler, A., Schwarzmann, M, and Lindinger, W., *Int. J. Mass Spectrom. Ion. Proc.*, **167/168**, 697 (1997).
81. Villinger, H., Futrell, J., Howorka, F., Djuric, N., and Lindinger, W., *J. Chem. Phys.*, **76**, 3529 (1982).
82. Tichy, M., Javahery, G., Twiddy, N.D., and Ferguson, E.E., *Int. J. Mass Spectrom. Ion Proc.*, **93**, 165 (1989).
83. Javahery, G., Glosik, J., Twiddy, N.D., and Ferguson, E.E., *Int. J. Mass Spectrom. Ion Proc.*, **98**, 225 (1990).
84. Glosik, J., Jordan, A., Skalsky, V., and Lindinger, W., *Int. J. Mass Spectrom. Ion Proc.*, **129**, 109 (1993).

85. Glosik, J., Skalsky, V., and Lindinger, W., *Int. J. Mass Spectrom. Ion Proc.*, **134**, 67 (1994).

86. Glosik, J., Skalsky, V., Praxmarer, C., Smith, D., Freysinger, W., and Lindinger, W., *J. Chem. Phys.*, **101**, 3792 (1994).

87. Glosik, J., Bánó, G., Ferguson, E.E., and Lindinger, W., *Int. J. Mass Spectrom.*, **176**, 177 (1998).

88. Barassin, J., Thomas, R., and Barassin, A., *Chem. Phys. Lett.*, **71**, 269 (1980).

89. de Gouw, J.A., Ding, L.N., Krishnamurty, M., Lee, H.S., Anthony, E.B., Bierbaum, V.M., and Leone, S.R., *J. Chem. Phys.*, **105**, 10398 (1996).

90. Krishnamurty, M., de Gouw, J.A., Ding, L.N., Bierbaum, V.M., and Leone, S.R., *J. Chem. Phys.*, **106**, 530 (1997).

91. de Gouw, J.A., Krishnamurty, M., and Leone, S.R., *J. Chem. Phys.*, **106**, 5937 (1997).

92. de Gouw, J.A., Krishnamurty, M., Bierbaum, V.M., and Leone, S.R., *Int. J. Mass Spectrom. Ion Proc.*, **167/168**, 281 (1997).

93. Clemmer, D.E., and Jarrold, M.F., *J. Mass Spectrom.*, **32**, 577 (1997).

94. Smith, D., and Adams, N.G., in *Rate Coefficients in Astrochemistry*, edited by Millar, T.J. and Williams, D.A., Kluwer, Dordrecht, 1988, p. 153.

95. Dotan, I., Lindinger, W., and Albritton, D.L., *J. Chem. Phys.*, **67**, 5968 (1977).

96. Baranov, V., and Bohme, D.K., *Int. J. Mass Spectrom. Ion Proc.*, **154**, 71 (1996).

97. Baranov, V., Petrie, S.A.H., and Bohme, D.K., *J. Am. Chem. Soc.*, **118**, 4500 (1996).

98. Ketvirtis, A.E., Baranov, V.I., Bohme, D.K., and Hopkinson, A.C., *Int. J. Mass Spectrom. Ion Proc.*, **153**, 161 (1996).

99. Ketvirtis, A.E., Baranov, V.I., Hopkinson, A.C., And Bohme, D.K., *J. Phys. Chem.*, **101**, 7258 (1997).

100. Baranov, V., Hopkinson, A.C., and Bohme, D.K., *J. Am. Chem. Soc.*, **119**, 7055 (1997).

101. Baranov, V., Wang, J.R., Javahery, G., Petrie, S., Hopkinson, A.C., and Bohme, D.K., *J. Am. Chem. Soc.*, **119**, 2040 (1997).

102. Baranov, V., Becker, H., and Bohme, D.K., *J. Phys. Chem.*, **101**, 5137 (1997).

103. Squires, R.R., *Int. J. Mass Spectrom. Ion Proc.*, **118/119**, 503 (1992).

104. Rowe, B.R., Fahey, D.W., Fehsenfeld, F.C., and Albritton, D.L., *J. Chem. Phys.*, **73**, 194 (1980).

105. Twiddy, N.D., Mohebati, A., and Tichy, M., *Int. J. Mass Spectrom. Ion Proc.*, **74**, 251 (1986).

106. van Koppen, P.A.M., Kemper, P.R., and Bowers, M.T., in *Organometallic Ion Chemistry*, edited by Freiser, B.S., Kluwer Academic Publishers, 1996.

107. Shvartsburg, A.A., and Jarrold, M.F., *Chem. Phys. Lett.*, **261**, 86 (1996).

108. Harland, P.W., McIntosh, B.J., Simpson, R.W., and Thomas, N.R., *J. Chem. Soc. Faraday Trans. 2*, **82**, 2039 (1986).

109. von Helden, G., Hsu, M.-T., Kemper, P.R., and Bowers, M.T., *J. Chem. Phys.*, **93**, 3835 (1991).

110. von Helden, G., Hsu, M.-T., Gotts, N., and Bowers, M.T., *J. Chem. Phys.*, **97**, 8182(1993).

111. Bowers, M.T., *Acc. Chem. Res.*, **27**, 324 (1994).

112. Gotts, N.G., von Helden, G., and Bowers, M.T., *Int. J. Mass Spectrom. Ion Proc.*, **150**, 217 (1995).

113. Shelimov, K.B., Hunter, J.M., and Jarrold, M.F., *Int. J. Mass Spectrom. Ion Proc.*, **138**, 17 (1994).

114. Hunter, J.M., and Jarrold, M.F., *J. Am. Chem. Soc.*, **117**, 10317 (1995).

115. Shvartsburg, A.A., Schatz, G.C., and Jarrold, M.F., *J. Chem. Phys.*, **108**, 2416 (1998).

116. Book, L.D., Xu, C., and Scuseria, G.E., *Chem. Phys. Lett.*, **222**, 281 (1984).

117. Jarrold, M.F. and Constant, V.A., *Phys. Rev. Lett.*, **67**, 2994 (1991).

118. Hunter, J.M., Fye, J.L., Jarrold, M.F., and Bower, J.E., *Phys. Rev. Lett.*, **73**, 2063 (1994).

119. Jarrold, M.F., *J. Phys. Chem.*, **99**, 11 (1995).

120. Clemmer, D.E., Hunter, J.M., Shelimov, K.B., and Jarrold, M.F., *Nature*, **372**, 248 (1994).

121. von Helden, G., Gotts, N.G., Maitre, P., and Bowers, M.T., *Chem. Phys. Lett.*, **227**,

601 (1994).

122. Strout, D.L., Miller, T.F., and Hall, M.B., *J. Phys. Chem. A*, **102**, 6307 (1998).
123. von Helden, G., Wyttenbach, T, and Bowers, M.T., *Science*, **267**, 1483 (1995).
124. Clemmer, D.E., Hudgins, R.R., and Jarrold, M.F., *J. Am. Chem. Soc.*, **117**, 10141 (1995).
125. Shelimov, K.B., Clemmer, D.E., Hudgins, R.R., and Jarrold, M.F., *J. Am. Chem. Soc.*, **119**, 2240 (1997).
126. Hudgins, R.R., Woenckhaus, J., and Jarrold, M.F., *Int. J. Mass Spectrom. Ion Proc.*, **165**, 497 (1997).
127. Dugourd, Ph., Hudgins, R.R., Clemmer, D.E., and Jarrold, M.F., *Rev. Sci. Instrum.*, **68**, 1122 (1997).
128. Krishnamurty, M, de Gouw, J.A., Bierbaum, V.M., and Leone, S.R., *J. Phys. Chem.*, **100**, 14908 (1996).
129. Patterson, P.L., *J. Chem. Phys.*, **56**, 3943 (1972).
130. Mesleh, M.F., Hunter, J.M., Shvartsburg, A.A., Schatz, G.C., and Jarrold, M.F., *J. Phys. Chem.*, **100**, 16082 (1996).
131. Blanc, A., *J. Phys.(Paris)*, **7**, 825 (1908).
132. Petrie, S., Freeman, C.G., Mautner, M., McEwan, M.J., and Ferguson, E.E., *J. Am. Chem. Soc.*, **112**, 7121 (1990).
133. Hansel, A., Glantschnig, M., Scheiring, Ch., Lindinger, W., and Ferguson, E.E., *J. Chem. Phys.*, **109**, 1743 (1998).
134. Freeman, C.G., Knight, J.S., Love, J.G., and McEwan, M.J., *Int. J. Mass Spectrom. Ion Proc.*, **80**, 255 (1987).
135. Cunje, A., Rodriquez, C.F., Bohme, D.K., and Hopkinson, A.C., *J. Phys. Chem.*, **102**, 478 (1997).
136. Hansel, A., Scheiring, Ch., Glantschnig, M., Lindinger, W., and Ferguson, E.E., *J. Chem. Phys.*, **109**, 1748 (1998).
137. Glosik, J., Zakouril, P., and Lindinger, W., *Int. J. Mass Spectrom. Ion Proc.*, **145**, 155 (1995).
138. Viggiano, A.A., Morris, R.A., Dale, F., Paulson, J.F., Giles, K., and Smith, D., *J.*

Chem. Phys., **93**, 1149 (1990).

139. Knight, J.S., *Selected-Ion Flow Tube Studies of Some Gaseous Ion-Molecule Reactions*, Ph.D. Thesis, University of Canterbury, New Zealand, (1986).
140. Petrie, S.A.H., *A Selected-Ion Flow Tube Study of Some Gas-Phase Ion-Molecule Reactions of Relevance to the Chemistry of Dense Interstellar Clouds*, Ph.D. Thesis, University of Canterbury, New Zealand, (1991).
141. Scott, G.B.I., *Experimental Studies of Astrochemical Ion-Atom and Ion-Molecule Reactions*, Ph.D. Thesis, University of Canterbury, New Zealand, (1997).
142. Upschulte, B.L., Shul, R.J., Passarella, R., Keesee, R.G., and Castleman, A.W., *Int. J. Mass Spectrom. Ion Proc.*, **75**, 27 (1987).
143. Van Doren, J.M., Barlow, S.E., DePuy, C.H., and Bierbaum, V.M., *Int. J. Mass Spectrom. Ion Proc.*, **81**, 85 (1987).
144. Smith, D. and Adams, N.G., *J. Phys. D*, **13**, 1267 (1980).
145. Mackay, G.I., Vlachos, G.D., Bohmę, D.K., and Schiff, H.I., *Int. J. Mass Spectrom. Ion Phys.*, **36**, 259 (1980).
146. SIMION 3D Ver. 6.00, Idaho National Engineering Laboratory, 1995.
147. Dupeyrat, G., Rowe, B.R., Fahey, D.W., and Albritton, D.L., *Int. J. Mass Spectrom. Ion Phys.*, **44**, 1 (1982).
148. Spanel, P., Private Communication, (1997).
149. ACE™-MCS Operators Manual Software Ver. 1.3, EG&G Ortec, Oak Ridge, Tennessee, U.S.A., 1987.
150. Thomas, R., Barassin, A., and Burke, R.R., *Int. J. Mass Spectrom. Ion Phys.*, **28**, 275 (1978).
151. Lindinger, W., Howorka, F., Lukac, P., Kuhn, S., Villinger, H., Alge, E., and Ramler, H., *Phys. Rev. A*, **23**, 2319 (1981).
152. Dotan, I. and Lindinger, W., *J. Chem. Phys.*, **76**, 4972 (1982).
153. Hamdan, M., Birkinshaw, K., and Twiddy, N.D., *Int. J. Mass Spectrom. Ion Proc.*, **57**, 225 (1984).
154. Viggiano, A.A., Van Doren, J.M., Morris, R.A., and Paulson, J.F., *J. Chem. Phys.*, **93**, 4761 (1990).

155. Smith, D. and Adams, N.G., *Phys. Rev. A*, **23**, 2327 (1981).

156. Anicich, V.G., *J. Phys. Chem. Ref. Data*, **22**, 1469 (1993) and subsequent software updates (http://astrochem.jpl.nasa.gov/asch/)

157. Lindinger, W. and Albritton, D.L., *J. Chem. Phys.*, **62**, 3517 (1975).

158. Curtiss, L.A., Raghavachari, K., Trucks, G.W., and Pople, J.A., *J.Chem. Phys.*, **94**, 7221 (1991).

159. Pople, J.A., Head-Gordon, M., Fox, D.J., Raghavachari, K., and Curtiss, L.A., *J.Chem. Phys.*, **90**, 5622 (1989).

160. Curtiss, L.A., Raghavachari, K., and Pople, J.A., *J. Chem. Phys.*, **98**, 1293 (1993).

161. Su, T. and Chesnavich, W.J., *J. Chem. Phys.*, **72**, 5183 (1982).

162. C.R.C. Handbook of Chemistry and Physics, 73rd edition, edited by Lide, D.R., C.R.C. Press Inc., Boca Raton, 1992.

163. Lias, S.G., Bartmess, J.E., Liebman, J.F., Holmes, J.L., Levin, R.D., and Mallard, W.G., *J. Phys. Chem. Ref. Data*, **17**, Suppl. 1 (1988).

164. Hunter, E.P. and Lias, S.G., *J. Phys. Chem. Ref. Data*, **27**, 413 (1998).

165. Snyder, L.E., in *Molecules in Space*, edited by Buckingham, D.A., Spectroscopy, Physical Chemistry, Ser. 1.6, 193; MTP Int. Rev. Sci. 3, Butterworth, London, 1972.

166. Jarrold, M.F., Kirchner, N.J., Liu, S., and Bowers, M.T., *J. Phys. Chem.*, **90**, 78 (1986).

167. Herbst, E., *Astrophys. J.*, **313**, 867 (1987).

168. Herbst, E., Smith, D., Adams, N.G., and McIntosh, B.J., *J. Chem. Soc. Faraday Trans. 2*, **85**, 1655 (1989).

169. Burgers, P.C., Terlouw, J.K., and Holmes, J.L., *Org. Mass Spectrom.*, **17**, 369 (1982).

170. McEwan, M.J., in *Advances in Gas Phase Ion Chemistry, Vol. 1*, edited by Adams, N.G. and Babcock, L.M., J.A.I. Press, Greenwich, CT, p.1 (1992).

171. Wilson, P.F., McEwan, M.J., and Mautner, M., *Int. J. Mass Spectrom. Ion Proc.*, **132**, 149 (1994).

172. Nobes, R.H., Rodwell, W.R., Bouma, W.J., and Radom, L., *J. Am. Chem. Soc.*, **103**, 1913 (1981).

173. Nobes, R.H. and Radom, L., *Chem. Phys. Lett.*, **99**, 107 (1983).

174. Curtiss, L.A., Lucas, D.J., and Pople, J.A., *J. Chem. Phys.*, **102**, 3292 (1995).

175. Jones, W.H., Mariani, R.D., and Lively, M.L., *Chem. Phys. Lett.*, **108**, 602 (1984).

176. Frisch, M.J., Head-Gordon, M., Trucks, G.W., Foresman, J.B., Schlegel, H.B., Raghavachari, K., Robb, M.A., Binkley, J.S., Gonzalez, C., DeFrees, D.J., Fox, D.J., Whiteside, R.A., Seeger, R., Melius, C.F., Baker, J., Martin, .L., Kahn, L.R., Stewart, J.J.P., Topiol, S., and Pople, J.A., GAUSSIAN 90, Gaussian Inc., Pittsburgh PA, 1990.

177. Frisch, M.J., Trucks, G.W., Head-Gordon, M., Gill, P.M.W., Wong, M.W., Foresman, J.B., Johnson, B.G., Schlegel, H.B., Robb, M.A., Replogle, E.S., Gomperts, R., Andres, J.L., Raghavachari, K., Binkley, J.S., Gonzalez, C., Martin, R.L., Fox, D.J., DeFrees, D.J., Baker, J., Stewart, J.J.P., and Pople, J.A., GAUSSIAN 92, Gaussian Inc., Pittsburgh PA, 1992.

178. Frisch, M.J., Trucks, G.W., Schlegel, H.B., Gill, P.M.W., Johnson, B.G., Robb, M.A., Cheeseman, J.R., Keith, T., Petersson, G.A., Montgomery, J.A., Raghavachari, K., Al-Laham, M.A., Zakrzewski, V.G., Ortiz, J.V., Foresman, J.B., Cioslowski, J., Stefanov, B.B., Nanayakkara, A., Challacombe, M., Peng, C.Y., Ayala, P.Y., Chen, W., Wong, M.W., Andres, J.L., Replogle, E.S., Gomperts, R., Martin, R.L., Fox, D.J., Binkley, J.S., DeFrees, D.J., Baker, J., Stewart, J.P., Head-Gordon, M., Gonzalez, C., and Pople, J.A., GAUSSIAN 94, Gaussian Inc., Pittsburgh PA, 1994.

179. Bock, C.W., George, P., and Glusker, J.P., *J. Org. Chem.*, **58**, 5816 (1993).

180. Smith, B.J. and Radom, L., *J. Am. Chem. Soc.*, **115**, 4885 (1993).

181. Smith, B.J. and Radom, L., *Chem. Phys. Lett.*, **231**, 345 (1994).

182. Smith, B.J. and Radom, L., *Chem. Phys. Lett.*, **245**, 123 (1995).

183. Smith, B.J. and Radom, L., *J. Phys. Chem.*, **99**, 6468 (1995).

184. Marcoccia, J.F., Csizmadia, I.G., Yates, P., and Krepinskyd, J.J., *J. Mol. Struct. (Theochem)*, **167**, 359 (1988).

185. Ford, G.P. and Smith, C.T., *J. Am.Chem. Soc.*, **109**, 1325 (1987).

186. Bouma, W.J. and Radom, L., *J. Mol. Struct.*, **43**, 267 (1978).

187. Bouma, W.J., Radom, L., and Rodwell, W.R., *Theor. Chim. Acta*, **56**, 149 (1980).

188. Smith, B.J. and Radom, L., *J. Am. Chem. Soc.*, **112**, 7525 (1990).

189. Smith, B.J., Nguyen, M.T., Bouma, W.J., and Radom, L., *J. Am. Chem. Soc.*, **113**, 6452 (1991).

190. Smith, B.J., Coffey, D., and Radom., L., *J. Chem. Phys.*, **97**, 6113 (1992).

191. Holmes, J.H. and Lossing, F.P., *J. Am. Chem. Soc.*, **104**, 2648 (1982).

192. Yamaguchi, Y., Schaefer, H.F., and Alberts, I.L., *J. Am. Chem. Soc.*, **115**, 5790 (1993).

193. Okada, S., Abe, Y., Taniguchi, S., and Yamabe, S., *J. Am. Chem. Soc.*, **109**, 295 (1987).

194. Ruscic, B. and Berkowitz, J., *J. Chem. Phys.*, **101**, 10936 (1994).

195. Traeger, J., private communication (1998), based on AE($C_2H_5O^+$) = 10.875 eV from ethanol, which yields a cationic heat of formation of 596.1 kJ mol^{-1} for CH_3CHOH^+.

196. Irvine, W.M., Goldsmith, P.F., Hjalmarson, A., in *Interstellar Processes*, edited by Hollenbach, D.J. and Thronson, H.A., Reidel, Dordrecht, p. 561 (1987).

197. Turner, B.E., *Astrophys. J. Suppl. Ser.*, **76**, 617 (1991).

198. Charnley, S.B., Kress, M.E., Tielens, A.G.G.M., and Millar, T.J., *Astrophys. J.*, **448**, 232 (1995).

199. Pearson, J.C., Sastry, K.V.L.N., Herbst, E., and De Lucia, F.C., *Astrophys. J.*, **480**, 420 (1997).

200. Miao, Y. and Snyder, L.E., *Astrophys. J.*, **480**, L67 (1997).

201. Zuckerman, B., Turner, B.E., Johnson, D.R., Clark, F.O., Lovas, F.J., Fourikis, N., Palmer, P., Morris, M., Lilley, A.E., Ball, J.A., Gottlieb, C.A., Litvak, M.M., and Penfield, H., *Astrophys. J.*, **196**, L99 (1975).

202. Ohishi, M., Ishikawa, S.I., Yamamoto, S., Saito, S., and Amano, T., *Astrophys. J.*, **446**, L43 (1995).

203. Millar, T.J., Olafsson, H., Hjalmarson, A., and Brown, P.D., *Astron. Astrophys.*, **205**, L5 (1988).

204. Herbst, E. and Leung, C.M., *Astrophys. J. Suppl. Ser.*, **69**, 271 (1989).

205. Bohme, D.K. and Mackay, G.I., *J. Am. Chem. Soc.*, **103**, 2173 (1981).

206. Matthews, K.K., Adams, N.G., and Fisher, N.D., *J. Phys. Chem. A*, **101**, 2841 (1997).

207. McIntosh, B.J., Adams, N.G., and Smith, D., *Chem. Phys. Lett.*, **148**, 142 (1988).

208. Radom, L., *Int. J. Mass Spectrom. Ion Proc.*, **118/119**, 339 (1992).

209. Bouchoux, G. and Hoppilliard, Y., *J. Am. Chem. Soc.*, **112**, 9110 (1990).

210. Audier, H.E., Koyanagi, G.K., McMahon, T.B., and Tholmann, D., *J. Phys. Chem.*, **100**, 8220 (1996).

211. Blake, J.F. and Jorgensen, W.L., *J. Org. Chem.*, **56**, 6052 (1991).

212. von Nagy-Felsobuki, E.I. and Kimura, K., *J. Phys. Chem.*, **94**, 8041 (1990).

213. Jones, W.H., Mezey, P.G., and Csizmadia, I.G., *J. Mol. Struct. (Theochem)*, **121**, 85 (1985).

214. Williams, T.L., Adams, N.G., Babcock, L.M., Herd, C.R., and Geoghegan, M., *Mon. Not. R. Astron. Soc.*, **282**, 413 (1996).

215. Andersen, L.H., Heber, O., Kella, D., Pedersen, H.B., Vejby-Christensen, L., and Zajfman, D., *Phys. Rev. Lett.*, **77**, 4891 (1996).

216. Vejby-Christensen, L., Andersen, l.H., Heber, O., Kella, D., Pedersen, H.B., Schmidt, H.T., and Zajfman, D., *Astrophys. J.*, **483**, 531 (1997).

217. Tielens, A. and Charnley, S., in *Planetary and Interstellar Processes Relevant to the Origins of Life*, edited by Whittet, D.C.B., Kluwer Academic Publishers, Dordrecht, p.23, 1997.

218. Miller, S.L., *Science*, **117**, 528 (1953).

219. Miller, S.L., *J. Am. Chem. Soc.*, **77**, 2351 (1955).

220. Goldanskii, V.I., *J. Phys. Chem. A*, **101**, 3424 (1997).

221. Bailey, J., Chrysostomou, A., Hough, J.H., Gledhill, T.M., McCall, A., Clark, S., Ménard, F., and Tamura, M., *Science*, **281**, 672 (1998).

222. Whittet, D.C.B., in *Planetary and Interstellar Processes Relevant to the Origins of Life*, edited by Whittet, D.C.B., Kluwer Academic Publishers, Dordrecht, p.249, 1997.

223. Snyder, L.E., in *Planetary and Interstellar Processes Relevant to the Origins of Life*, edited by Whittet, D.C.B., Kluwer Academic Publishers, Dordrecht, p.115, 1997.

224. Stepanian, S.G., Reva, I.D., Radchenko, E.D., Rosado, M.T.S., Duarte, M.L.T.S., Fausto, R., and Adamowicz, L., *J. Phys. Chem. A*, **102**, 1041 (1998).

225. Meot-Ner(Mautner), M., Hunter, E.P., and Field, F.H., *J. Am. Chem. Soc.*, **101**, 686 (1979).

226. Bohme, D.K., in *Structure/Reactivity and Thermochemistry of Ions*, edited by Ausloos, P. and Lias, S.G., Reidel Publishing Co., Dordrecht, p.219, 1987.

227. Mehringer, D.M., Snyder, L.E., and Miao, Y., *Astrophys. J. Lett.*, **480**, L71 (1997).

228. Spanel, P. and Smith, D., *Int. J. Mass Spectrom. Ion Proc.*, **172**, 137 (1998).

229. Freeman, C.G., Harland, P.W., and McEwan, M.J., *Aust. J. Chem.*, **31**, 2157 (1978).

230. Beranová, Š., Cai, J., and Wesdemiotis, C., *J. Am. Chem. Soc.*, **117**, 9492 (1995).

231. Topol, I.A., Burt, S.K., Toscano, M., and Russo, N., *J. Mol. Struct. (Theochem)*, **430**, 41 (1998).

232. Bouchoux, G., Bourcier, S., Hoppilliard, Y., and Mauriac, C., *Org. Mass Spectrom.*, **28**, 1064 (1993).

233. Ausloos, P., Lias, S.G., Buckley, T.J., and Rogers, E.E., *Int. J. Mass Spectrom. Ion Proc.*, **92**, 65 (1989).

234. Tasaka, M., Ogata, M., and Ichikawa, H., *J. Am. Chem. Soc.*, **103**, 1885 (1981).

235. Bernadi, F., Grandinetti, F., Guarino, A., and Robb, M.A., *Chem. Phys. Lett.*, **153**, 309 (1988).

236. Grandinetti, F. and Speranza, M., *Chem. Phys. Lett.*, **229**, 581 (1994).

237. Speranza, M., Sefcik, M.D., Henis, J.M.S., and Gaspar, P.P., *J. Am. Chem. Soc.*, **99**, 2051 (1977).

238. Brill, F.W. and Eyler, J.R., *J. Phys. Chem.*, **85**, 1091 (1981).

239. Eyler, J.R. and Campana, J.E., *Int. J. Mass Spectrom. Ion Proc.*, **55**, 171 (1983/84).

240. Knight, J.S., Freeman, C.G., McEwan, M.J., Anicich, V.G., and Huntress, W.T., *J. Phys. Chem.*, **91**, 3898 (1987).

241. Giles, K., Adams, N.G., and Smith, D., *Int. J. Mass Spectrom. Ion Proc.*, **89**, 303 (1989).

242. Jackson, J.A., Lias, S.G., and Ausloos, P., *J. Am. Chem. Soc.*, **99**, 7515 (1977).

243. Ausloos, P., *J. Am. Chem. Soc.*, **104**, 5259 (1982).

244. Ausloos, P. and Lias, S.G., *J. Am. Chem. Soc.*, **103**, 6505 (1981).

245. Rakshit, A.B. and Warneck, P., *J. Chem. Soc. Faraday Trans. 2*, **76**, 1084 (1980).

246. Lee, S., Gotts, N., von Helden, G., and Bowers, M.T., *J. Phys. Chem. A*, **101**, 2096 (1997).

247. Rylander, P.N., Meyerson, S., and Grubb, H.M., *J. Am. Chem. Soc.*, **79**, 842 (1957).

248. Winkler, J. and McLafferty, F.W., *J. Am. Chem. Soc.*, **95**, 7533 (1973).

249. McLafferty, F.W. and Winkler, J., *J. Am. Chem. Soc.*, **96**, 5182 (1974).

250. Shen, J., Dunbar, R.C., and Olah, G.A., *J. Am. Chem. Soc.*, **96**, 6227 (1974).

251. Dunbar, R.D., *J. Am. Chem. Soc.*, **97**, 1382 (1975).

252. Fu, E.W., Dymerski, P.P., and Dunbar, R.C., *J. Am. Chem. Soc.*, **98**, 337 (1976).

253. McLafferty, F.W. and Bockhoff, F.M., *J. Am. Chem. Soc.*, **101**, 1783 (1979).

254. Ausloos, P., Jackson, J.A., and Lias, S.G., *Int. J. Mass Spectrom. Ion Phys.*, **33**, 269 (1980).

255. Andrews, L. and Keelan, B.W., *J. Am. Chem. Soc.*, **103**, 99 (1981).

256. Bombach, R., Dannacher, J., and Stadelmann, J-P., *J. Am. Chem. Soc.*, **105**, 4205 (1983).

257. Bombach, R., Dannacher, J., and Stadelmann, J-P., *Chem. Phys. Lett.*, **95**, 259 (1983).

258. Cacace, F., Ciranni, G., Sparapani, C., and Speranza, M., *J. Am. Chem. Soc.*, **106**, 8046 (1984).

259. Buschek, J.M., Ridal, J.J., and Holmes, J.L., *Org. Mass Spectrom.*, **23**, 543 (1988).

260. Baer, T., Morrow, J.C., Shao, J.D., and Olesik, S.J., *J. Am. Chem. Soc.*, **110**, 5633 (1988).

261. Traeger, J.C. and Kompe, B.M., *Int. J. Mass Spectrom. Ion Proc.*, **101**, 111 (1990).

262. Heath, T.G., Allison, J., and Watson, J.T., *J. Am. Soc. Mass Spectrom.*, **2**, 270 (1991).

263. Zhao, G. and Gäumann, T., *Org. Mass Spectrom.*, **27**, 428 (1992).

264. Lifshitz, C., Gotkis, Y., Ioffe, A., Laskin, J., and Shaik, S., *Int. J. Mass Spectrom. Ion Proc.*, **125**, R7 (1993).

265. Basic, C., Eyler, J.R., and Yost, R.A., *Org. Mass Spectrom.*, **29**, 329 (1994).

266. Lin, C.Y. and Dunbar, R.C., *J. Phys. Chem.*, **98**, 1369 (1994).

267. Lifshitz, C., *Acc. Chem. Res.*, **27**, 138 (1994).

268. Shin, S.K., Han, S-J., and Kim, B., *Int. J. Mass Spectrom. Ion Proc.*, **157/158**, 345 (1996).

269. Xu, Y.C., Garcia, E., Freiser, B.S., and Bauschlicher, C.W., *Int. J. Mass Spectrom. Ion Proc.*, **157/158**, 249 (1996).

270. Ellison, G.B., Davico, G.E., Bierbaum, V.M., and DePuy, C.H., *Int. J. Mass Spectrom. Ion Proc.*, **156**, 109 (1996).

271. Kim, B. and Shin, S.K., *J. Chem. Phys.*, **106**, 1411 (1996).

272. Kretzschmar, I., Schröder, D., and Schwarz, H., *Int. J. Mass Spectrom. Ion Proc.*, **167/168**, 103 (1997).

273. Abboud, J.L.M., Hehre, W.J., and Taft, R.W., *J. Am. Chem. Soc.*, **98**, 6072 (1976).

274. Cone, C., Dewar, M.J.S., and Landman, D., *J. Am. Chem. Soc.*, **99**, 372 (1977).

275. Dewar, M.J.S. and Landman, D., *J. Am. Chem. Soc.*, **99**, 2446 (1977).

276. Nicolaides, A. and Radom, L., *J. Am. Chem. Soc.*, **116**, 9769 (1994).

277. Nicolaides, A. and Radom, L., *J. Am. Chem. Soc.*, **118**, 10561 (1996).

278. Smith, B.J. and Hall, N.E., *Chem. Phys. Lett.*, **279**, 165 (1997).

279. Lee, E.P.F. and Wright, T.G., *J. Phys. Chem. A*, **102**, 4007 (1998).

280. NIST/EPA/NIH Mass Spectral Library.

281. Smyth, K.C., Lias, S.G., and Ausloos, P., *Comb. Sci. Tech.*, **28**, 147 (1982).

282. McEwan, M.J., McConnell, C.L., Freeman, C.G., and Anicich, V.G., *J. Phys. Chem.*, **98**, 5068 (1994).

283. Houriet, R., Elwood, T.A., and Futrell, J.H., *J. Am. Chem. Soc.*, **100**, 2320 (1978).

284. Ozturk, F., Baykut, G., Moini, M., Eyler, J.R., *J. Phys. Chem.*, **91**, 4360 (1987).

285. Ozturk, F., Moini, M., Brill, F.W., Eyler, J.R., Buckley, T.J., Lias, S.G., and Ausloos, P., *J. Phys. Chem.*, **93**, 4038 (1989).

286. Lossing, F.P., *Can. J. Chem.*, **49**, 357 (1971); **50**, 3973 (1972).

287. Dewar, M.J.S. and Kirschner, *J. Am. Chem. Soc.*, **93**, 4290 (1971).

288. Radom, L., Hariharan, P.C., Pople, J.A., and Schleyer, P.v.R., *J. Am. Chem. Soc.*, **95**, 6531 (1973).

289. Radom, L., Pople, J.A., and Schleyer, P.v.R., *J. Am. Chem. Soc.*, **95**, 8193 (1973).

290. Merlet, P., Peyerimhoff, R.J., Buenker, R.J., and Shih, S., *J. Am. Chem. Soc.*, **96**, 959 (1974).

291. Aue, D.H., Davidson, W.R., and Bowers, M.T., *J. Am. Chem. Soc.*, **98**, 6700 (1976).

292. Houriet, R., Eldwood, T.A., and Futrell, J.H., *J. Am. Chem. Soc.*, **100**, 2320 (1978).

293. Köhler, H.J. and Lischka, H., *J. Am. Chem. Soc.*, **101**, 3479 (1979).

294. Bowen, R.D., Williams, D.H., Schwarz, H., and Wesdemiotis, C., *J. Am. Chem. Soc.*, **101**, 4681 (1979).

295. Bowers, M.T., Shuying, L., Kemper, P., Stradling, R., Webb, H., Aue, D.H., Gilbert, J.R., and Jennings, K.R., *J. Am. Chem. Soc.*, **102**, 4830 (1980).

296. Raghavachari, K., Whiteside, R.A., Pople, J.A., and Schleyer, P.v.R., *J. Am.* Chem. Soc., **103**, 5649 (1981).

297. Lay, J.O., and Gross, M.L., *J. Am. Chem. Soc.*, **105**, 3445 (1983).

298. Fornarini, S., Speranza, M., Attina, M., Cacace, F., and Giacomello, P., *J. Am. Chem. Soc.*, **106**, 2498 (1984).

299. My, N.K., Schilling, M., and Schwarz, H., *Org. Mass Spectrom.*, **22**, 254 (1987).

300. Martin, P.S., Yates, K., and Csizmadia, I.G., *Can. J. Chem.*, **67**, 2178 (1989).

301. Martin, P.S., Yates, K., and Csizmadia, I.G., *J. Mol. Struc. (Theochem.)*, **170**, 107 (1988).

302. Riveros, J.M. and Zhu, Z., *Rapid Commun. Mass Spectrom.*, **5**, 387 (1991).

303. McAllister, M., Tidwell, T.T., Peterson, M.R., and Csizmadia, I.G., *J. Org. Chem.*, **56**, 575 (1991).

304. Foresman, J.B., Wong, M.W., Wiberg, K.B., and Frisch, M.J., *J. Am. Chem. Soc.*, **115**, 2220 (1993).

305. van der Rest, G., Mourgues, P., LeBlanc, D., and Audier, H.E., *Eur. Mass Spectrom.*, **3**, 323 (1997).

306. Reindl, B., Clark, T., and Schleyer, P.v.R., *J. Comput. Chem.*, **18**, 533 (1997).

307. Houle, F.A. and Beauchamp, J.L., *J. Am. Chem. Soc.*, **100**, 3290 (1978).

308. Traeger, J.C., *Int. J. Mass Spectrom. Ion Proc.*, **58**, 259 (1984).

309. Dyke, J., Ellis, A., Jonathan, N., and Morris, A., *J. Chem. Soc. Faraday Trans. 2*, **81**,

1573 (1985).

310. Milligan, D.B., Fairley, D.A., Mautner, M., and McEwan, M.J., *Int. J. Mass Spectrom.*, in press (1998).
311. Smith, D., *Chem. Rev.*, **92**, 1473 (1992).
312. Adams, N.G., Smith, D., and Millar, T.J., *Mon. Not. R. Astr. Soc.*, **211**, 857 (1984).
313. Millar, T.J., Adams, N.G., Smith, D., Lindinger, W., and Villinger, H., *Mon. Not. R. Astr. Soc.*, **221**, 673 (1986).
314. Luine, J.A. and Dunn, G.H., *Astrophys. J. Lett.*, **299**, L67 (1985).
315. Adams, N.G., Smith, D., and Paulson, J.F., *J. Chem. Phys.*, **72**, 288 (1980).
316. Adams, N.G., and Smith, D., *Chem. Phys. Lett.*, **117**, 67 (1985).
317. Smith, D., Adams, N.G., and Ferguson, E.E., *Int. J. Mass Spectrom. Ion Proc.*, **61**, 15 (1984).
318. Smith, D. and Adams, N.G., *Int. J. Mass Spectrom. Ion Proc.*, **76**, 307 (1987).
319. Wong, M.W. and Radom, L., *J. Am. Chem. Soc.*, **115**, 1507 (1993).
320. Prodnuk, S.D., DePuy, C.H., and Bierbaum, V.M., *Int. J. Mass Spectrom. Ion Proc.*, **100**, 693 (1990).
321. Schiff, H.I., Hemsworth, R.S., Payzant, J.D., and Bohme, D.K., *Astrophys. J.*, **191**, L49 (1974).
322. Kim, J.K., Theard, L.P., and Huntress, W.T., *J. Chem. Phys.*, **62**, 45 (1975).
323. Fehsenfeld, F.C., Lindinger, W., Schmeltekopf, A.L., Albritton, D.L., and Ferguson, E.E., *J. Chem. Phys.*, **62**, 2001 (1975).
324. Smith, D. and Adams, N.G., *Mon. Not. R. Astron. Soc.*, **197**, 377 (1981).
325. Adams, N.G. and Smith, D., *Int. J. Mass Spectrom. Ion Proc.*, **61**, 133 (1984).
326. Marquette, J.B., Rowe, B.R., Dupeyrat, G., and Roueff, E., *Astron. Astrophys.*, **147**, 115 (1985).
327. Böhringer, H., *Chem. Phys. Lett.*, **122**, 185 (1985).
328. Barlow, S.E. and Dunn, G.H., *Int. J. Mass Spectrom. Ion Proc.*, **80**, 227 (1987).
329. Hawley, H., Mazely, T.L., Randeniya, L.K., Smith, R.S., Zeng, X.K., and Smith, M.A., *Int. J. Mass Spectrom. Ion Proc.*, **97**, 55 (1990).
330. Herbst, E., DeFrees, D.J., Talbi, D., Pauzat, F., Koch, W., and McLean, A.D., *J.*

Chem. Phys., **94**, 7842 (1991).

331. Herbst, E., *Chem. Phys. Lett.*, **222**, 297 (1994).
332. Knight, J.S., Freeman, C.G., McEwan, M.J., Adams, N.G., and Smith, D., *Int. J. Mass Spectrom. Ion Proc.*, **67**, 317 (1985).
333. Knight, J.S., Freeman, C.G., McEwan, M.J., Smith, S.C., Adams, N.G., and Smith, D., *Mon. Not. R. Astron. Soc.*, **219**, 89 (1986).
334. Fox, A., Raksit, A.B., Dheandhanoo, S., and Bohme, D.K., *Can. J. Chem.*, **64**, 399 (1986).
335. Petrie, S.A.H., Chirnside, T.J., Freeman, C.G., and McEwan, M.J., *Int. J. Mass Spectrom. Ion Proc.*, **107**, 319 (1991).
336. Smith, D. and Adams, N.G., *Astrophys. J.*, **298**, 827 (1985).
337. Scott, G.B.I., Fairley, D.A., Freeman, C.G., McEwan, M.J., Spanel, P., and Smith, D., *J. Chem. Phys.*, **106**, 3982 (1997).
338. Smith, D., Private Communication, (1996).
339. Böhringer, H., Durup-Ferguson, M., and Fahey, D.W., *J. Chem. Phys.*, **79**, 1974 (1983).
340. Smith, D., Glosik, J., Skalsky, V., Spanel, P., and Lindinger, W., *Int. J. Mass Spectrom. Ion Proc.*, **129**, 145 (1993).
341. Ma, M.L., Smith, B.J., Pople, J.A. and Radom, L., *J. Am. Chem. Soc.*, **113**, 7903 (1991).
342. Durant, J.L. and Rohlfing, C.M., *J. Chem. Phys.*, 98, 8031 (1993).
343. Malick, D.K., Petersson, G.A., and Montgomery, J.A., *J. Chem. Phys.*, **108**, 5704 (1998).
344. Szulejko, J.E., Normann, K., and McMahon, T.B., University of Waterloo HPMS PA Database, 1998.
345. Bohme, D.K., in *Interaction Between Ions and Molecules*, edited by Ausloos, P., Plenum, New York, p.489, 1975.
346. Hawley, M. and Smith, M.A., *J. Am. Chem. Soc.*, **111**, 8293 (1989).
347. Phillips, M., *Scientific American*, July 1992, p. 52.
348. Smith, D. and Spanel, P., *Int. Rev. Phys. Chem.*, **15**, 231 (1996).

349. Spanel, P. and Smith, D., *Med. Biol. Eng. Comput.*, **34**, 409 (1996).

350. Smith, D. and Spanel, P., *Rapid Commun. Mass Spectrom.*, **10**, 1183 (1996).

351. Lindinger, W., Hansel, A., and Jordan, A., *Int. J. Mass Spectrom. Ion Proc.*, **173**, 191 (1998).

352. Spanel, P. and Smith, D., *Int. J. Mass Spectrom. Ion Proc.*, **167/168**, 375 (1997).

353. Spanel, P. and Smith, D., *Int. J. Mass Spectrom. Ion Proc.*, **172**, 239 (1998).

354. Spanel, P. and Smith, D., *Int. J. Mass Spectrom.*, **176**, 203 (1998).

355. Spanel, P., Ji, Y., and Smith, D., *Int. J. Mass Spectrom. Ion Proc.*, **165/166**, 25 (1997).

356. Spanel, P. and Smith, D., *Int. J. Mass Spectrom.*, **176**, 167 (1998).

357. Meot-Ner, M., in *Gas Phase Ion Chemistry Vol. 1*, edited by Bowers, M.T., Academic Press, New York, 1979, p. 198.

358. Reents, W.D. and Freiser, B.S., *J. Am. Chem. Soc.*, **103**, 2791 (1981).

359. Weddle, G. and Dunbar, R.C., *Int. J. Mass Spectrom. Ion. Proc.*, **134**, 73 (1994).

360. Ryzhov, V., Klippenstein, S.J., and Dunbar, R.C., *J. Am. Chem. Soc.*, **118**, 5462 (1996).

361. Klippenstein, S.J., Yang, Y.-C., Ryzhov, V., and Dunbar, R.C., *J. Chem. Phys.*, **104**, 4502 (1996).

362. Dunbar, R.C., *Int. J. Mass Spectrom. Ion. Proc.*, **160**, 1 (1997).

363. Ryzhov, V. and Dunbar, R.C., *Int. J. Mass Spectrom. Ion Proc.*, **167/168**, 627 (1997).

364. Saxer, A., Richter, R., Villinger, H., Futrell, J.H., and Lindinger, W., *J. Chem. Phys.*, **87**, 2105 (1987).

365. Zangerle, R., Hansel, A., Richter, R., and Lindinger, W., *Int. J. Mass Spectrom. Ion Proc.*, **129**, 117 (1993).

366. Dobler, W., Federer, W., Howorka, F., Lindinger, W., Durup-Ferguson, M., and Ferguson, E.E., *J. Chem. Phys.*, **79**, 1543 (1983).

367. Federer, W., Dobler, W., Howorka, F., Lindinger, W., Durup-Ferguson, M., and Ferguson, E.E., *J. Chem. Phys.*, **83**, 1032 (1985).

368. Durup-Ferguson, M., Böhringer, H., Fahey, D.W., Fehsenfeld, F.C., and Ferguson,

E.E., *J. Chem. Phys.*, **81**, 2657 (1984).

369. Bass, L. and Jennings, K.R., *Int. J. Mass Spectrom. Ion Proc.*, **58**, 307 (1984).
370. Deakyne, C.A. and Meot-Ner, M., *J. Phys. Chem.*, **94**, 232 (1990).
371. Smith, S.C., Wilson, P.F., Sudkeaw, P., Maclagan, R.G.A.R., McEwan, M.J., Anicich, V.G., and Huntress, W.T., *J. Chem. Phys.*, **98**, 1944 (1993).
372. McEwan, M.J., Denison, A.B., Huntress, W.T., Anicich, V.G., Snodgrass, J., and Bowers, M.T., *J. Phys. Chem.*, **93**, 4064 (1989).
373. Petrie, S.A.H., Freeman, C.G., McEwan, M.J., and Meot-Ner, M., *Int. J. Mass Spectrom. Ion Proc.*, **90**, 241 (1989).
374. McEwan, M.J., Fairley, D.A., Scott, G.B.I., and Anicich, V.G., *J. Phys. Chem.*, **100**, 4032 (1996).
375. Rodler, M., *J. Mol. Spectrosc.*, **114**, 23 (1985).

APPENDICES

I. Computer programs.

II. Fairley, D.A., Scott, G.B.I., Freeman, C.G., Maclagan, R.G.A.R., and McEwan, M.J., *J. Chem. Soc., Faraday Trans.*, **92**, 1305 (1996).
Ion-molecule association of H_3O^+ and C_2H_2: Interstellar CH_3CHO.

III. Fairley, D.A., Scott, G.B.I., Freeman, C.G., Maclagan, R.G.A.R., and McEwan, M.J., *J. Phys. Chem. A*, **101**, 2848 (1997).
$C_2H_7O^+$ potential surface and ion-molecule association between H_3O^+ and C_2H_4.

IV. Fairley, D.A., Scott, G.B.I., Milligan, D.B., Maclagan, R.G.A.R., and McEwan, M.J., *Int. J. Mass Spectrom. Ion Proc.*, **172**, 79 (1998).
SIFDT study of the SO_2^+/H_2 H-atom abstraction reaction.

APPENDIX I: COMPUTER PROGRAMS

MCSREAD (QuickBASIC)

```
100 ON ERROR GOTO 1490
110 KEY OFF
120 CLS
130 DIM F$(8)
140 CHANNEL.NUMBER% = 0
150 DEF FNLONG! (LOW$, HIGH$) = CVI(LOW$) + CVI(HIGH$) * 65536!
160 INPUT "ENTER MCS FILENAME (INCLUDE EXTENSION): ", FILNM$
170 OPEN FILNM$ FOR RANDOM AS #1 LEN = 256
180 PRINT
200 INPUT "NAME FOR SAVED FILE (INCLUDE EXTENSION): ", NAME$
210 PRINT
560 FIELD #1, 2 AS F1$, 1 AS F2$, 1 AS F3$, 1 AS F4$, 1 AS F5$, 2 AS F6$, 2 AS
F7$, 2 AS F8$, 2 AS F9$, 2 AS F10$, 2 AS F11$, 2 AS F12$, 8 AS F13$, 8 AS F14$, 3
AS F15$, 1 AS F16$, 4 AS F17$, 20 AS F18$, 1 AS F19$, 63 AS F20$, 1 AS F21$, 63
AS F22$, 64 AS F23$
580 GET #1
600 TEMP$ = F2$
610 GOSUB 1440
620 EXTERN.START% = TEMP%
630 TEMP$ = F3$
640 EXTERN.DWELL% = TEMP%
660 TEMP$ = F5$
670 GOSUB 1440
680 SUM% = TEMP%
690 DWELL.TIME.LOW$ = F6$
700 DWELL.TIME.HIGH$ = F7$
710 DWELL.TIME! = FNLONG(DWELL.TIME.LOW$, DWELL.TIME.HIGH$)
720 IF CVI(DWELL.TIME.LOW$) < 0 THEN DWELL.TIME! = DWELL.TIME! +
65536!
730 PASS.LENGTH% = CVI(F8$)
740 PASS.CNT.LOW$ = F9$
750 PASS.CNT.HIGH$ = F10$
760 PASS.COUNT! = FNLONG(PASS.CNT.LOW$, PASS.CNT.HIGH$)
770 IF CVI(PASS.CNT.LOW$) < O THEN PASS.COUNT! = PASS.COUNT! + 65536!
780 PAS.PRE.LOW$ = F11$
790 PAS.PRE.HIGH$ = F12$
800 PASS.CNT.PRESET! = FNLONG(PAS.PRE.LOW$, PAS.PRE.HIGH$)
810 IF CVI(PAS.PRE.LOW$) < 0 THEN PASS.CNT.PRESET! = PASS.CNT.PRESET!
+ 65536!
820 START.TIME$ = F13$
```

```
830 START.DATE$ = F14$
840 TEMP$ = F16$
850 GOSUB 1440
860 CALIBRATED% = TEMP%
870 CAL.UNIT$ = F17$
880 TEMP$ = F19$
890 GOSUB 1440
900 DET.DESC.LENGTH% = TEMP%
910 DET.DESCRIPTION$ = LEFT$(F20$, DET.DESC.LENGTH%)
920 TEMP$ = F21$
930 GOSUB 1440
940 SAMPLE.LENGTH% = TEMP%
950 SAMPLE.DESC$ = LEFT$(F22$, SAMPLE.LENGTH%)
1221 ICHAN = FREEFILE
1222 PATH$ = "C:\"
'1223 NAME$ = "DAF.DAF"
1226 OPEN PATH$ + NAME$ FOR OUTPUT AS #ICHAN LEN = 256
1230 FIELD #1, 32 AS F$(1), 32 AS F$(2), 32 AS F$(3), 32 AS F$(4), 32 AS F$(5), 32
AS F$(6), 32 AS F$(7), 32 AS F$(8)
1240 FOR RECORD% = 1 TO INT(PASS.LENGTH% * 4 / 256) + 1
1250 GET 1
1260 FOR FIELD.CNT% = 1 TO 8
1270 PRINT "CH";
1280 PRINT USING "#####"; CHANNEL.NUMBER%;
1290 FOR CHANNEL.PER.FIELD% = 0 TO 7
1300 CHAN.DATA.LOW$ = MID$(F$(FIELD.CNT%), CHANNEL.PER.FIELD% * 4 +
1, 2)
1310 CHAN.DATA.HI$ = MID$(F$(FIELD.CNT%), CHANNEL.PER.FIELD% * 4 + 3,
2)
1320 CHAN.DATA! = FNLONG(CHAN.DATA.LOW$, CHAN.DATA.HI$)
1330 IF CVI(CHAN.DATA.LOW$) < 0 THEN CHAN.DATA! = CHAN.DATA! +
65536!
1332 PRINT USING "#########"; CHAN.DATA!;
1335 PRINT #ICHAN, USING "#####"; CHANNEL.NUMBER% * DWELL.TIME!;
1340 PRINT #ICHAN, USING "#########"; CHAN.DATA!
1350 CHANNEL.NUMBER% = CHANNEL.NUMBER% + 1
1360 IF CHANNEL.NUMBER% >= PASS.LENGTH% THEN GOTO 1540
1370 NEXT CHANNEL.PER.FIELD%
1380 PRINT
1390 NEXT FIELD.CNT%
1400 NEXT RECORD%
1440 TEMP% = ASC(TEMP$)
1450 RETURN
1490 IF (ERR = 5) THEN TEMP% = 0 ELSE PRINT "ERROR NUMBER "; ERR; "
LINE "; ERL
```

```
1500 RESUME NEXT
1540 CLOSE #1
1550 END
```

DAFPROG (Borland Pascal)

```
uses wincrt,wfforms;
const kb=1.38054e-23 { J/K };
    pi=3.14159265;
    au=1.67261e-24{g};
    T0=273.16;
    NA=6.022e23{mol-1};
    Rtube=3.015{cm};
    Patm=760{Torr};
    Dist8r=43.4{cm};
    Dist31r=20.4{cm};
    n1torr=3.23974e16{cm-3};
    ev=96.485e3{J mol-1 per eV};
    Logfile='c:\SIFDT.TXT';
    var nrings,voltage,time8r,time31r,timemo,vionzero,press,Temp,mion,massbuff,field,
        Atube:real;
    var Vbuff,Vdrift,vion,eovern,fc,mobility,massneut:real;
    var Er,Ec,redmob,KEion,run:real;
    var ch:char;
    var f:text;
    var date,reacn:string;
begin
 nrings:=50; Temp:=300; mion:=39.95; massneut:=28.01; massbuff:=4.00; fc:=117.0;
press:=0.340;
 run:=1;date:='12/12/95';reacn:='Ar+ + N2';vionzero:=1.5;
repeat
  clrscr;
  writeln;
  writeln('This program will calculate reduced mobilities and centre-of-mass energies
from input drift tube data.');
  writeln('Input parameters as prompted (displayed value is default)...');
  writeln('Enter arrival times for two rings - make the other one zero');
  writeln;
  inputs('Date [dd/mm/yy]: ',date,8);
  inputs('Reaction description or ion name: ',reacn,20);
  inputr('Number of rings voltage applied to = ',nrings,3,0);
  inputr('Temperature(K) = ',Temp,8,3);
  inputr('Ion mass(g/mol) = ',mion,8,3);
  inputr('Neutral reactant mass(g/mol) = ',massneut,8,3);
  inputr('Buffer gas mass(g/mol) = ',massbuff,8,3);
```

```
inputr('Buffer gas pressure(torr) = ',press,8,3);
inputr('Buffer gas flow(torr l/s) = ',fc,8,3);
inputr('Voltage applied to drift tube(V) = ',voltage,8,3);
inputr('Measured arrival time from ring 8 (us) = ',time8r,8,3);
inputr('Measured arrival time from ring 31 (us) = ',time31r,8,3);
inputr('Measured arrival time from Mo disc (us) = ',timemo,8,3);
inputr('Ion velocity/buffer gas velocity at zero field = ',vionzero,8,3);
field:=voltage/nrings;
Atube:=pi*Rtube*Rtube{cm2};
if time8r=0 then vion:=20.9/((time31r-timemo)*1e-6){cm/sec}else if
time31r=0 then vion:=43.9/((time8r-timemo)*1e-6){cm/s} else if
timemo=0 then  vion:=(dist8r-dist31r)/((time8r-time31r)*1e-6){cm/s};
eovern:=field/(press*n1torr);
eovern:=eovern/1e-17{Td};
Vbuff:=1000*fc/press/Atube;
Vdrift:=vion-vionzero*vbuff{cm/s};
mobility:=vdrift/field;
redmob:=mobility*(press/Patm)*(T0/Temp);
vdrift:=vdrift/100;
massbuff:=massbuff/1000{kg/mol};
mion:=mion/1000{kg/mol};
massneut:=massneut/1000{kg/mol};
KEion:=(1.5*kb*NA*Temp)+(0.5*massbuff*vdrift*vdrift)+(0.5*mion*vdrift*vdrift){J/
mol};
Er:=(massneut/(mion+massneut))*(KEion-1.5*kb*NA*Temp)+1.5*kb*NA*Temp;
Ec:=(massbuff/(mion+massbuff))*(KEion-1.5*kb*NA*Temp)+1.5*kb*NA*Temp;
mion:=mion*1000;
massbuff:=massbuff*1000;
massneut:=massneut*1000;
writeln;
writeln('Run #',run:1:0);
writeln('Reaction: ',reacn);
writeln;
write('Ion velocity = ',vion:8:3);writeln(' cm/s');
write('Carrier gas velocity = ',Vbuff:8:3);writeln(' cm/s');
write('Ion drift velocity = ',Vdrift*100:8:3);writeln(' cm/s');
writeln('Ion velocity/buffer gas velocity = ',(vion/Vbuff):8:3);
writeln;
write('E/N = ',eovern:8:3);writeln(' Td');
write('Ionic mobility = ',mobility:8:3);writeln(' cm2/V.s');
write('Reduced mobility = ',redmob:8:3);writeln(' cm2/V.s');
writeln;
write('KE ion = ',KEion:8:3);writeln(' J/mol');
write('       = ',KEion/eV:8:3);writeln(' eV');
write('Ion/reactant neutral centre-of-mass energy = ',Er:8:3);writeln(' J/mol');
```

```
 write('                                    = ',Er/eV:8:3);writeln(' eV');
 Write('Ion/carrier gas centre-of-mass energy = ',Ec:8:3);writeln(' J/mol');
 write('                                  = ',Ec/eV:8:3);writeln('eV');
 assign(f,Logfile);
 append(f);
 writeln(f,'');writeln(f,'');
 writeln(f,'Date: ',date);
 writeln(f,'Reaction: ',reacn);
 writeln(f,'');
 writeln(f,'Run # ',run:1:0);
 write(f,'Time#1= ',time8r:8:3);write(f,' us');write(f,'   ');write(f,'Time#2=
',time31r:8:3);writeln(f,' us');
 write(f,'Time#3= ',timemo:8:3);writeln(f,' us');
 writeln(f,'Ion velocity/buffer gas velocity = ',vionzero:8:3);
 write(f,'Temperature= ',Temp:8:3);write(f,' K   ');write(f,'Pressure= ',press:8:3);writeln(f,'
Torr');
 write(f,'Ion mass= ',mion:8:3);write(f,' g/mol   ');write(f,'Neutral mass=
',massneut:8:3);writeln(f,' g/mol');
 write(f,'Carrier flow= ',fc:8:3);write(f,' Torr l/s   ');write(f,'Drift tube voltage=
',voltage:8:3);writeln(f,' V');
 writeln(f,'');
 write(f,'Ion velocity = ',vion:8:3);writeln(f,' cm/s');
 write(f,'Carrier gas velocity = ',Vbuff:8:3);writeln(f,' cm/s');
 write(f,'Ion drift velocity = ',Vdrift*100:8:3);writeln(f,' cm/s');
 writeln(f,'Ion velocity/buffer gas velocity = ',(vion/Vbuff):8:3);
 writeln(f,'');
 write(f,'E/N = ',eovern:8:3);writeln(f,' Td');
 write(f,'Ionic mobility = ',mobility:8:3);writeln(f,' cm2/V.s');
 write(f,'Reduced mobility = ',redmob:8:3);writeln(f,' cm2/V.s');
 writeln(f,'');
 write(f,'KE ion = ',KEion:8:3);writeln(f,' J/mol');
 write(f,'       = ',KEion/eV:8:3);writeln(f,' eV');
 write(f,'Ion/reactant neutral centre-of-mass energy = ',Er:8:3);writeln(f,' J/mol');
 write(f,'                                    = ',Er/eV:8:3);writeln(f,' eV');
 Write(f,'Ion/carrier gas centre-of-mass energy = ',Ec:8:3);writeln(f,' J/mol');
 write(f,'                                  = ',Ec/eV:8:3);writeln(f,' eV');
 close(f);
 run:=run+1;
 writeln;
 writeln('This data has been appended to the file "SIFDT.TXT" for printing"');
 writeln;
 writeln('Another calculation?[Y/N]');
 ch:=readkey;
until upcase(ch)<>'Y';
end.
```

Ion–molecule association of H_3O^+ and C_2H_2: Interstellar CH_3CHO

David A. Fairley, Graham B. I. Scott, Colin G. Freeman, Robert G. A. R. Maclagan and Murray J. McEwan

Department of Chemistry, University of Canterbury, Christchurch, New Zealand

The $C_2H_2 \cdot H_3O^+$ product of the ion–molecule association reaction between H_3O^+ and C_2H_2 is found to consist of a *ca.* 50 : 50 mixture of two isomeric ions. These two isomeric ions are identified in a selected ion flow tube, by their different proton transfer behaviour with the neutral reagents C_2H_5Br, 4-fluorotoluene, CH_3OH and benzene, as protonated vinyl alcohol, $CH_2CHOH_2^+$ and either protonated acetaldehyde, CH_3CHOH^+ or the electrostatic complex $H_3O^+ \cdot C_2H_2$. These conclusions are supported by Gaussian G2 level calculations based on *ab initio* molecular orbital theory, which are applied to calculate the proton affinities of CH_3CHO, CH_2CHOH, oxirane and acyclic CH_2OCH_2. Reaction rate coefficients and product ratios are also reported for the reactions of specific $C_2H_5O^+$ isomers, *viz*: CH_3CHOH^+, $CH_3OCH_2^+$ and $\underline{CH_2OHCH_2}^+$ with CH_3OH, 4-fluorotoluene and C_6H_6. The implications of the current results to the interstellar synthesis of CH_3CHO are discussed briefly.

Acetaldehyde is one of the molecules known to exist in interstellar clouds, having been first identified in 1971 from its emission spectrum at 1065.075 MHz.[1] Among the reactions considered as responsible for its production in the interstellar medium is the radiative association of H_3O^+ and C_2H_2:[2,3]

$$H_3O^+ + C_2H_2 \rightarrow C_2H_5O^+ + h\nu \qquad (1)$$

followed by dissociative recombination

$$CH_3CHOH^+ + e \rightarrow CH_3CHO + H \qquad (2)$$

There are, however, several isomeric forms of the $C_2H_5O^+$ product ion of reaction (1) and it is not immediately obvious whether protonated acetaldehyde, CH_3CHOH^+, is the structure formed in reaction (1).

Indirect evidence from Herbst *et al.*[4] suggested that the structure of the product ion of the association reaction (3)

$$H_3O^+ + C_2H_2 + M \rightarrow C_2H_5O^+ + M \qquad (3)$$

did not correspond to CH_3CHOH^+ which is the lowest energy $C_2H_5O^+$ isomer. In their study they compared the measured rate coefficient for reaction (3) with that calculated assuming the $C_2H_5O^+$ association ion has the CH_3CHOH^+ structure. The calculated rate coefficient did not match the measured value and they concluded that the $C_2H_5O^+$ isomer formed in the association reaction has a structure higher in energy than CH_3CHOH^+.

Jarrold *et al.*,[2] from their laboratory collision-induced dissociation (CID) investigation of the $C_2H_5O^+$ ion formed in reaction (3), concluded that the product ion of association has the structure of either CH_3CHOH^+ or O-protonated ethylene oxide (protonated oxirane).

In the present work we have examined the reactivity of the $C_2H_5O^+$ ion formed in reaction (3) and have also undertaken an *ab initio* study of the $C_2H_5O^+$ potential surface.

Experimental

The experiments reported here were carried out at room temperature (298 ± 5) K and at a helium-bath gas pressure of 0.300 Torr using the Canterbury selected ion flow tube (SIFT) system described previously.[5] The $C_2H_5O^+$ association ion, which we designate $C_2H_2 \cdot H_3O^+$, was produced in the flow tube by injecting mass-selected H_3O^+ from the SIFT ion source and adding C_2H_2 at the first inlet port.

$$H_3O^+ + C_2H_2 + M \rightarrow C_2H_2 \cdot H_3O^+ + M \qquad (4)$$

The rate coefficient for reaction (4) was reported by Herbst *et al.*[4] as $k = 8 \times 10^{-28}$ cm^6 s^{-1} at 300 K. Our measured pseudo-second-order rate coefficient for this reaction is 1.1×10^{-11} cm^3 s^{-1} at a helium-bath gas pressure of 0.3 Torr which is consistent with the Herbst *et al.* measurement. In our experiments we added sufficient C_2H_2 to reduce the H_3O^+ signal to less than 1% of the background H_3O^+ signal in most experiments. The presence of the excess C_2H_2 did not affect the subsequent reactions of $C_2H_2 \cdot H_3O^+$ with neutral reactants added at the second inlet port.

The existence of different isomeric ions is apparent by their differing reactivities with selected reagents. We have earlier discussed at some length the possibility that vibrational excitation of ions formed *via* an association reaction might also give rise to curved semilogarithmic decays of ln(ion signal) *vs.* neutral flow.[5] In the present case, eight atoms in the $C_2H_2 \cdot H_3O^+$ complex yield 19 normal modes for distribution of vibrational energy, which makes collisional stabilization by the bath gas a more efficient process than for smaller ions. The distance of 28.0 cm between the first and second ports in our flow tube means that under typical operating conditions (298 K, $P = 0.300$ Torr) the association ion would experience an average of *ca.* 11 000 collisions with the bath gas before its reaction with the diagnostic neutral species. Further, the curved decays, of which Fig. 1(a) is representative, were found only for those neutral reagents which had proton affinities such that one isomer exhibited proton transfer and the other did not. For the reactant molecules allene (proton affinity, $E_{pa} = 779$ kJ mol^{-1}) and 2-fluorotoluene ($E_{pa} = 781$ kJ mol^{-1}), linear semilogarithmic decays were observed [Fig. 1(b)] whereas for C_2H_5Br, 4-fluorotoluene, CH_3OH and C_6H_6 curved decays were observed.

All reagents used in the study were obtained from commercial suppliers and were further purified by freeze–pump–thaw cycles.

Results

Ab initio studies

An earlier investigation of the $C_2H_5O^+$ potential-energy surface found four low-lying stable isomers of $C_2H_5O^+$.[6,7] These are CH_3CHOH^+ (protonated acetaldehyde), $CH_2CHOH_2^+$ (protonated vinyl alcohol), $CH_3OCH_2^+$ (methoxymethyl cation) and $\underline{CH_2OHCH_2}^+$ (protonated oxirane). A recent re-examination of these structures and the relevant neutral C_2H_5O structures was reported by Curtiss *et*

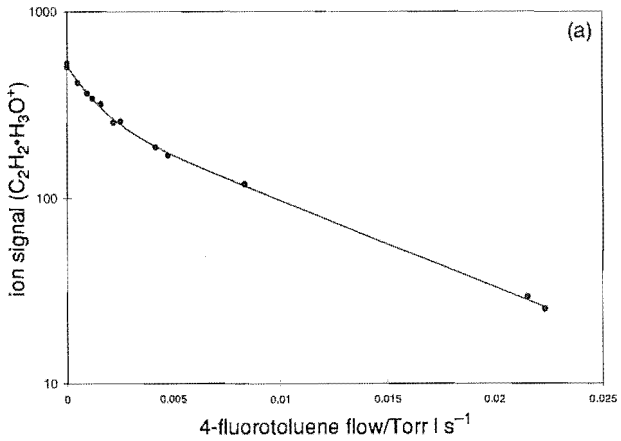

Fig. 1 Semilogarithmic plots of the $C_2H_2 \cdot H_3O^+$ ion count rate at $m/z = 45$ *vs.* (a) 4-fluorotoluene and (b) allene flow. In (a) the points are experimental and the line is a computer-generated least-mean-square fit to the data points based on the assumption that only two isomeric forms of $C_2H_5O^+$ are present; (b) is the conventional semilogarithmic decay observed for pseudo-first-order kinetics.

al.[8] We have also repeated the study of Nobes *et al.*[6] at a higher level of theory and have explored further reaction pathways for interconversion between $C_2H_5O^+$ isomers. Some of our results are summarized in Table 1 which lists the enthalpies of formation and proton affinities for the neutral species derived from the four most stable $C_2H_5O^+$ isomers calculated using the G2 procedure.[11] Smith and Radom[12] have also calculated the proton affinity of CH_3CHO at the G2 level of theory as 770 kJ mol^{-1}. We also note that the *ab initio* study identified an electrostatic complex of $C_2H_2 \cdot H_3O^+$ which lies 79 kJ mol^{-1} below the reactant energies. The proton affinity of the C_2H_2–H_2O complex was calculated to be 761 kJ mol^{-1}. All calculations were performed using the GAUSSIAN 92 program.[13] The energies of the different $C_2H_5O^+$ isomers relative to $H_3O^+ + C_2H_2$ are shown in Fig. 2.

Table 1 Calculated enthalpies of formation and proton affinities of C_2H_4O isomers

	$\Delta_f H^0$/kJ mol^{-1}		E_{pa}/kJ mol^{-1}	
structure	calc.[a]	exp.[b]	calc.[c]	exp.
CH_3CHO	−173.2	−165.8	767.5	781,[b] ≥769[d]
CH_2CHOH	−122.9	−125	719.2	
oxirane	−59.8	−52.6	766.6	786[b]
CH_2OCH_2[e]	127.3		995.5	

[a] Calculated enthalpies of formation at 298 K at the G2 level of theory using $E_{G2}(C_2H_4O) - E_{G2}(H_2O) - E_{G2}(C_2H_2) = \Delta_f H^0(C_2H_4O) - \Delta_f H^0(H_2O) - \Delta_f H^0(C_2H_2)$. Substitution of $\Delta_f H^0(H_2O)$ and $\Delta_f H^0(C_2H_2)$ from ref. 9 yields $\Delta_f H^0(C_2H_4O)$. [b] Experimental values are from ref. 9. [c] Calculated proton affinities at 298 K at the G2 level of theory. [d] Value from ref. 10. [e] Planar (edge-to-edge) structure.

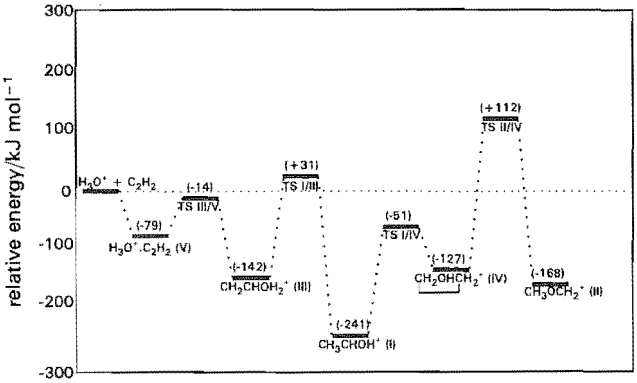

Fig. 2 Energies of $C_2H_5O^+$ species relative to $H_3O^+ + C_2H_2$

SIFT experiments

The *ab initio* calculations have shown some $C_2H_5O^+$ isomers to have proton affinities that are sufficiently different for proton transfer to be used as a probe of the structure. We selected several neutral reactants on the basis of their known proton affinities and examined the reactivities of different isomers of $C_2H_5O^+$ with them. The neutral reactants chosen were C_2H_5Br ($E_{pa} \approx 715$ kJ mol^{-1}), 4-fluorotoluene ($E_{pa} = 757$ kJ mol^{-1}), C_6H_6 ($E_{pa} = 759$ kJ mol^{-1}) and CH_3OH ($E_{pa} = 761$ kJ mol^{-1}). Not all isomeric ions were examined with all neutral reagents. The reactions of the known $C_2H_5O^+$ isomers were then compared with those of $C_2H_2 \cdot H_3O^+$ formed in reaction (4). The designated $C_2H_5O^+$ isomers were produced in the following ways: CH_3CHOH^+ was formed *via* electron impact on CH_3CHO in a high-pressure ion source; $CH_3OCH_2^+$ was made from electron impact on dimethoxymethane and $CH_2OHCH_2^+$ from electron impact on oxirane in a high-pressure ion source. The desired $C_2H_5O^+$ isomer was then mass selected and injected into the flow tube in the usual manner. These $C_2H_5O^+$ isomers have substantial barriers to isomerization (Fig. 2) and retain their identity in the flow tube as the reaction chemistry described next bears out.

CH_3CHOH^+ reactions

The reactions of protonated acetaldehyde, CH_3CHOH^+, with 4-fluorotoluene and CH_3OH were examined. Similar rate coefficients were obtained for each neutral reactant and both reagents gave the association adduct as the only product. The pseudo-second-order rate coefficients are $k = 4.5 \times 10^{-10}$ cm^3 s^{-1} (4-fluorotoluene) and $k = 4.4 \times 10^{-10}$ cm^3 s^{-1} (CH_3OH) at a helium pressure of 0.300 Torr.

$CH_3OCH_2^+$ reactions

Three reagents were used to examine the reactions of $CH_3OCH_2^+$: C_6H_6, 4-fluorotoluene and CH_3OH (CD_3OD) with the following results:

$$CH_3OCH_2^+ + C_6H_6 \xrightarrow{1.0} C_7H_7^+ + CH_3OH \quad (5)$$

$$k = 5.0 \times 10^{-10} \text{ cm}^3 \text{ s}^{-1}$$

$$CH_3OCH_2^+ + C_7H_7F \xrightarrow{ca.\ 0.85} C_8H_8F^+ + CH_3OH \quad (6a)$$

$$\xrightarrow{ca.\ 0.15} C_8H_9F^+ + CH_3O \quad (6b)$$

$$\xrightarrow{<0.05} \text{adduct} \quad (6c)$$

$$k = 2.6 \times 10^{-10} \text{ cm}^3 \text{ s}^{-1}$$

Table 2 Reaction rate coefficients and product ratios for the $C_2H_5O^+$ ions: protonated acetaldehyde, CH_3CHOH^+; protonated oxirane, $CH_2OHCH_2^+$; and methoxymethyl cation, $CH_3OCH_2^+$ with the specified reactant

reactant	products	branching ratio	k_{obs} /10^{-9} cm^3 s^{-1}	k_{coll}[b] /10^{-9} cm^3 s^{-1}	E_{pa}[a] /kJ mol^{-1}
		CH_3CHOH^+			
C_7H_7F[c]	adduct	1.0	0.45	2.3	757
CH_3OH	adduct	1.0	0.44	2.1	761
		$CH_3OCH_2^+$			
C_6H_6	$C_7H_7^+ + CH_3OH$	1.0	0.50	1.4	759
C_7H_7F[c]	$C_8H_8F^+ + CH_3OH$	~0.85			
	$C_8H_9F^+ + CH_3O$	~0.15	0.26	2.3	757
	adduct	<0.05			
CD_3OD	adduct	>0.9	0.02	2.1	761
	$CD_3OCH_2^+ + CH_3OD$	<0.1			
		$CH_2OHCH_2^+$			
C_7H_7F[c]	$C_9H_{10}F^+ + H_2O$	0.90	0.63	2.3	757
	adduct	0.10			
CH_3OH	$C_3H_7O^+ + H_2O$	0.50	0.50	2.1	761
	adduct	0.50			

[a] Proton affinities are from ref. 9. [b] Calculated using the theory of ref. 15 for molecules containing a permanent dipole and Langevin theory for C_6H_6. [c] Reactant is 4-fluorotoluene.

$$CH_3OCH_2^+ + CD_3OD \xrightarrow{>0.9} \text{adduct} \quad (7a)$$

$$\xrightarrow{<0.1} CD_3OCH_2^+ + CH_3OD \quad (7b)$$

$$k = 2 \times 10^{-11} \text{ cm}^3 \text{ s}^{-1}$$

$CH_2OHCH_2^+$ reactions

The reactions of protonated oxirane with 4-fluorotoluene and CH_3OH were examined.

$$CH_2OHCH_2^+ + C_7H_7F \xrightarrow{0.90} C_9H_{10}F^+ + H_2O \quad (8a)$$

$$\xrightarrow{0.10} \text{adduct} \quad (8b)$$

$$k = 6.3 \times 10^{-10} \text{ cm}^3 \text{ s}^{-1}$$

$$CH_2OHCH_2^+ + CH_3OH \xrightarrow{0.50} C_3H_7O^+ + H_2O \quad (9a)$$

$$\xrightarrow{0.50} \text{adduct} \quad (9b)$$

$$k = 5.0 \times 10^{-10} \text{ cm}^3 \text{ s}^{-1}$$

$C_2H_2 \cdot H_3O^+$ reactions

Six reagents were used to examine the product ion of the association reaction between H_3O^+ and C_2H_2: *viz.* C_2H_5Br, 4-fluorotoluene, CH_3OH, C_6H_6, 2-fluorotoluene and allene (propadiene). For the first four reagents the reaction behaviour was very different from the behaviour exhibited by the $C_2H_5O^+$ isomers discussed previously. For each reagent, curved semilogarithmic decays were found which shows that more than one structural form of $C_2H_5O^+$ is produced in the association reaction (4).[5,14] An example of one of these decays obtained for the reaction of $C_2H_2 \cdot H_3O^+$ and 4-fluorotoluene is shown in Fig. 1(a). The data points are fitted in the usual way[5,14] using eqn. (I) which assumes that two isomeric forms [$C_2H_5O^+$ (1) and $C_2H_5O^+$ (2)] are present in the reaction mixture of $C_2H_2 \cdot H_3O^+$.

$$I_{C_2H_5O^+} = C'_1 \exp(-k'_1 f_{C_7H_7F}) + C'_2 \exp(-k'_2 f_{C_7H_7F}) \quad (I)$$

The solid curve in Fig. 1(a) is the computer-generated best fit modelled according to eqn. (I). C'_1 and C'_2 are the respective initial ion signals of $C_2H_5O^+$ (1) and $C_2H_5O^+$ (2); k'_1, k'_2 are related to the respective rate coefficients for $C_2H_5O^+$ (1) and $C_2H_5O^+$ (2); and $f_{C_7H_7F}$ is the flow of 4-fluorotoluene. Because of uncertainties in the curve-fitting procedure, the rate coefficients derived have larger uncertainties (±50%) than rate coefficients usually obtained using the SIFT technique.

$$C_2H_2 \cdot H_3O^+ + C_2H_5Br \rightarrow C_2H_5BrH^+ + C_2H_4O \quad (10a)$$

$$\rightarrow \text{adduct} \quad (10b)$$

$$C_1 = 0.45, \quad k_1 = 1.8 \times 10^{-9} \text{ cm}^3 \text{ s}^{-1}$$

$$C_2 = 0.55, \quad k_2 = 5.8 \times 10^{-11} \text{ cm}^3 \text{ s}^{-1}$$

$$C_2H_2 \cdot H_3O^+ + C_7H_7F \rightarrow C_7H_8F^+ + C_2H_4O \quad (11a)$$

$$\rightarrow \text{adduct} \quad (11b)$$

$$C_1 = 0.50, \quad k_1 = 3.9 \times 10^{-9} \text{ cm}^3 \text{ s}^{-1};$$

$$C_2 = 0.50, \quad k_2 = 5.4 \times 10^{-10} \text{ cm}^3 \text{ s}^{-1}$$

Table 3 Reaction rate coefficients and isomer ratio for the $C_2H_5O^+$ species, $C_2H_2 \cdot H_3O^+$, formed in the association reaction between H_3O^+ and C_2H_2 and the specified reactant

reactant	products	E_{pa}[a] /kJ mol^{-1}	k_1[b] /10^{-9} cm^3 s^{-1}	k_2[c] /10^{-9} cm^3 s^{-1}	C_1[d]	k_{coll}[e] /10^{-9} cm^3 s^{-1}
C_2H_5Br	$C_2H_5BrH^+ + C_2H_4O$/adduct	*ca.* 715	1.8	0.058	0.45	2.1
C_7H_7F[f]	$C_7H_8F^+ + C_2H_4O$/adduct	757	3.9	0.54	0.50	2.3
CH_3OH	$CH_3OH_2^+ + C_2H_4O$/adduct	761	3.9	0.47	0.40	2.1
C_6H_6	multiple products	759	2.1	0.20	0.50	1.4
C_7H_7F[g]	$C_7H_8F^+ + C_2H_4O$	781	1.7[h]	—	—	1.9
C_3H_4[i]	products	779	1.0[h]	—	—	1.2

[a] Ref. 9. [b] Observed rate coefficients for the more reactive isomer. Uncertainty (±50%). [c] Observed rate coefficients for the less reactive isomer. Uncertainty (±50%). [d] Estimated proportion of the more reactive isomer. [e] Calculated collision rate using the theory of ref. 15 for molecules containing a permanent dipole and Langevin theory for C_6H_6. [f] 4-Fluorotoluene. [g] 2-Fluorotoluene. [h] A linear semilogarithmic decay is observed. [i] Allene.

$$C_2H_2 \cdot H_3O^+ + CH_3OH \rightarrow CH_3OH_2^+ + C_2H_4O \quad (12a)$$

$$\rightarrow \text{adduct} \quad (12b)$$

$$C_1 = 0.40, \quad k_1 = 3.9 \times 10^{-9} \text{ cm}^3 \text{ s}^{-1}$$

$$C_2 = 0.60, \quad k_2 = 4.7 \times 10^{-10} \text{ cm}^3 \text{ s}^{-1}$$

$$C_2H_2 \cdot H_3O^+ + C_6H_6 \rightarrow C_6H_7^+ + C_2H_4O \quad (13)$$

plus other products

$$C_1 = 0.50, \quad k_1 = 2.1 \times 10^{-9} \text{ cm}^3 \text{ s}^{-1}$$

$$C_2 = 0.50, \quad k_2 = 2.0 \times 10^{-10} \text{ cm}^3 \text{ s}^{-1}$$

C_1 and C_2 are the fractions of isomer 1 and 2 present in the mixture. The rate coefficient k_1 is the rate coefficient for the proton-transfer channel and corresponds to the initial rapid decay component in Fig. 1(a). The rate coefficient k_2 is the rate coefficient for the slower adduct-formation channel.

The reactions of $C_2H_2 \cdot H_3O^+$ with 2-fluorotoluene and allene gave linear semilogarithmic decays [Fig. 1(b)] corresponding to exothermic proton transfer from both isomeric species in $C_2H_2 \cdot H_3O^+$.

A summary of all the measurements of designated $C_2H_5O^+$ isomer reactions is presented in Table 2 and the reactions of $C_2H_2 \cdot H_3O^+$ in Table 3.

Discussion

The flow tube measurements show that the $C_2H_5O^+$ species produced by association between H_3O^+ and C_2H_2 in reaction (3) is a mixture of $C_2H_5O^+$ isomers. The more reactive isomer accounts for *ca.* 50% of the total $C_2H_5O^+$ signal and exhibits collision-rate proton transfer reactions with C_2H_5Br ($E_{pa} \approx$ 715 kJ mol^{-1}), 4-fluorotoluene (E_{pa} = 759 kJ mol^{-1}), CH_3OH (E_{pa} = 761 kJ mol^{-1}) and C_6H_6 (E_{pa} = 759 kJ mol^{-1}). Clearly, proton transfer is an exothermic process in all reactions. There is only one structure with a proton affinity close to 715 kJ mol^{-1} on the list of proton affinities of C_2H_4O isomers in Table 1. That isomer is vinyl alcohol, CH_2CHOH which has a calculated proton affinity of 717 kJ mol^{-1}. Accordingly, we identify the more reactive $C_2H_5O^+$ component, contributing *ca.* 50% to the isomeric mixture of $C_2H_5O^+$ ions from $C_2H_2 \cdot H_3O^+$, as protonated vinyl alcohol (or the vinyloxonium cation), $CH_2CHOH_2^+$. An ideal experimental confirmation of this identification would be to examine the reactions of pure vinyloxonium cations in the flow tube. Unfortunately no source we tried produced the $CH_2CHOH_2^+$ ion free from other isomeric forms.

Burgers *et al.*[16] report that they prepared the vinyloxonium cation by electron impact on either *n*-butanol or propane-1,3-diol. Their identification of the $C_2H_5O^+$ ion from these precursors as $CH_2CHOH_2^+$ came from collisional activation and charge-stripping experiments. When we subjected *n*-butanol and propane-1,3-diol to electron impact in our ion source at *ca.* 10^{-3} Torr, the resultant $C_2H_5O^+$ ion, after mass selection and injection into the flow tube, did not transfer protons to 4-fluorotoluene or methanol. The rate coefficient we observed for this ion with 4-fluorotoluene and methanol ($k \leqslant 5 \times 10^{-10}$ cm^3 s^{-1}) is faster than the rate coefficient observed for $CH_3OCH_2^+$ with methanol ($k = 2 \times 10^{-11}$ cm^3 s^{-1}). We therefore conclude that the $C_2H_5O^+$ ion produced by fragmentation electron impact is either CH_3CHOH^+ or $\underline{CH_2OHCH_2}^+$. It clearly was not the $CH_2CHOH_2^+$ ion but we acknowledge that the conditions in our SIFT experiment were quite different from those of Burgers *et al.*[16] High repeller energies in the ion source were required in order to generate sufficient ion signal.

The question of the identity of the less reactive isomer present in the $C_2H_2 \cdot H_3O^+$ mixture of isomers, identified by its unreactivity to proton transfer, is not so easily answered. The less reactive $C_2H_5O^+$ component in the isomeric mixture reacted at *ca.* 25% of the collision rate with three reagents (see Table 3) and we therefore eliminate the methoxymethyl cation, $CH_3OCH_2^+$, from the list of contenders. $CH_3OCH_2^+$ reacts with CH_3OH more slowly by a factor of ten (2×10^{-11} cm^3 s^{-1}) than the less reactive component in the isomeric mixture (4.7×10^{-10} cm^3 s^{-1}). We are therefore left with CH_3CHOH^+, $\underline{CH_2OHCH_2}^+$ or the electrostatic complex, $H_3O^+ \cdot C_2H_2$, as the species contributing to the less-reactive component in the isomeric mixture. The adduct of $C_2H_2 \cdot H_3O^+$ and 4-fluorotoluene was observed in the reaction with 4-fluorotoluene. From Table 2 we find that the adduct was not seen as a major component in the product ions from the reaction between $\underline{CH_2OHCH_2}^+$ and 4-fluorotoluene but it was present as the major product of the reaction with CH_3CHOH^+. Although not providing unequivocal evidence, the product distribution comparison favours either CH_3CHOH^+ as the isomer giving rise to the less reactive component in the $C_2H_2 \cdot H_3O^+$ decays, or alternatively, the electrostatic adduct, $H_3O^+ \cdot C_2H_2$, identified in the *ab initio* study. The proton affinities of the neutrals formed from these ions are similar and are in the range where proton transfer from either CH_3CHOH^+ or $H_3O^+ \cdot C_2H_2$ to C_2H_5Br, 4-fluorotoluene, CH_3OH and C_6H_6 is endothermic. Proton transfer to both 2-fluorotoluene and allene is, however, exothermic and for each of these species a single decay was observed, as in these cases both isomeric forms reacted at, or close to, the collision rate.

Conclusions

Reactivity, in the present case through proton-transfer reactions, has proven to be a sensitive probe of structure. The results of this study show that at least two isomeric species are formed in the association reaction between H_3O^+ and C_2H_2:

$$H_3O^+ + C_2H_2 + M \xrightarrow{ca.\ 0.5} CH_2CHOH_2^+ + M \quad (14a)$$

$$\xrightarrow{ca.\ 0.5} CH_3CHOH^+(?) + M \quad (14b)$$

The $C_2H_5O^+$ association product ions are present as a *ca.* 50 : 50 mixture of protonated vinyl alcohol ($CH_2CHOH_2^+$) and either protonated acetaldehyde (CH_3CHOH^+) or the electrostatic complex $H_3O^+ \cdot C_2H_2$. These results differ from the conclusions of Jarrold *et al.*[2] who examined the product of the association reaction (3) using the technique of CID. They concluded that the likely product of the association was CH_3CHOH^+. Their conclusions must now be modified, however, as they did not consider $CH_2CHOH_2^+$ as a possible structure.

In our laboratory experiment, the $C_2H_5O^+$ product ions of the association reaction are stabilized by collision with the bath gas. In interstellar clouds, however, the $(C_2H_5O^+)^*$ complex formed in the association process is stabilized by photon emission. Although these two stabilizing mechanisms differ, it is unlikely that the outcomes of the different stabilizing mechanisms will result in different structures. If reaction (14) followed by dissociative recombination [reaction (2)] is responsible for some of the interstellar CH_3CHO then the question must also be raised as to the possibility of detecting interstellar vinyl alcohol in regions where acetaldehyde has been observed.

We thank the New Zealand Lottery Grants Board for financial support.

References

1 L. E. Snyder, in *Molecules in Space*, ed. D. A. Buckingham, Spectroscopy, Physical Chemistry, Ser. 1.6, 193; MTP Int. Rev. Sci., 3, Butterworth, London 1972.

2 M. F. Jarrold, N. J. Kirchner, S. Liu and M. T. Bowers, *J. Phys. Chem.*, 1986, **90**, 78.
3 E. Herbst, *Astrophys. J.*, 1987, **313**, 867.
4 E. Herbst, D. Smith, N. G. Adams and B. J. McIntosh, *J. Chem. Soc., Faraday Trans. 2*, 1989, **85**, 1655.
5 M. J. McEwan, in *Advances in Gas Phase Ion Chemistry*, ed. N. G. Adams and L. M. Babcock, J.A.I. Press, Greenwich, CT, 1992, vol. 1, p. 1.
6 R. H. Nobes, W. R. Rodwell, W. J. Bouma and L. Radom, *J. Am. Chem. Soc.*, 1981, **103**, 1913.
7 R. H. Nobes and L. Radom, *Chem. Phys. Lett.*, 1983, **99**, 107.
8 L. A. Curtiss, D. J. Lucas and J. A. Pople, *J. Chem. Phys.*, 1995, **102**, 3292.
9 S. G. Lias, J. E. Bartmess, J. F. Liebman, J. L. Holmes, R. D. Levin and W. G. Mallard, *J. Phys. Chem. Ref. Data*, 1988, 17, Suppl. No. 1.
10 B. Ruscic and J. Berkowitz, *J. Chem. Phys.*, 1994, **101**, 10936.
11 L. A. Curtiss, K. Raghavachari, G. W. Trucks and J. A. Pople, *J. Chem. Phys.*, 1991, **94**, 7221.
12. B. J. Smith and L. Radom, *J. Am. Chem. Soc.*, 1993, **115**, 4885.
13 M. J. Frisch, G. W. Trucks, M. Head-Gordon, P. M. W. Gill, M. W. Wong, J. B. Foresman, B. G. Johnson, H. B. Schlegel, M. A. Robb, E. S. Replogle, R. Gomperts, J. L. Andres, K. Raghavachari, J. S. Binkley, C. Gonzalez, R. L. Martin, D. J. Fox, D. J. DeFrees, J. Baker, J. J. P. Stewart and J. A. Pople, GAUSSIAN 92, Gaussian Inc., Pittsburgh PA, 1992.
14 C. G. Freeman, J. S. Knight, J. G. Love and M. J. McEwan, *Int. J. Mass Spectrom. Ion Proc.*, 1987, **80**, 255.
15 T. Su and W. J. Chesnavich, *J. Chem. Phys.*, 1982, **76**, 5183.
16 P. C. Burgers, J. K. Terlouw and J. L. Holmes, *Org. Mass Spectrom.*, 1982, **17**, 369.

Paper 5/04067A; *Received* 23*rd June*, 1995

2848 *J. Phys. Chem. A* **1997**, *101*, 2848−2851

$C_2H_7O^+$ Potential Surface and Ion−Molecule Association between H_3O^+ and C_2H_4

David A. Fairley, Graham B. I. Scott, Colin G. Freeman, Robert G. A. R. Maclagan, and Murray J. McEwan*

Department of Chemistry, University of Canterbury, Christchurch, New Zealand

Received: October 22, 1996; In Final Form: January 30, 1997[⊗]

The $C_2H_7O^+$ potential surface has been explored using the G2 procedure. Four stable structures were identified: protonated ethanol, $C_2H_5OH_2^+$, protonated dimethyl ether, $(CH_3)_2OH^+$, and the electrostatic complexes $C_2H_4\cdots H\cdots OH_2^+$ and $CH_3^+\cdots HOCH_3$. Experiments conducted using a selected ion flow tube identify the $H_3O^+\cdot C_2H_4$ product of the ion−molecule association reaction $H_3O^+ + C_2H_4$ as $C_2H_5OH_2^+$, protonated ethanol. Rate coefficients and branching ratios are reported for reactions of the $C_2H_7O^+$ ions—$H_3O^+\cdot C_2H_4$ formed in the reaction of $H_3O^+ + C_2H_4$, $C_2H_5OH_2^+$, and $(CH_3)_2OH^+$—with acrylonitrile and 2-fluorotoluene.

Introduction

Ethanol is one of the molecules observed in interstellar clouds, and although it is not found in cold, dark clouds, it is present in appreciable abundances in regions where stars are formed.[1−3] Model calculations have used a variety of reactions, both gas phase and heterogeneous reactions on grain surfaces, as sources of C_2H_5OH in the interstellar medium.[3−5] Among the gas phase reactions considered in the models are the following ion−molecule association reactions:

$$CH_3^+ + CH_3OH \rightarrow (CH_3)_2OH^+ + h\nu \quad (1a)$$

$$\rightarrow C_2H_5OH_2^+ + h\nu \quad (1b)$$

$$H_3O^+ + C_2H_4 \rightarrow C_2H_5OH_2^+ + h\nu \quad (2)$$

C_2H_5OH has been assumed in the models to be formed from $C_2H_5OH_2^+$ in a dissociative recombination reaction.

$$C_2H_5OH_2^+ + e \rightarrow C_2H_5OH + H \quad (3)$$

Several stable isomers of $C_2H_7O^+$ are possible, and it is not certain which isomeric species or mixture of species might be produced from an ion−molecule association process. Likely stable isomers of association reactions coincide with valleys on the $C_2H_7O^+$ potential surface and include $C_2H_5OH_2^+$ (protonated ethanol), $(CH_3)_2OH^+$ (protonated dimethyl ether), $C_2H_4\cdots H\cdots OH_2^+$, and $CH_3^+\cdots HOCH_3$ (electrostatic-type complexes). Jarrold *et al.*[6] examined the collision-induced dissociation (CID) spectra of $C_2H_5OH_2^+$ and $(CH_3)_2OH^+$ and concluded that the association product of reaction 1 has predominantly the $(CH_3)_2OH^+$ structure while the product of reaction 2 has mainly the $C_2H_5OH_2^+$ structure.

In this study we have probed the structure of the $C_2H_7O^+$ ion formed in the termolecular analogue of reaction 2 by examining its proton transfer reactions using a selected ion flow tube (SIFT) with the neutral reagents 2-fluorotoluene and acrylonitrile. The technique has been used previously to probe the structures of several other products of ion−molecule association.[7,8] We have also undertaken ab initio calculations of the $C_2H_7O^+$ energy surface to assist in the interpretation of our experiments.

Experimental Section

The experiments reported here were carried out using the SIFT at Canterbury University operating at room temperature (300 ± 5) K as described previously.[9] The $C_2H_7O^+$ ions examined in this work were produced in the following ways. The product ion of the association reaction 4b, which we designate $H_3O^+\cdot C_2H_4$, was formed in the flow tube by injecting H_3O^+ into a stream of C_2H_4 introduced at the first inlet port.

$$H_3O^+ + C_2H_4 \rightarrow C_2H_5^+ + H_2O \quad (4a)$$

$$\xrightarrow{M} H_3O^+\cdot C_2H_4 \quad (4b)$$

Sufficient C_2H_4 was added to remove >99% of the H_3O^+ ion signal. In the process, $C_2H_5^+$ produced in reaction 4a was completely converted into predominantly $(C_2H_4)_2H^+$ and $C_5H_9^+$, neither of which reacted further with 2-fluorotoluene and CH_2-CHCN.

The products of reaction 4 were first established by Bohme and Mackay[10] and also by McIntosh *et al.*[11] Our measurement of the rate coefficient for the reaction ($k = 8.4 \times 10^{-11}$ cm^3 s^{-1}) and of the branching ratio ($H_3O^+\cdot C_2H_4 = 30\%$) at 0.35 Torr of helium is in reasonable agreement with the earlier measurements when allowance is made for the different bath gas pressures between different experiments. (McIntosh *et al.*[11] report a rate coefficient of 1×10^{-10} cm^3 s^{-1} with a branching ratio of 60% adduct at a helium pressure of 0.45 Torr.) Our measurement is also in excellent agreement with that given in the accompanying paper by Matthews *et al.* of $k = 7.8 \times 10^{-11}$ cm^3 s^{-1}.[12]

The $C_2H_5OH_2^+$ ion was generated in the ion source by initial electron impact on C_2H_5OH, followed by H atom abstraction (reaction 5).

$$C_2H_5OH^+ + C_2H_5OH \rightarrow C_2H_5OH_2^+ + C_2H_5O \quad (5)$$

Alternatively $C_2H_5OH_2^+$ was formed in the flow tube by injecting H_2CN^+ into the helium carrier gas and adding C_2H_5-OH at the first neutral inlet. This prevents any breakup from $C_2H_5OH_2^+$ that occurs during the injection process. A similar technique was used to produce the $(CH_3)_2OH^+$ ion by subjecting

[⊗] Abstract published in *Advance ACS Abstracts*, March 15, 1997.

S1089-5639(96)03294-X CCC: $14.00

$(CH_3)_2O$ to electron impact in the ion source and, after mass selection, injecting $(CH_3)_2OH^+$ into the flow tube.

All reagents were obtained from commercial sources. A trace of the radical inhibitor, 4-methoxyphenol, was added to acrylonitrile to prevent polymerization in the absence of oxygen.

Results

SIFT Experiments. We examined the reactions of three $C_2H_7O^+$ isomers ($H_3O^+\cdot C_2H_4$, $C_2H_5OH_2^+$, and $(CH_3)_2OH^+$) with the reagents 2-fluorotoluene, C_7H_7F, and acrylonitrile, CH_2-CHCN. We also examined the reaction of $H_3O^+\cdot C_2H_4$ with CH_3OH. These three reagents were selected on the basis of their known proton affinities (PAs) which are (in kJ mol^{-1}) C_7H_7F (PA = 782); CH_2CHCN (PA = 794), and CH_3OH (PA = 761).[13] The following results were obtained:

$$H_3O^+\cdot C_2H_4 + CH_3OH \rightarrow \text{adduct} \quad (1.0) \qquad (6)$$

$$k = 6.9 \times 10^{-10}\ cm^3\ s^{-1}$$

$$H_3O^+\cdot C_2H_4 + C_7H_7F \rightarrow C_7H_8F^+ + C_2H_5OH \quad (0.65) \quad (7)$$

$$\rightarrow \text{adduct} \quad (0.35)$$

$$k = 5.4 \times 10^{-10}\ cm^3\ s^{-1}$$

$$H_3O^+\cdot C_2H_4 + CH_2CHCN \rightarrow CH_2CHCNH^+ + C_2H_5OH \quad (0.40) \quad (8)$$

$$\rightarrow \text{adduct} \quad (0.60)$$

$$k = 3.2 \times 10^{-9}\ cm^3\ s^{-1}$$

$$C_2H_5OH_2^+ + C_7H_7F \rightarrow C_7H_8F^+ + C_2H_5OH \quad (\sim 0.70) \quad (9)$$

$$\rightarrow \text{adduct} \quad (\sim 0.30)$$

$$k = 4.3 \times 10^{-10}\ cm^3\ s^{-1}$$

$$C_2H_5OH_2^+ + CH_2CHCN \rightarrow CH_2CHCNH^+ + C_2H_5OH \quad (0.50) \quad (10)$$

$$\rightarrow \text{adduct} \quad (0.50)$$

$$k = 3.2 \times 10^{-9}\ cm^3\ s^{-1}$$

$$(CH_3)_2OH^+ + C_7H_7F \rightarrow \text{adduct} \quad (1.0) \qquad (11)$$

$$k = 1.9 \times 10^{-10}\ cm^3\ s^{-1}$$

$$(CH_3)_2OH^+ + CH_2CHCN \rightarrow \text{adduct} \quad (1.0) \qquad (12)$$

$$k = 2.3 \times 10^{-9}\ cm^3\ s^{-1}$$

Branching ratios for the product channels are shown in parentheses following the stated channel, and the rate coefficients for each reaction are also given. Although the rate coefficients for adduct formation are presented as simple bimolecular processes, the adducts are undoubtedly formed via collisional stabilization of the $(AB^+)^*$ complex. The rate coefficient for adduct formation may therefore exhibit some sensitivity to pressure, although the rate coefficients observed in most of the reactions 6−12 suggest that collisional stabilization is approaching the pressure-saturation regime at our operating pressure of 0.35 Torr of helium bath gas.

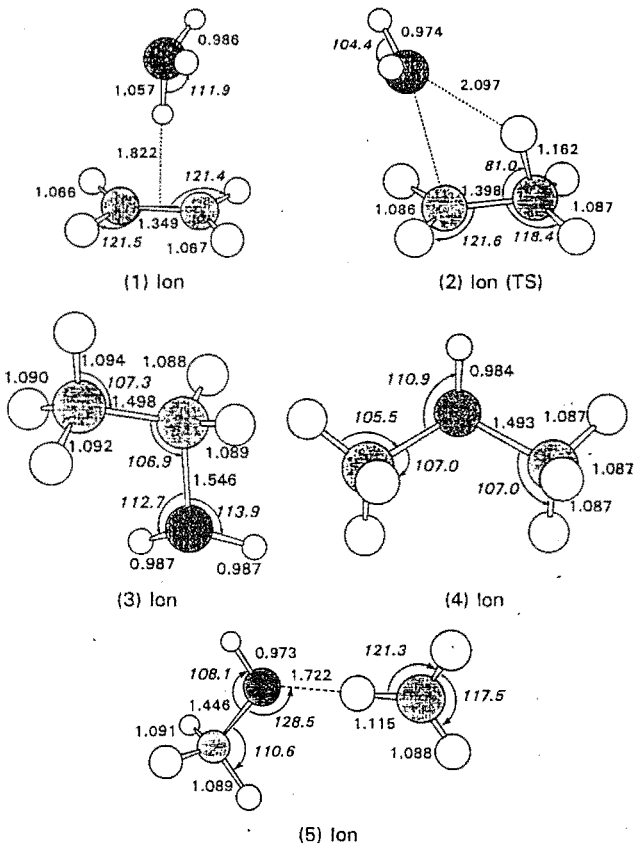

Figure 1. MP2/6-31G* optimized geometries for the designated $C_2H_7O^+$ species with bond lengths in Å and bond angles in deg.

We have presented the neutral products of $H_3O^+\cdot C_2H_4$ in reactions 7 and 8 as C_2H_5OH rather than $H_2O + C_2H_4$. Evidence presented in the Discussion section will show that the C_2H_5OH representation of the neutral product is a likely outcome in these two reactions.

A summary of the experimental results is presented in Table 1.

Ab Initio Studies. Two isomers of $C_2H_7O^+$, protonated ethanol, $C_2H_5OH_2^+$, and protonated dimethyl ether, $(CH_3)_2OH^+$, have been well characterized and identified experimentally as distinct isomeric species that retain their identifies under a wide range of conditions. Their enthalpies of formation have been determined.[13] Bouchoux and Hoppilliard in an ab initio study[15] characterized an electrostatic complex $C_2H_4\cdots H\cdots OH_2^+$ that is readily accessible from $C_2H_5OH_2^+$. Recently Audier *et al.*[16] also identified an electrostatic complex $CH_3^+\cdots HOCH_3$ formed from the association of CH_3^+ and CH_3OH, which they predicted to be separated by a small potential barrier from $(CH_3)_2OH^+$. In our calculations we identified four stable $C_2H_7O^+$ structures corresponding to minima on the potential energy surface using the G2 procedure.[17,18] These structures, in order of decreasing stability are: protonated ethanol, protonated dimethyl ether, and electrostatic complexes $C_2H_4\cdots H_2\cdots OH_2^+$, and $CH_3^+\cdots HOCH_3$. Our calculations of the $C_2H_7O^+$ potential surface are the first extended calculations of this surface at the G2 level of theory.

Formation of the $H_3O^+\cdot C_2H_4$ electrostatic π complex involves approach of the oxygen atom of H_3O^+ toward the midpoint of the C−C double bond with the formation of a hydrogen bond directed toward the center of the double bond (i.e. the most basic site). (See **1** in Figure 1.) The transition state between $H_3O^+\cdot C_2H_4$ and $C_2H_5OH_2^+$ resembles a loose association between a classical $C_2H_5^+$ ion and a water molecule. (See **2** in

TABLE 1: Reaction Rate Coefficients and Product Ratios with the Specified Reagent for the Three $C_2H_7O^+$ Ions: $H_3O^+ \cdot C_2H_4$, Protonated Ethanol, $C_2H_5OH_2^+$, and Protonated Dimethyl Ether, $(CH_3)_2OH^+$

reactant	products	branching ratio	k_{obs} (10^{-9} cm^3 s^{-1})	k_{coll}[a] (10^{-9} cm^3 s^{-1})
		$H_3O^+ \cdot C_2H_4$		
CH_3OH	adduct	1.0	0.69	2.1
C_7H_7F[b]	$C_7H_8F^+ + C_2H_5OH$[c]	0.65	0.54	1.9
	adduct	0.35		
CH_2CHCN	$CH_2CHCNH^+ + C_2H_5OH$[c]	0.40	3.2	3.8
	adduct	0.60		
		$C_2H_5OH_2^+$		
C_7H_7F[b]	$C_7H_8F^+ + C_2H_5OH$	~0.70	0.43	1.9
	adduct	~0.30		
CH_2CHCN	$CH_2CHCNH^+ + C_2H_5OH$	0.50	3.2	3.8
	adduct	0.50		
		$(CH_3)_2OH^+$		
C_7H_7F[b]	adduct	1.0	0.19	1.9
CH_2CHCN	adduct	1.0	2.3	3.8

[a] Reference 14. [b] 2-fluorotoluene. [c] See text for discussion.

TABLE 2: Calculated Enthalpies of Formation and Proton Affinities of C_2H_6O Isomers

	$\Delta_f H^\circ$ (kJ mol^{-1})		E_{pa}/kJ mol^{-1}	
structure	calc[a]	exp[b]	calc[c]	exp
CH_3CH_2OH	−233.6	−234.7	780.4	788[b]
$(CH_3)_2O$	−190.2	−184.0	791.1	804[b]
$H_2O + C_2H_4$	−180.2	−189.5	767.5[d]	

[a] Calculated enthalpies of formation at 298 K at the G2 level of theory using $E_{G2}(C_2H_6O) - E_{G2}(H_2O) - E_{G2}(C_2H_4) = \Delta_f H^\circ(C_2H_6O) - \Delta_f H^\circ(H_2O) - \Delta_f H^\circ(C_2H_4)$. Substitution of $\Delta_f H^\circ(H_2O)$ and $\Delta_f H^\circ(C_2H_4)$ from ref 13 yields $\Delta_f H^\circ(C_2H_6O)$. [b] Experimental values are from ref 13. [c] Calculated proton affinities at 298 K at the G2 level of theory. [d] Calculated in the usual way using the equation $H_2O + C_2H_4 + H^+ \rightarrow H_3O^+ \cdot C_2H_4$.

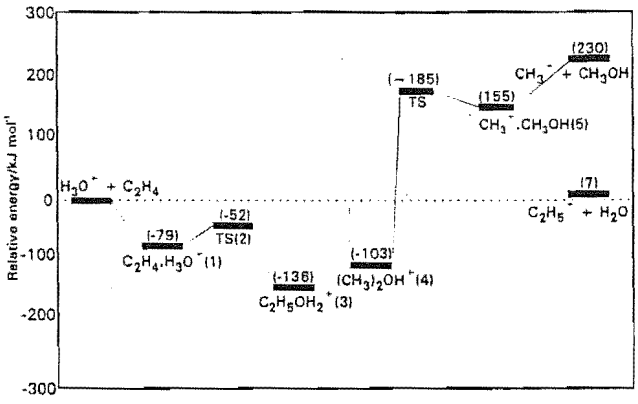

Figure 2. $C_2H_7O^+$ energy surface calculated using the G2 procedure. The energies are expressed in kJ mol^{-1} relative to $H_3O^+ + C_2H_4$ and are corrected to 298 K and for zero-point energy.

Figure 1.) Collision complexes with sufficient excitation energy may dissociate to $C_2H_5^+ + H_2O$ (reaction 4a): this proton transfer is calculated to be 7 kJ mol^{-1} endothermic. Complexes below this threshold can either dissociate back to reactants or be stabilized to form $C_2H_5OH_2^+$, which lies 136 kJ mol^{-1} below the reactants, $H_3O^+ + C_2H_4$. This mechanism supports the intuitive assumption that formation of $C_2H_5OH_2^+$ is more likely than $(CH_3)_2OH^+$ since the latter requires significantly more rearrangement.

In the reaction of CH_3^+ with CH_3OH, an electrostatic complex is formed with the CH_3^+ moiety attached by a H atom to the O atom of CH_3OH, with a binding energy of 75 kJ mol^{-1}. If the C−O bond distance is decreased, the energy of the system is raised until, at approximately R(C−O) = 2.6 Å, the CH_3^+ moiety is flipped to allow bonding between the C atom of CH_3^+ and the O atom of CH_3OH. The barrier between the

TABLE 3: G2 Energies and Relative Energies of $C_2H_7O^+$ Species at 298 K

		$\Delta E(G2)$[a]	$\Delta_f H^\circ$ (kJ mol^{-1})	
structure	E(G2)	(kJ mol^{-1})	calc	expt[b]
$H_3O^+ + C_2H_4$	−155.00200	0.0	657.4	642.3
$H_3O^+ \cdot C_2H_4$	−155.03212	−79.1	563.2	
$C_2H_5OH_2^+$	−155.05385	−136.1	506.2	506.3
TS (2)	−155.02195	−52.4		
$(CH_3)_2OH^+$	−155.04141	−103.5	538.8	544.0
$C_2H_5^+ + H_2O$	−154.99953	6.5	669.4	660.2
$CH_3^+ \cdot HOCH_3$	−154.94289	155.2	816.7	
$CH_3^+ + CH_3OH$	−154.91435	230.1	883.8	891.6

[a] Relative to $H_3O^+ + C_2H_4$. [b] Values from ref 13.

$CH_3^+ \cdots HOCH_3$ electrostatic complex and $(CH_3)_2OH^+$ is about 30 kJ mol^{-1}. An experimental investigation of the $CH_3^+ + CH_3OH$ reaction is presented in the accompanying paper by Matthews *et al.*[12]

A summary of some of the ab initio results showing the calculated proton affinities of the different C_2H_6O species is given in Table 2. Smith and Radom[18] have also calculated the proton affinity of $(CH_3)_2O$ using the G2 procedure as 792 kJ mol^{-1}.

The potential energy diagram relevant to the ion−molecule association reactions $H_3O^+ + C_2H_4$ and $CH_3^+ + CH_3OH$ incorporating our calculations is shown in Figure 2. The G2 energies of some of the ions and transition states on the $C_2H_7O^+$ surface are summarized in Table 3.

Discussion

The reaction chemistry summarized in Table 1 distinguishes clearly between the isomeric species, $C_2H_5OH_2^+$ and $(CH_3)_2OH^+$, on the basis of the different proton affinities of C_2H_5OH and $(CH_3)_2O$. Both ions exhibited near collision rate reactions with CH_2CHCN (PA = 794 kJ mol^{-1}), but protonated ethanol, $C_2H_5OH_2^+$, yielded a 50% proton transfer product channel whereas protonated dimethyl ether, $(CH_3)_2OH^+$, yielded only adduct. Both ions underwent slower reactions with 2-fluorotoluene (PA = 782 kJ mol^{-1}), but whereas $C_2H_5OH_2^+$ yielded a 70% proton transfer product channel and a faster reaction, no proton transfer was found for $(CH_3)_2OH^+$. These findings are in accord with the established proton affinities of C_2H_5OH (PA = 788 kJ mol^{-1}) and $(CH_3)_2O$ (PA = 804 kJ mol^{-1}).

What is also evident from the experimental studies is that the association adduct, $H_3O^+ \cdot C_2H_4$, formed in reaction 4b is indistinguishable in our experiments from $C_2H_5OH_2^+$. The calculated G2 proton affinity of $(H_2O + C_2H_4)$ is 768 kJ mol^{-1}.

Our choice of CH_3OH (PA = 761 kJ mol^{-1}) as a neutral reagent for $H_3O^+ \cdot C_2H_4$ was influenced by this value. If the $H_3O^+ \cdot C_2H_4$ association ion product is the electrostatic ion, $C_2H_4 \cdots H \cdots OH_2^+$, identified in the ab initio studies, then proton transfer to CH_3OH might be expected. None was observed. Further, the rate coefficients and product distributions of the reactions of $H_3O^+ \cdot C_2H_4$ with C_7H_7F and CH_2CHCN are identical (within the experimental uncertainty) with those of $C_2H_5OH_2^+$ giving strong support to the identification of $H_3O^+ \cdot C_2H_4$ as $C_2H_5OH_2^+$. The transition state barrier between the two structures is only 27 kJ mol^{-1} relative to $C_2H_4 \cdot H_3O^+$ (Figure 2), and it is apparent that at the entrance level of $H_3O^+ + C_2H_4$ there is ample energy to overcome this small barrier and sample the surface above the $C_2H_5OH_2^+$ global minimum.

We conclude therefore that the experimental evidence supports the structure of the $H_3O^+ \cdot C_2H_4$ association adduct being $C_2H_5OH_2^+$. Although the accompanying paper of Matthews *et al.*[12] provides evidence for some fraction of the $C_2H_7O^+$ ion formed in the association reaction 4b being in the electrostatic form, some interconversion to $C_2H_5OH_2^+$ is possible. Our results from the product ratios of the two reagents studied (C_7H_7F and CH_2CHCN) do not allow us to state unequivocally that the electrostatic form is accessed. Two earlier studies also favor $C_2H_5OH_2^+$ as the structure of the $H_3O^+ \cdot C_2H_4$ adduct. Jarrold *et al.*[6] found supporting evidence from CID studies. Herbst *et al.*[19] compared the measured ternary reaction rate coefficient of reaction 4b with calculated values that were based on a designated structure of the $C_2H_7O^+$ product ion. They obtained satisfactory agreement between theory and experiment when they assumed an adduct structure of $C_2H_5OH_2^+$.

Conclusions

Proton transfer reactions can be used as a sensitive probe of structure.[7-9] We have utilized ab initio calculations of the $C_2H_7O^+$ energy surface and experimental observations of the proton transfer reactivity of the $C_2H_7O^+$ isomers, $C_2H_5OH_2^+$ and $(CH_3)_2OH^+$, to identify the $H_3O^+ \cdot C_2H_4$ product of reaction 4b as $C_2H_5OH_2^+$. Thus sources of C_2H_5OH in interstellar models utilizing the ion–molecule association reaction 2 remain valid although we note that the products of the subsequent ion–electron recombination reaction 3 have not yet been determined.

The observation of the endothermic proton transfer channel in reaction 4a ($C_2H_5^+ + H_2O$, $\Delta H^\circ = +10.5$ kJ mol^{-1}),[13] which competes with formation of the $H_3O^+ \cdot C_2H_4$ adduct, shows that the exit channel from the $(H_3O^+ \cdot C_2H_4)^*$ complex to $C_2H_5^+ + H_2O$ is found before collisional stabilization can occur. In this work our measurement of the rate coefficient for endothermic proton transfer is 5.9×10^{-11} cm^3 s^{-1} at 0.35 Torr of helium. At 0.45 Torr of helium, McIntosh *et al.*[11] report a rate coefficient for proton transfer of 4.0×10^{-11} cm^3 s^{-1} and Bohme and Mackay[10] report a value of 6.3×10^{-11} cm^3 s^{-1} in a hydrogen carrier gas. The slight variation in rate coefficient in these three measurements is close to the experimental uncertainty. We conclude that the proton transfer channel takes place on a time scale that is much shorter than the time between collisions, *viz.* <125 ns, and proceeds independently of complex stabilization. The branching ratio is therefore expected to vary with pressure because of the variation in the termolecular rate.

Acknowledgment. We thank the Marsden Fund for financial support.

References and Notes

(1) Irvine, W. M.; Goldsmith, P. F.; Hjalmarson, Å. In *Interstellar Processes*; Hollenbach, D. J., Thronson, H. A., Jr., Eds.; Dordrecht: Reidel, 1987; p 561.
(2) Turner, B. E. *Astrophys. J., Suppl. Ser.* **1991**, *76*, 617.
(3) Charnley, S. B.; Kress, M. E.; Tielens, A. G. G. M.; Millar, T. J. *Astrophys. J.* **1995**, *448*, 232.
(4) Herbst, E.; Leung, C. M. *Astrophys. J., Suppl. Ser.* **1989**, *69*, 271.
(5) Herbst, E. *Astrophys. J.* **1987**, *313*, 867.
(6) Jarrold, M. F.; Kirchner, N. J.; Liu, S.; Bowers, M. T. *J. Phys. Chem.* **1986**, *90*, 78.
(7) Scott, G. B. I.; Fairley, D. A.; Freeman, C. G.; Maclagan, R. G. A. R.; McEwan, M. J. *Int. J. Mass Spectrom. Ion Processes* **1995**, *149/150*, 251.
(8) Fairley, D. A.; Scott, G. B. I.; Freeman, C. G.; Maclagan, R. G. A. R.; McEwan, M. J. *J. Chem. Soc., Faraday Trans.* **1996**, *92*, 1305.
(9) McEwan, M. J. In *Advances in Gas Phase Ion Chemistry*; Adams, N. G., Babcock, L. M., Eds.; JAI Press: Greenwich, CT, 1992; Vol. 1, p 1.
(10) Bohme, D. K.; Mackay, G. I. *J. Am. Chem. Soc.* **1981**, *103*, 2173.
(11) McIntosh, B. J.; Adams, N. G.; Smith, D. *Chem. Phys. Lett.* **1988**, *148*, 142.
(12) Matthews, K. K.; Adams, N. G.; Fisher, N. D. *J. Phys. Chem. A* **1997**, *101*, 2841.
(13) Lias, S. G.; Bartmess, J. E.; Liebman, J. F.; Holmes, J. L.; Levin, R. D.; Mallard, W. G. *J. Phys. Chem. Ref. Data* **1988**, *17*, Suppl. 1.
(14) Su, T.; Chesnavich, W. J. *J. Chem. Phys.* **1982**, *76*, 5183.
(15) Bouchoux, G.; Hoppilliard, Y. *J. Am. Chem. Soc.* **1990**, *112*, 9110.
(16) Audier, H. E., Koyanagi, G. K., McMahon, T. B., Tholmann, D. *J. Phys. Chem.* **1996**, *100*, 8220.
(17) Curtiss, L. A.; Raghavachari, K.; Trucks, G. W.; Pople, J. A. *J. Chem. Phys.* **1991**, *94*, 7221.
(18) Smith, B. J.; Radom, L. *J. Am. Chem. Soc.* **1993**, *115*, 4885.
(19) Herbst, E.; Smith, D.; Adams, N. G.; McIntosh, B. J. *J. Chem. Soc., Faraday Trans. 2* **1989**, *85*, 1655.

Reprinted from

International Journal of

Mass Spectrometry and Ion Processes

International Journal of Mass Spectrometry and Ion Processes 172 (1998) 79–87

SIFDT study of the SO_2^+/H_2 H-atom abstraction reaction

David A. Fairley, Graham B.I. Scott, Daniel B. Milligan, Robert G.A.R. Maclagan, Murray J. McEwan*

Department of Chemistry, University of Canterbury, Christchurch, New Zealand

Received 11 July 1997; accepted 4 September 1997

ELSEVIER

INTERNATIONAL JOURNAL OF MASS SPECTROMETRY AND ION PROCESSES

GENERAL INFORMATION

Scope of the journal

The journal contains papers which consider fundamental aspects of mass spectrometry and ion processes, and the application of mass spectrometric techniques to specific problems in chemistry and physics. The following topics, amongst others, can be found in the journal: theoretical and experimental studies of ion formation (i.e. by electrons, laser or other forms of radiation, heavy ions, high-energy particles, etc.), ion separation and ion detection processes; the design and performance of instruments (or their parts) and accessories; measurements of natural isotopic abundances, precise isotopic masses, ionization, appearance and excitation energies, ionization cross-sections; development of techniques related to determining molecular structures, geological age determination, studies of thermodynamic properties, chemical kinetics, surface phenomena, radiation chemistry, and chemical analyses; theory of mass spectra, application of computer techniques to mass spectral data; chemistry and physics of cluster ions; spectroscopy of gaseous ions including studies related to interstellar chemistry; mechanistic studies of unimolecular processes and ion/molecule reactions in the gas phase including computational aspects (ion trajectory calculations, quantum mechanical studies of potential energy surfaces); physical organic chemistry of isolated ions; biological applications of mass spectrometry.

The journal is of interest to all mass spectrometrists and other scientists interested in the chemistry and physics of charged particles.

Categories of manuscripts

The journal welcomes the following types of papers.

Full-length articles: Comprehensive description and discussion of original research investigations; the experimental techniques must be described in detail.

Letters: Brief reports (no longer than 4 printed pages or 2000 words) of significant, original and timely research. In considering the suitability of a letter for publication, the editors pay particular attention to the originality of the research and the desirability of rapid publication. **Letters will be published within 6–8 weeks** after acceptance of the article by the editor concerned. No proofs will be sent to the authors.

Reviews: Timely, critical reviews will focus on recent developments while keeping historical documentation to a minimum. Reviews will often be solicited, but prospective authors are also encouraged to contact the editors or editorial board members regarding the appropriateness of the subject matter. In general the length should not exceed 30–40 printed pages. The publisher provides authors of Reviews with a modest honorarium.

Book Reviews: Normally invited by the editors, the style should conform to that of previously published Book Reviews.

 0168-1176/98/$17.00

ELSEVIER

International Journal of Mass Spectrometry and Ion Processes 172 (1998) 79–87

International Journal of Mass Spectrometry and Ion Processes

SIFDT study of the SO_2^+/H_2 H-atom abstraction reaction

David A. Fairley, Graham B.I. Scott, Daniel B. Milligan, Robert G.A.R. Maclagan, Murray J. McEwan*

Department of Chemistry, University of Canterbury, Christchurch, New Zealand

Received 11 July 1997; accepted 4 September 1997

Abstract

The exothermic H-atom abstraction reaction of SO_2^+ with H_2 has been studied in a selected ion flow drift tube (SIFDT) over a range of center-of-mass energies from thermal (300 K) to about 0.12 eV. The measured rate coefficient at 300 K is 4.2×10^{-12} cm^3 s^{-1} which is very much less than the Langevin capture rate. The increase in rate coefficient with ion kinetic energy gives a linear Arrhenius-type plot with a slope that indicates a barrier of ~5 kJ mol^{-1} exists on the potential surface. The $H_2SO_2^+$ potential surface is also explored in an ab initio investigation using the G2 procedure. An $(SO_2^+.H_2)^*$ transition state between reactants and products is identified, corresponding to the barrier found from experiments. © 1998 Elsevier Science B.V.

Keywords: SIFDT; H-atom abstraction; Ab initio; Potential barrier; Ion-molecule

1. Introduction

Hydrogen atom abstraction reactions are an important class of ion/molecule reactions that are responsible for the hydrogenation of many ionic species in the interstellar medium [1]. For many types of positive ions it appears that if H-atom abstraction is exothermic, it is fast [2,3], although there are a number of notable exceptions to this general rule. One such exception is the $NH_3^+ + H_2$ reaction which although exothermic to $NH_4^+ + H$ is very slow at room temperature [4] but at very low temperatures the rate coefficient increases due to tunnelling through a potential barrier [5]. Another well-studied example of H-atom abstraction is the reaction between ℓ–C_3H^+ and H_2

$$\ell-C_3H^+ + H_2 \rightarrow c-C_3H_2^+ + H \quad (1)$$

which was observed to be slow and from its rate coefficient predicted to be endothermic by about 4 kJ mol^{-1} [6]. Further experiments on H-atom abstraction led Prodnuk et al. [3] to propose that reaction (1) was actually exothermic by 24 kJ mol^{-1}. Their conclusion was based on the H-atom abstraction reaction $c-C_3H_2^+ + H_2O$ which they observed to be slow. Because it was slow they concluded that it was endothermic. Their basis for this assumption was that H-atom abstraction reactions, if exothermic, are generally fast except when the neutral reagent is molecular hydrogen [3]. Later theoretical calculations by Wong and Radom [7] however found reaction (1) was in fact endothermic by 4 kJ mol^{-1} and that the reason for the slow H-atom abstraction between $c-C_3H_2^+$ and H_2O was because of a 23 kJ mol^{-1} barrier on the reaction path.

The conclusion from these and other studies is that small rate coefficients for H-atom abstraction

* Corresponding author.

PII S0168-1176(97)00242-5

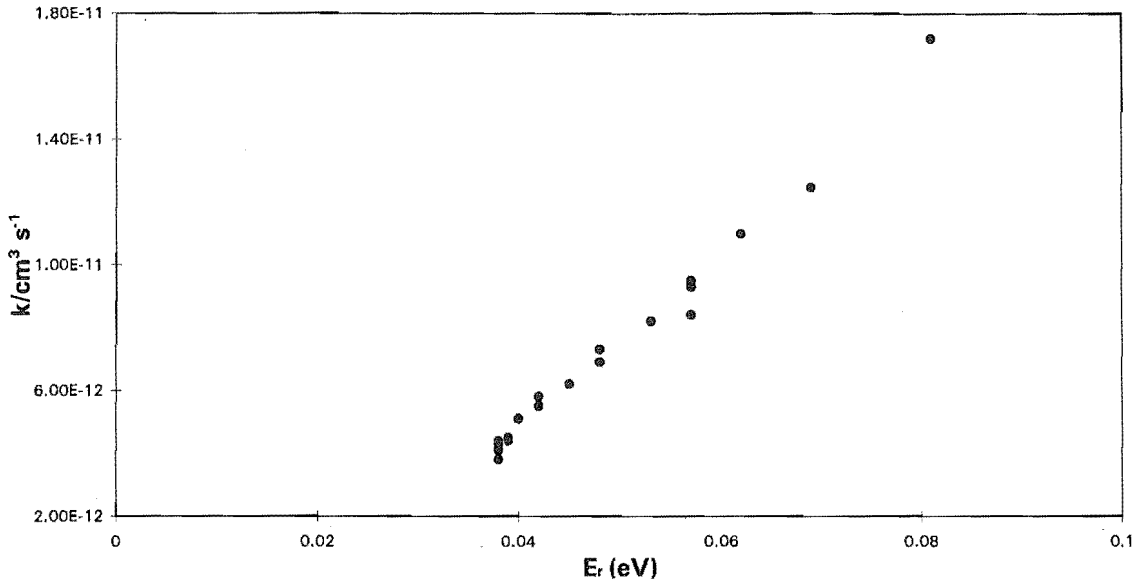

Fig. 1. Variations in the rate coefficient k for the H-atom abstraction reaction $SO_2^+ + H_2$ with E_r.

reactions do not necessarily provide a reliable guide for the thermochemistry. Several of these reactions appear to have barriers on the potential surface. H-atom abstraction reactions possessing kinetic barriers may not be important at the low temperatures of the interstellar environment unless a new mechanism takes over as quantum tunnelling is assumed to in the $NH_3^+ + H_2$ reaction [5].

The investigation of H-atom abstraction reactions in a drift tube may, in favourable circumstances, provide information on the nature of any barrier. In the present study we examine the behaviour of the H-atom abstraction reaction between $SO_2^+ + H_2$ in a selected ion flow drift tube (SIFDT). Although reaction (2) is exothermic by

$$SO_2^+ + H_2 \rightarrow OSOH^+ + H \quad (2)$$

75 kJ mol^{-1} [8] and should therefore be fast, the reported rate coefficient is only $k \sim 5 \times 10^{-12}$ cm^3 s^{-1} [9] which is much less than the Langevin rate coefficient of 1.5×10^{-9} cm^3 s^{-1}. One other measurement of 1.7×10^{-11} cm^3 s^{-1} has also been reported [10]. There appears to be a barrier to H-atom abstraction and we examine the nature of this barrier in a SIFDT experiment as well as in an ab initio investigation of the $H_2SO_2^+$ potential surface.

2. Experimental

The SIFT used in this work has been described previously [11] so the description will not be repeated here. The drift tube assembly has not been described before. In brief it is similar in design to the drift tube described by Smith and Adams [12] and consists of 50 stainless steel rings (6.03 cm diam. and 9 mm width) held 1 mm apart by ceramic insulators. A 17.5 cm field free extension to the drift tube is attached to the upstream end to ensure the bath gas has settled to laminar flow before entry to the drift field reaction region. The drift time of the ions is measured by applying a 20 μs, 50 V pulse to one of the rings in the drift tube assembly to perturb the ion signal and monitoring the arrival time distribution of the ions using a multichannel scaler. A correction for the transit time of the ions in the detection system is obtained by pulsing a second ring near the nose cone to the

downstream quadrupole mass filter. The ion velocity is then obtained by dividing the distance between the two pulsing rings by the difference between the two flight times. Two excellent reviews of the SIFDT technique have been given by Smith and Adams [12] and Lindinger and Smith [13].

All measurements were made at (300 ± 5) K in a helium bath gas. The SO_2^+ ions in the study were prepared by subjecting a 10% mixture of SO_2 in argon to low energy electron impact in a high pressure ion source. The presence of argon reduced variability in emission from the rhenium filament by pure SO_2.

3. Results and discussion

Rate coefficients for reaction (2) were measured at different values of E/N between 0 and 60 Td, Fig. 1. It is the value of E/N which controls the drift velocity, v_d, of the ions. The drift velocities were calculated from the mobility data for SO_2^+ from B öhringer et al. [14] which were confirmed by measurements of the SO_2^+ ion arrival time distributions at selected E/N values as described above. Our measurements of drift velocities agreed within experimental error, with those of Böhringer et al. At zero field and 0.35 Torr our measured rate coefficient for reaction (2) was 4.2×10^{-12} cm^3 s^{-1}.

It has been traditional to examine the variation in rate coefficient with ion energy by plotting k against the mean ion-reactant gas center-of-mass energy, E_r, where the ion kinetic energy is defined by the Wannier formula [13,15,16]

$$KE_{ion} = \frac{3}{2}k_B T + \frac{M_i v_d^2}{2} + \frac{M_c v_d^2}{2} \quad (3)$$

In Eq. (3), M_i = mass of the ion and M_c = mass of the carrier gas atoms. Converting to the center-of-mass frame of reference gives [17]

$$E_r = [M_r/(M_i + M_r)](KE_{ion} - \frac{3}{2}k_B T) + \frac{3}{2}k_B T \quad (4)$$

where M_r is the mass of the reactant neutral and T is the reactant neutral and bath gas temperature.

For reactions which are predicted to be endothermic or possess an activation barrier it is usual to plot ln k vs. E_r^{-1} to test for Arrhenius behaviour.

$$k = A \exp(-E_a/RT) \quad (5)$$

Implicit in this is the assumption that the effective reaction temperature is equilibrated on E_r, i.e. $E_r = 3/2k"T_{eff}"$. Substitution into (5) yields

$$k = A \exp(-3/2(E_a/E_r)) \quad (6)$$

We plot ln k vs. E_r^{-1} in Fig. 2(a).

Is E_r the best indicator of the reaction energy? The question of energy partitioning in polyatomic ions in a drift tube is a subject of considerable interest. The rotational and vibrational state populations of polyatomic ions are not clearly defined and are different from their zero field thermal distribution. Sufficient evidence exists to expect the rotational state population to equilibrate rapidly to the ion-buffer gas center-of-mass energy [18] and an ion rotational temperature can generally be defined [12,19]. The same cannot be said of the vibrational state population which may exhibit considerable non-thermal excitation at high E/N values and particularly when bath gases heavier than helium are used [20,21]. To assist in the understanding of how the ion energy is partitioned, Glosik et al. [22] and Smith et al. [23] distinguished between two different mean center-of-mass energies: E_r (defined in Eq. (4)) and E_c, where E_c is the reactant ion-carrier gas atom mean center-of-mass energy for a carrier gas of atomic mass M_c

$$E_c = [M_c/(M_i + M_c)](KE_{ion} - \frac{3}{2}k_B T) + \frac{3}{2}k_B T \quad (7)$$

As collisions of the reactant ion with the He bath gas are much more frequent than those with H_2, the internal energy state of the ions prior to their encounter with reactant molecules is described by E_c rather than by E_r [22]. Smith et al. [23] note that as the E_r energy from the ion-reactant

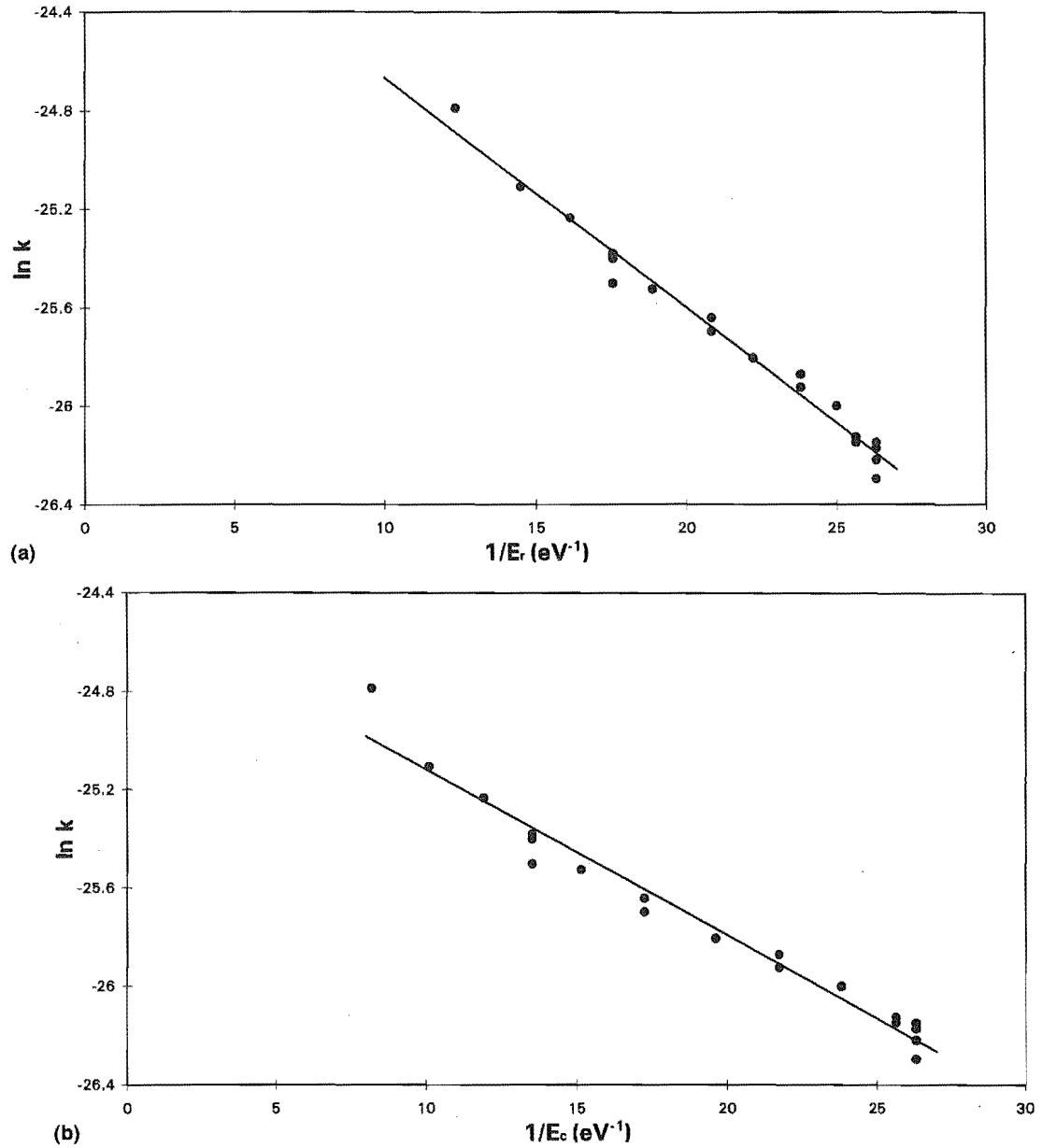

Fig. 2. SIFDT data for the reaction $SO_2^+ + H_2$. Plotted in the form of an Arrhenius type plot of ln k against (a) $E_r^{-1}/(eV^{-1})$ and (b) $E_c^{-1}/(eV^{-1})$.

gas collisions is distributed amongst the several modes of the ion-reactant gas complex, then the energy input from E_r is effectively smaller than E_c. It is E_c that has the dominant influence on the reaction. We therefore plot $\ln k$ against E_c^{-1} in Fig. 2(b).

In the present case, the difference between E_r and E_c is not large ($M_c = 4$ and $M_r = 2$) and Fig. 2 indicates the plots of $\ln k$ vs. $E_{r,c}^{-1}$ are linear over most of the range of energies accessed in this work. Linear Arrhenius-type plots have been observed in several drift tube investigations [23–25] and are to be interpreted with care [26].

3.1. The barrier to H-atom abstraction

Can we infer a barrier height for H-atom abstraction from the results shown in Fig. 2? The slope of $\ln k$ against $1/E_r$ (Fig. 2(a)) and against $1/E_c$ (Fig. 2(b)) correspond to barriers of 6.0 kJ mol^{-1} and 4.3 kJ mol^{-1} respectively. Having taken cognizance of potential problems in using drift tubes to evaluate thermodynamic data, we note that sufficient linear Arrhenius type plots using flow drift tubes have been made [23–25] for us to have some confidence in equating the activation energy from the slope of the lines in Fig. (2(a)) and (2(b)) with the barrier height to H-atom abstraction. We compare next our evaluated barrier height with that calculated from an ab initio investigation of the $H_2SO_2^+$ surface.

3.2. Ab initio calculations

All calculations were performed using the Gaussian 94 program [27] and follow the prescription detailed in the original description of the G2(MP2) procedure [28].

The structures of the reactants, possible products, and transition states, with geometric parameters calculated at the MP2 = FU/6–31G* level of theory are shown in Fig. 3. The calculated energies of the possible reactants, products and transition states are listed in Table 1. In the $OSOH_2^+$ structures there is a long (2.022 Å trans,

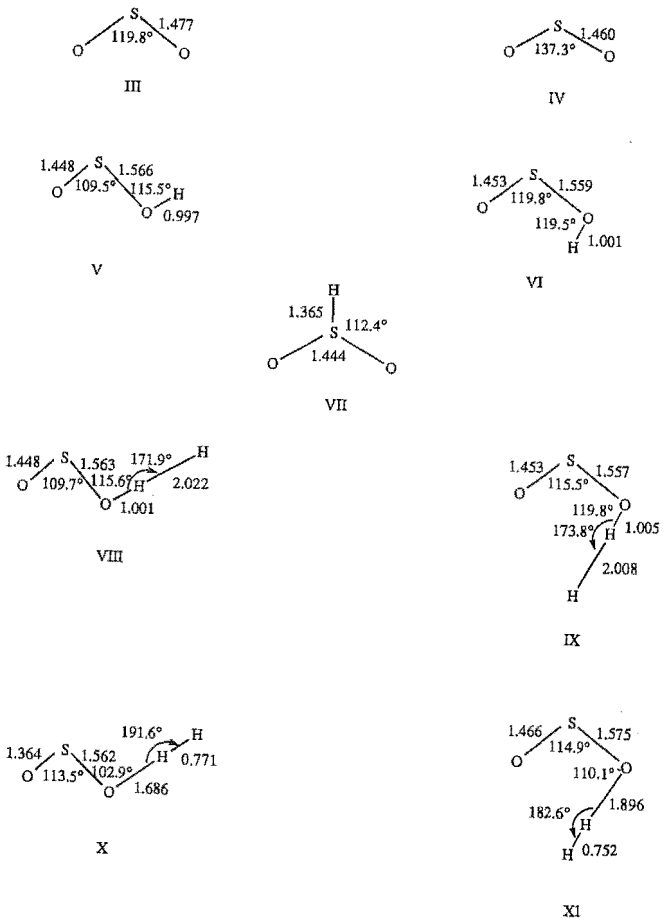

Fig. 3. Calculated structures of transition states, reactants and products in the reaction $SO_2^+ + H_2 \rightarrow OSOH^+ + H$.

Table 1
Calculated energies at 0 K (in hartrees) for the designated structures

Structure	Species	HF/6-31G*	MP2 = FU/6-31G*	G2(MP2)
I	H_2	− 1.14414	− 1.16832	− 1.16832
II	H	− 0.49823	− 0.49823	− 0.50000
III	SO_2^+	− 546.73386	− 547.25021	− 547.36248
IV	SO_2	− 547.16901	− 547.70010	− 548.00709
V	trans $OSOH^+$	− 547.42155	− 547.94340	− 548.24605
VI	cis $OSOH^+$	− 547.42762	− 547.94950	− 548.24933
VII	HSO_2^+	− 547.33948	− 547.87562	− 548.18073
VIII	trans $OSOH_2^+$	− 547.92090	− 548.44339	− 548.74855
IX	cis $OSOH_2^+$	− 547.92697	− 548.44950	− 548.75157
X	trans $OSOH_2^+$ TS	− 547.87288	− 548.36509	− 548.71152
XI	cis $OSOH_2^+$ TS	− 547.87765	− 548.38512	− 548.71170

2.008 Å cis) H–H bond. In the $OSOH_2^+$ TS structures there is a long O–H bond (1.686 Å trans, 1.896 Å cis) with the H–H bond only slightly elongated (0.738 Å to 0.771 Å (trans) and 0.752 (cis)). The weak interaction between SO_2^+ and H_2 means that considerable H–H bonding energy is lost before a gain in O–H bonding occurs with a barrier to H-atom abstraction resulting. Attachment to the S atom is energetically unfavourable giving the reaction a significant steric factor. The strength of the cis $OSOH^+$ O–H bond is calculated to be 512.4 kJ mol^{-1} compared with 436.8 kJ mol^{-1} calculated for the H_2 H–H bond. The energies of the various $H_2SO_2^+$ species relative to $SO_2^+ + H_2$ are given in Table 2. From these Tables we find that the calculated proton affinities (PAs) of SO_2 at 0 K are: 627 kJ mol^{-1} for trans $OSOH^+$, 636 kJ mol^{-1} for cis $OSOH^+$ and 456 kJ mol^{-1} for HSO_2^+ protonated at the S atom. The PA measured for SO_2 at room temperature is 636 kJ mol^{-1} [8] in good agreement with the calculated values.

Table 2
Relative energies of the stated structure to $SO_2^+ + H_2$ in kJ mol^{-1} at 0 K and 298 K

	0 K	298 K
$SO_2^+ + H_2$	0.0	0.0
trans $OSOH_2^+$	− 73.5	− 73.8
cis $OSOH_2^+$	− 81.5	− 82.0
trans $OSOH_2^+$ TS	23.7	20.3
cis $OSOH_2^+$ TS	23.2	19.9
trans $OSOH^+ + H$	− 67.0	− 69.0
cis $OSOH^+ + H$	− 75.6	− 77.7
$HSO_2^+ + H$	+ 104.5	+ 102.1

Lastly the transition state corresponding to the barrier height for H-atom abstraction (Fig. 4) is calculated to be 19.9 kJ mol^{-1} at 298 K and 23.2 kJ mol^{-1} above $SO_2^+ + H_2$ at 0 K.

3.3. Comparison of experiment and theory

The agreement between theory (19.9 kJ mol^{-1}) and experiment (6.0 kJ mol^{-1} (E_r) and 4.3 kJ mol^{-1} (E_c) for the barrier height is fair bearing in mind the difficulties inherent in calculating the energies of transition states. For example, in the study by Herbst et al. [5], the barrier calculated for the reaction of $NH_3^+ + H_2$ of 20.1 kJ mol^{-1} was larger than the experimental determination of 8.8 kJ mol^{-1}. Smith et al. [23] in a SIFDT study of the H-atom abstraction reaction $C_2H_2^+ + H_2$ found that the E_c function (Eq. (5)) gave better agreement with other techniques than did E_r (Eq. (4)). We cannot come out in favour of which function, E_r or E_c, best represents the effective reaction temperature in this study except to note that the difference between the activation barriers calculated using the two approaches is within the experimental uncertainty.

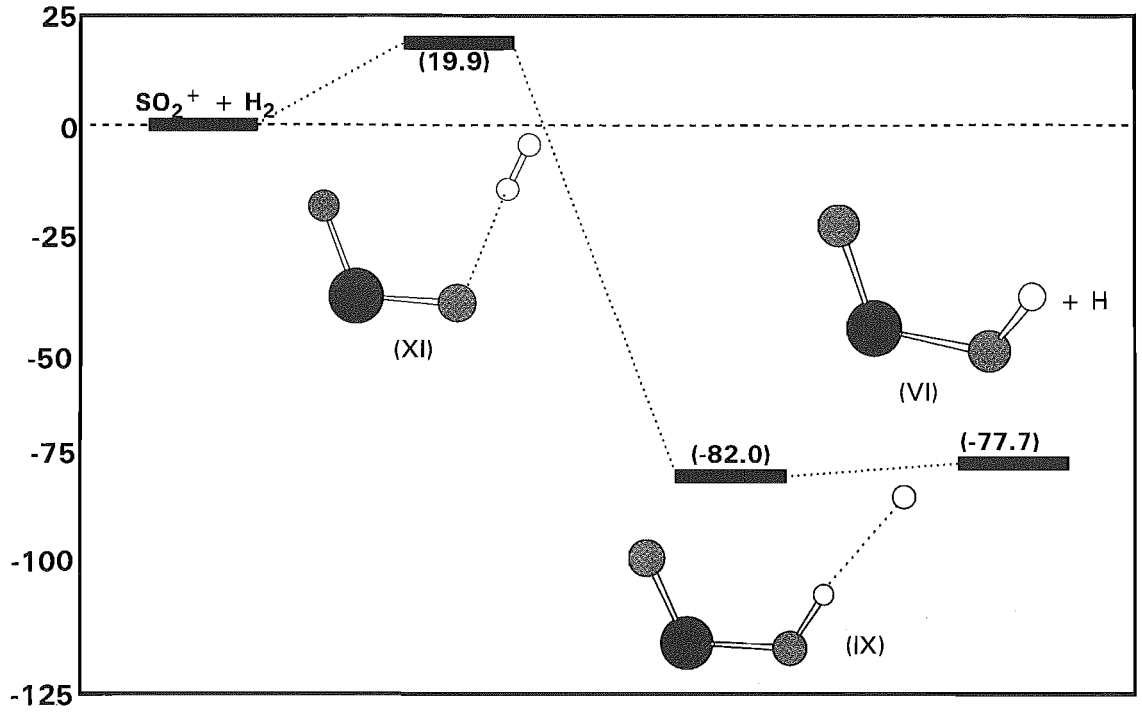

Fig. 4. $H_2SO_2^+$ energy surface calculated using the G2 procedure. The energies are expressed in kJ mol^{-1} relative to $SO_2^+ + H_2$ and are corrected to 298 K and for zero-point energy.

The excellent linearity of the two Arrhenius-type plots indicates that significant vibrational excitation of SO_2^+ in collisions with the He bath gas does not occur at energies < 0.1 eV (9.7 kJ mol^{-1}). This observation is in agreement with the results of Durup–Ferguson et al. [29,30] who found that SO_2^+ ions were not significantly vibrationally excited in a helium bath gas at E_c energies near, or even above the threshold for vibrational excitation. Accordingly our results satisfy the criterion that in order to obtain accurate thermodynamic data from drift tube measurements, it is necessary to work in a regime where vibrational energy is not a factor [26]. Smith et al. [23] attributed the non-linearity in their Arrhenius-type plots at higher center-of-mass energies to population of the C=C stretch in $C_2H_2^+$. In their case, the H-atom abstraction reaction was about 6 kJ mol^{-1} endothermic and population of higher vibrational levels provides a mechanism for driving the reaction.

4. Concluding remarks

A kinetic barrier has been identified from both theory and experiment, between the reactants and products in the exothermic H-atom abstraction reaction of SO_2^+ and H_2. This barrier accounts for the small rate coefficient observed at 300 K.

It is apparent from this and other studies that kinetic barriers occur in several H-atom abstraction reactions. For example, barriers have been observed in a number of reactions with H_2, including NH_3^+ [4,5], c–$C_3H_2^+$ [7], C_6H^+ [2] and have been predicted for $C_2H_2^+$ [23]. Of thirty exothermic ion H-atom abstraction reactions of H_2 listed in the literature [10], about 30% exhibit

rate coefficients that are less than half the collision rate. There is therefore a marked contrast between H-atom abstraction and exothermic proton transfer reactions which are invariably fast. H-atom abstraction from H_2 requires the H_2 molecule to be bound to the ion before eventual H-atom loss rather than exchange of a proton. It is this binding process and subsequent loss of H that may result in a barrier (e.g. see Fig. 4). The presence of kinetic barriers has important implications for interstellar cloud chemistry [31] which, for the most part, takes place at temperatures < 50 K.

We also note that not all H-atom abstraction reactions having rate coefficients much less than their capture rates have kinetic barriers. Of the five H-atom abstraction reactions of $C_nH_m^+$ ions with H_2 investigated by Giles et al. [2], only one, $C_6H^+ + H_2$, has a rate coefficient that is less at 80 K than it is at 300 K indicating a kinetic barrier. The remaining four rate coefficients have rate coefficients that are substantially less than the collision rate at 300 K yet all show noticeable increases in rate coefficient at 80 K. In these cases the lifetime of the $(C_nH_m^+.H_2)^*$ complex (which is greater at 80 K than it is at 300 K) may be the major factor contributing to the low efficiency of the reaction.

Acknowledgements

We thank the Marsden Fund for financial support and acknowledge helpful discussions with Prof. David Smith.

References

[1] E. Herbst, C.M. Leung, Astrophys. J. Suppl. Ser. 69 (1989) 271.
[2] K. Giles, N.G. Adams, D. Smith, Int. J. Mass Spectrom. Ion Proc. 89 (1989) 303.
[3] S.D. Prodnuk, C.H. DePuy, V.M. Bierbaum, Int. J. Mass Spectrom. Ion Proc. 100 (1990) 693.
[4] N.G. Adams, D. Smith, J.F. Paulson, J. Chem. Phys. 72 (1980) 288.
[5] E. Herbst, D.J. DeFrees, D. Talbi, F. Pauzat, W. Koch, A.D. McLean, J. Chem. Phys. 94 (1991) 7842.
[6] D. Smith, N.G. Adams, Int. J. Mass Spectrom. Ion Proc. 76 (1987) 307.
[7] M.W. Wong, L. Radom, J. Amer. Chem. Soc. 115 (1993) 1507.
[8] S.G. Lias, J.E. Bartmess, J.F. Liebman, J.L. Holmes, R.D. Levin, W.G. Mallard, J. Phys. Chem. Ref. Data, 17 (1988) Suppl. No. 1.
[9] G.B.I. Scott, D.A. Fairley, C.G. Freeman, M.J. McEwan, P. Spanel, D. Smith, J. Chem. Phys. 106 (1997) 3982.
[10] V.G. Anicich, J. Phys. Chem. Ref. Data 22 (1993) 1469.
[11] M.J. McEwan, in: N.G. Adams, L.M. Babcock (Eds.), Advances in Gas Phase Ion Chemistry, Vol. 1, J.A.I. Press, CT, 1992, p. 1.
[12] D. Smith, N.G. Adams, in: D. Bates, B. Bederson (Eds.), Advances in Atomic and Molecular Physics, Vol. 24, Academic Press, 1988, p. 1.
[13] W. Lindinger, D. Smith, in: A. Fontijn, M.A.A. Clyne (Eds.), Reactions of Small Transient Species, Academic Press, London, 1983, p. 387.
[14] H. Böhringer, M. Durup-Ferguson, D.W. Fahey, J. Chem. Phys. 79 (1983) 1974.
[15] D.L. Albritton in P. Ausloos (Ed.), Kinetics of Ion Molecule Reactions, Plenum, 1979, p. 119.
[16] W. Lindinger, Int. J. Mass Spectrom. Ion Proc. 80 (1987) 115.
[17] M. McFarland, D.L. Albritton, F.C. Fehsenfeld, E.E. Ferguson, A.L. Schmeltekopf, J. Chem. Phys. 59 (1973) 6620.
[18] M.A. Duncan, V.M. Bierbaum, G.B. Ellison, S.R. Leone, J. Chem. Phys. 79 (1983) 5448.
[19] L.A. Viehland, R.E. Robson, Int. J. Mass Spectrom. Ion Proc. 90 (1989) 167.
[20] W. Lindinger, M. McFarland, F.C. Fehsenfeld, D.L. Albritton, A.L. Schmeltekopf, E.E. Ferguson, J. Chem. Phys. 63 (1975) 2175.
[21] W. Federer, H. Ramler, H. Villinger, W. Lindinger, Phys. Rev. Lett. 54 (1985) 540.
[22] J. Glosik, D. Smith, P. Spanel, W. Freysinger, W. Lindinger, Int. J. Mass Spectrom. Ion Proc. 129 (1993) 131.
[23] D. Smith, J. Glosik, V. Skalsky, P. Spanel, W. Lindinger, Int. J. Mass Spectrom. Ion Proc. 129 (1993) 145.
[24] M. Tichy, G. Javahery, N.D. Twiddy, E.E. Ferguson, Int. J. Mass Spectrom. Ion Proc. 93 (1989) 165.
[25] D. Smith, N.G. Adams, in: T.J. Millar, D.A. Williams (Eds.), Rate Coefficients in Astrochemistry, Kluwer Academic, 1988, p. 153.
[26] M. Henchman, in: K.R. Jennings (Ed.), Fundamentals of Gas Phase Ion Chemistry, NATO ASI series, Kluwer Academic, 1991, p. 267.
[27] M.J. Frisch, G.W. Trucks, H.B. Schlegel, P.M.W. Gill, B.G. Johnson, M.A. Robb, J.R. Cheeseman, T. Keith, G.A. Petersson, J.A. Montgomery, K. Raghavachari, M.A. Al-Laham, V.G. Zakrzewski, J.V. Ortiz, J.B. Foresman, J. Cioslowski, B.B. Stefanov, A. Nanayakkara, M. Challacombe, C.Y. Peng, P.Y. Ayala, W. Chen, M.W. Wong, J.L. Andres, E.S. Replogle, R. Gomperts, R.L. Martin, D.J. Fox, J.S. Binkley, D.J. DeFrees, J. Baker, J.P. Stewart, M. Head-Gordon, C.

Gonzalez, J.A. Pople, Gaussian 94, Gaussian, Inc., Pittsburgh, PA, 1995.
[28] L.A. Curtiss, K. Raghavachari, J.A. Pople, J. Chem. Phys. 98 (1993) 1293.
[29] M. Durup-Ferguson, H. Böhringer, D.W. Fahey, E.E. Ferguson, J. Chem. Phys. 79 (1983) 265.
[30] E.E. Ferguson, in: P. Ausloos, S.G. Lias (Eds.), Structure/Reactivity and Thermochemistry of Ions, NATO ASI Series, D. Reidel, Dordrecht, 1987, p. 81.
[31] D.K. Bohme, in: P. Ausloos, S.G. Lias (Eds.), Structure/Reactivity and Thermochemistry of Ions, NATO ASI series, D. Reidel Publishing Co., Dordrecht, 1987, p. 219.

Submission of papers (in English, French or German (English is preferred))

Papers should be sent to:

M.T. BOWERS, Department of Chemistry, University of California, Santa Barbara, CA 93106, USA (Fax: +1 805 893 8703)
or to: H. SCHWARZ, Department of Chemistry, Technical University, Strasse des 17. Juni 135, +1 D-10623 Berlin, Germany (Fax: +49 30 3142 1102)
or to: J.F.J. TODD, Chemistry Department, University of Kent, Canterbury, Kent CT2 7NH, UK (Fax: +44 (0) 1227 827724)

Submission of an article is understood to imply that the article is original and unpublished and is not being considered for publication elsewhere. Upon acceptance of an article by the journal, author(s) will be asked to transfer the copyright of the article to the publisher. This transfer will ensure the widest possible dissemination of information.

Publication

International Journal of Mass Spectrometry and Ion Processes (ISSN 0168-1176). For 1997 volumes 160–173 are scheduled for publication.
Subscription prices are available on request from the publisher. Subscriptions are accepted on a prepaid basis only and are entered on a calendar year basis. Issues are sent by surface mail except to the following countries where air delivery via SAL (Surface Air Lift) mail is ensured: Argentina, Australia, Brazil, Canada, Hong Kong, India, Israel, Japan, Malaysia, Mexico, New Zealand, Pakistan, PR China, Singapore, South Africa, South Korea, Taiwan, Thailand, USA. For all other countries airmail rates are available upon request. Claims for missing issues must be made within six months of our publication (mailing) date.
Orders, claims and product enquiries: please contact the Customer Support Department at the Regional Office nearest you:
New York: Elsevier Science, P.O. Box 945, New York, NY 10159-0945, USA; Tel. (+1) 212-633-33730, [Toll free number for North American customers: 1-888-4ES-INFO (437-4636)], Fax (+1)212-633-3680, E-mail usinfo-f@elsevier.com
Amsterdam: Elsevier Science, P.O. Box 211, 1000 AE Amsterdam, The Netherlands; Tel. (+31)20-4853757, Fax (+31)20-4853432, E-mail nlinfo-f@elsevier.nl
Tokyo: Elsevier Science, 9-15 Higashi-Azabu 1-chome, Minato-ku, Tokyo 106, Japan: Tel. (+81)3-5561-5033, Fax (+81)3-5561-5047, E-mail. kyf04035@niftyserve.or.jp
Singapore: Elsevier Science, No. 1 Temasek Avenue, #17-01 Millenia Tower, Singapore 039192; Tel. (+65)434-3727, Fax (+65)337-2230. E-mail asiainfo@elsevier.com.sg

US **mailing notice**—International Journal of Mass Spectrometry and Ion Processes (ISSN 0168-1176) is published semi-monthly (except in January when it will appear monthly) by Elsevier Science B.V., Molenwerf 1, Postbus 211, 1000 AE Amsterdam. Annual subscription price in the USA US$2985.00 (valid in North, Central and South America only), including air speed delivery. Second class postage is paid at Jamaica, NY 11431.

USA **POSTMASTERS**: Send address changes to International Journal of Mass Spectrometry and Ion Processes, Publications Expediting, Inc., 200 Meacham Avenue, Elmont, NY 11003. Airfreight and mailing in the USA by Publication Expediting.

The International Journal of Mass Spectrometry and Ion Processes **has no page charges.**
Fifty reprints will be supplied free of charge. Additional reprints (minimum 100) can be ordered at quoted prices.

INSTRUCTIONS TO AUTHORS

Manuscripts

Authors should submit the original and two copies in double-spaced type with adequate margins on pages of uniform size. Manuscripts should be written in English. Instructions for the preparation of compuscripts are available from the publisher.

Acknowledgements and references should be placed at the end of the paper. It is recommended that authors use the nomenclature and symbols adopted by IUPAC (Quantities, Units and Symbols in Physical Chemistry, Blackwell Scientific, Oxford, 1993). See also the IUPAC Recommendations for Symbolism and Nomenclature for Mass Spectrometry, Pure Appl. Chem., 63 (1991) 1541–1566, and reprinted in Int. J. Mass Spectrom. Ion Processes, 142 (1995) 211–240.

Tables should be typed on separate pages and numbered with Arabic numerals in the order in which they are mentioned in the text. All tables should have descriptive titles. The use of chemical formulae and conventional abbreviations is encouraged in tables and figures but chemical formulae should not be used in the text unless they are necessary for clarity. Units of weight, volume, etc., when used with numerals should be abbreviated and unpunctuated (e.g. 2%, 2 ml, 2 g, 2 μl, 2 μg, 2 ng, 2 cm, 200 nm).

Figures should be drawn in black, waterproof drawing ink on drawing or tracing paper. Standard symbols should be used in line drawings; the following are available to the typesetter:

○ ⊕ ● × + △ ▲ ◇ ◆ □ ■ ☆ ★ –

Photographs should be submitted as clear black-and-white glossy prints. Figures and photographs should be of the same size as the typed pages. Legends for figures should be typed on a separate page. Figures should be numbered with Arabic numerals in the order in which they are mentioned in the text.

References in text should be numbered (on the line and in square brackets) in the order of their appearance. The reference list at the end of the article should be in numerical order of appearance in the text. Abbreviations of journal titles should conform to those adopted by the Chemical Abstract Service (Bibliographic Guide for Editors and Authors, The American Chemical Society, Washington, DC, 1974). The recommended form for references to journal papers and books is as follows: 1 J.J. Lingane and A.M. Hartley, Anal. Chim. Acta, 11 (1954) 475. 2 F. Feigl, Spot Tests in Organic Analysis, 7th edn., Elsevier, Amsterdam, 1966, p. 516. For multi-author references, all authors must be named, and initials given, in the reference list, although the use of, for example, Smith et al., is desirable in the text.

An abstract of not more than 500 words should be provided. It should be a concise and factual description of the contents and conclusions as well as an indication of any new findings. References should be avoided in the abstract if at all possible. If they are necessary, they should be given in full and not included as part of the numbered list. Illustrations (e.g. formulae and schemes which cannot be typeset) should be avoided in the abstract if at all possible.

Detailed suggestions and instructions to authors are published in Int. J. Mass Spectrom. Ion Processes, 154 (1996) 229–234. A free copy of these instructions is available from the publisher on request.